KfK 3789
November 1986

Temperature Escalation in PWR Fuel Rod Simulator Bundles due to the Zircaloy/Steam Reaction: Post Test Investigations of Bundle Test ESBU-2A

S. Hagen, H. Kapulla, H. Malauschek,
K. P. Wallenfels, B. Buescher

Hauptabteilung Ingenieurtechnik
Projekt Nukleare Sicherheit

Kernforschungszentrum Karlsruhe

KERNFORSCHUNGSZENTRUM KARLSRUHE
HAUPTABTEILUNG INGENIEURTECHNIK
PROJEKT NUKLEARE SICHERHEIT

KfK 3789

Temperature Escalation in PWR Fuel Rod Simulator Bundles due to the Zircaloy/Steam Reaction: Post Test Investigations of Bundle Test ESBU-2A

S. Hagen, H. Kapulla, H. Malauschek, K.P. Wallenfels, B. Buescher[+])

[+]) USNRC Delegate to Kernforschungszentrum Karlsruhe
from EG&G, Idaho Falls, Idaho

KERNFORSCHUNGSZENTRUM KARLSRUHE GMBH, KARLSRUHE

Kernforschungszentrum Karlsruhe GmbH
Postfach 3640, 7500 Karlsruhe 1

ISSN 0303-4003

Summary

This KfK report describes the post test investigation of bundle experiment ESBU-2a. ESBU-2a was the second of two bundle tests on the temperature escalation of zircaloy clad fuel rods. The investigation of the temperature escalation is part of the program of out-of-pile experiments performed within the frame work of the PNS - Severe Fuel Damage program.

The bundle was composed of a 3x3 fuel rod array of our fuel rod simulators (central tungsten heater, UO_2- ring pellet and zircaloy cladding). The length was 0.4 meter. The bundle was heated to a maximum temperature of 2175°C. Molten cladding which dissolved part of the UO_2 pellets and slumped away from the already oxidized cladding formed a lump in the lower part of the bundle. After the test the bundle was embedded in epoxy and sectioned with a diamand saw, in the region of the refrozen melt. The cross sections were investigated by metallographic examination.

The refrozen (U, Zr, O) melt consists variously of three phases with increasing oxygen content (metallic α-Zry, metallic (U,Zr)alloy and a $(U,Zr)O_2$ mixed oxide), two phases (α-Zry, $(U,Zr)O_2$ mixed oxide), or one phase ($(U,Zr)O_2$ mixed oxide).

The cross sections show the increasing oxidation of the cladding with increasing elevation (temperature). A strong azimuthal dependency of the oxidation is found. In regions where the initial oxidized cladding is contacted by the melt one can recognize the interaction between the metallic melt and ZrO_2 of the cladding. Oxygen is taken away from the ZrO_2. If the melt is in direct contact with steam a relatively well defined oxide layer is formed.

...

Temperatureskalation in DWR Brennstabbündeln infolge der Zircaloy/Dampf-Reaktion: Nachuntersuchung des Bündels ESBU-2a.

Kurzfassung

Dieser KfK-Bericht beschreibt die metallographische Nachuntersuchung des Bündelversuchs ESBU-2a. ESBU-2a war der zweite von zwei Bündelversuchen für die Untersuchung der Temperatureskalation von zirkaloy-umhüllten Brennelementstäben. Die Untersuchung des Eskalationsverhaltens gehört zum Programm der out-of-pile-Experimente (CORA), die im Rahmen der Severe Fuel Damage Untersuchungen des PNS durchgeführt werden.

Das Bündel war in einer 3x3 Anordnung aus den üblichen Brennstabsimulatoren aufgebaut (zentraler W-Heizer, UO_2-Ringpellets und Zircaloy-Hüllrohre). Die Länge betrug 40 cm. Die maximale Temperatur im Bündel betrug 2175°C. Im oberen Bereich des Bündels geschmolzenes Zry der Hülle hat die äußere Schichten des UO_2-Pellets aufgelöst und die anfänglich entstandene Oxid-Schicht mit herabgespült. Im unteren Bereich des Bündels hat sich daraus ein Schmelzklumpen gebildet.

Nach dem Versuch wurde das Bündel in Epoxidharz eingebettet und im Bereich des Klumpens mit einer Diamantsäge geschnitten. Die Querschnitte wurden mit einem Metallmikroskop untersucht. Die gefrorene (U,Zr,O)Schmelze bildet mit zunehmendem Sauerstoffgehalt 3 Phasen (metallisches α-Zry, eine metallische (U,Zr)-Legierung und $(U,Zr)O_2$ Mischoxid), 2 Phasen (α-Zry, Mischoxid) oder 1 Phase (nur Mischoxid).

Die Querschnitte zeigen die mit der Höhenlage (Temperatur) ansteigende Oxidschichtdicke, die eine stark azimutale Abhängigkeit aufweist. In Bereichen, in denen das zu Beginn des Versuches oxidierte Hüllrohr in Kontakt mit der Schmelze tritt, kommt es zur Wechselwirkung zwischen dem ZrO_2 und der metallischen Schmelze. Sauerstoff wird dem ZrO_2 entzogen. Wenn die Schmelze dagegen in direktem Kontakt zum Dampf kommt, bildet sich eine relativ gut definierte Oxidschicht aus.

...

Contents

1. Introduction

Within the Project of Nuclear Safety (PNS) at the Kernforschungszentrum Karlsruhe (KfK), a comprehensive program /1/ for the investigation of Severe Fuel Damage (SFD) is scheduled. As part of this program, out-of-pile experiments (CORA Program /2/) are being conducted at the Hauptabteilung Ingenieurtechnik (IT). These experiments provide information on the mechanisms causing damage to PWR fuel rods for temperatures up to 2200 °C. These experiments are designed to give information on the integral behaviour of the processes, which are investigated in detail and under well defined conditions in the separate effect tests /3,4/ of the SFD-program. The out-of-pile experiments will also be used for the assessment of the SFD computer codes to simulate the integral behaviour of the fuel rods under Severe Fuel Damage conditions. In addition, these experiments directly complement integral in-pile bundle tests being conducted at PBF, ACRR, NRU and PHEBUS.

Earlier experiments have shown that the behaviour of fuel rods at high temperatures is strongly dependent on the degree of cladding oxidation. Highly oxidized rods are very brittle and can fragment during operation or during quenching, whereas relatively unoxidized cladding melts, dissolves UO_2, and runs down the rod. The extent of oxidation depends, in part, on the temperature rise rate, which in turn is influenced by the exothermic oxidation process. If the heat of reaction is not removed fast enough, the exponential increase of the reaction with temperature can give rise to a rapid temperature escalation. Therefore, oxidation-induced temperature escalation plays an important role in determining fuel behaviour. To investigate the temperature escalation and the processes leading to a turnaround of the escalation, a series of single rod and bundle experiments with fuel rod simulators are being performed.

The results of single rod tests are given in the KfK-report 3507, 3557 and 3567 /5, 6, 7/. The bundle tests ESBU-1 and ESBU-2 are described in the KfK-reports 3508 and 3509 /8, 9/. This paper reports on the posttest investigations on the bundle test ESBU-2A.

2. Experimental Facility

The test was performed in the NIELS facility located in the Hauptabteilung Ingenieurtechnik at KfK. Figure 1 shows side and top cross sections of the 3x3 bundle of fuel rod simulators. The simulators conformed as nearly as possible to German PWR dimensions and pitch, using zircaloy cladding of 10.75 mm outer and 9.29 mm inner diameter, UO_2 ring pellets of 9.2 mm outer and 6.1 mm inner diameter, and a tungsten heater element 6.0 mm in diameter. The overall length of the simulators was 400 mm. Figure 3 illustrates the pretest appearance of the bundle.

To simulate the exothermic reaction energy of neighbouring rods, a zircaloy shroud was installed around the rod bundle (Figure 3). Radial heat losses were reduced by wrapping the shroud in a ceramic fiber insulation (6 mm). Steam was inlet to the bottom of the bundle at 16 locations so that the flow would be evenly distributed across the bundle cross section.

3. Test Conduct

The time dependent power input together with the temperatures at 255 mm elevation is given in Figure 2. The maximum power input reached a value of about 17.5 kW. A steam flow of about 0.7 g/sec was inlet to the bundle beginning at 21 minutes. The drop in voltage at 57 minutes was unintentional and was caused by failure of the power supply. This resulted in a discontinuity of the temperature rise. So only during the last 35 minutes a mean temperature increase of about 0.5 °C/sec was reached at 255 mm elevation. The maximum temperature of 2175 °C was measured on the center rod. The experiment was terminated by turning off the electric power at 99 minutes into the test.

Escalation of the temperature can be seen at 255 mm elevation in the time after 70 minutes. As discussed in the test results report /10/ the escalation is assumed to have a higher influence at the lower elevation of 155 mm. This may be caused partly by low steam supply or improper functioning of the steam supply system.

First melting in the bundle may have happened at about 75 minutes into the test. This is assumed from the change of the character of the upper end steam

temperature, which reflects a change in the bundle geometry. We assume, that from this time on, there is some blockage by molten material.

4. Posttest Appearance

The posttest appearance of the bundle is shown in Figures 4 to 10. The insulation and shroud were still intact following the test. However, both were severely embrittled, as the removal of the insulation from the shroud showed. The insulation, originally a flexible mat, broke into pieces. Even though the insulation was carefully removed, pieces of the shroud broke off. The shroud was severely oxidized over the center region of the bundle and broke away in several places, revealing the fuel rod simulators (Figure 4). Powdery rubble was found at the lower end of the bundle.

Figure 5 shows the fuel rod simulators after removal of the shroud. From the appearance of the bundle we assume the following sequence of events. The cladding from all nine rods melted in the center region of the bundle, liquefied some fuel. The oxide layers formed were too thin to restrain the melt and were carried down together with the melt, and refroze in a solid mass near the bottom of the bundle. The frozen material substantially blocked the coolant flow channels, and the shroud adhered to the refrozen mass. A large amount of powdery rubble, probably fuel fractured during cooldown, was found on top of the blockage . Due to the the smooth surface of the molten material the powdery material must have fallen down after refreezing, i.e., during cooldown. Figures 6 to 8 show this powdery rubble in detail.

The appearance of the bundle after removal of the rubble is shown in Figures 9 and 10. The smooth surface is clearly recognized. In particular, the right-hand photo in Figure 9 shows the sequence of formation of the blockage from single droplets which have been frozen in the lower end of the bundle . Then more and more melt refroze on top of these droplets blocking the whole bundle, so that more and more melt was blocked within the bundle region.The lower part of the refrozen melt shows pure wetting of the solid surface as indicated by the large wetting angles and small contact areas. Melt viscosity , oxygen content and relatively cold fuel rods simulators were probably the main influence on the refreezing behaviour in this region.

The upper surface of the blockage (Figure 10) has a smooth surface and wets the remaining simulators rather well (small wetting angle and large contact surface).

This indicates that the melt interacted with the oxidized fuel rod simulators and steam. The composition of the melt and these interactions will be the primary subject of the posttest examination in this region .

The upper end of the bundle contains intact but oxidized zircaloy cladding. Below this region the remains of fuel pellets that stuck to the tungsten heater rod can be seen. Below the blockage (Figure 9) the cladding appears metallic near the steam inlet, changing to oxidized zircaloy near the lower end of the blockage.

5. Cross section of the blocked region

After disassembling of the shroud and collecting the debris from top of the lump the bundle was encapsulated in epoxy and cut into sections. The elevations of the cross sections are shown in Figure 11. The saw kerf had a thickness of 2 mm. The summary of these cross sections is given at Figure 12. Both sides of the resulting discs were polished and the photographs of the top side and bottom side of each disc is given on Figure 12. The top view is right/left reversed compared to the bottom view. Therefore the photographs of the cross sections in Figure 12 are always marked with the word "oben" for the top view and the word "unten" for the bottom view. To clarify this situation, all numbers of the rods are given.

The white zircaloy area on which the above mentioned numbers are written are the cross sections of the tungsten rod heaters. Around this white area we can recognize the black annulus of the UO_2 pellet. With the exception of some other cross sections in this area of the investigation the UO_2 pellets have survived. At the beginning of the test the UO_2 pellets were surrounded by the zircaloy cladding. The cladding in its original form can be seen in the lower cross sections. With increasing elevation one can recognize that an oxide layer is forming. This oxide layer has a black colour. A large number of droplets is first seen at an elevation of 60 mm. The fuel blockage starts at about 80 mm and continue to about 120 mm. Thus, the fuel blockage length is nearly 40 mm. The comparison of the cross section at 71 mm to the cross sections at the higher elevations shows that in the area of the frozen melt the oxidation is drastically reduced, since steam flow is precluded in that region.

5.1 Discussion of the cross sections (Fig. 13-22)

The photographs of the single cross sections are given from Figure 13 to Figure 22. In Figure 13 the cross section at 135 mm shows the bundle just above the blockage. Here only on the center rod is half of one UO_2 pellet sticking to the tungsten rod. On all the other rods the UO_2 has broken away. Only thin remnants of the pellets are sticking to the surface, glued by the melt which had run into the gap between the tungsten rod and the pellet.

At 121 mm elevation already the whole internal area of the bundle is filled with melt. The black annular UO_2 pellets can be recognized around the brighter tungsten rod cross sections. With the exception of the center rod and an even smaller part of side rod number 4 the cladding of the fuel rod simulators has disappeared at this elevation. They have been dissolved by the surrounding melt.

2 mm lower, at 119 mm elevation, the cross section shown in the photo is nearly the same. Most of the cladding has disappeared. Only in the direction of the missing fuel rod simulator some remnants of the cladding can be seen. At 111 mm elevation in this region much larger remnants of the cladding are visible. At 101 mm the cladding can be recognized around nearly all fuel rods. The cladding has survived at all lower elevations. Remarkable is the behaviour of the oxidized cladding of the fuel rod simulators 1 and 4. The cladding on this fuel rod shows some type of bursting on the outside of the bundle by moving away the cladding from the UO_2 pellet. This behaviour can be recognized down to an elevation of about 80 mm.

Also of interest is the dark seam around the cladding in the region of the former melt. The seam can be seen at all elevations where the cladding has survived in contact with the melt.

During heat up the oxide layer of the cladding has been formed. When the oxidized cladding is surrounded by the metallic melt the zircaloy of the melt starts to take away the oxygen from the oxide layer in the same way as with the interaction with the UO_2. This oxidation uptake by the melt in the surrounding of the fuel rod is the reason for the colour change in this area.

In the cross sections below 71 mm two phenomena are remarkable. First, the large difference in the azimuthal oxidation around the same fuel rods, and second, the formation of thick oxide layers around the former melt droplets. As

we have even steam distribution in the lower end of the bundle the difference in the oxide layer around the rod means a difference in temperature. It is assumed that an initial difference in temperature is increased by the exothermic reaction energy of the oxidation. The higher initial temperature again produces a higher reaction energy. We have some type of temperature escalation . On all cross sections we can recognize a sharp boundary between the oxidized and unoxidized region of the refrozen melt droplets.

5.2 Variation of elevation for the special rods (Fig. 23-30)

In Figures 23 to 30 for the 8 different fuel rod simulators the cross sections at the different elevations are given. Compared to Figures 12 to 22 the photographs are rotated counter clock wise by 90°C. The pictures illustrate the development of the interaction between melt, cladding and UO_2 with changing elevation, that is, with changing temperature.

5.3 Change of structure in cladding area for different elevations (Fig. 31-55)

The change of the structure in the cladding at the different elevations can be even better recognized in Figures 31 to 55. In these Figures of the fuel rod simulators the lower right-hand side of the picture shows enlargements of the cladding area. There are always two pictures from opposite sides of the same fuel rod at the same elevation, signified by left and right. For each fuel rod simulator the photos begin with the 135 mm elevation and continue to the 31 mm elevation.

The photos of the center fuel rod simulator 5 are given in Figures 31 to 35. The oxidation of the original cladding can be best recognized by starting with the lower elevations in Figure 35. On Figure 34 at the 51 mm elevation nearly half of the cladding is oxidized. The cross sections at 59 mm show a strong increase of the oxide layer with elevation, that is, with increasing temperature. Compared to the thickness at the elevation 8 mm lower, the oxide layer has doubled. Also of interest is the remarkable difference in oxidation on the two opposite sides of the same rod at the same elevation. The side of the central fuel rod simulator directed towards the side rod (r) has the higher temperature, which produces higher oxidation, and in turn a larger contribution to the exothermic reaction energy.

The gaps between UO_2 and oxidized cladding, filled with epoxy in the cross sections, are the result of slumping of molten cladding before oxidation. It can be seen, that the molten material which remained, was oxidized. The same behaviour was found in the single rod tests. Also of interest is the crack behaviour. Many of the cracks are continuous from the pellet into the cladding layers. This means that the cracks have developed during cooldown, and this is another indication that fragmentation takes place during cooldown.

At the 69 mm elevation both sides are fully oxidized. At the higher elevation, where the oxidized cladding is surrounded by the melt, the oxide layer has been attacked by the metallic melt. The ZrO_2 of the oxidized cladding is partly reduced to $\alpha(Zr)$.

In Figures 36 to 40 the cladding regions of the side rod 8 are compared for various elevations. Starting again from the lower end at 31 mm on Figure 40, that the oxide layer increases with elevation, that is, with increasing temperature. Compared to the central rod this increase is slower. On the outer side of this fuel rod even at 71 mm the cladding was not fully oxidized. Also here at the higher elevations the attack from the surrounding melt on the oxide layer is apparent.

The change of the structure in the cladding region with elevation is shown for corner rod 3 in Figures 41 to 45, for rod number 6 in Figures 46 to 50, and rod number 9 in Figures 51 to 55. These photographs show the same general behaviour and tendencies as the rods discussed above.

5.4 Melt/Cladding interaction of the center rod (Fig. 56-63)

Figures 56 to 63 show an enlargement of the cladding region for center rod 5 between 121 and 79 mm elevations. In these figures the uranium oxide is at the bottom and the refrozen melt at the top of the photos. The middle region contains the oxidized cladding. At all elevations the attack of the melt on the oxidized cladding can be seen.

5.5 Azimuthal dependency of oxidation (Fig. 64-67)

Figures 64 to 67 illustrate the azimuthal dependance of the oxide layer thickness. At all elevations the oxide layer thickness in the inner part of the bundle is much larger than on the outside for the same fuel rod. This implies a corresponding difference in temperature around the periphery of the fuel rod. It is also apparent that the thickness of the oxide layer is strongly influenced by accessiblity of steam. Positions which are covered locally by melt droplets have a much thinner oxide layer.

5.6 Oxidation Behaviour of the Melt (Fig. 68-90).

Figures 68 to 90 illustrate the oxidation behaviour of the melt in the lower part of the bundle. The oxidized region of the cross section is always dark compared to the nearly white colour of the unoxidized zircaloy. The transition from the oxidized to the unoxidized region is relatively well-defined but much less distinct than the oxidized cladding. The appearance in the transition region is shown in the photos with the large magnification. The lower left photo (Fig. 34) in Figure 80 shows how the thickness of the oxide layer is influenced by the access of steam.

5.7 Thermocouple behaviour

FIgure 91 shows cross sections of a NiCrNi-thermocouple at various elevations in the region between 49 and 61 mm. Note that with increasing temperature the deformation of the thermocouple sheath is increasing. It appears that at elevations where the sheath is already melting the insulation maintains its original shape.

5.8 Change of melt structure with elevations (Fig. 92-94)

The change in the structure of the refrozen melt at different elevations for 3 different positions within the cross sections is given in Figures 92 to 94. It can be seen that the amount of oxidation decreases rapidly from the upper elevation at 121 mm to the lower elevation at 51 mm.

...

5.9 Sieve analysis of the debris (Fig. 96, 97)

The powdery rubble underwent sieve analysis. Figure 96 shows the remnants of this analysis with a mass size of larger than 1 mm. In Figure 97 the sieve analysis of the powdery rubble is given. About 25% of the powdery rubble has a grain size between 20 and 56 µ, and more than half of the grains have a size less than 0.2 mm.

6. Acknowledgement

The authors would like to thank Mr. Seibert for the preparation of the microscopic pictures and Mrs. Ivanitsch for her careful typing of the manuscript.

7. References

1. A. Fiege, Severe Fuel Damage Investigations of KfK/PNS, KfK 3431B, 1983

2. S. Hagen et.al., CORA-Program, KfK 3677, 1986

3. P. Hofmann et.al., UO_2/Zircaloy-4 Chemical Interactions and Reaction Kinetics, KfK 3552, 1983

4. S. Leistikow, G. Schanz, Zircaloy-4 Oxidation Results 600-1600°C, OECD-NEA-CSNI/IAEA Specialists Meeting on Water Reactor Fuel Safety, Riso National Laboratory (Denmark), 16-20 May, 1983

5. S.Hagen et.al., Temperature Escalation in PWR Fuel Rod Simulators due to the Zircaloy/Steam Reaction: Tests ESSI 1-3, Test Results Report, KfK 3507, 1983

6. S.Hagen et.al. Temperature Escalation in PWR Fuel Rod Simulators due to the Zircaloy/Steam Reaction: Tests ESSI 4-11, Test Results Report, KfK 3557, 1984

7. S.Hagen, Out-of-pile Experiments on the High Temperature Behaviour of Zry-4 Clad Fuel Rods, KfK 3567, 1983

8. S. Hagen et.al., Temperature Escalation in PWR Fuel Rod Bundles due to the Zircaloy/Steam Reaction: Bundle Test ESBU-1, Test Results Report, KfK 3508, 1983

9. S. Hagen et.al., Temperature Escalation in PWR Fuel Rod Bundles due to the Zircaloy/Steam Reaction: Bundle Test ESBU-2A, Test Results Report,KfK 3509, 1984

List of Figures

Fig. 22: Cross sections of ESBU-2A at the given elevation above the bottom of the bundle.

Fig. 23: Enlarged views of the region around center rod 5 for different cross sections ESBU-2A.

Fig. 24: Enlarged views of the region around side rod 8 for different cross sections ESBU-2A.

Fig. 25: Enlarged views of the region around corner rod 1 for different cross sections ESBU-2A.

Fig. 26: Enlarged views of the region around corner rod 3 for different cross sections ESBU-2A.

Fig. 27: Enlarged views of the region around side rod 4 for different cross sections ESBU-2A.

Fig. 28: Enlarged views of the region around side rod 6 for different cross sections ESBU-2A.

Fig. 29: Enlarged views of the region around corner rod 7 for different cross sections ESBU-2A.

Fig. 30: Enlarged views of the region around corner rod 9 for different cross sections ESBU-2A.

Fig. 31: Comparison of opposite sides of center rod 5 at various elevations. Test ESBU-2A.

Fig. 32: Comparison of opposite sides of center rod 5 at various elevations. Test ESBU-2A.

Fig. 33: Comparison of opposite sides of center rod 5 at various elevations. Test ESBU-2A.

Fig. 34: Comparison of opposite sides of center rod 5 at various elevations. Test ESBU-2A.

Fig. 35: Comparison of opposite sides of center rod 5 at various elevations. Test ESBU-2A.

Fig. 36: Comparison of opposite sides of side rod 8 at various elevations. Test ESBU-2A.

Fig. 37: Comparison of opposite sides of side rod 8 at various elevations. Test ESBU-2A.

Fig. 38: Comparison of opposite sides of side rod 8 at various elevations. Test ESBU-2A.

Fig. 39: Comparison of opposite sides of side rod 8 at various elevations. Test ESBU-2A.

Fig. 40: Comparison of opposite sides of side rod 8 at various elevations. Test ESBU-2A.

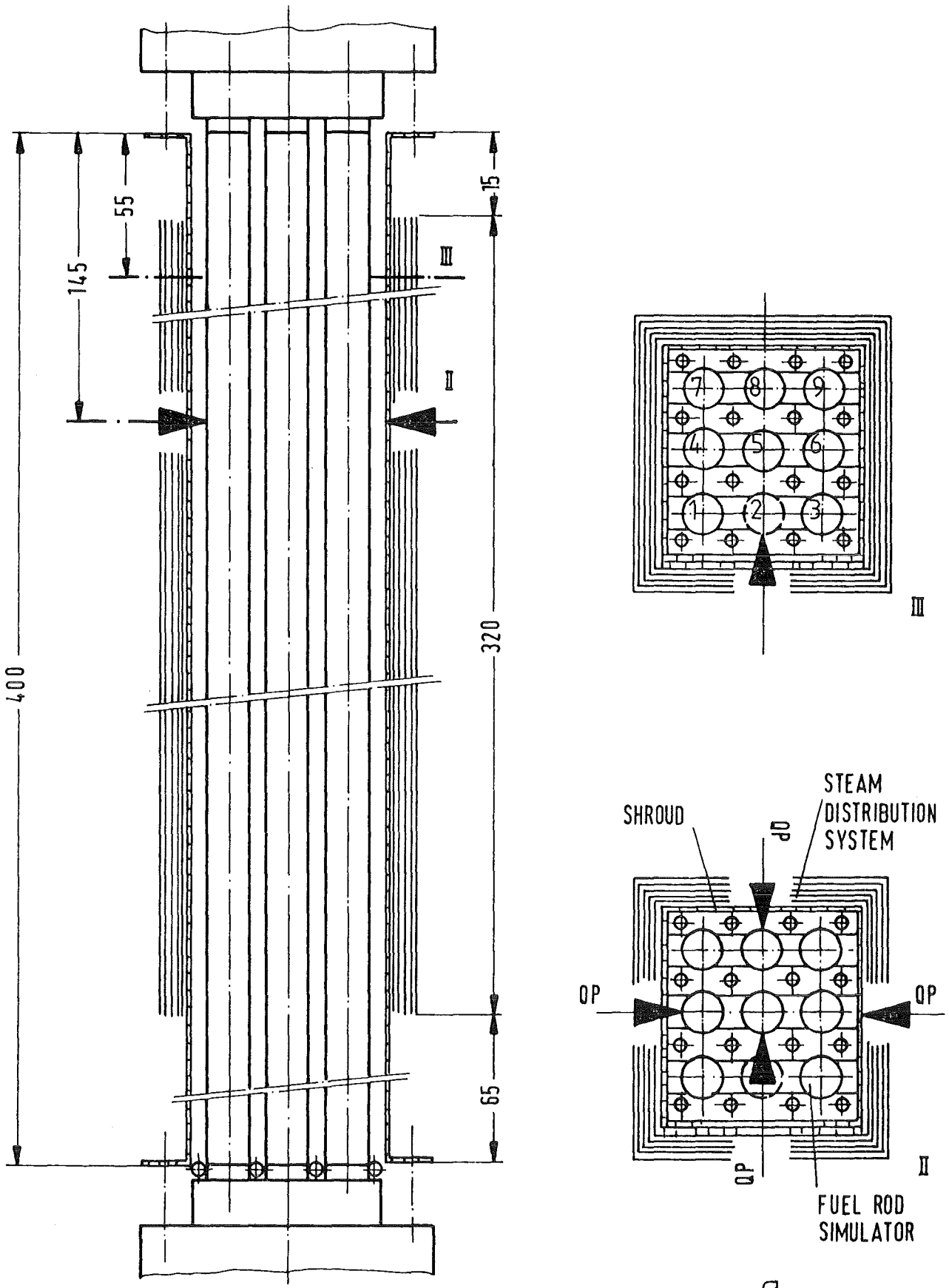

FIGURE 1: ESBU-2A AXIAL AND RADIAL CROSS SECTIONS AND THE LOCATIONS OF THE TWO-COLOR PYROMETERS

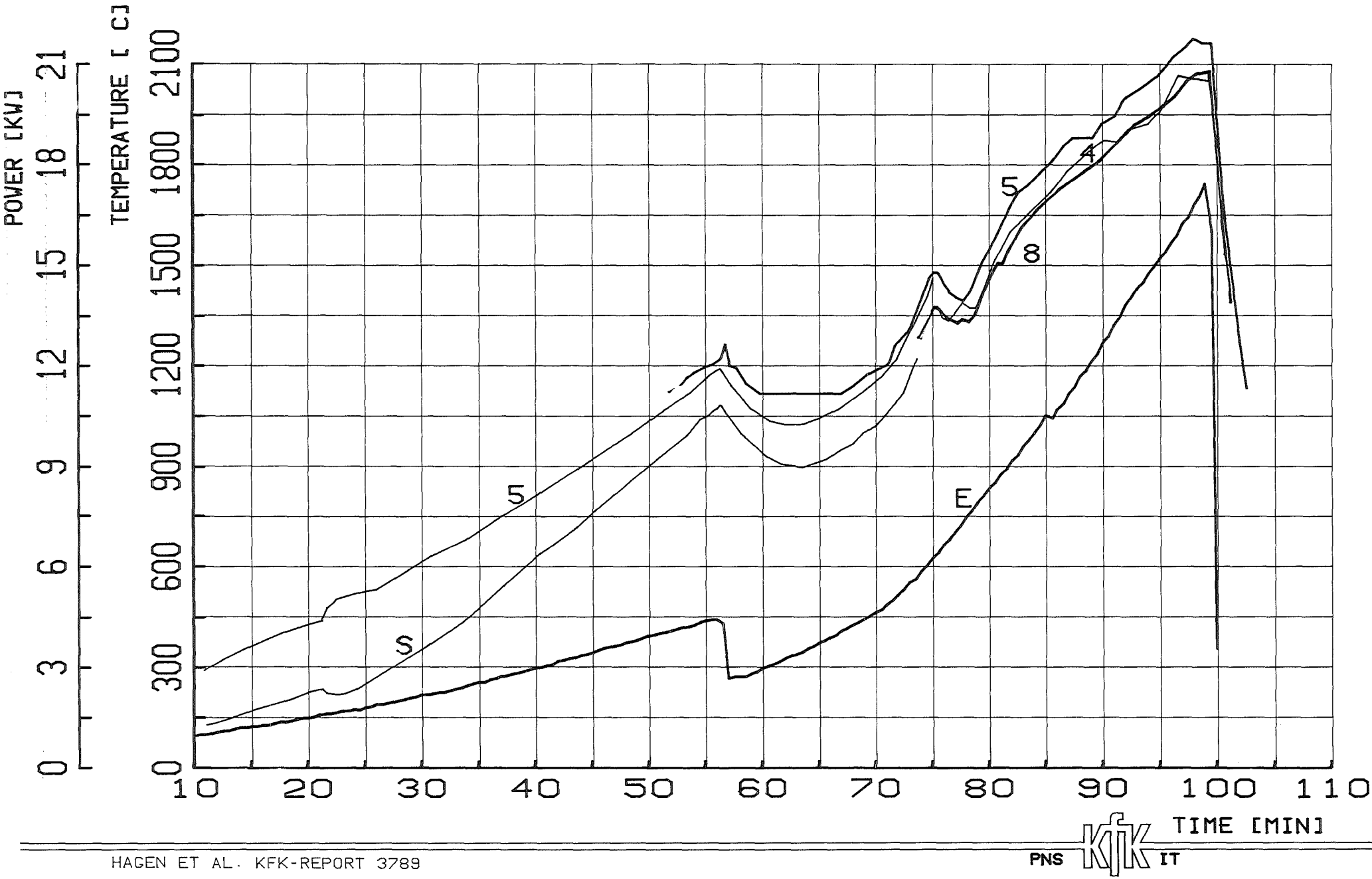

HAGEN ET AL. KFK-REPORT 3789

PNS KfK IT

FIG. 2 : TEMPERATURES AT THE 255 MM MIDPLANE ON THE CENTRAL ROD (5). SIDE RODS (4+8) AND SHROUD (S) COMPARED TO THE ELECTRIC POWER (E). : ESBU-2A

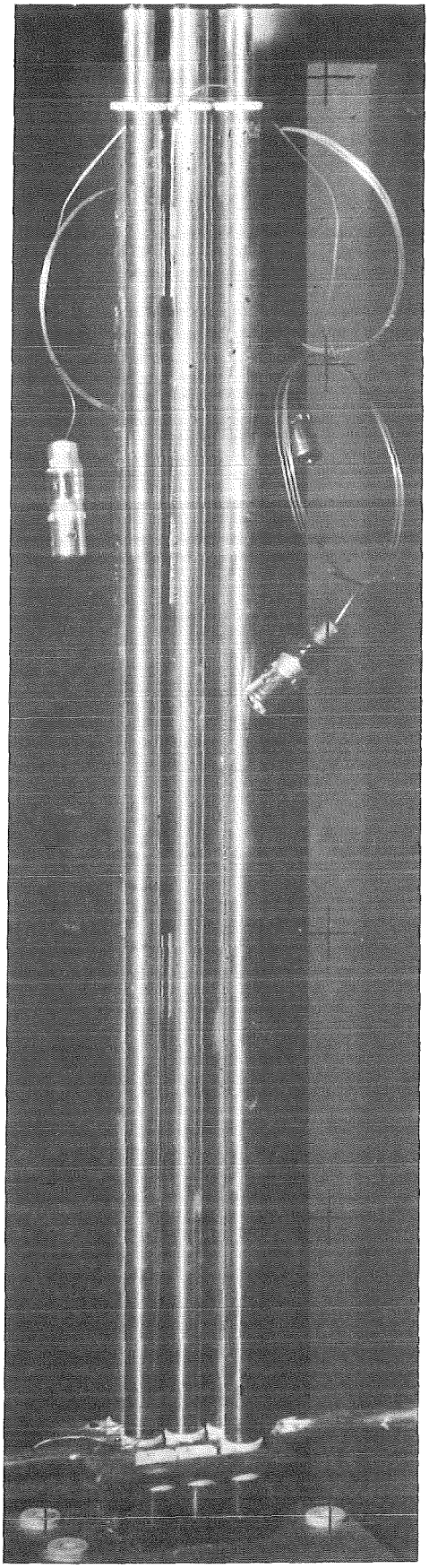

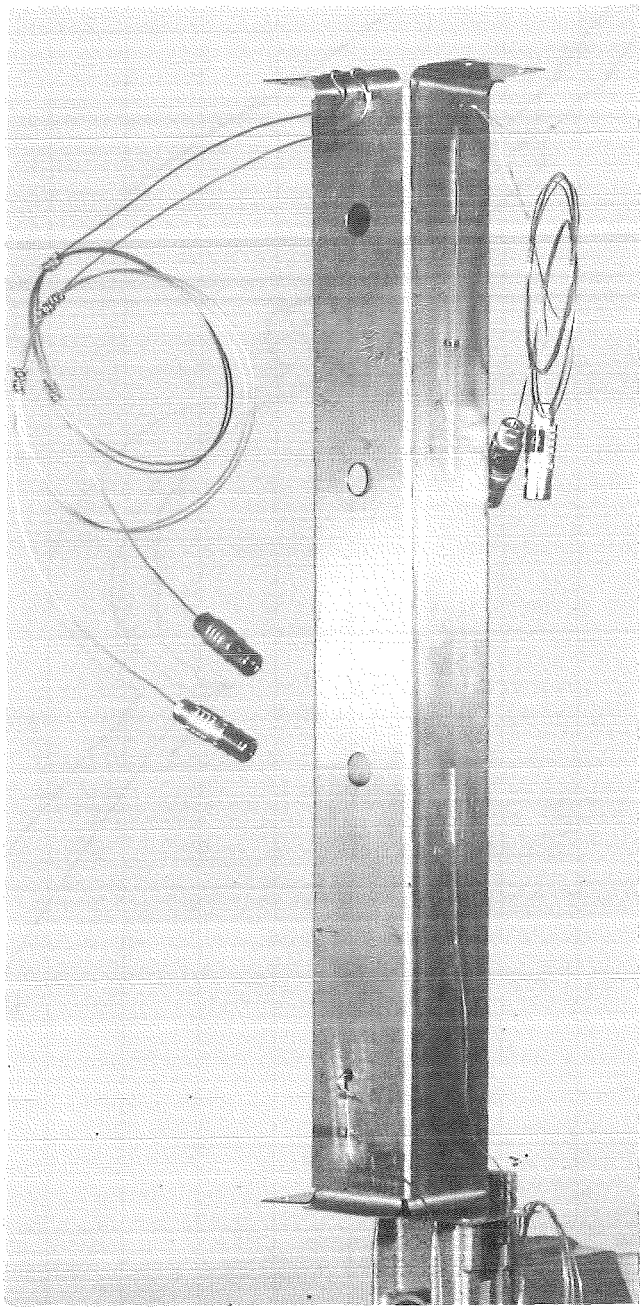

FIGURE 3: PRETEST APPEARANCE OF THE ESBU-2A BUNDLE AND SHROUD

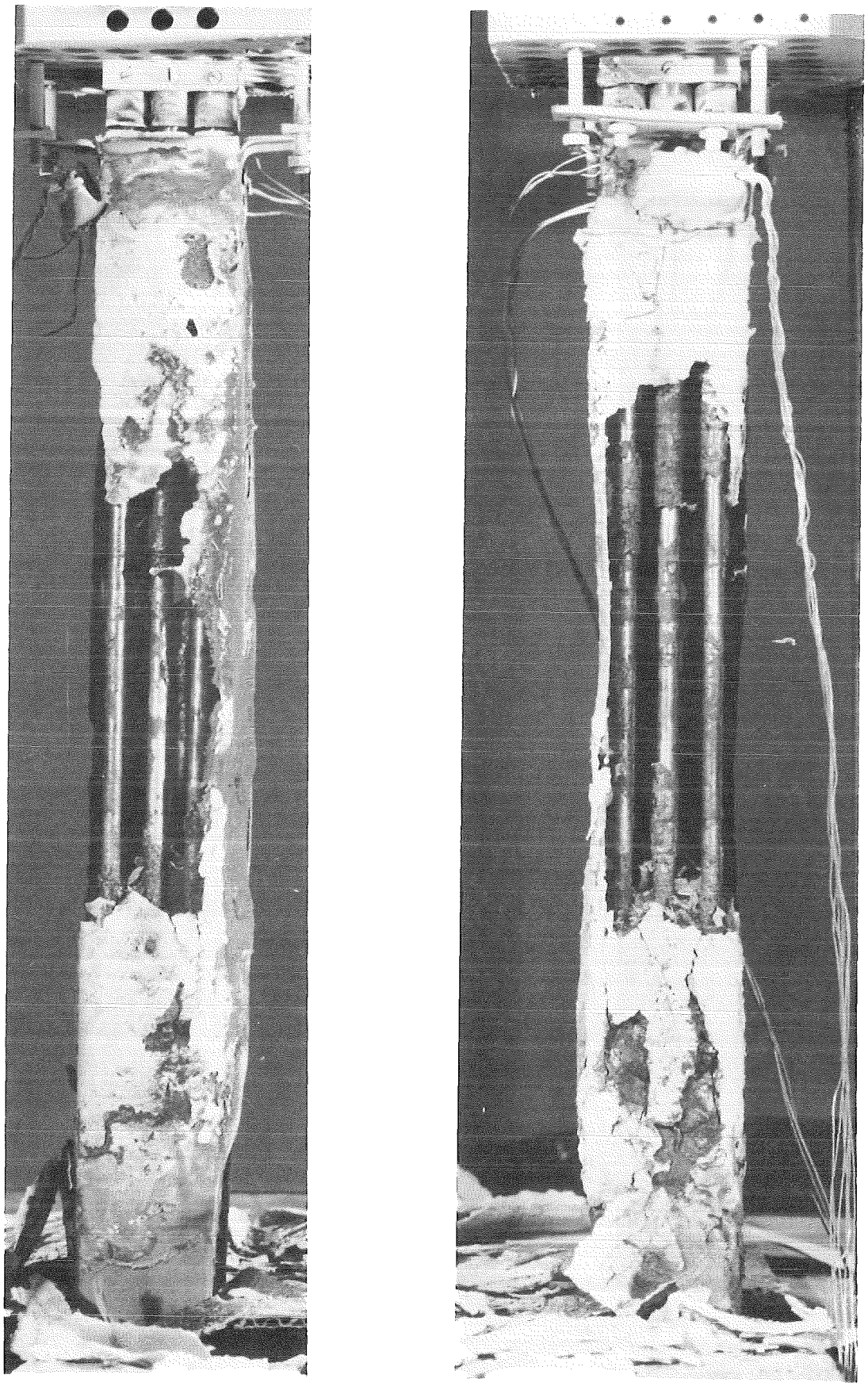

FIGURE 4: PARTIAL DISASSEMBLY OF THE HIGHLY EMBRITTLED ESBU-2A SHROUD

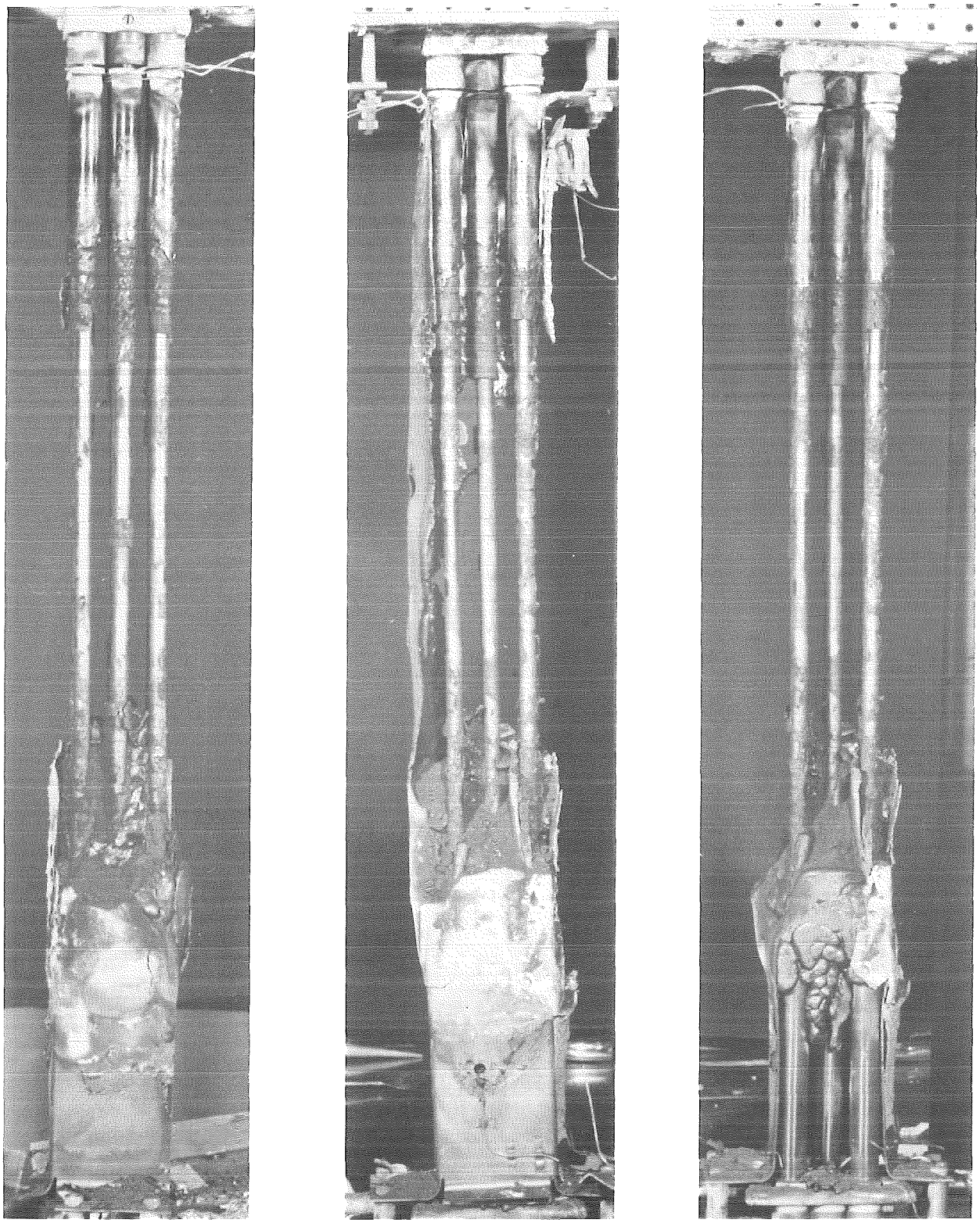

FIGURE 5: POSTTEST APPEARANCE OF THE ESBU-2A BUNDLE

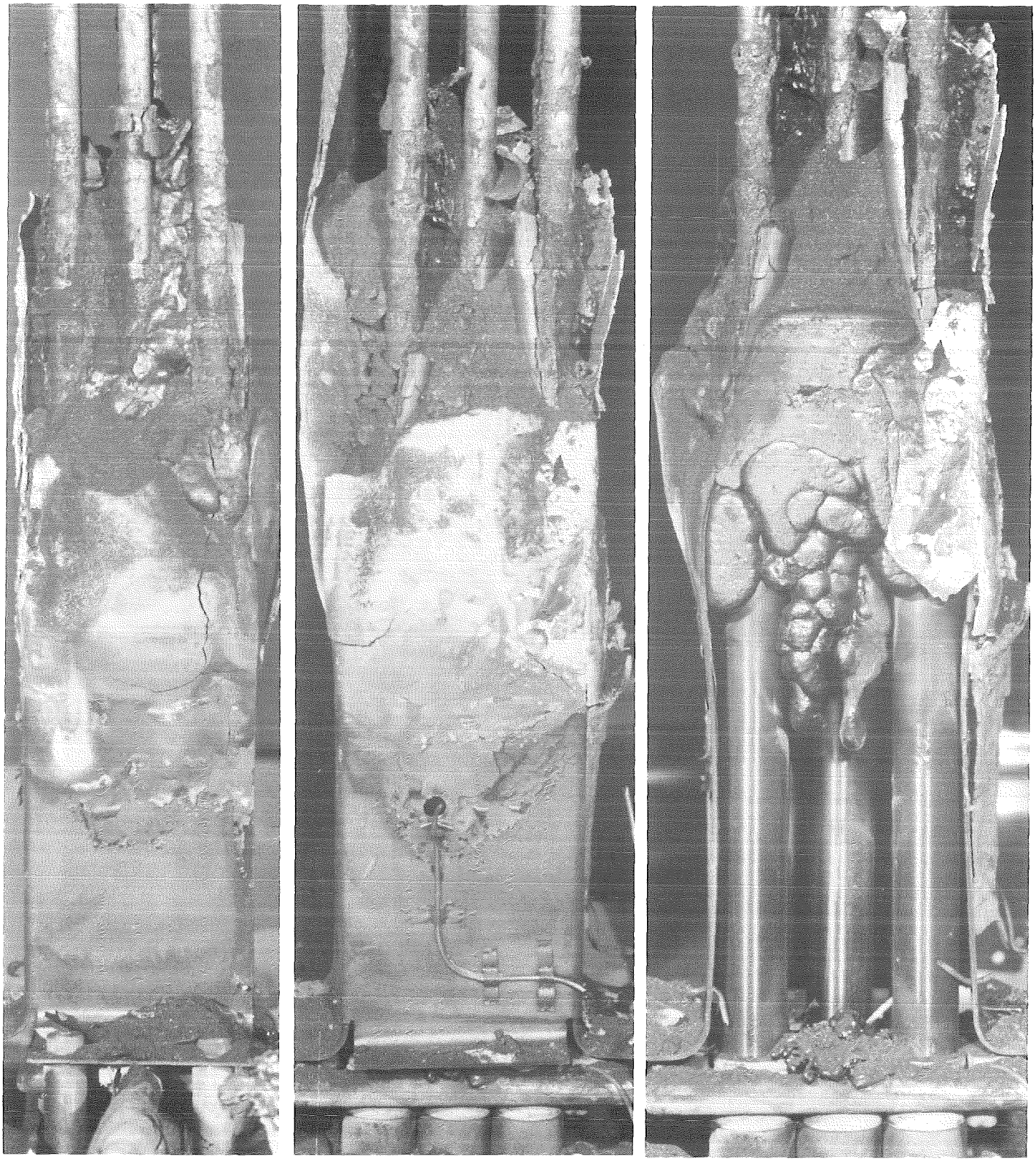

FIGURE 6: CLOSE-UP OF THE BLOCKED REGION OF ESBU-2A INCLUDING POWDERY RUBBLE

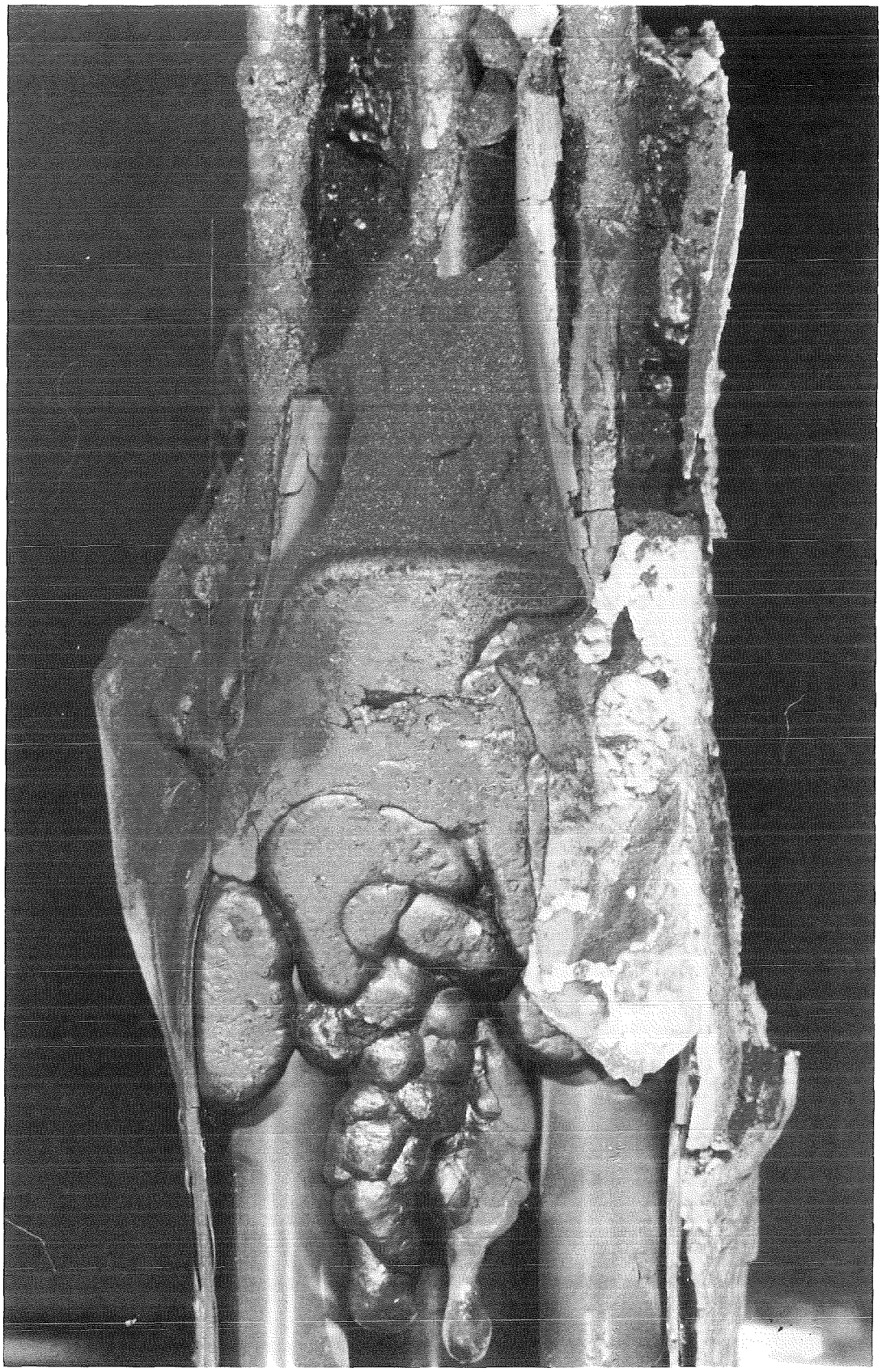

FIGURE 7: ENLARGEMENT OF THE REFROZEN MELT AND POWDERY RUBBLE FROM ESBU-2A

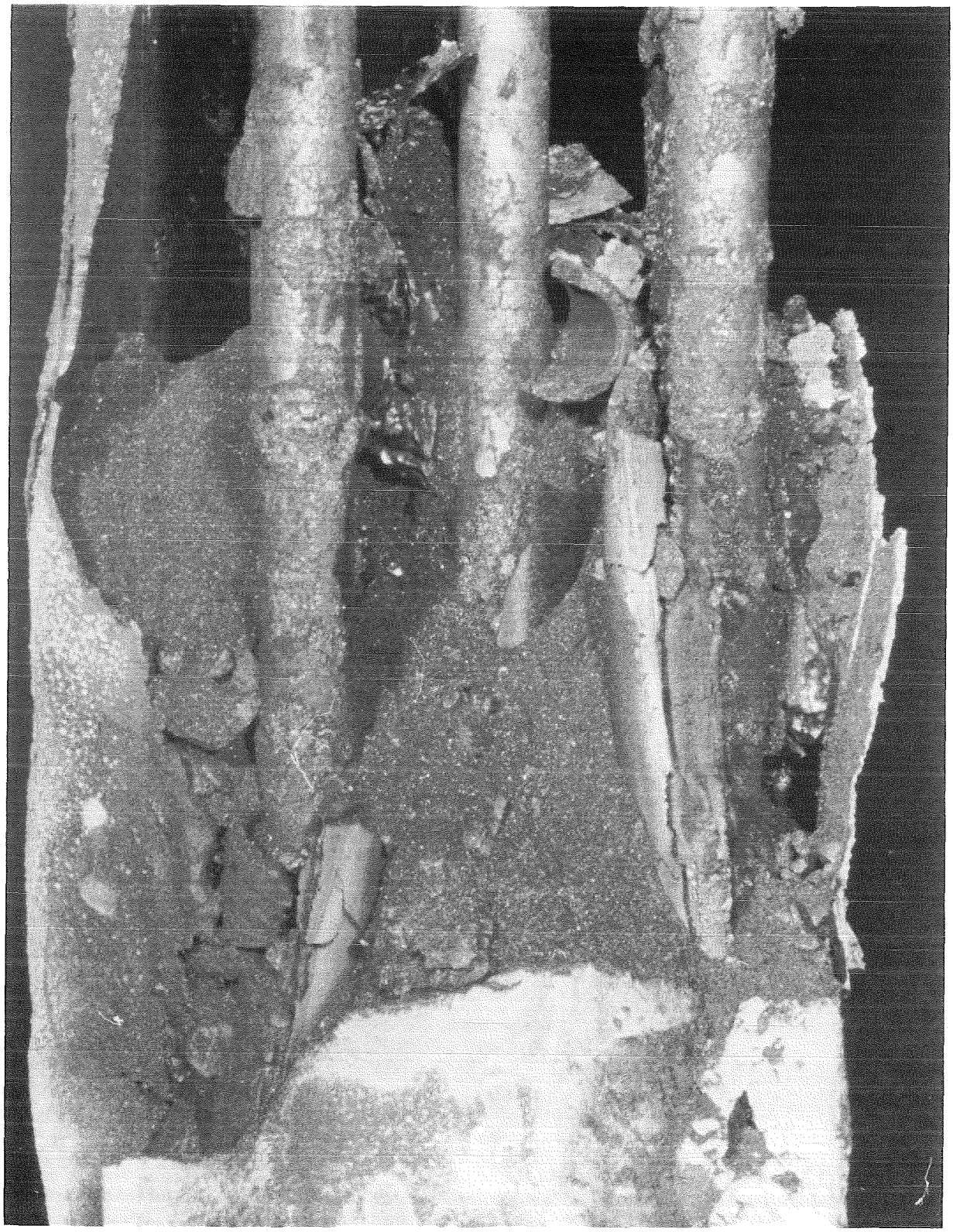

FIGURE 8: ENLARGEMENT OF THE RUBBLE FOUND ABOVE THE REFOZEN MELT IN ESBU-2A

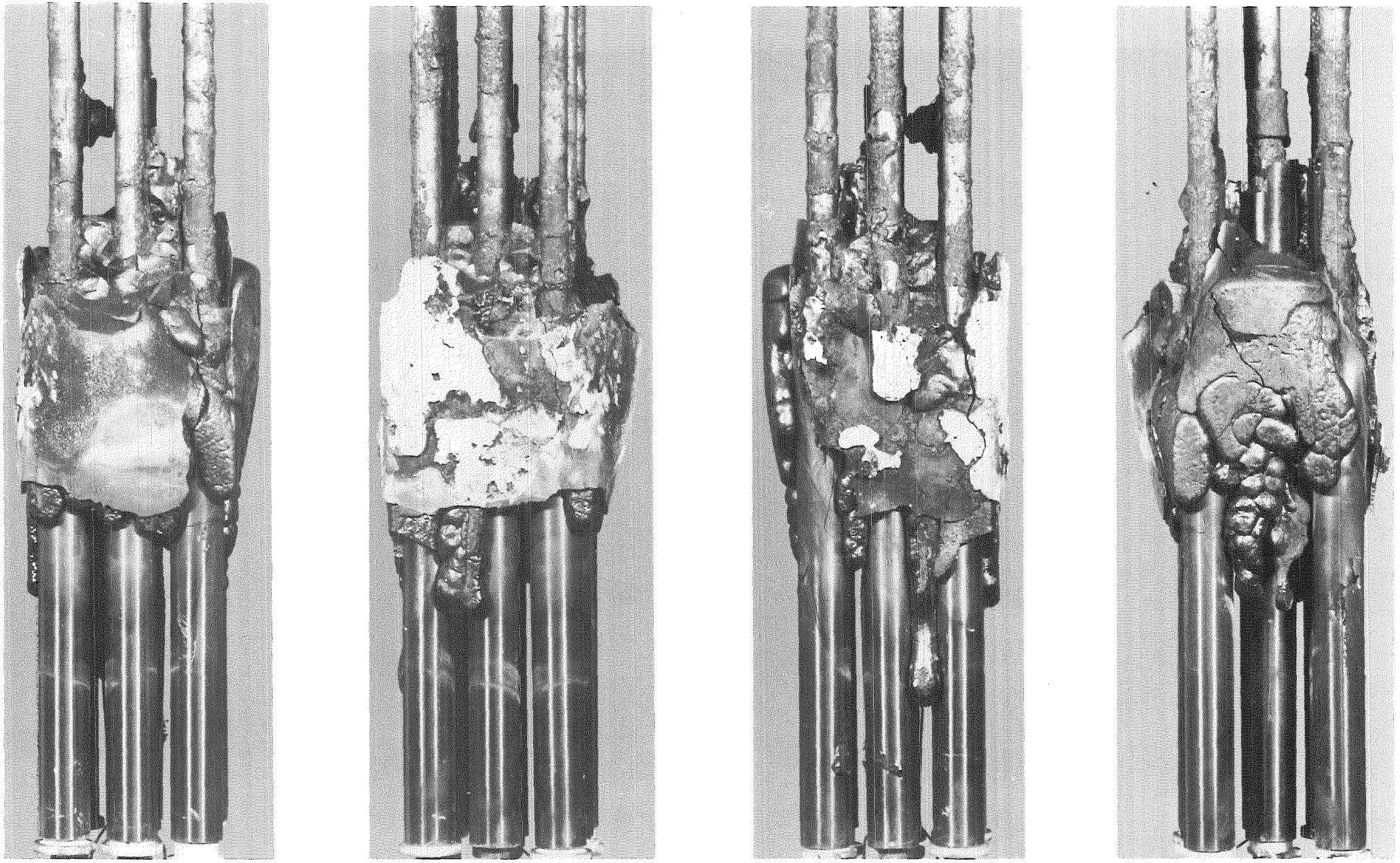

FIGURE 9: CLOSE-UP OF THE LOWER PORTION OF THE ESBU-2A BUNDLE

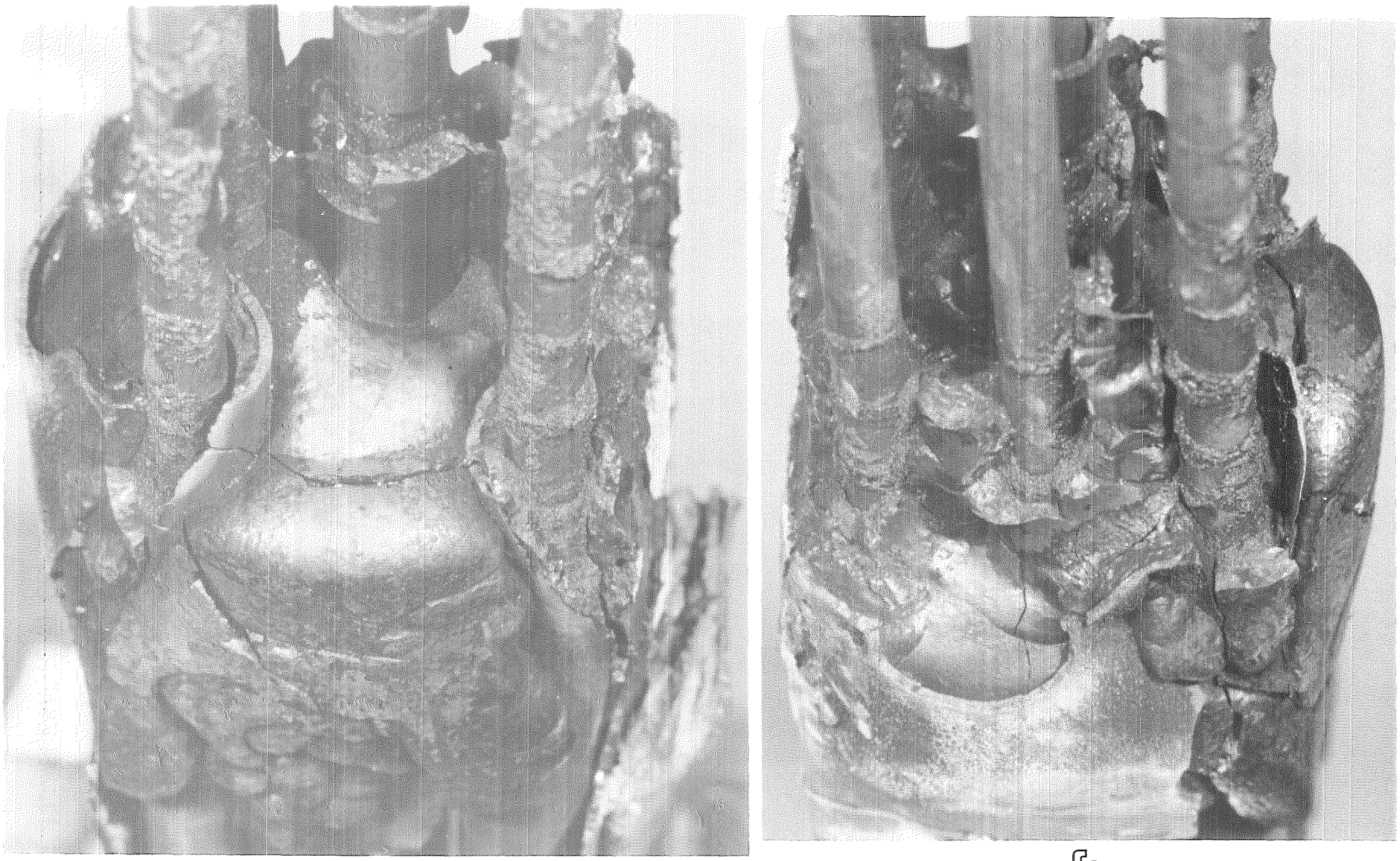

FIGURE 10: ENLARGED VIEW OF THE ESBU-2A BLOCKED REGION FROM ABOVE: TWO ORIENTATIONS

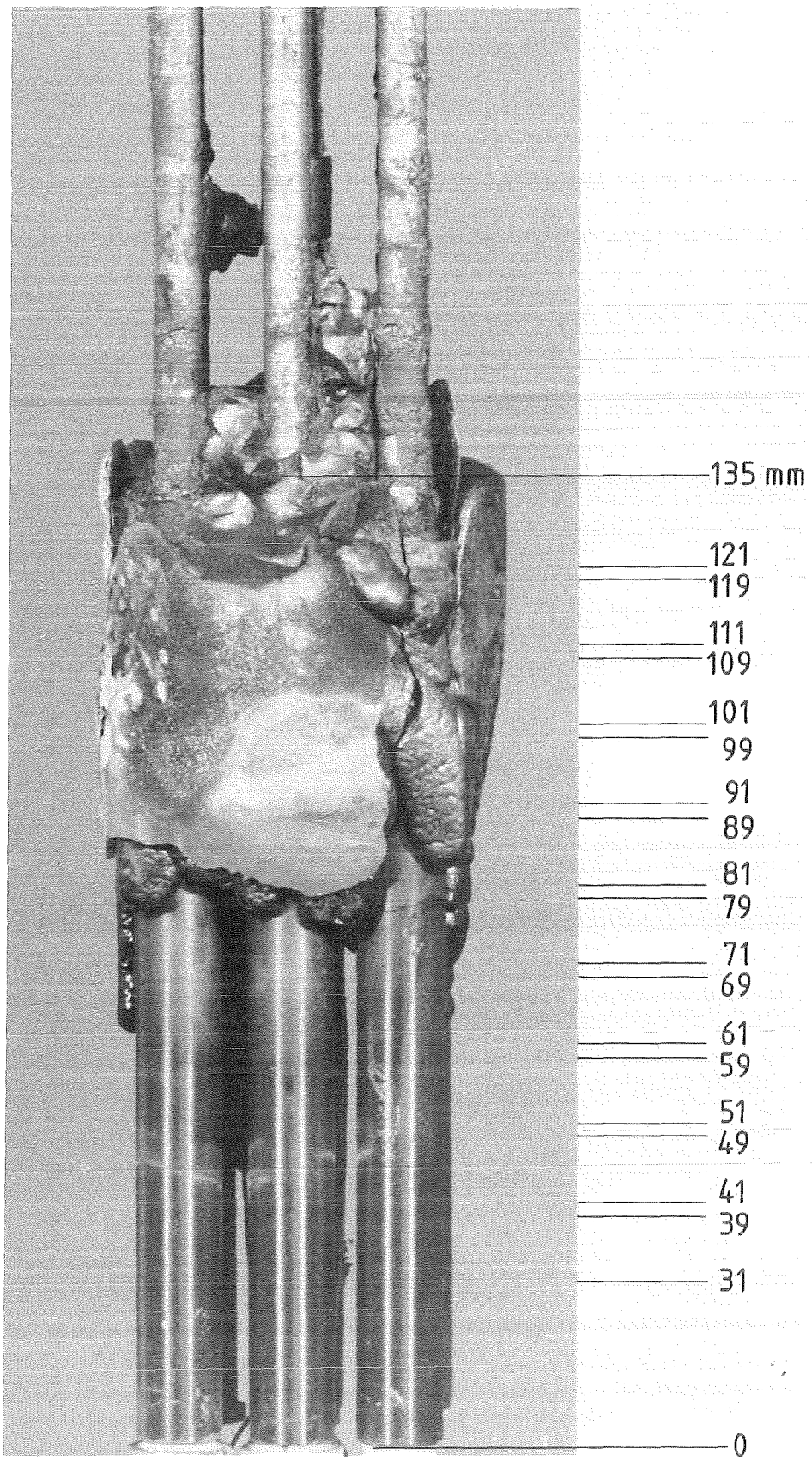

FIG.11: ELEVATIONS OF CROSS SECTIONS FOR TEST ESBU-2A.

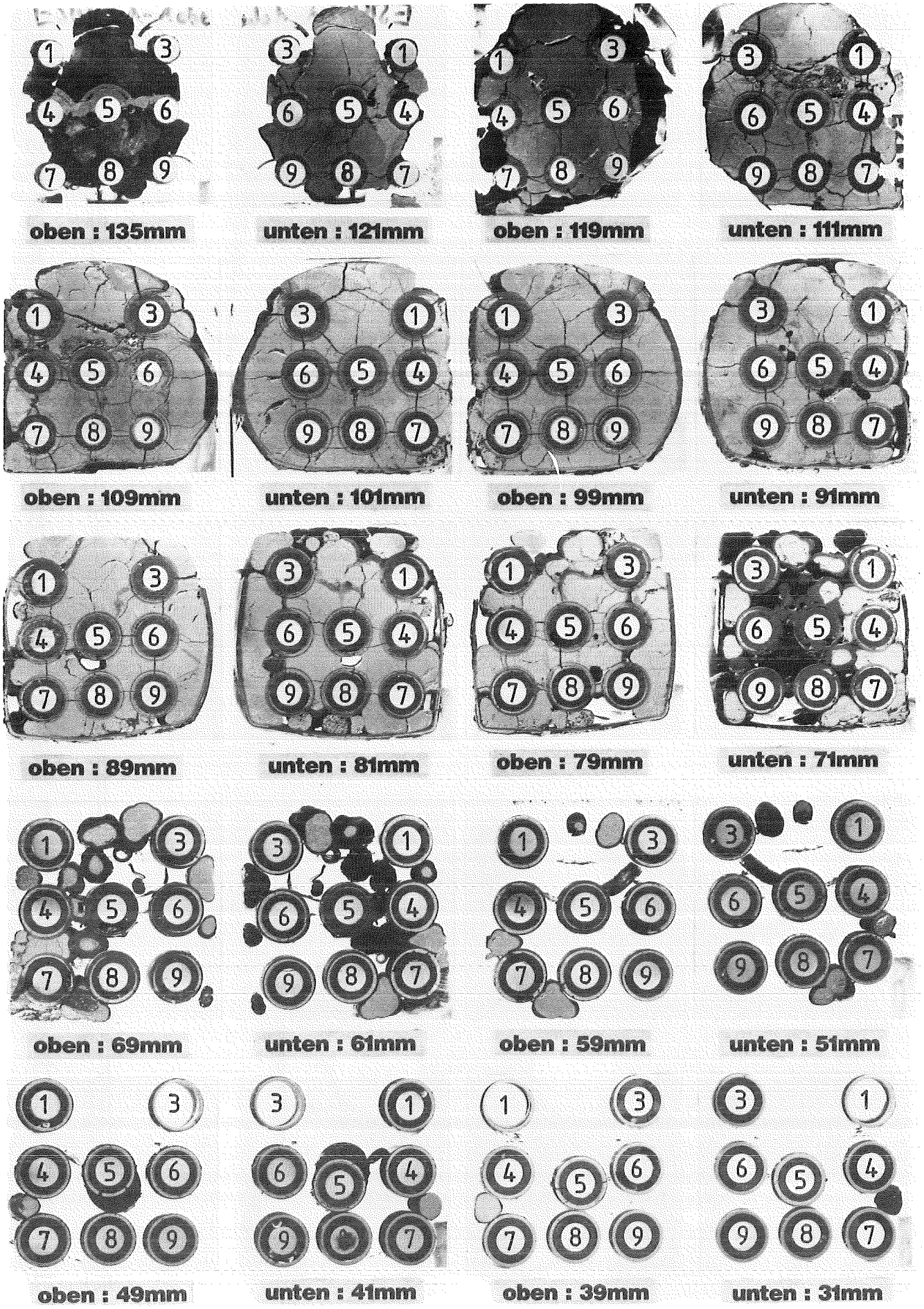

FIG.12: BUNDLE CROSS SECTION SUMMARY ESBU-2A.

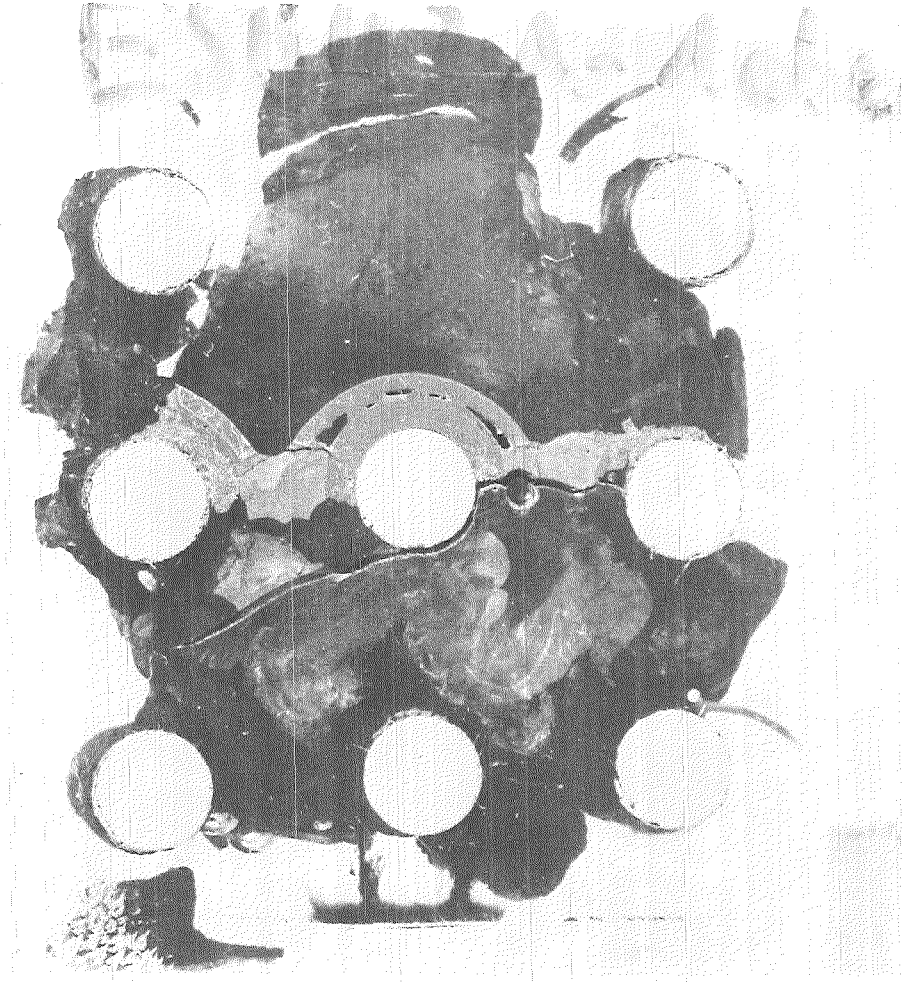

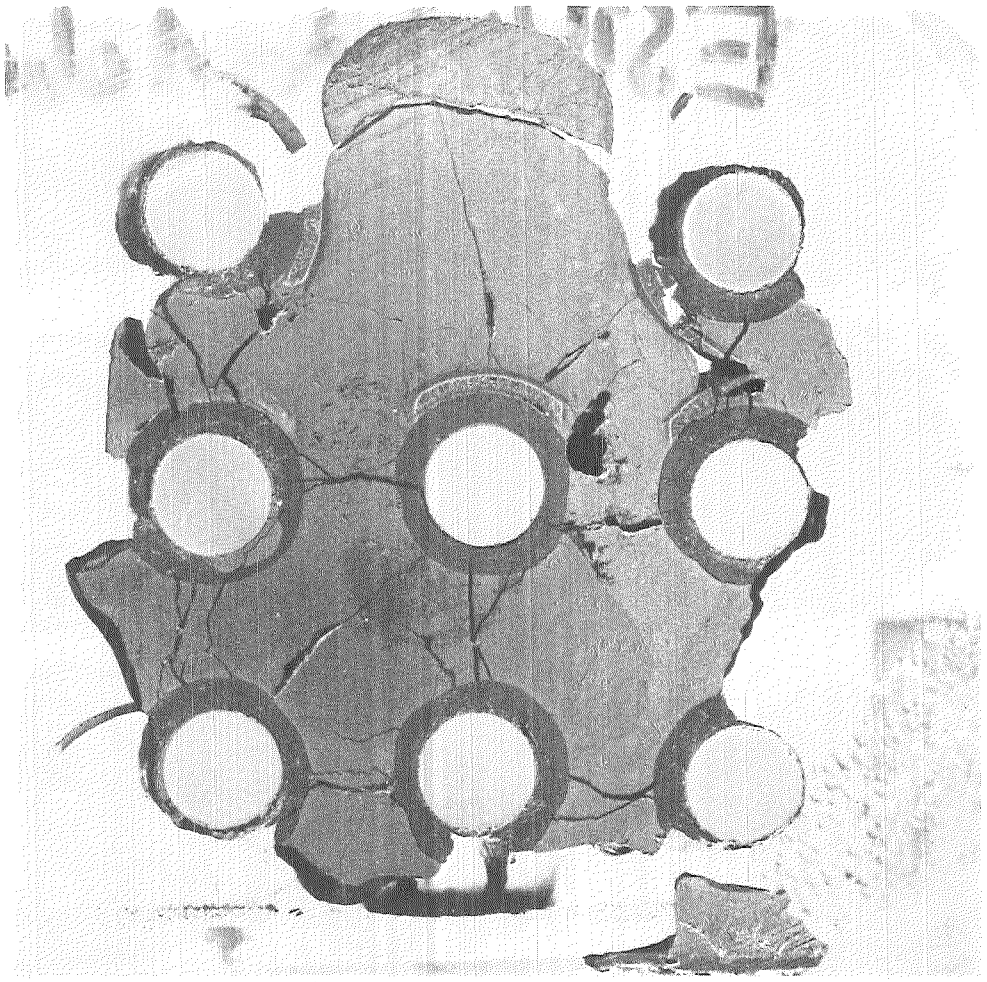

FIG.13: CROSS SECTIONS OF ESBU-2A AT THE GIVEN ELEVATION ABOVE THE BOTTOM OF THE BUNDLE

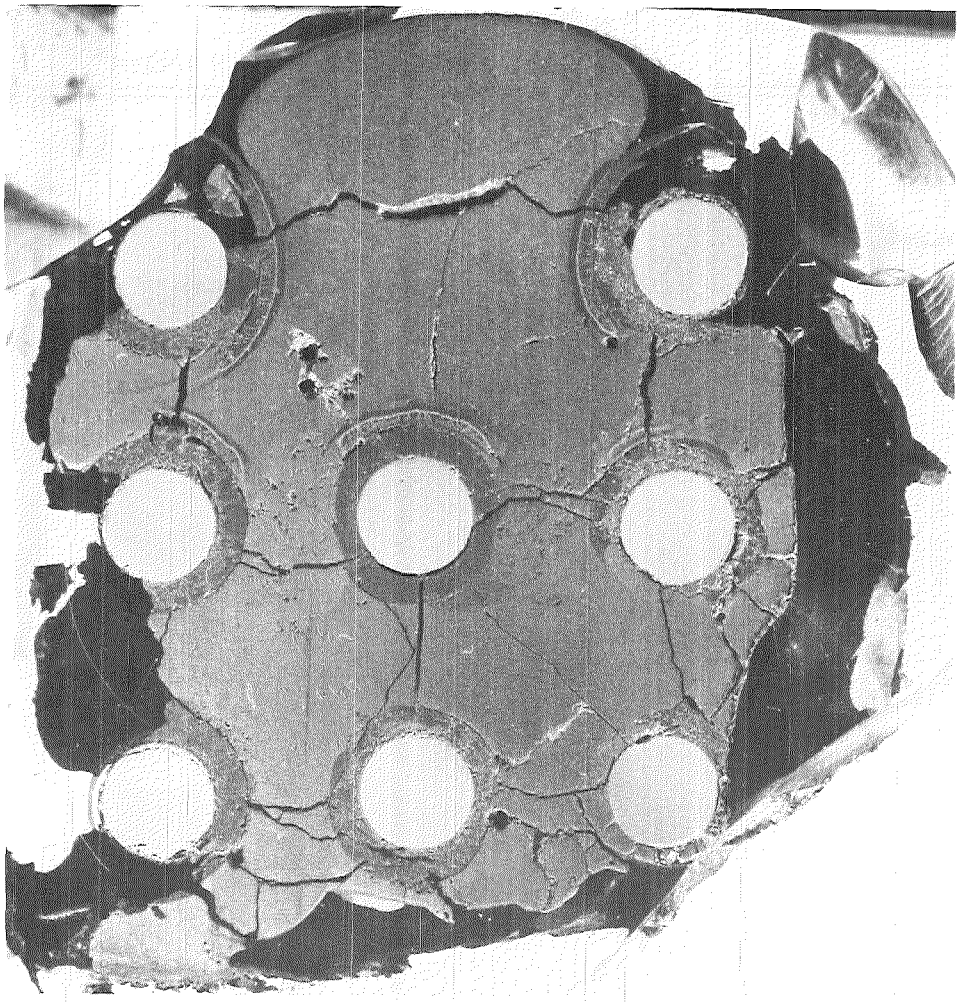

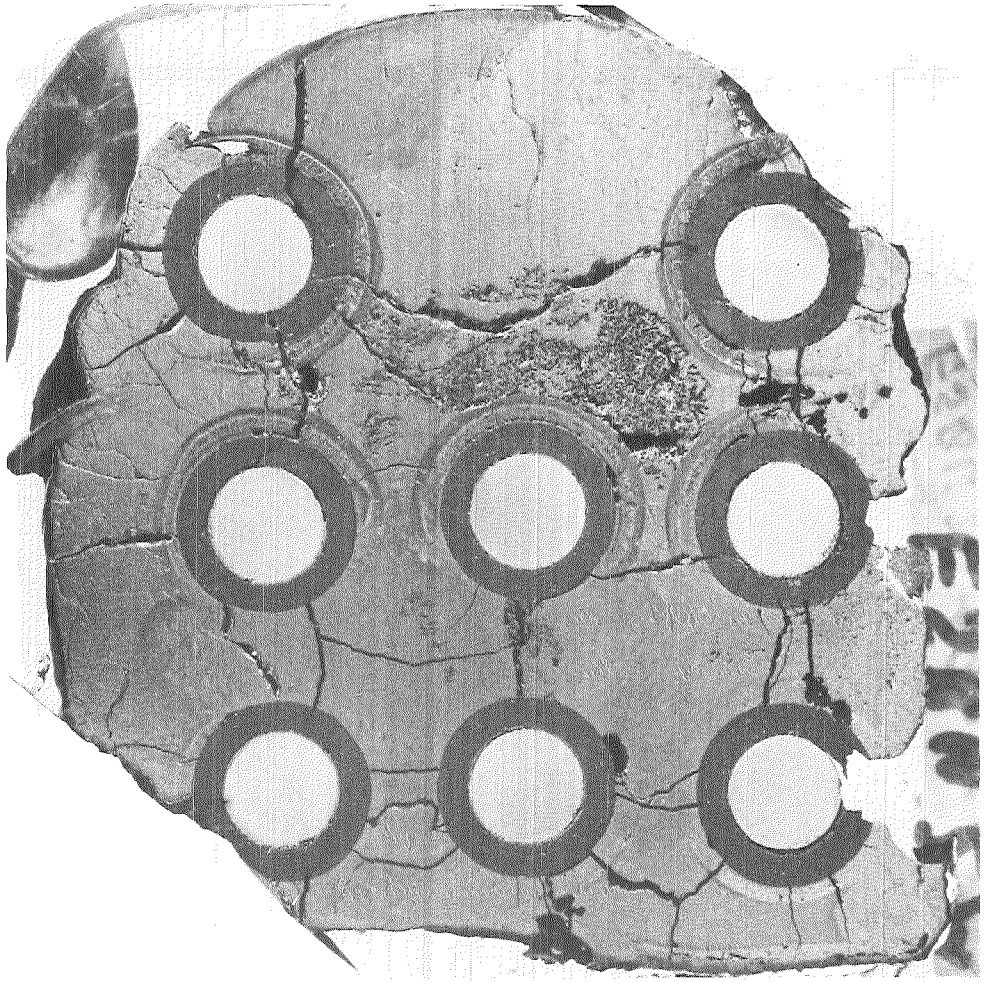

FIG.14: CROSS SECTIONS OF ESBU-2A AT THE GIVEN ELEVATION ABOVE THE BOTTOM OF THE BUNDLE

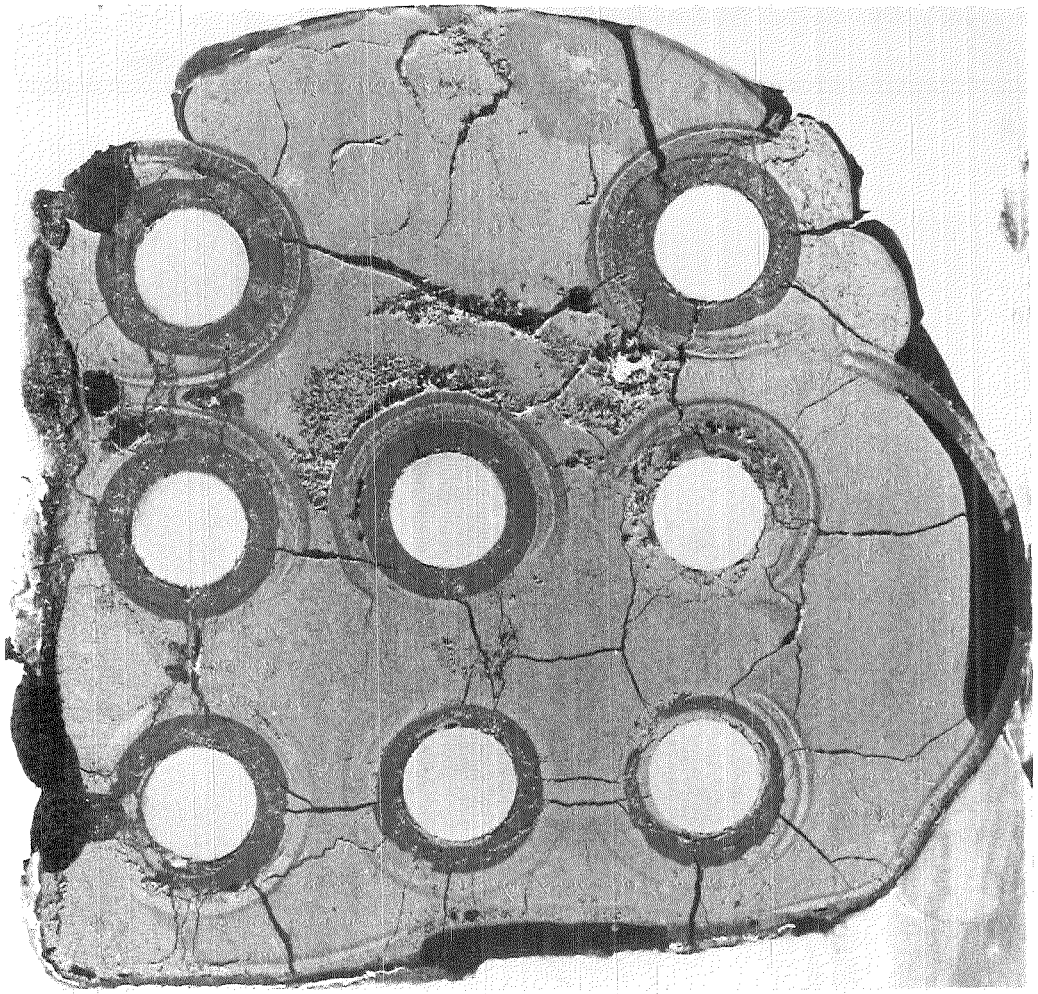

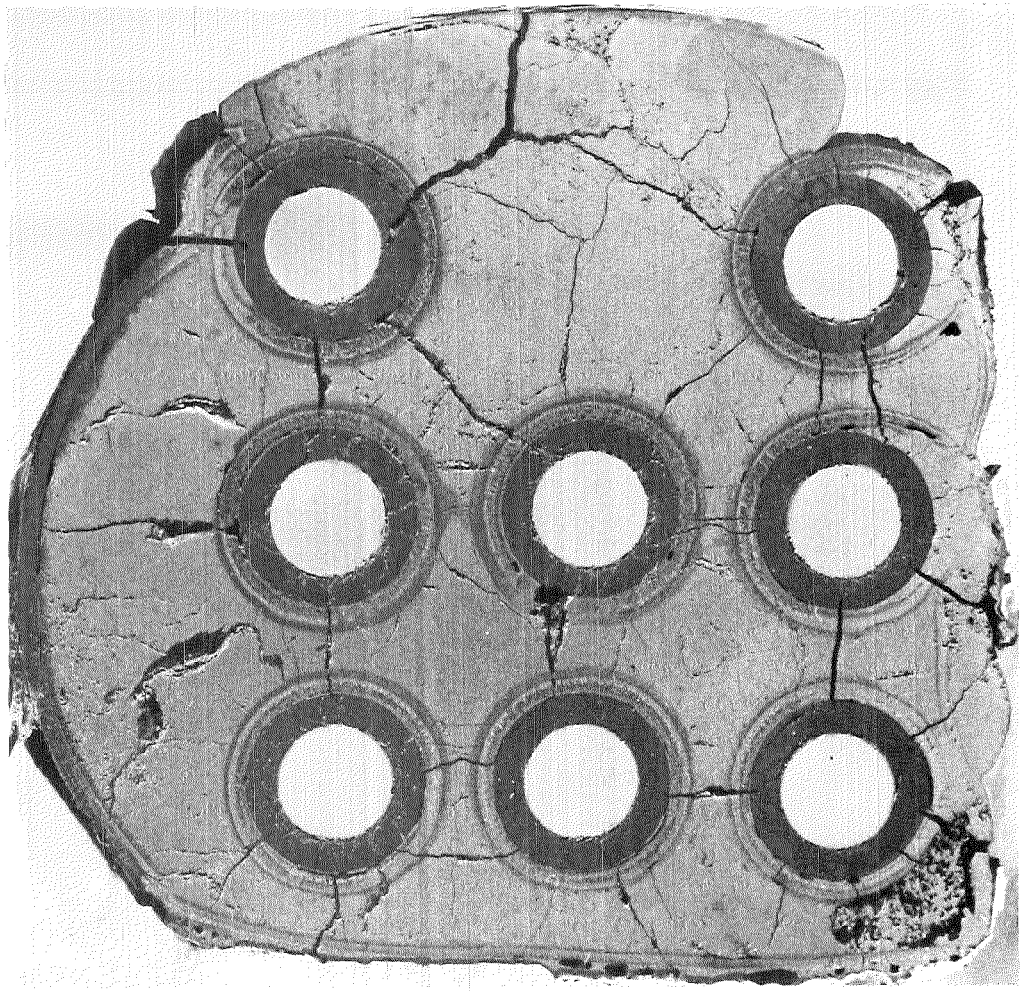

FIG.15: CROSS SECTIONS OF ESBU-2A AT THE GIVEN ELEVATION ABOVE THE BOTTOM OF THE BUNDLE

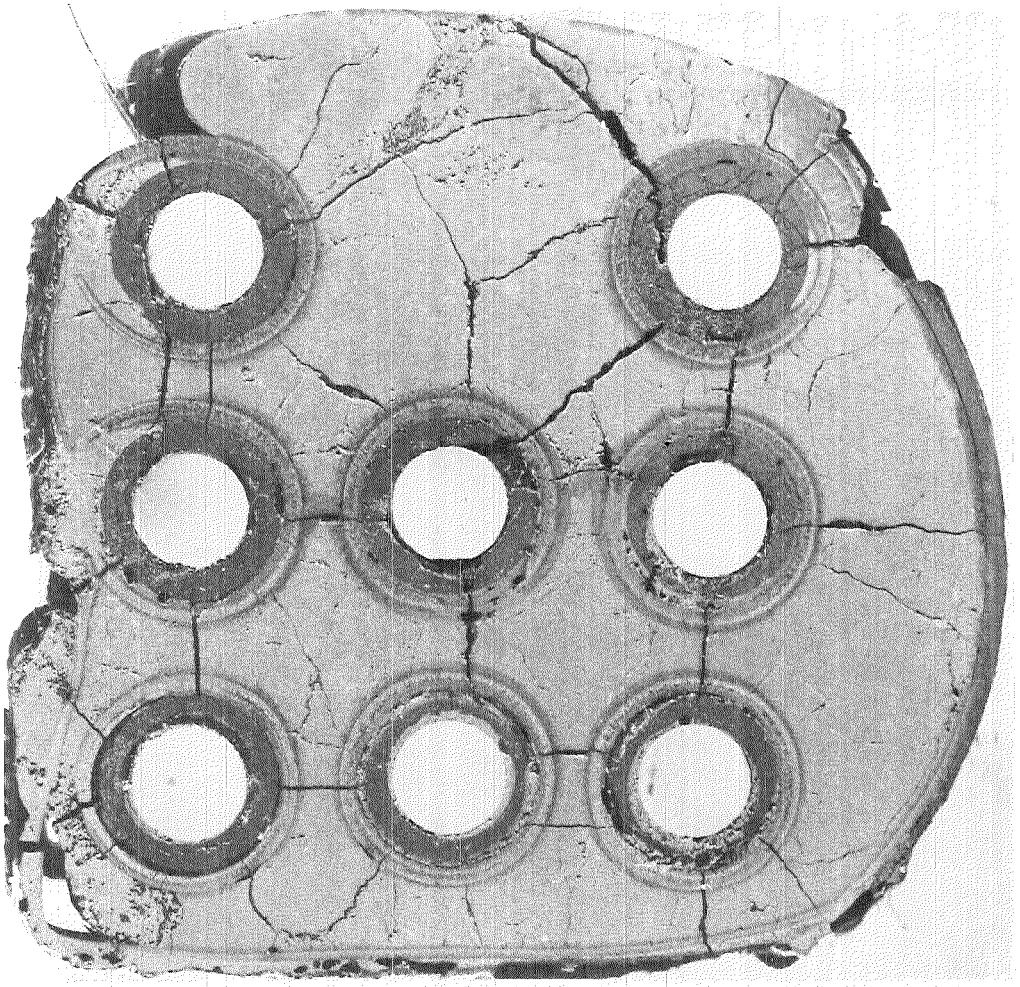

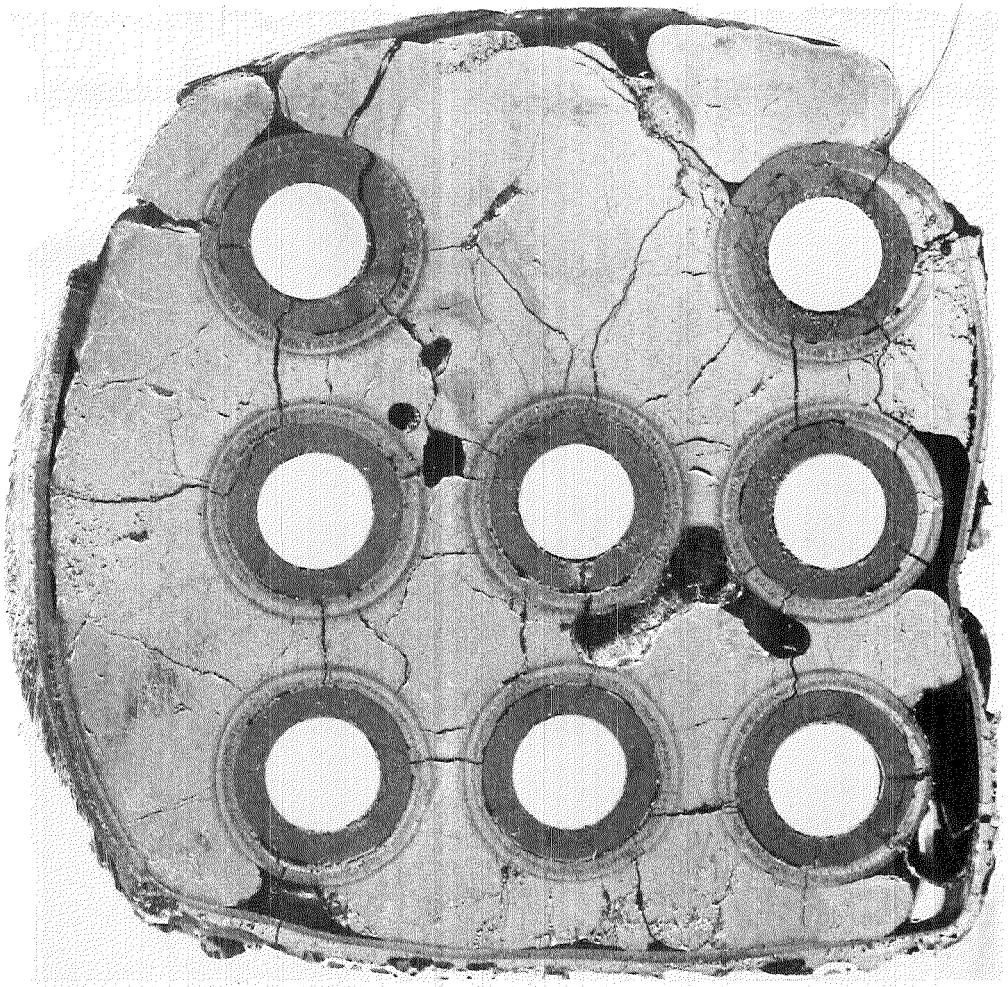

FIG. 16: CROSS SECTIONS OF ESBU-2A AT THE GIVEN ELEVATION ABOVE THE BOTTOM OF THE BUNDLE

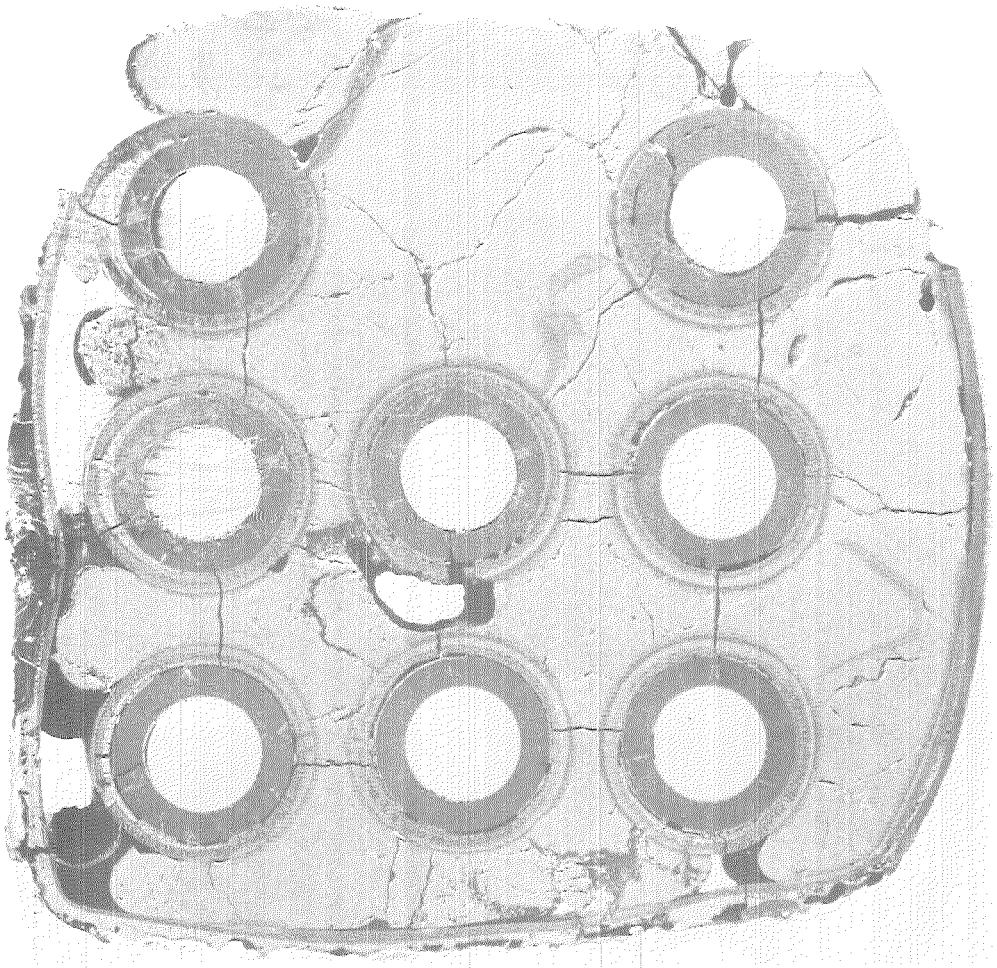

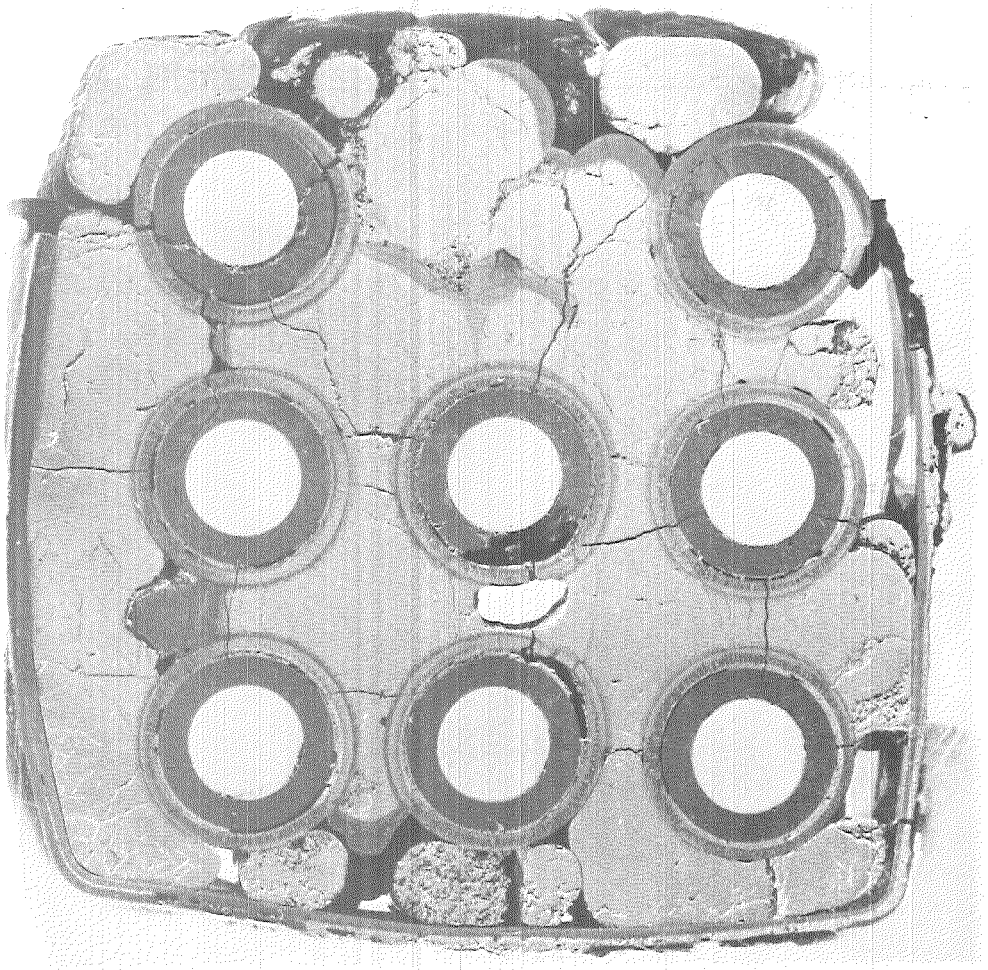

FIG.17: CROSS SECTIONS OF ESBU-2A AT THE GIVEN ELEVATION ABOVE THE BOTTOM OF THE BUNDLE

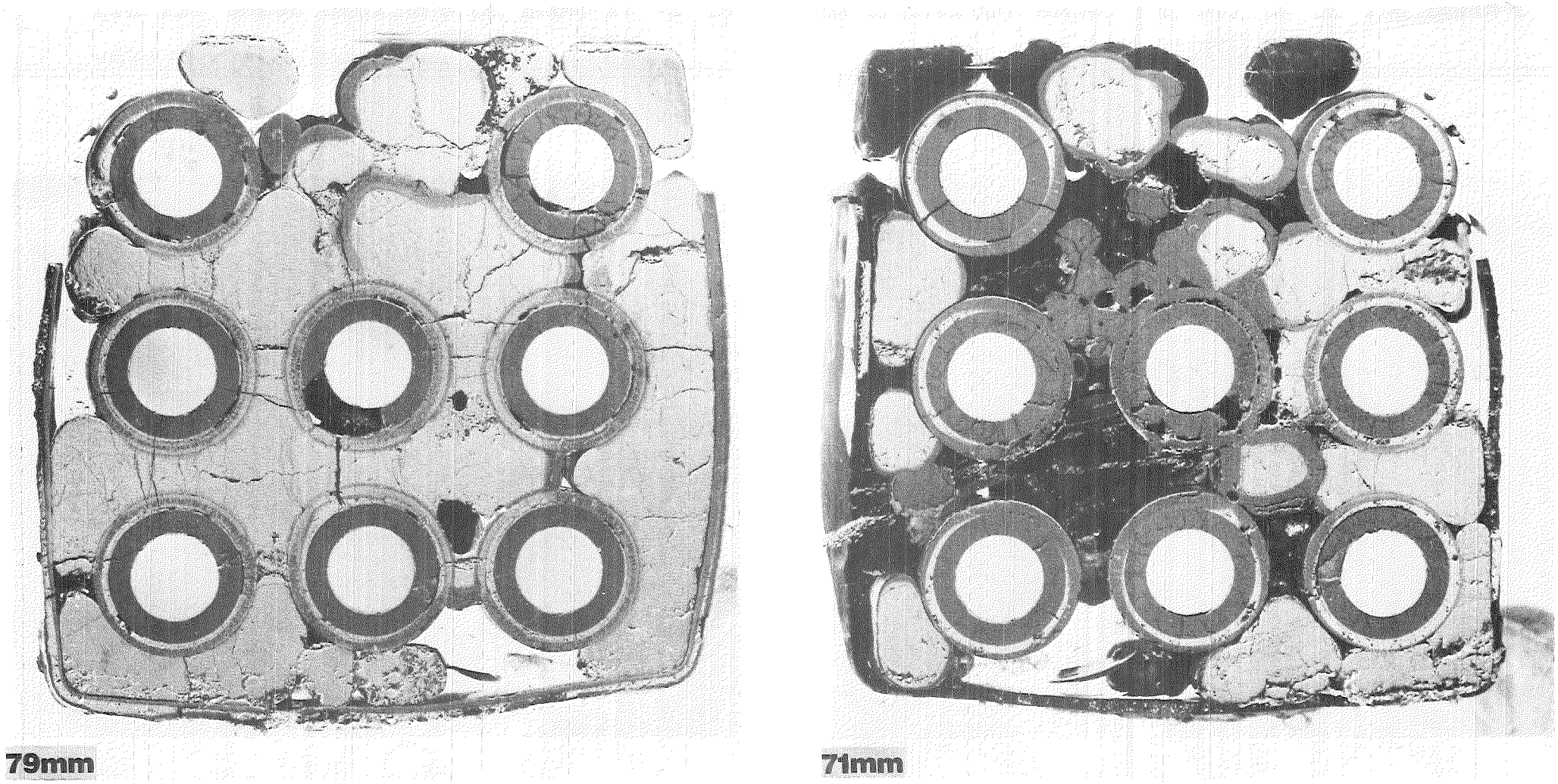

FIG.18: CROSS SECTIONS OF ESBU-2A AT THE GIVEN ELEVATION ABOVE THE BOTTOM OF THE BUNDLE

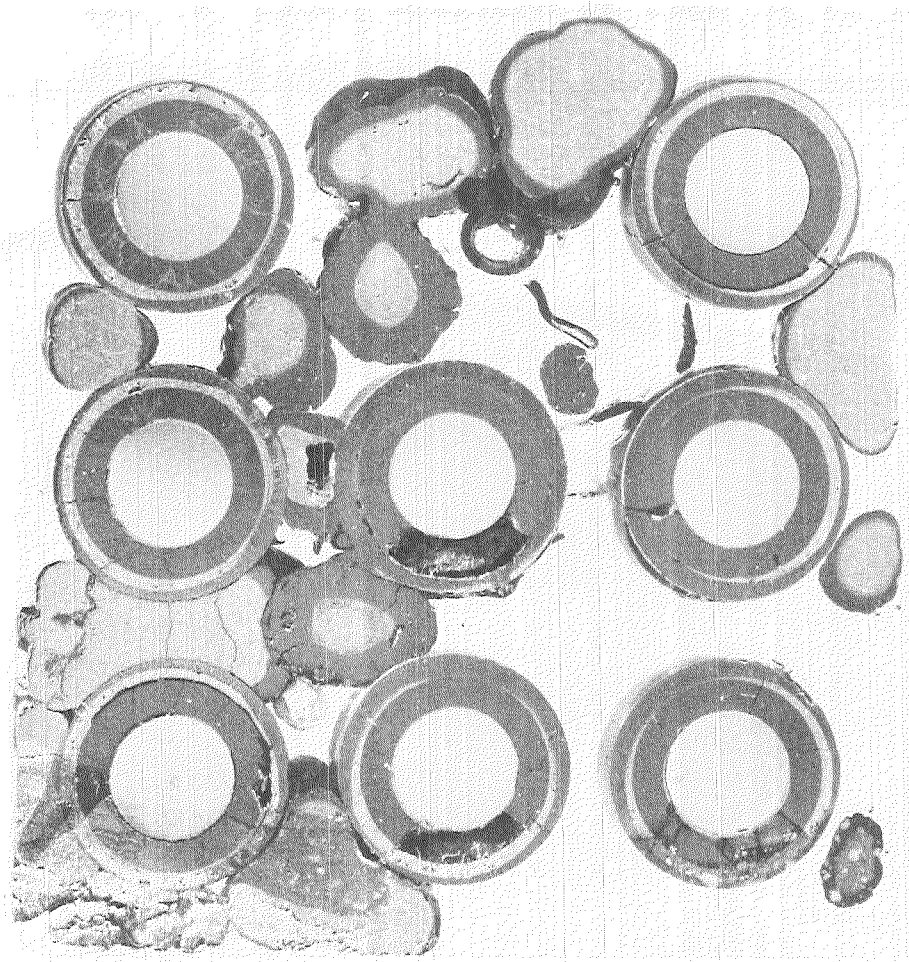

69mm

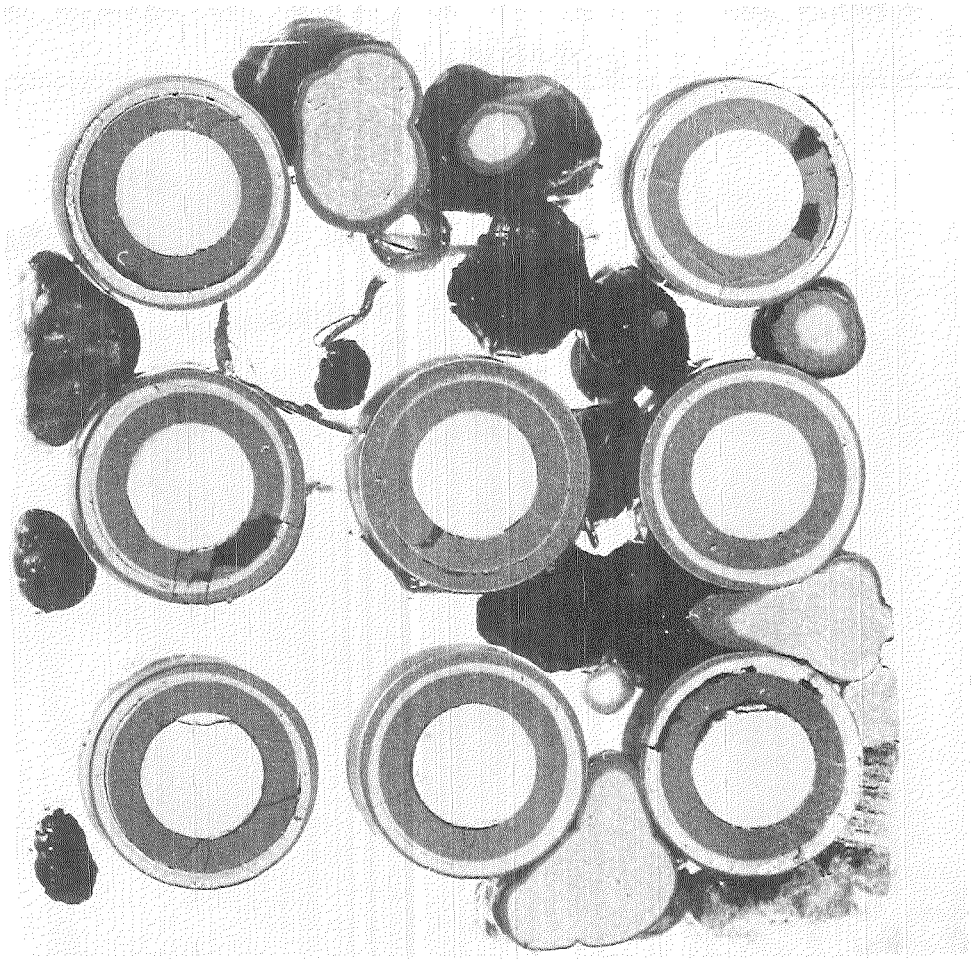

61mm

FIG.19: CROSS SECTIONS OF ESBU-2A AT THE GIVEN ELEVATION ABOVE THE BOTTOM OF THE BUNDLE

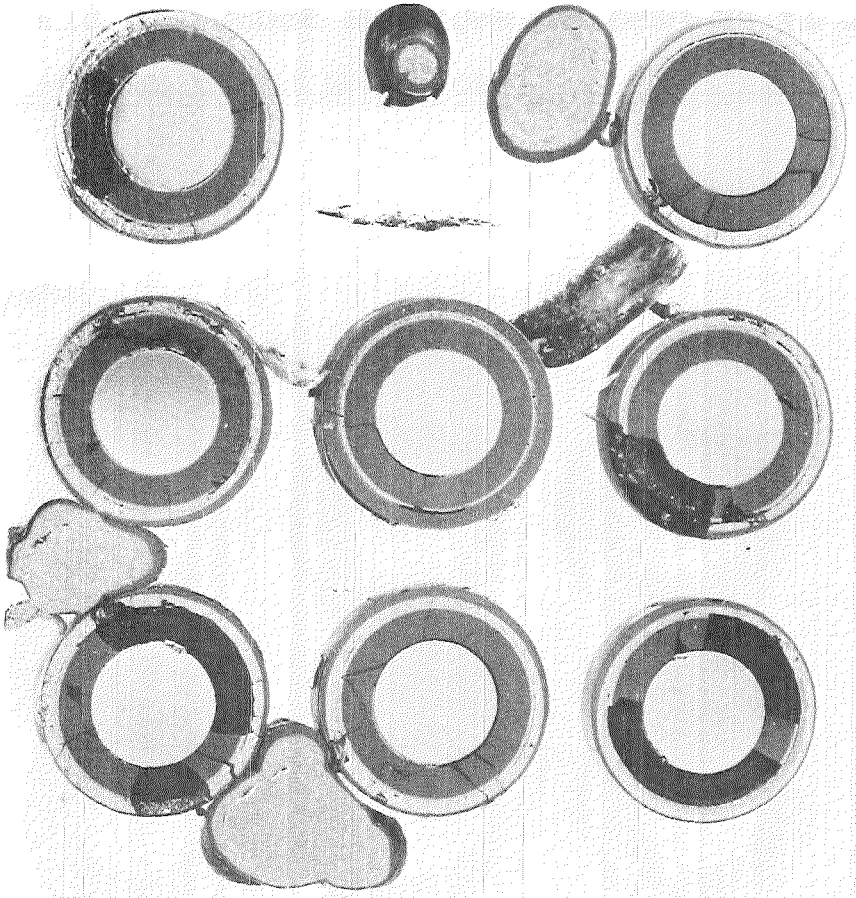

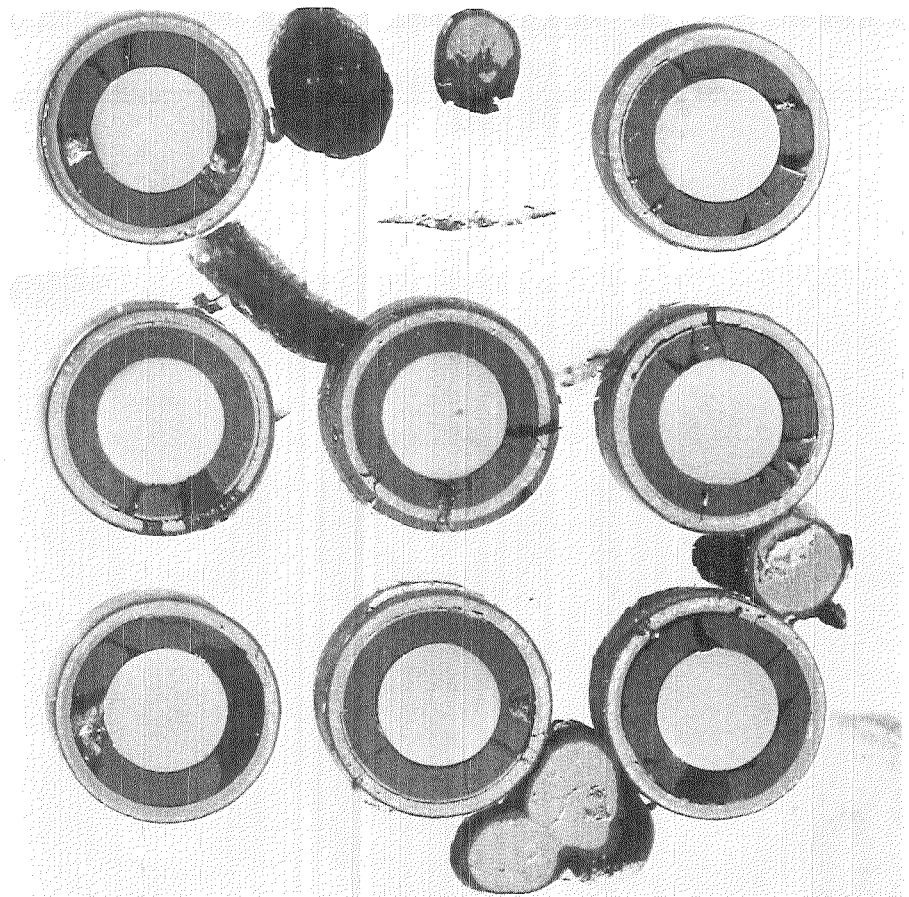

FIG.20: CROSS SECTIONS OF ESBU-2A AT THE GIVEN ELEVATION ABOVE THE BOTTOM OF THE BUNDLE

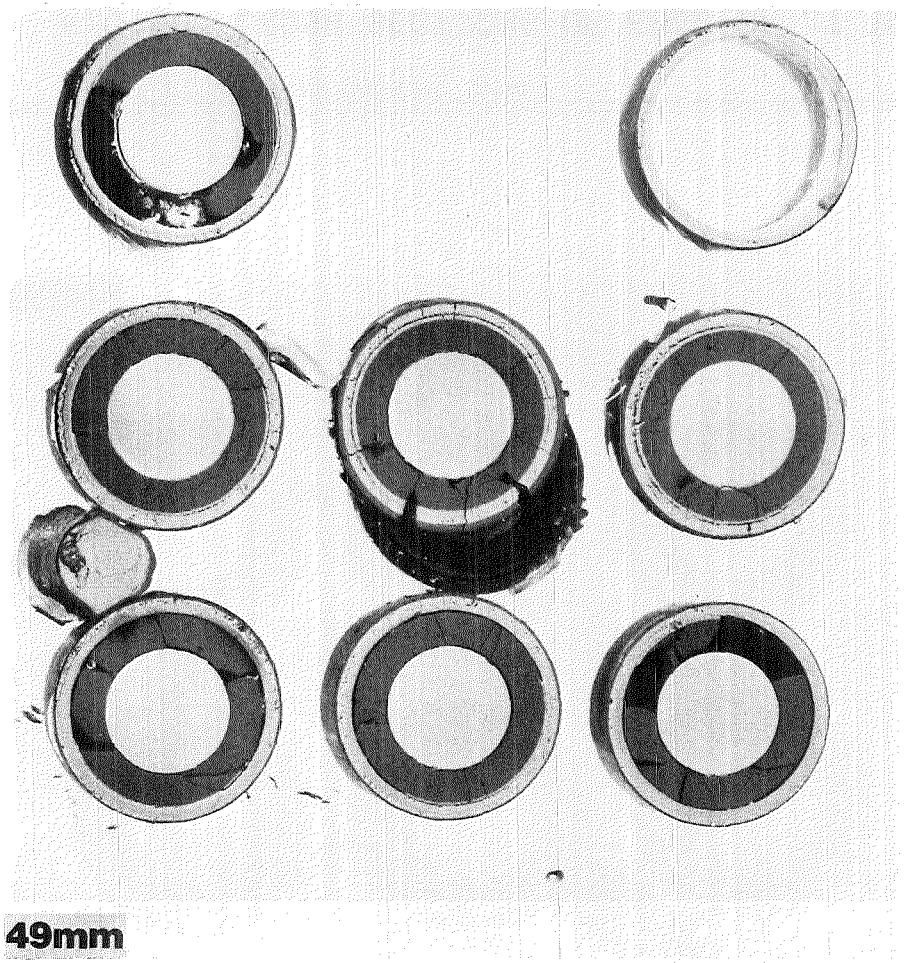

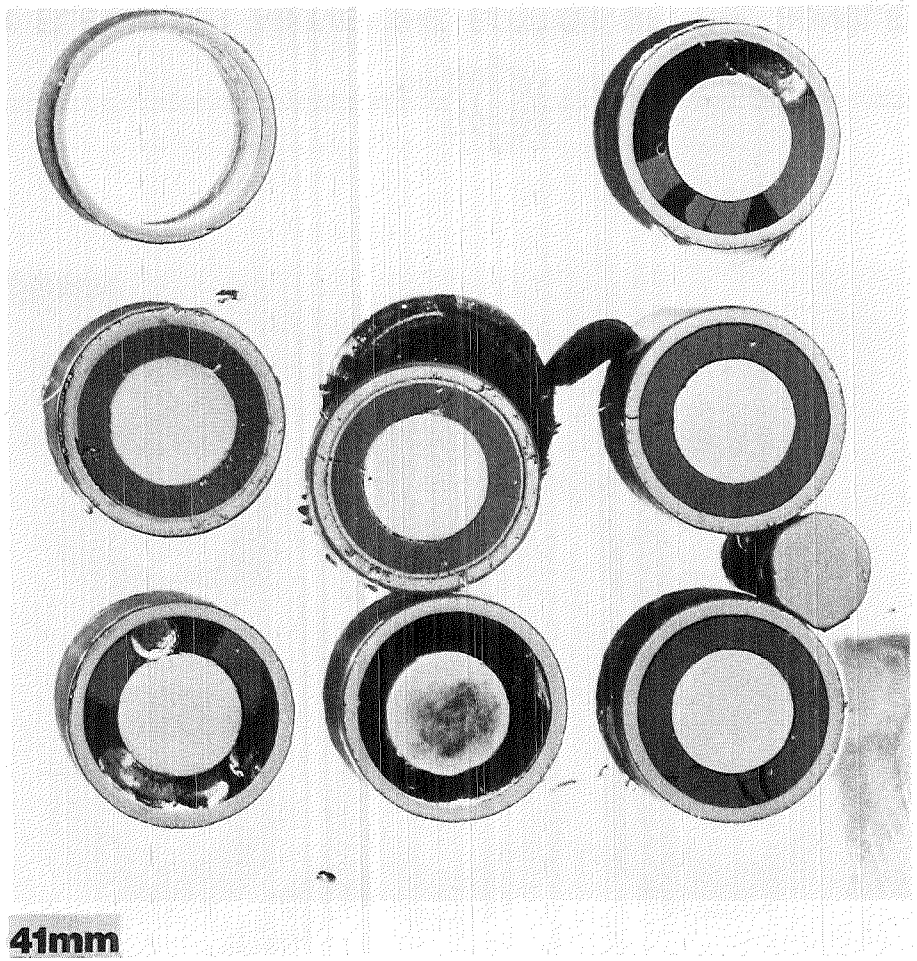

FIG.21: CROSS SECTIONS OF ESBU-2A AT THE GIVEN ELEVATION ABOVE THE BOTTOM OF THE BUNDLE

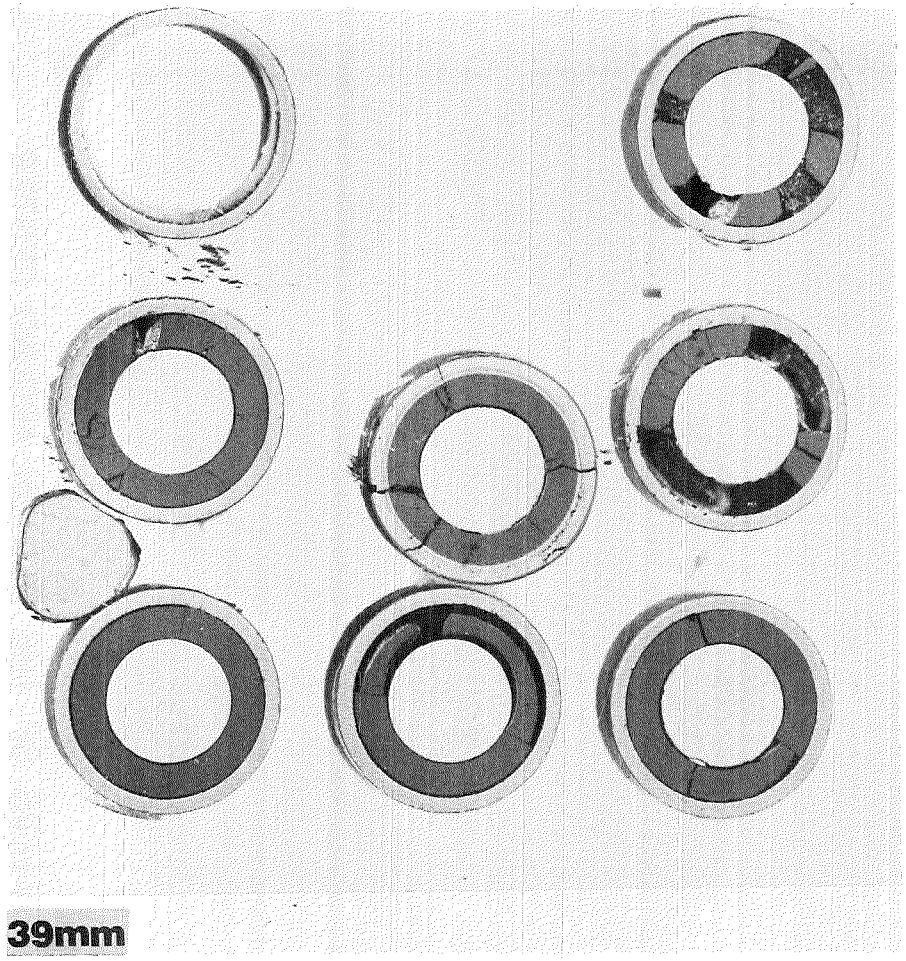

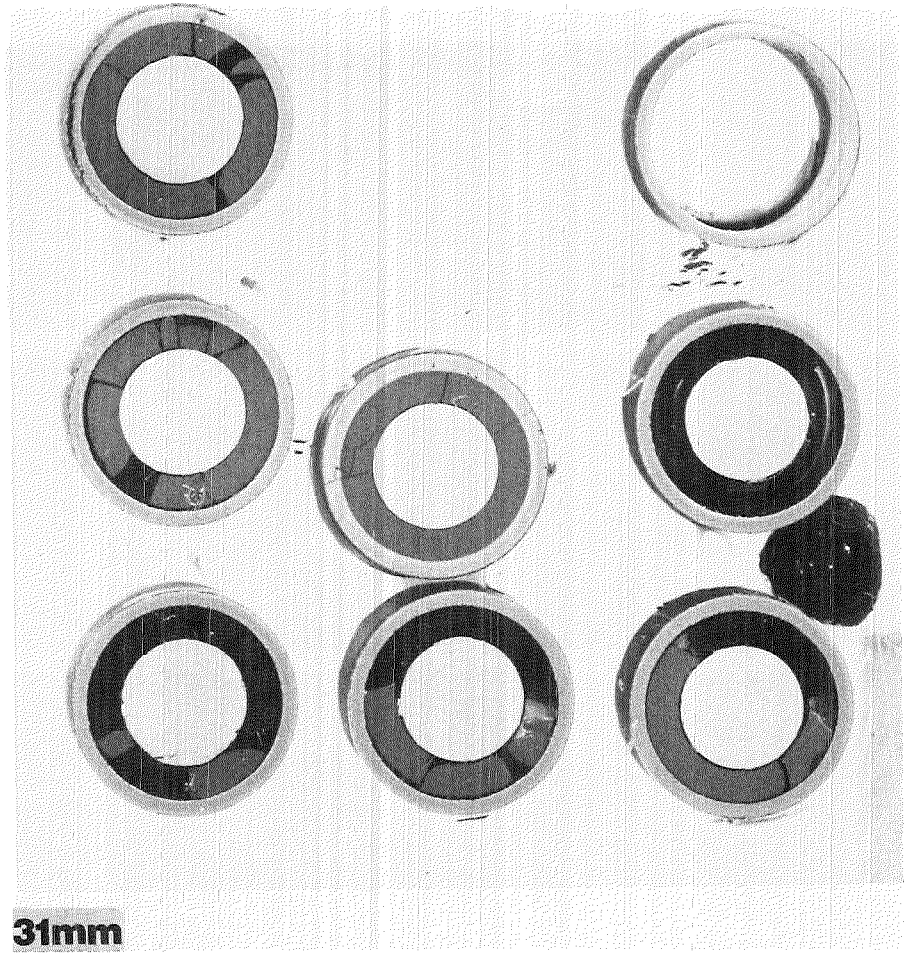

FIG.22: CROSS SECTIONS OF ESBU-2A AT THE GIVEN ELEVATION ABOVE THE BOTTOM OF THE BUNDLE

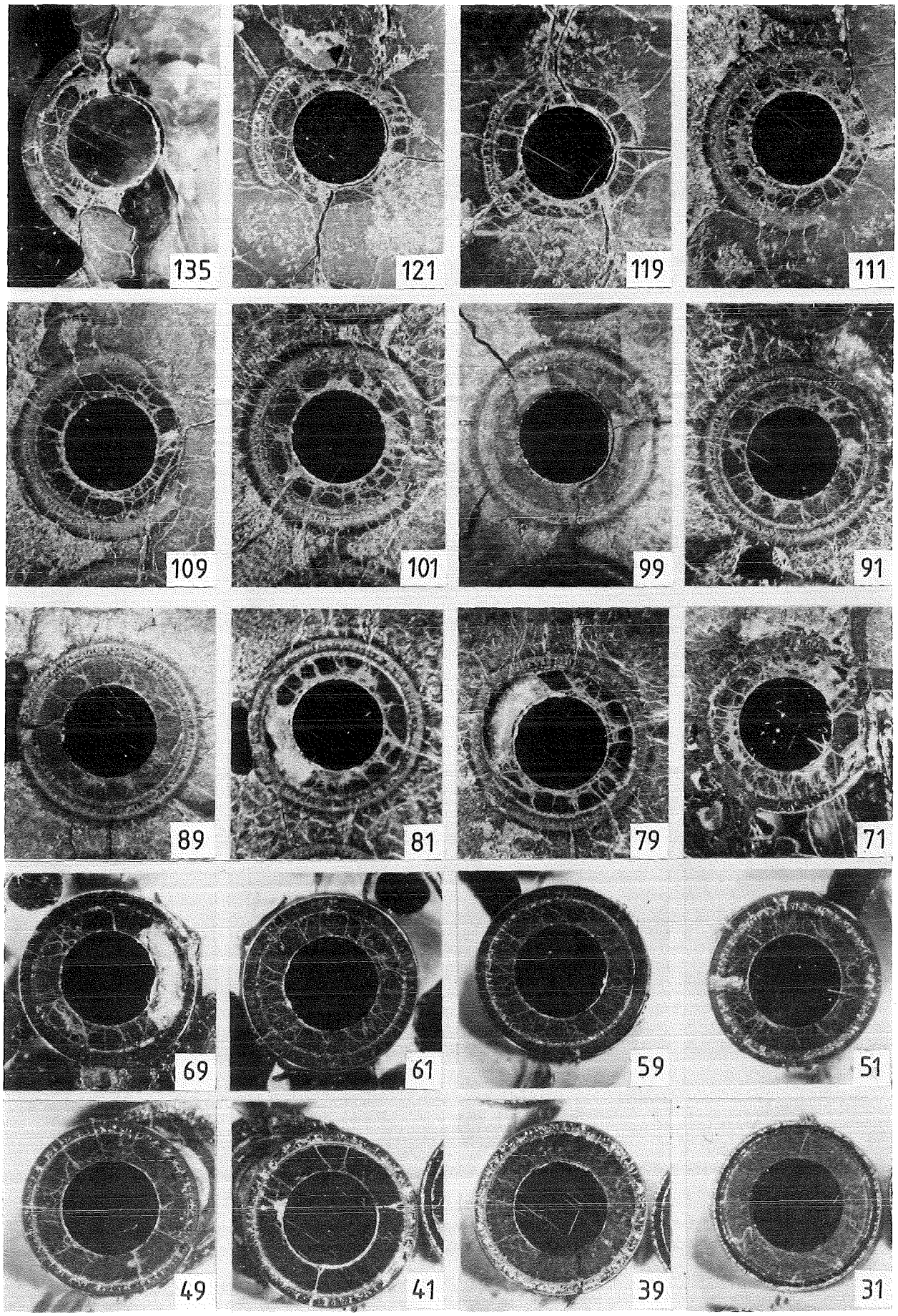

FIG.23: ENLARGED VIEWS OF THE REGION AROUND CENTER ROD 5 FOR DIFFERENT CROSS SECTIONS ESBU-2A.

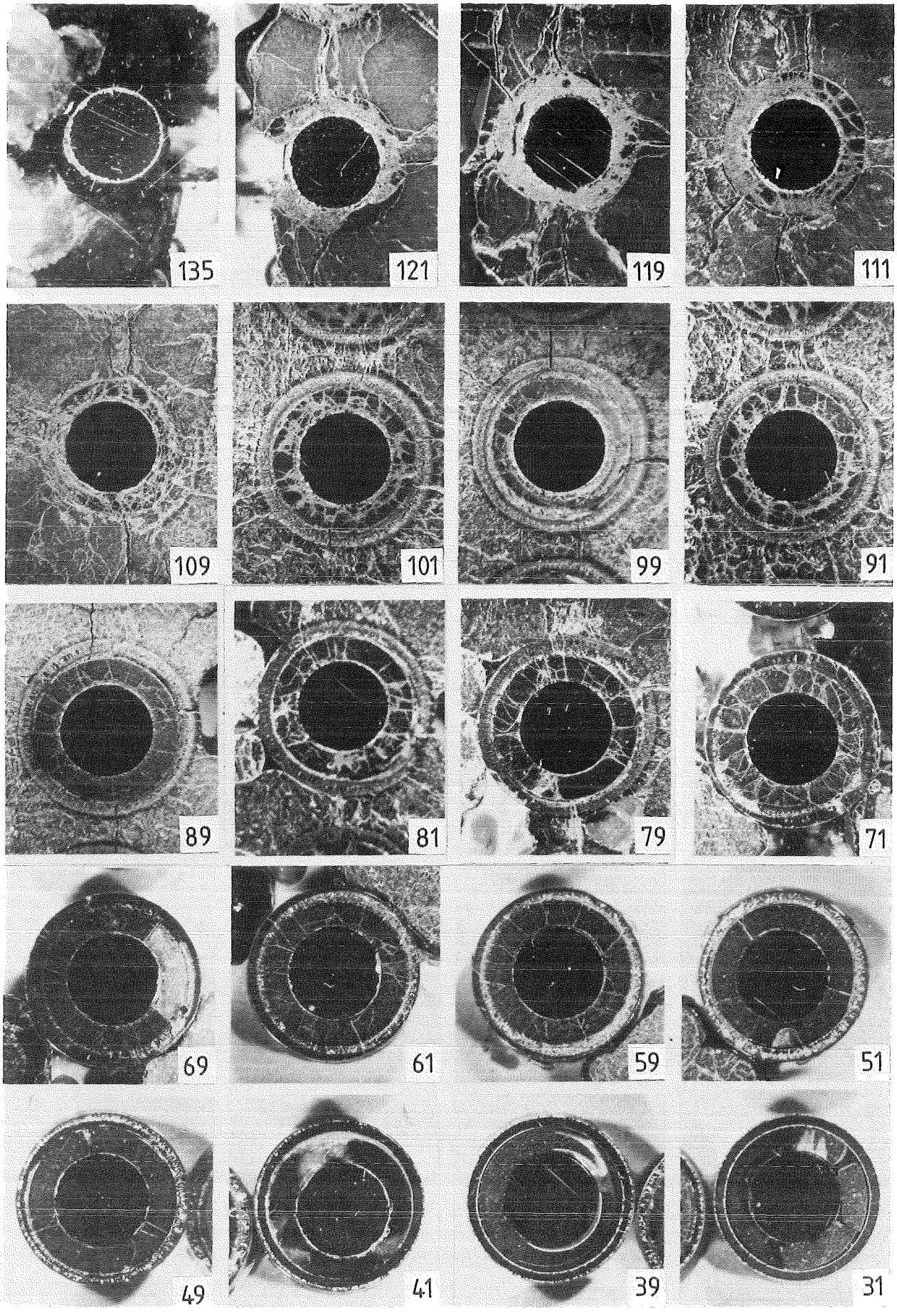

FIG.24: ENLARGED VIEWS OF THE REGION AROUND SIDE ROD 8 FOR DIFFERENT CROSS SECTIONS ESBU-2A.

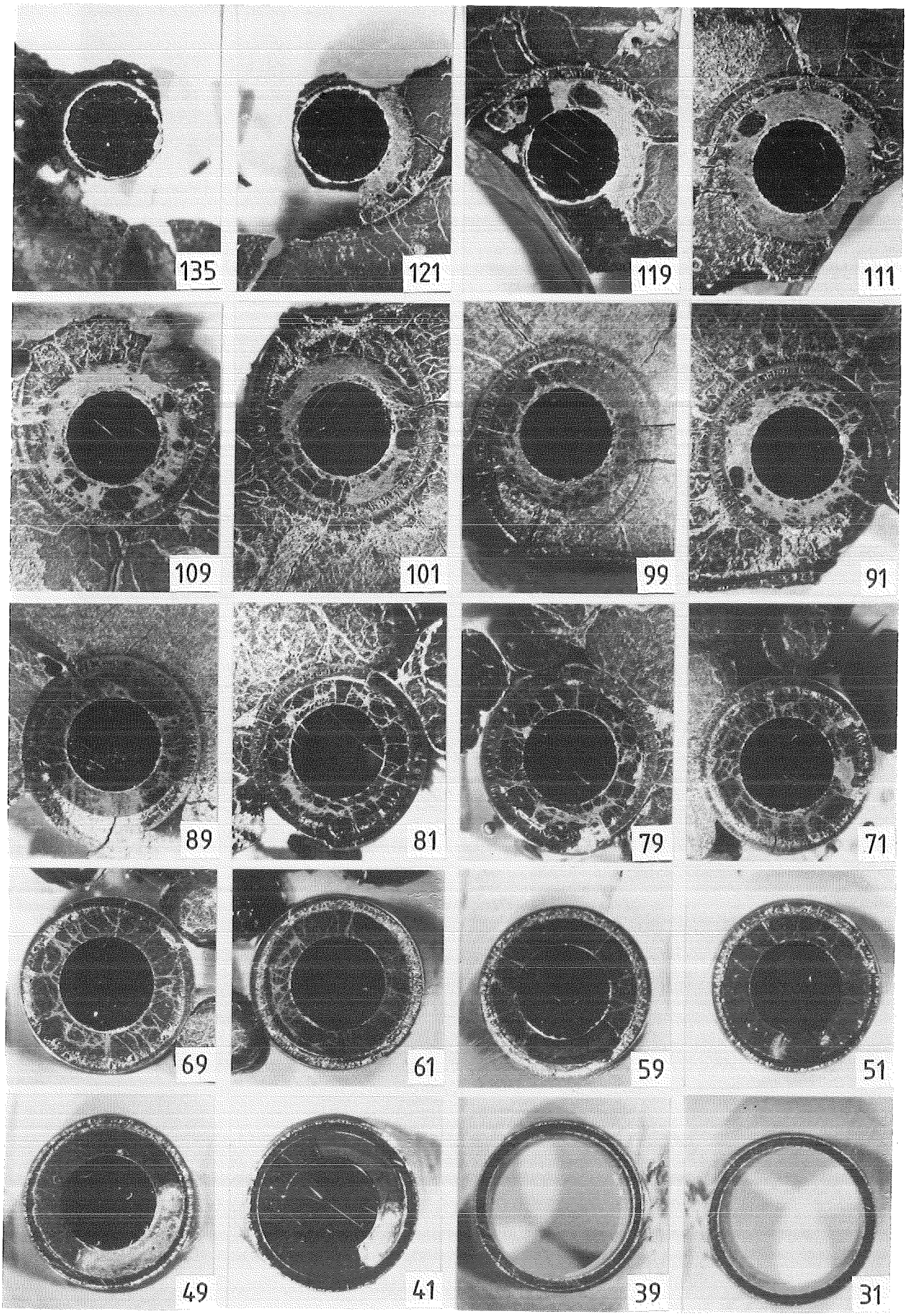

FIG.25: ENLARGED VIEWS OF THE REGION AROUND CORNER ROD 1 FOR DIFFERENT CROSS SECTIONS ESBU-2A.

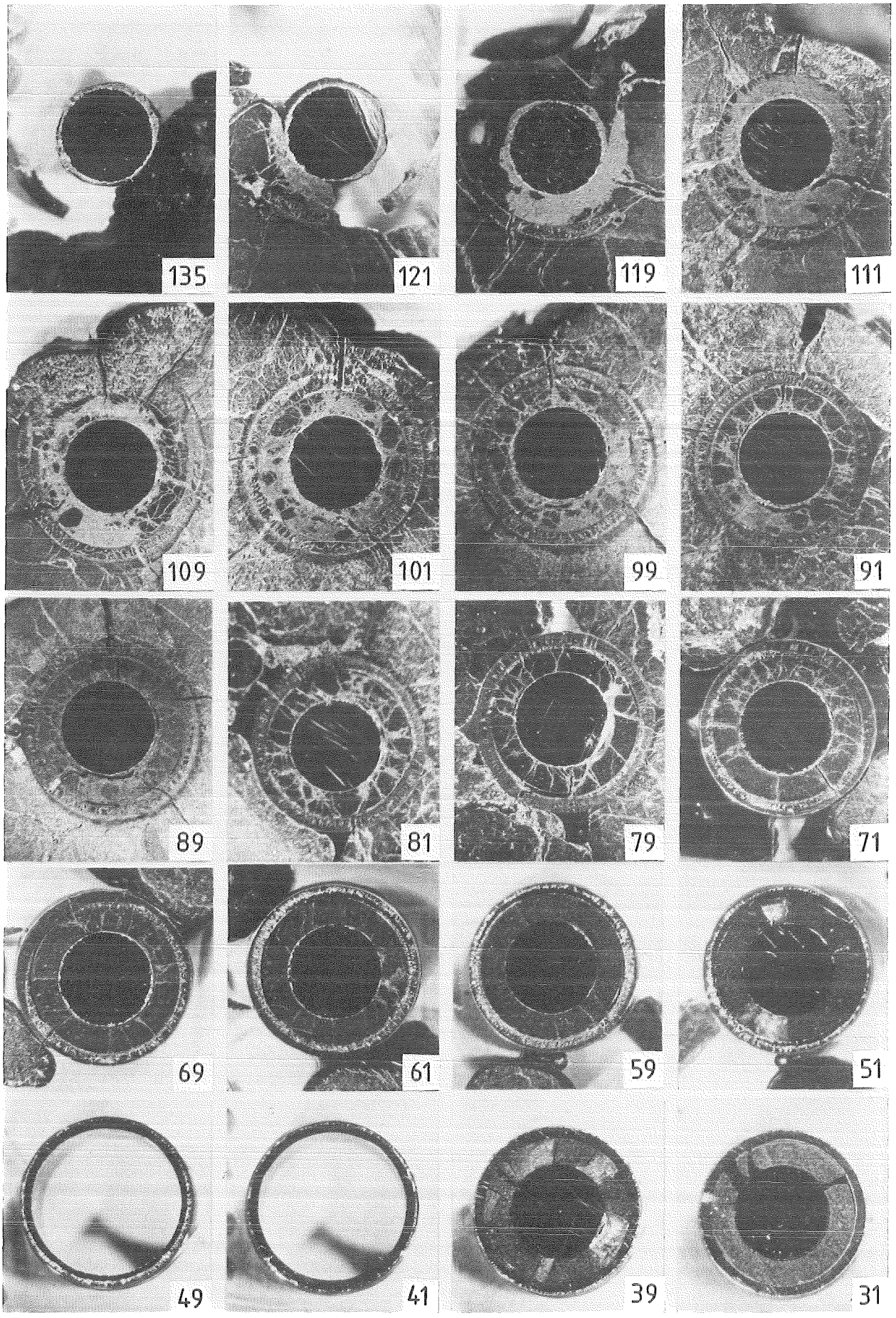

FIG.26: ENLARGED VIEWS OF THE REGION AROUND CORNER ROD 3 FOR DIFFERENT CROSS SECTIONS ESBU-2A.

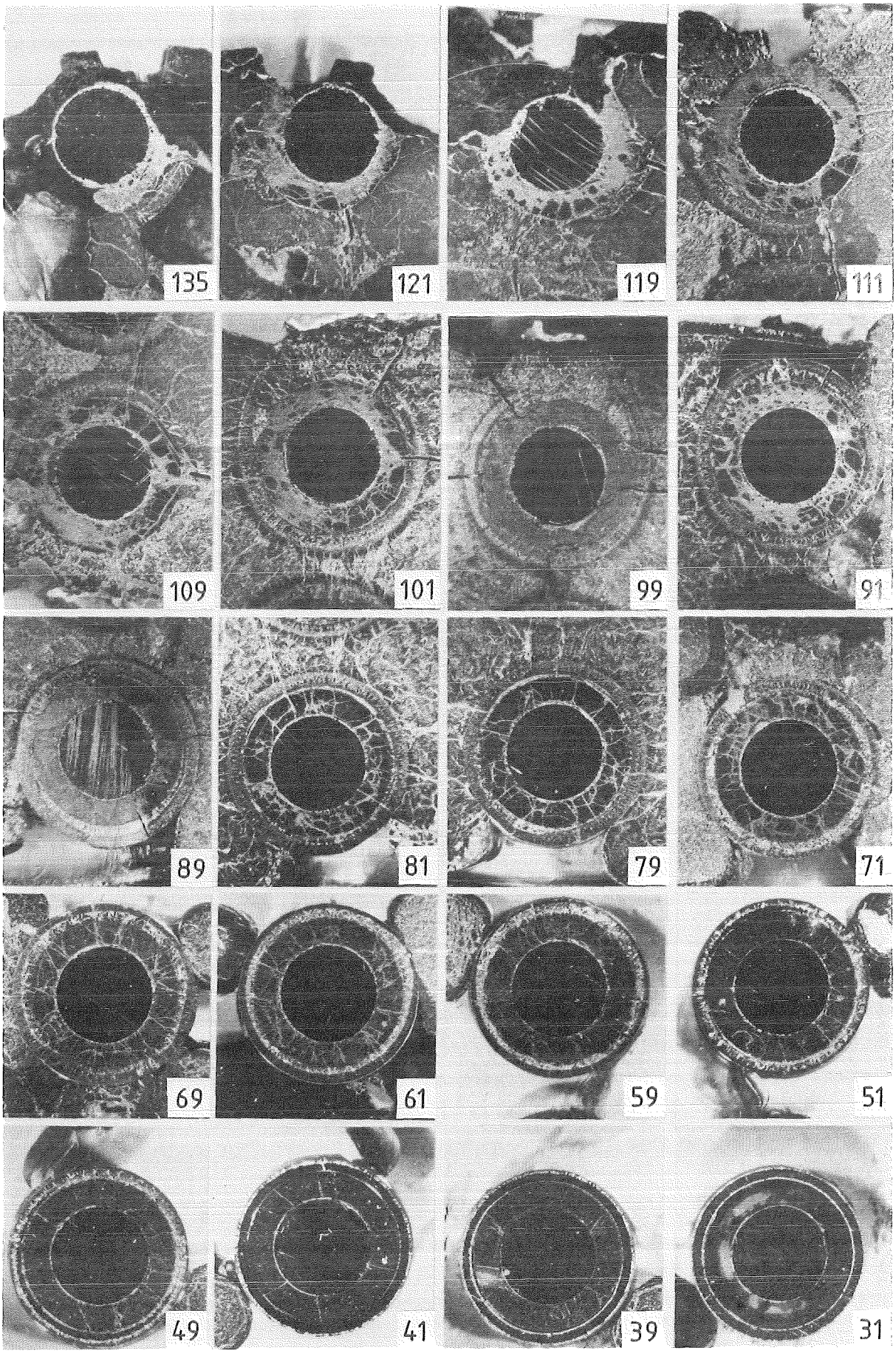

FIG.27: ENLARGED VIEWS OF THE REGION AROUND SIDE ROD 4 FOR DIFFERENT CROSS SECTIONS ESBU-2A.

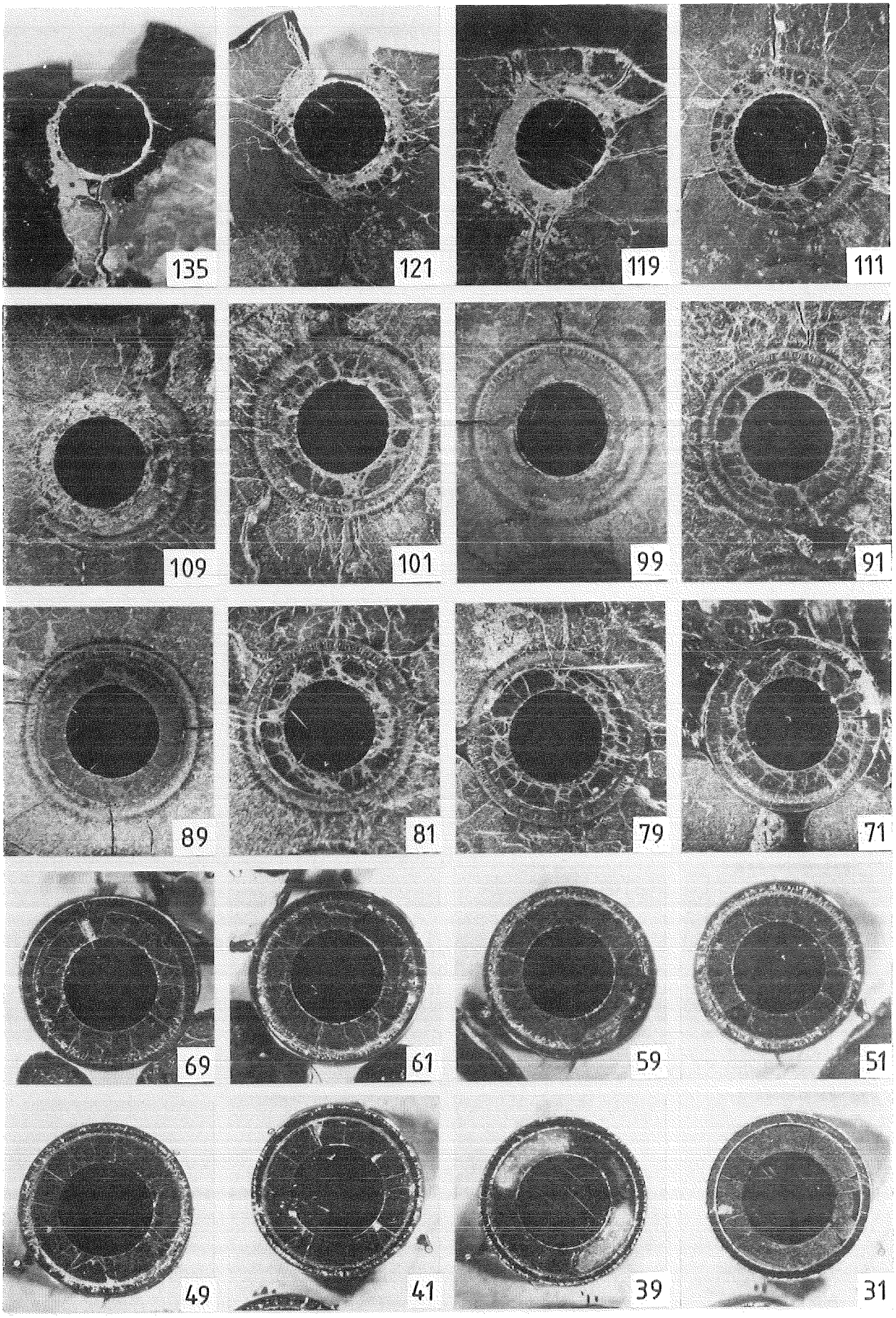

FIG.28: ENLARGED VIEWS OF THE REGION AROUND SIDE ROD 6 FOR DIFFERENT CROSS SECTIONS ESBU-2A.

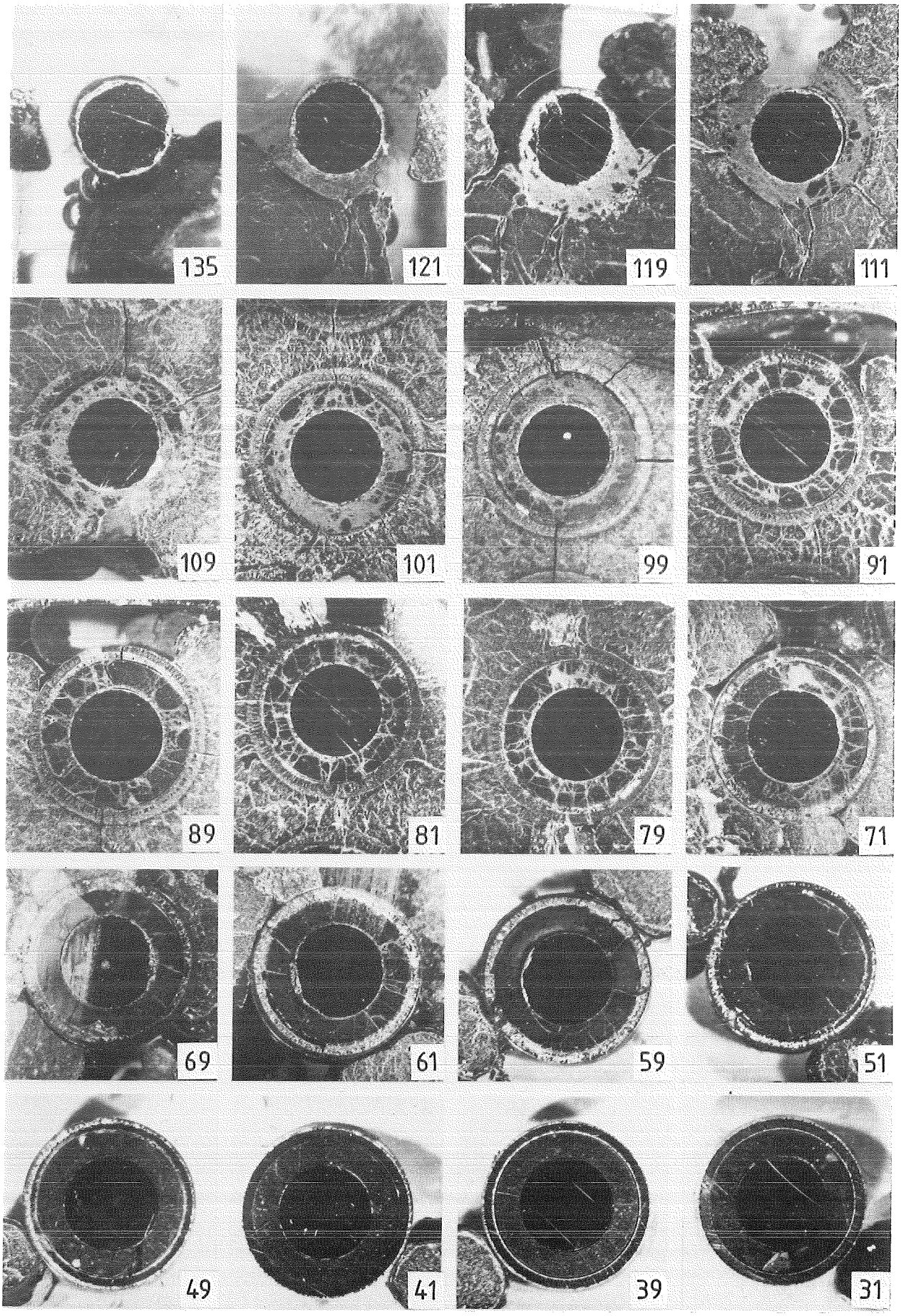

FIG.29: ENLARGED VIEWS OF THE REGION AROUND CORNER ROD 7 FOR DIFFERENT CROSS SECTIONS ESBU-2A.

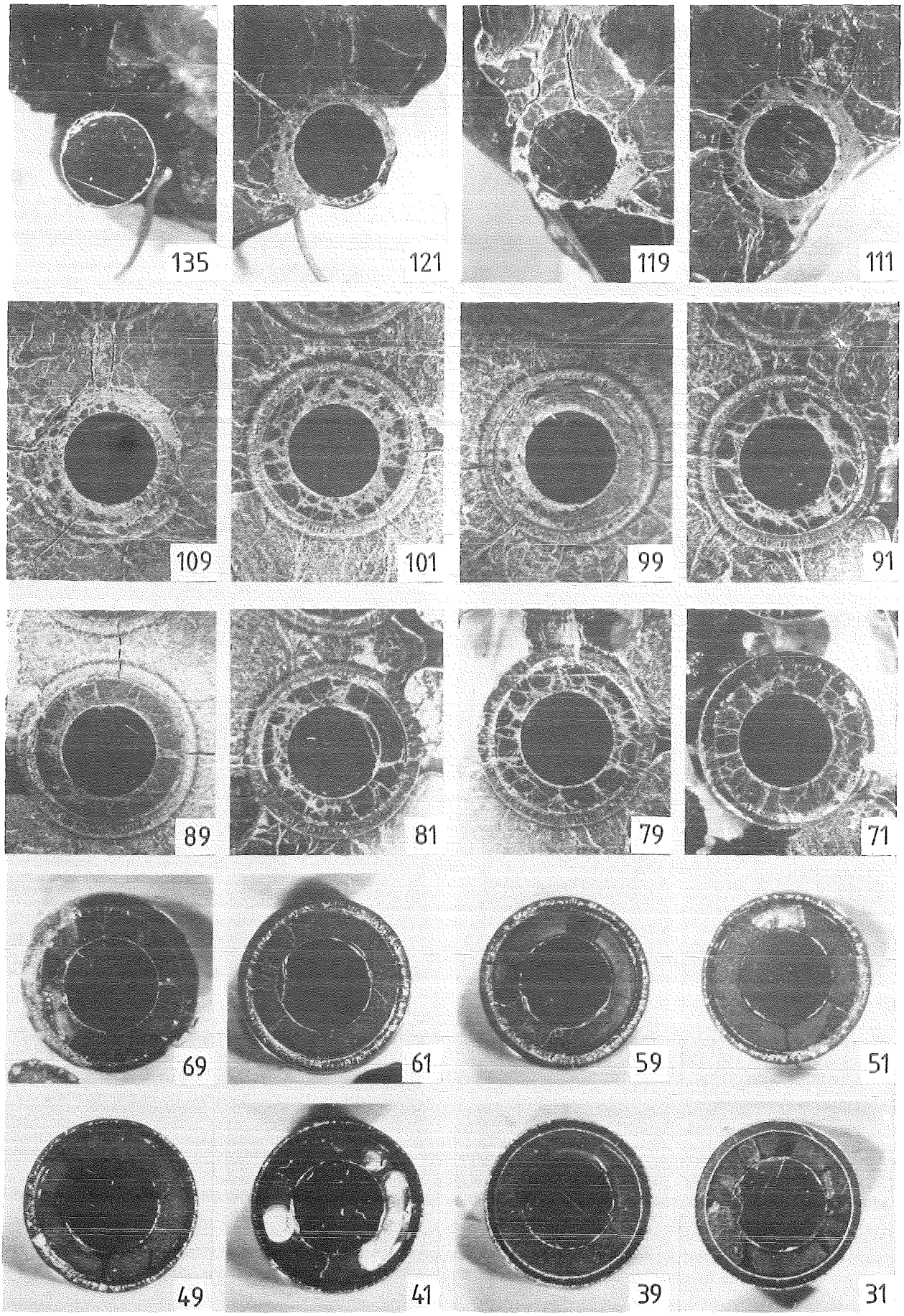

FIG.30: ENLARGED VIEWS OF THE REGION AROUND CORNER ROD 9 FOR DIFFERENT CROSS SECTIONS ESBU-2A.

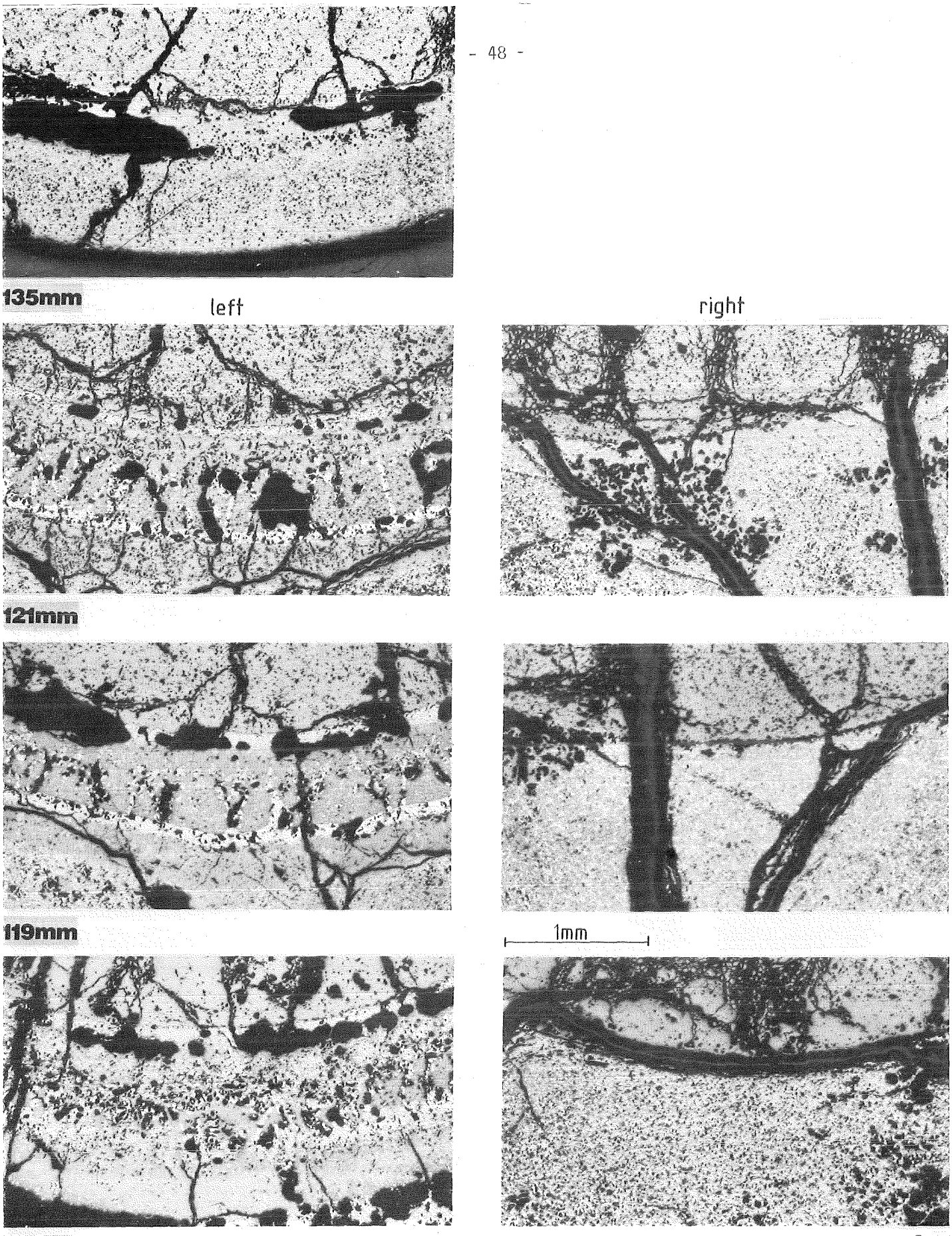

FIG.31: COMPARISON OF OPPOSITE SIDES OF CENTER ROD 5 AT VARIOUS ELEVATIONS. TEST ESBU-2A

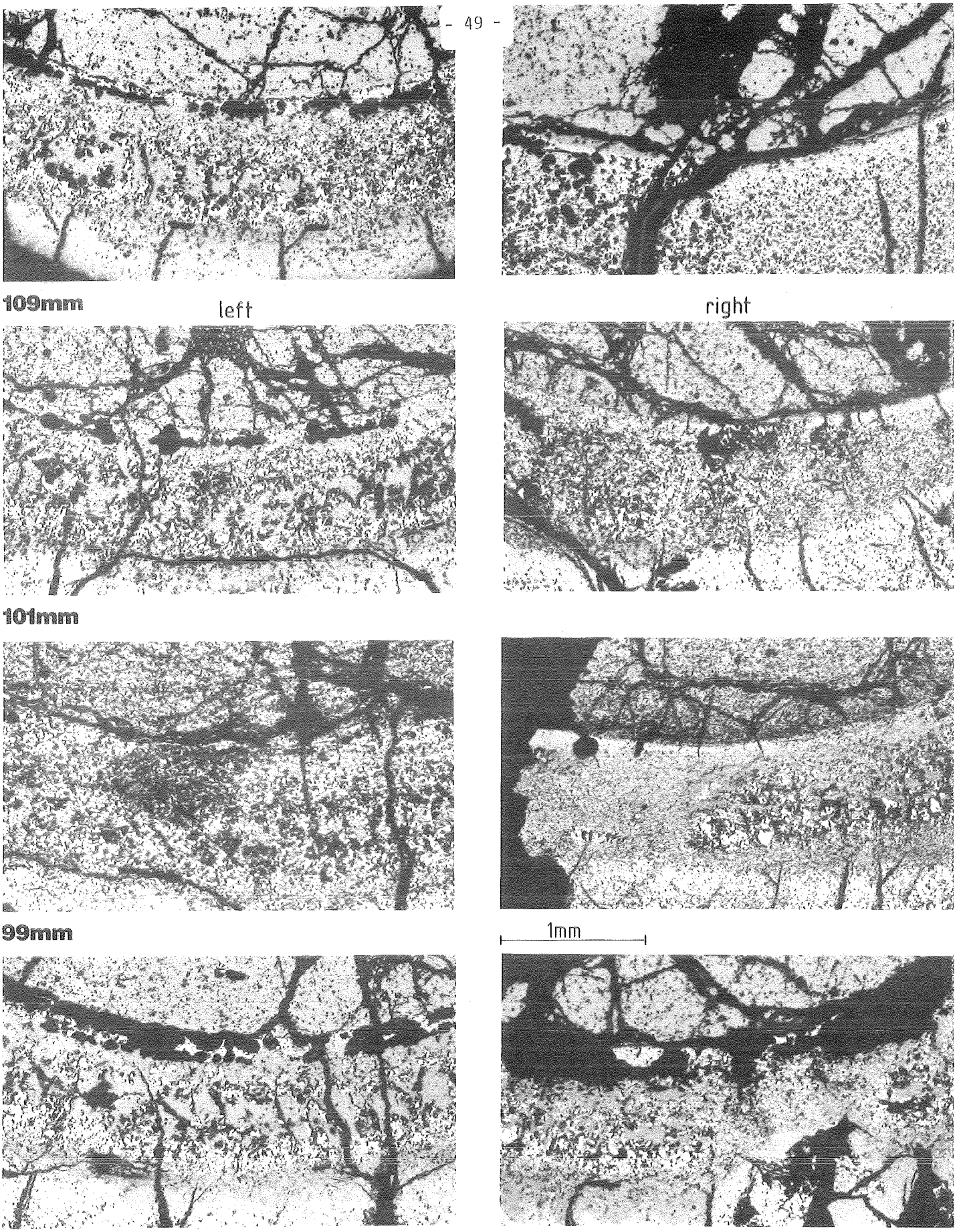

FIG.32: COMPARISON OF OPPOSITE SIDES OF CENTER ROD 5 AT VARIOUS ELEVATIONS. TEST ESBU-2A

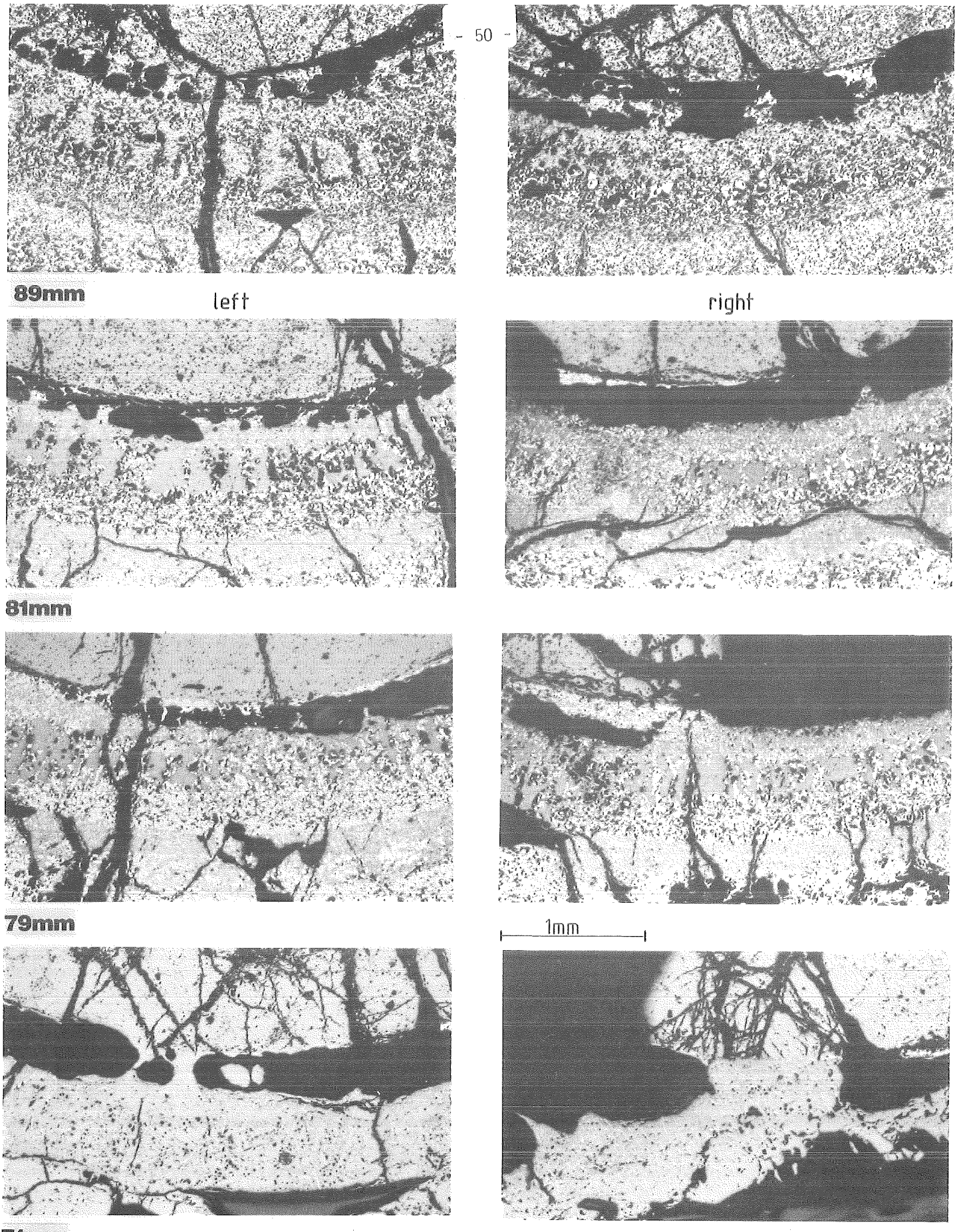

FIG.33: COMPARISON OF OPPOSITE SIDES OF CENTER ROD 5 AT VARIOUS ELEVATIONS. TEST ESBU-2A

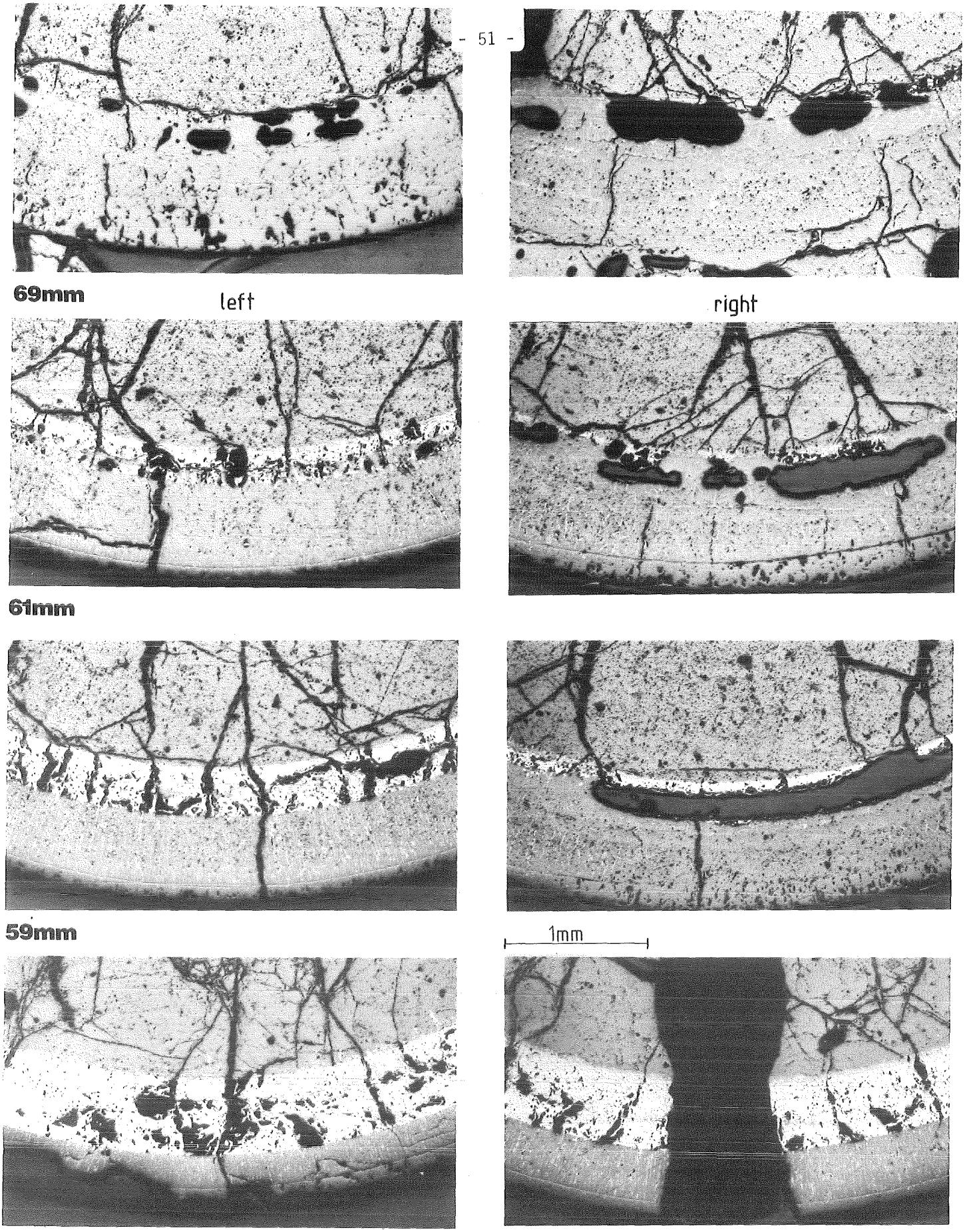

FIG.34: COMPARISON OF OPPOSITE SIDES OF CENTER ROD 5 AT VARIOUS ELEVATIONS. TEST ESBU-2A

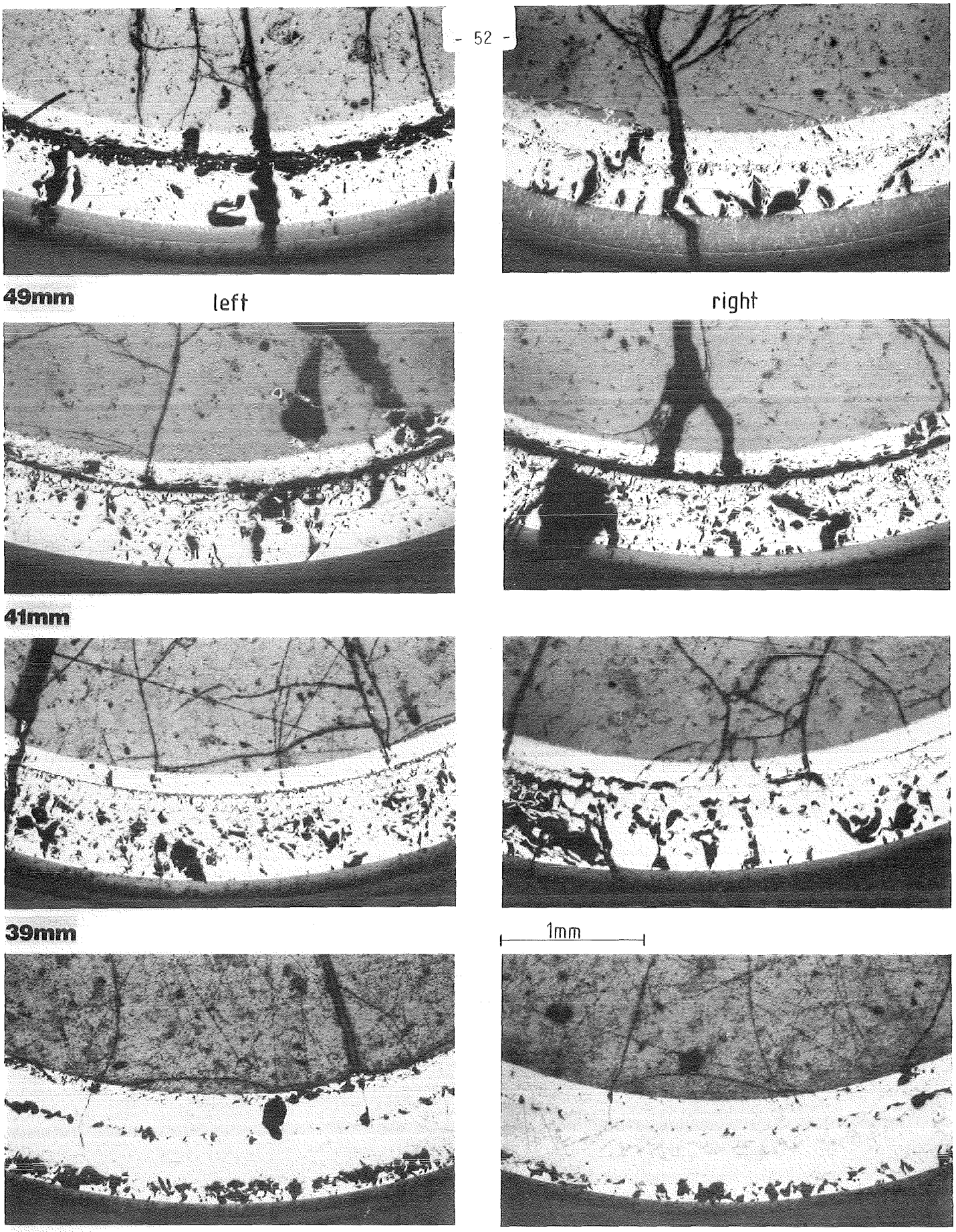

FIG.35: COMPARISON OF OPPOSITE SIDES OF CENTER ROD 5 AT VARIOUS ELEVATIONS. TEST ESBU-2A

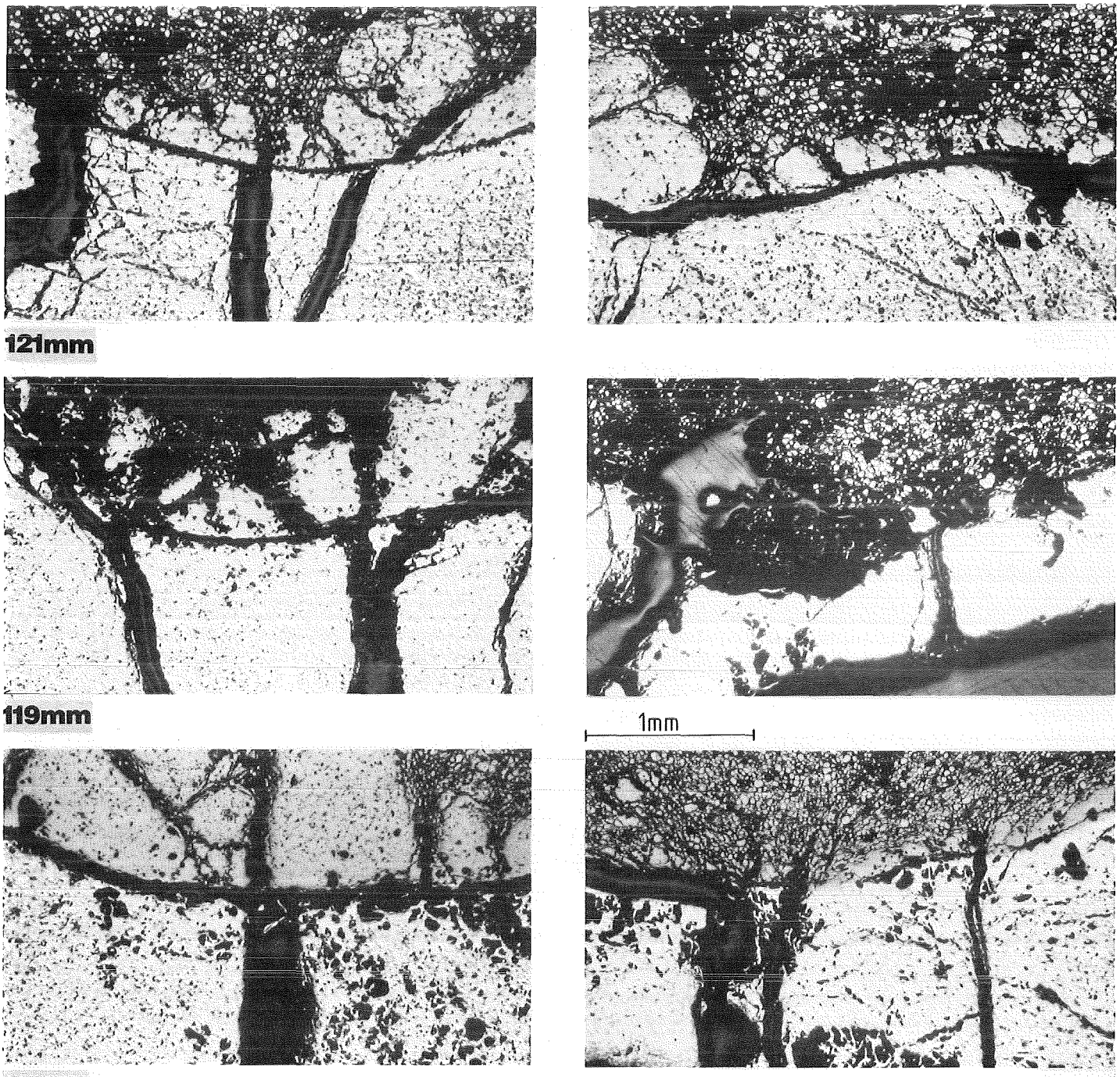

FIG.36: COMPARISON OF OPPOSITE SIDES OF SIDE ROD 8
AT VARIOUS ELEVATIONS. TEST ESBU-2A

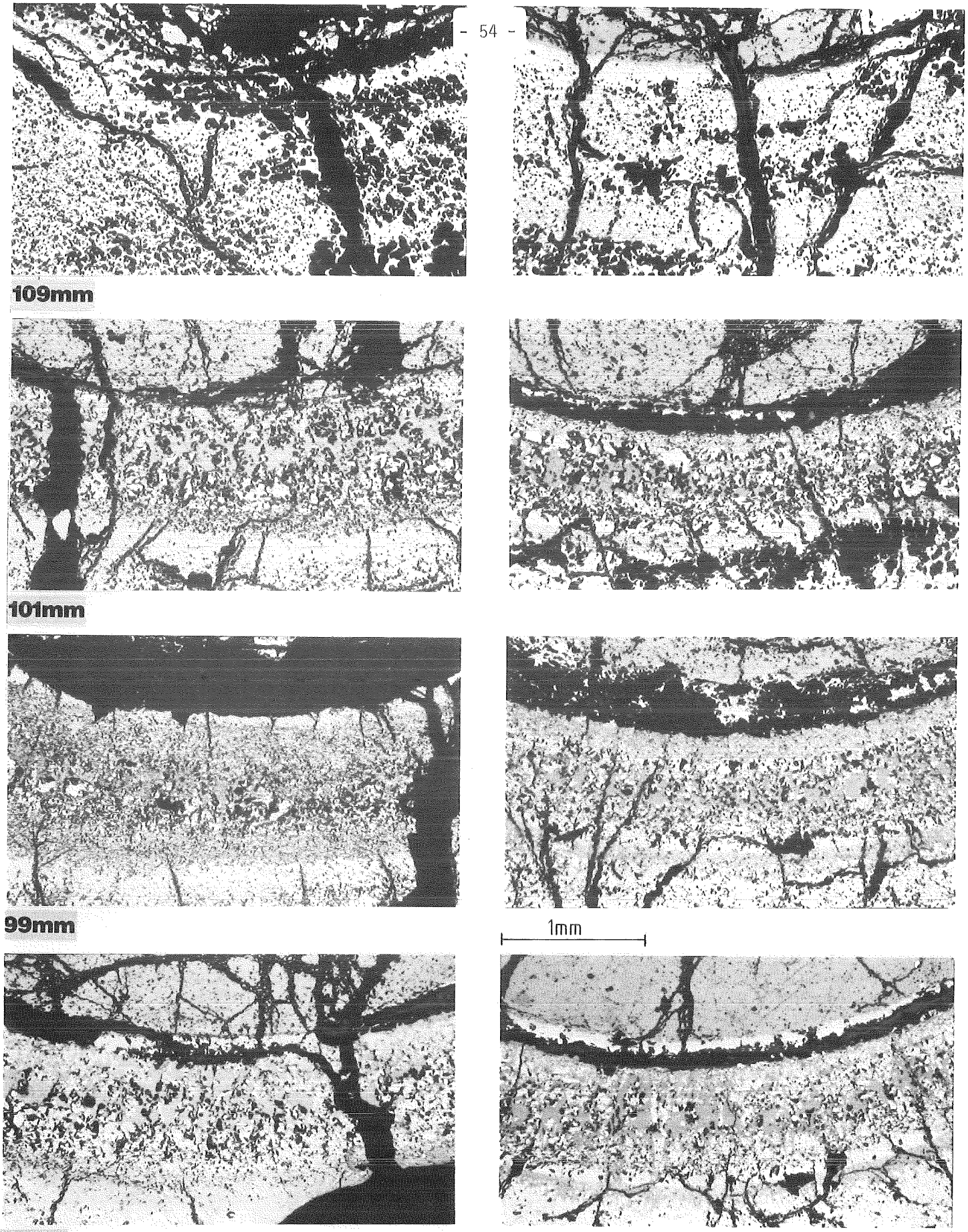

FIG.37: COMPARISON OF OPPOSITE SIDES OF SIDE ROD 8 AT VARIOUS ELEVATIONS. TEST ESBU-2A

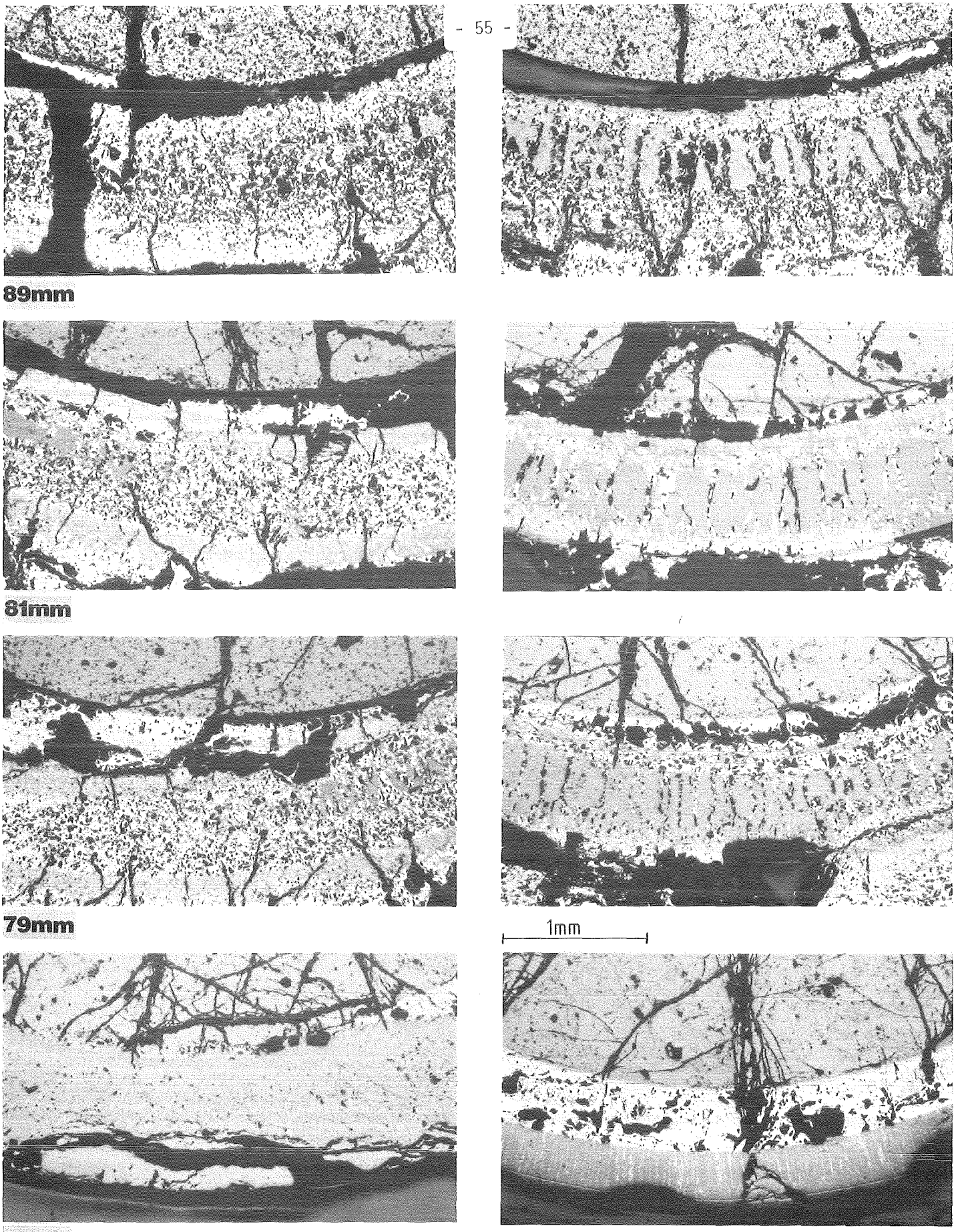

FIG.38: COMPARISON OF OPPOSITE SIDES OF SIDE ROD 8 AT VARIOUS ELEVATIONS. TEST ESBU-2A

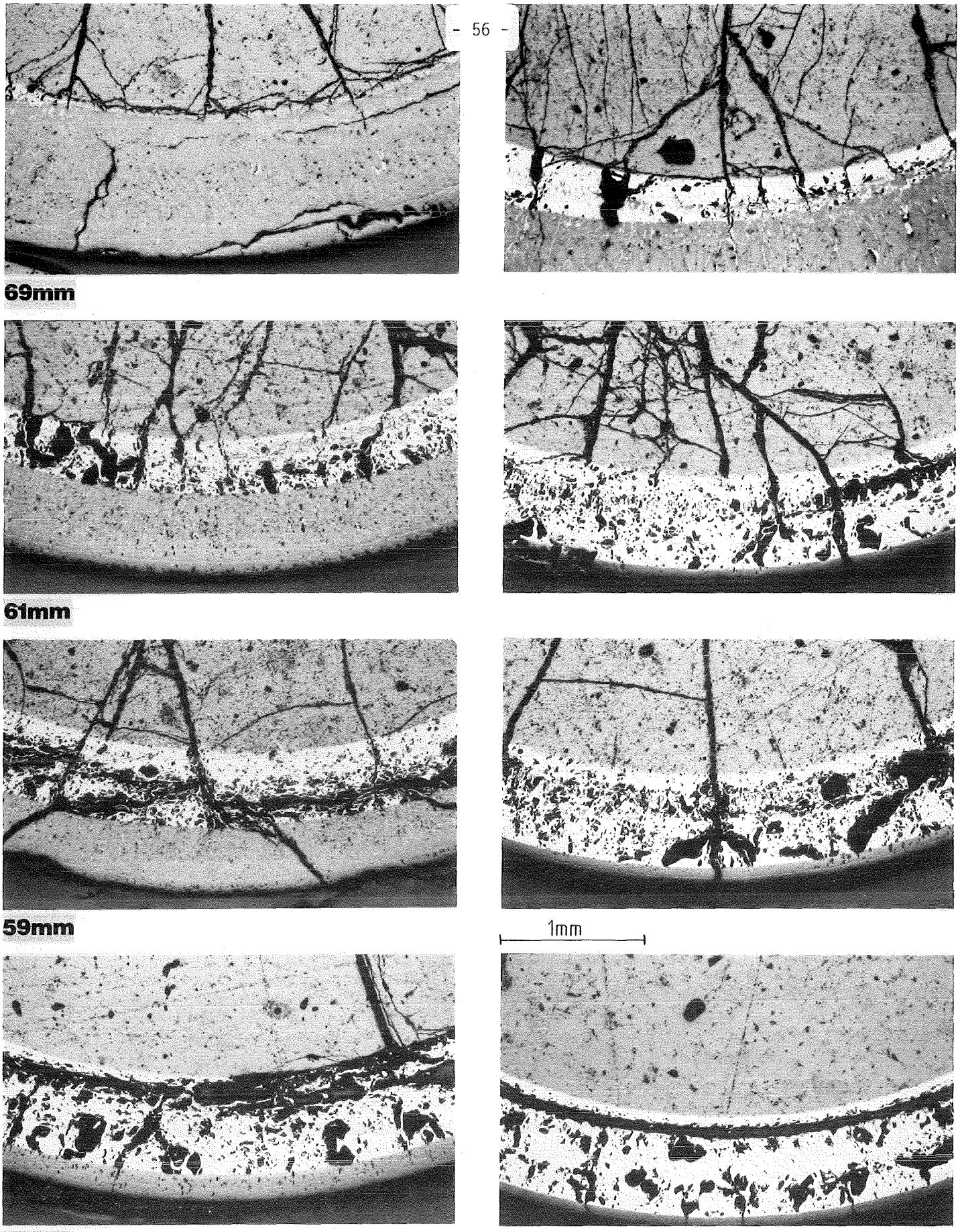

FIG.39: COMPARISON OF OPPOSITE SIDES OF SIDE ROD 8 AT VARIOUS ELEVATIONS. TEST ESBU-2A

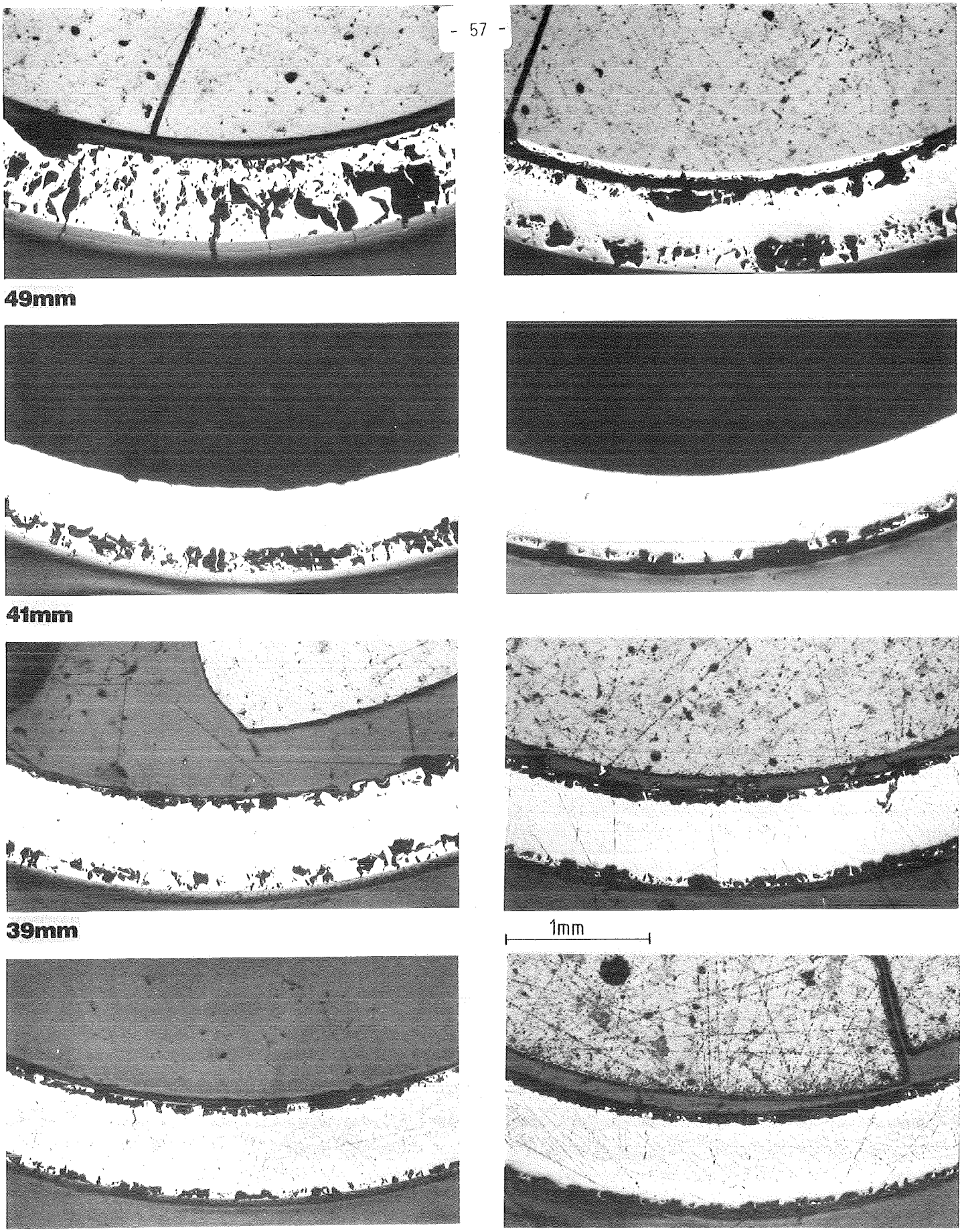

FIG.40: COMPARISON OF OPPOSITE SIDES OF SIDE ROD 8 AT VARIOUS ELEVATIONS. TEST ESBU-2A

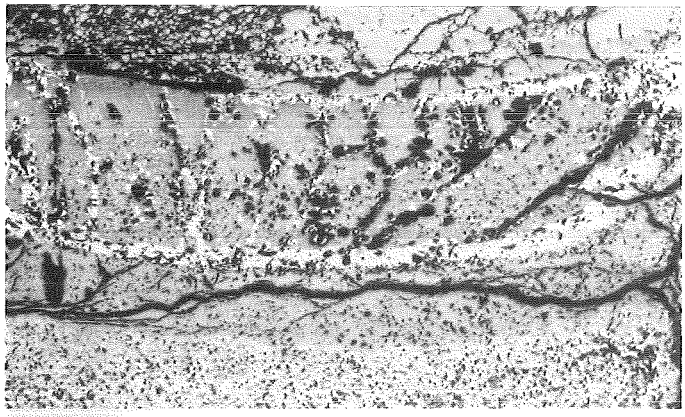

121mm

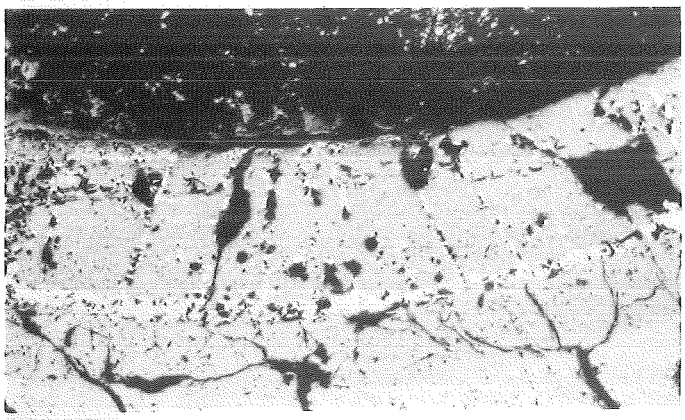

119mm

1mm

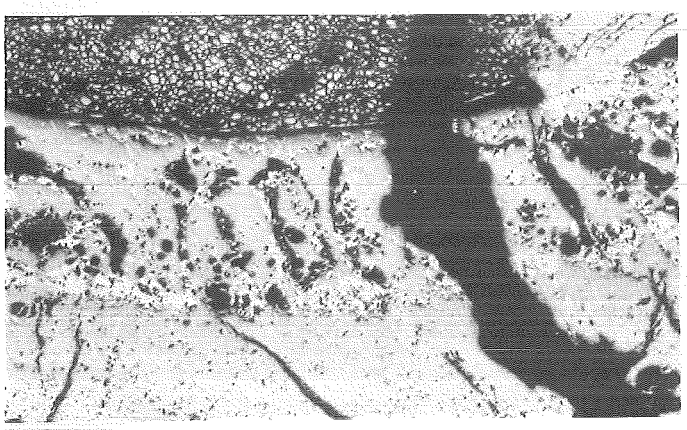

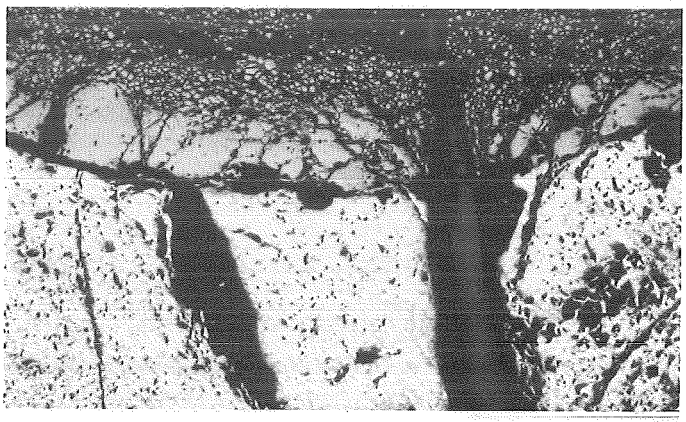

111mm

FIG.41: COMPARISON OF OPPOSITE SIDES OF CORNER ROD 3 AT VARIOUS ELEVATIONS. TEST ESBU-2A

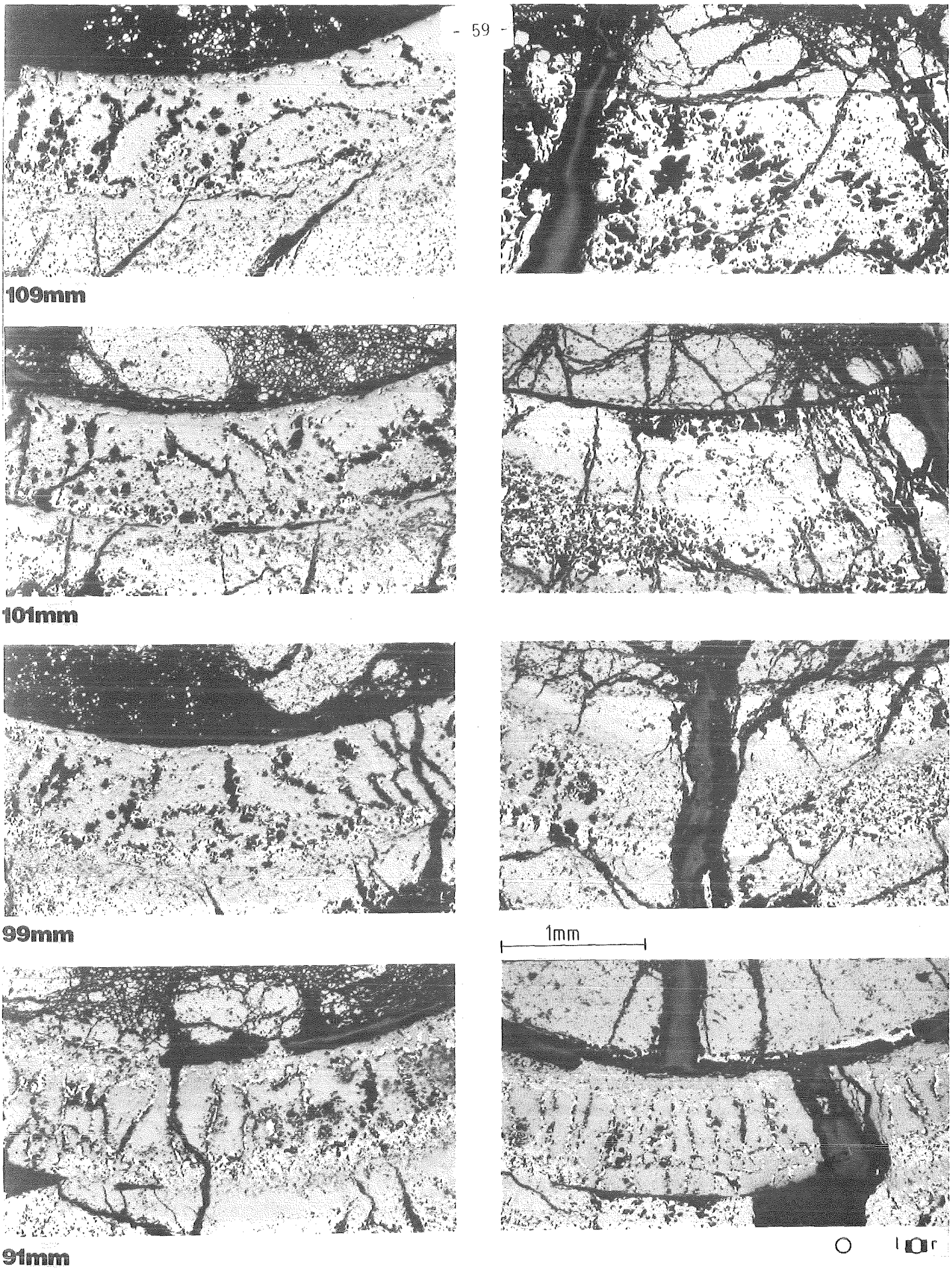

FIG.42: COMPARISON OF OPPOSITE SIDES OF CORNER ROD 3 AT VARIOUS ELEVATIONS. TEST ESBU-2A

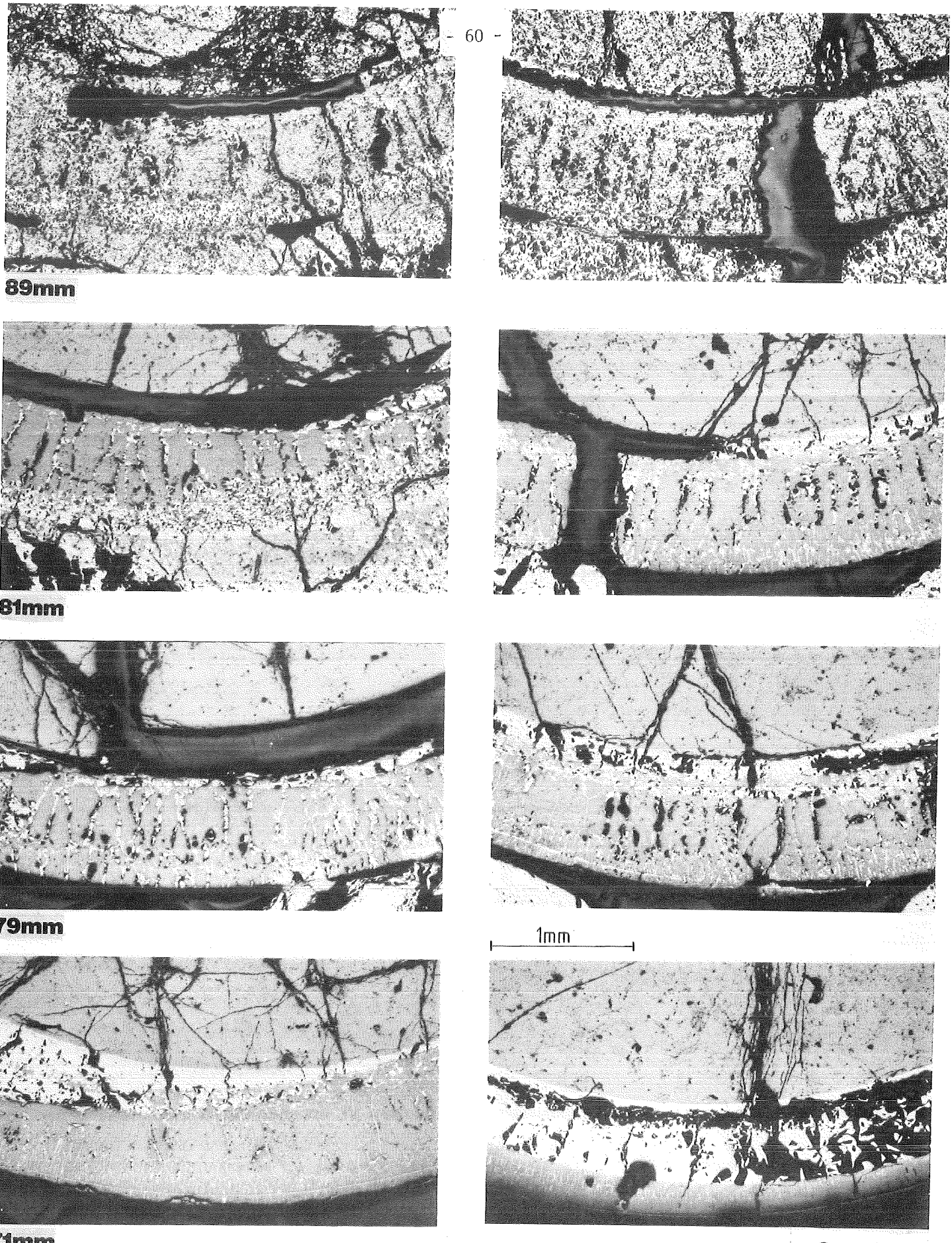

FIG.43: COMPARISON OF OPPOSITE SIDES OF CORNER ROD 3 AT VARIOUS ELEVATIONS. TEST ESBU-2A

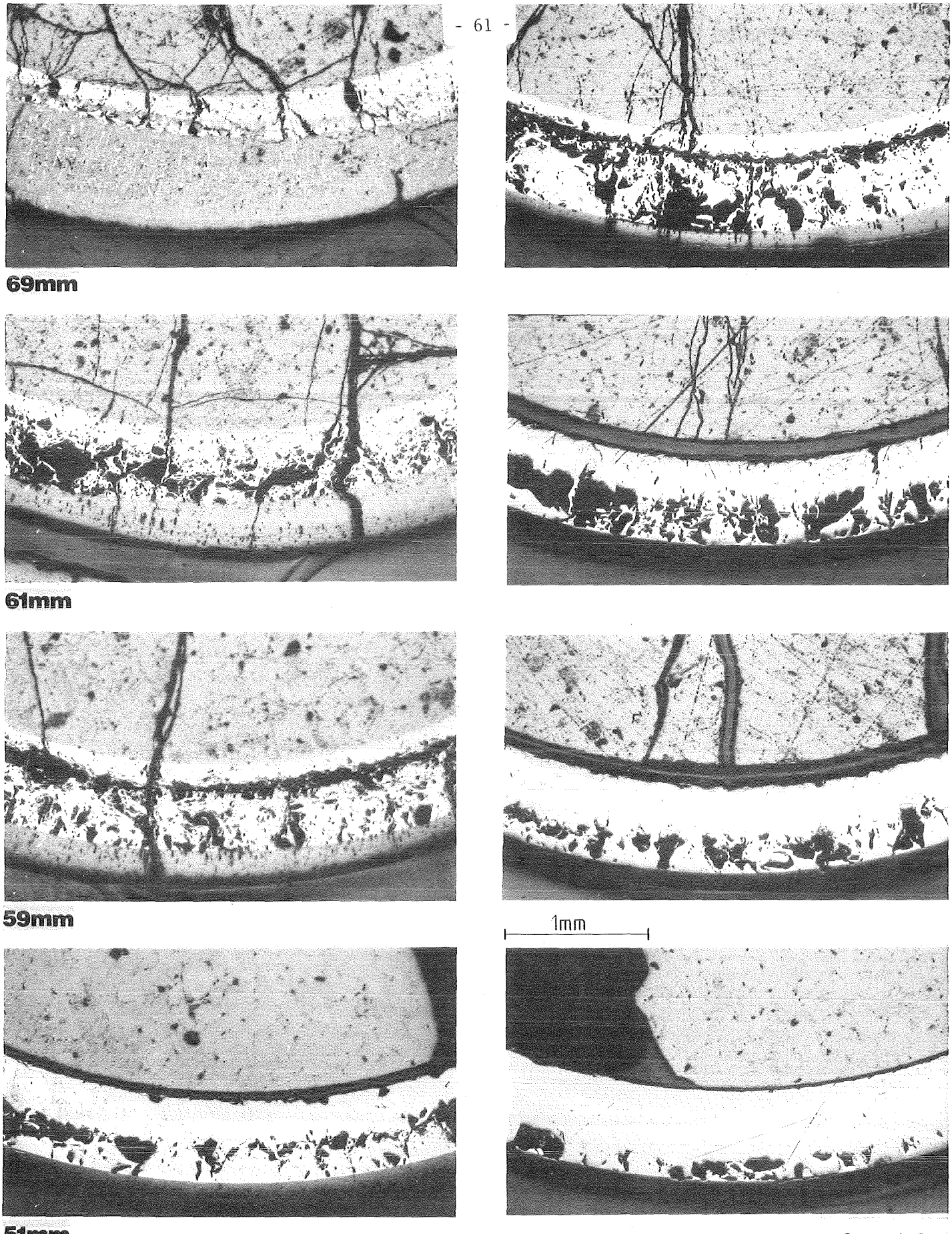

FIG.44: COMPARISON OF OPPOSITE SIDES OF CORNER ROD 3 AT VARIOUS ELEVATIONS. TEST ESBU-2A

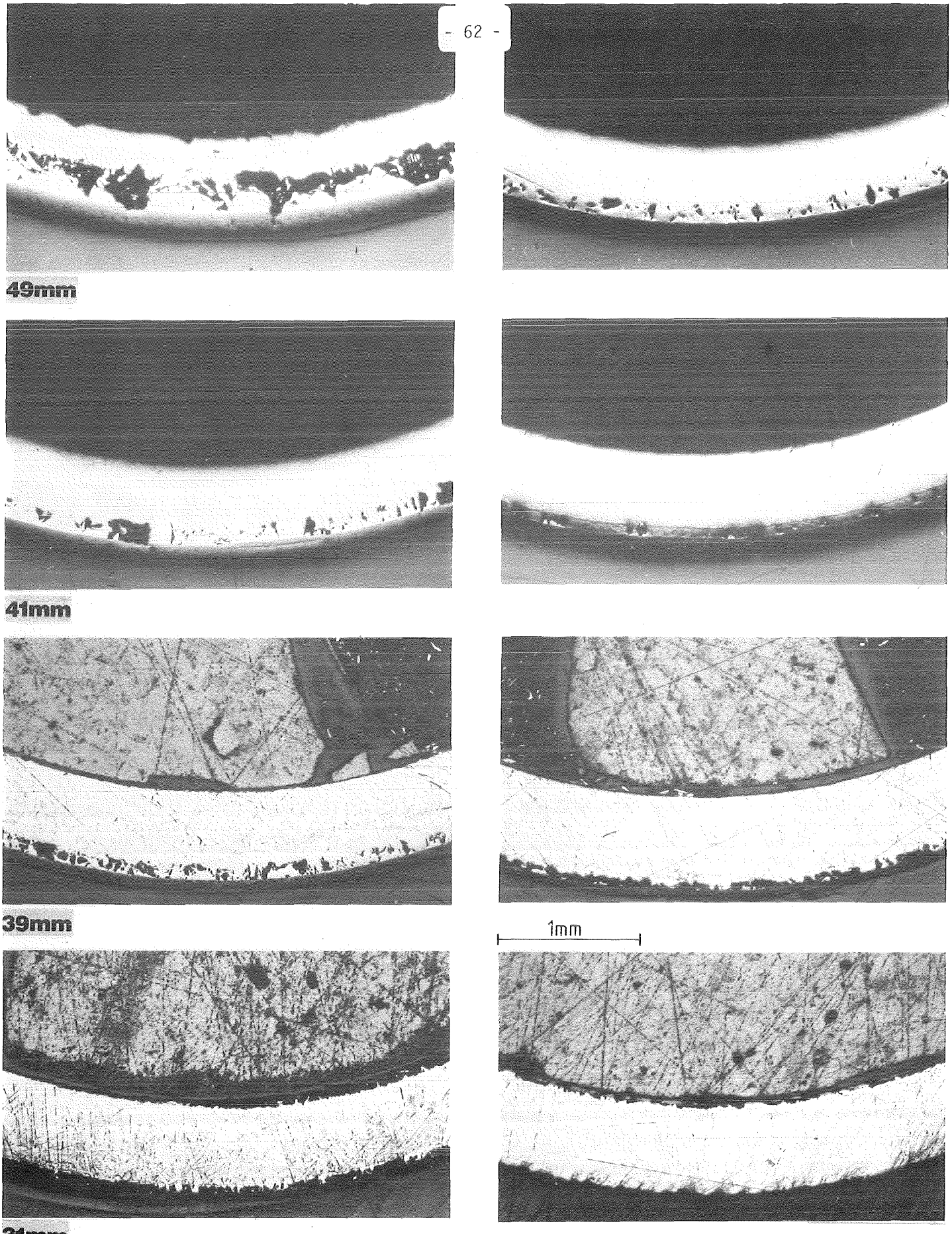

FIG.45: COMPARISON OF OPPOSITE SIDES OF CORNER ROD 3 AT VARIOUS ELEVATIONS. TEST ESBU-2A

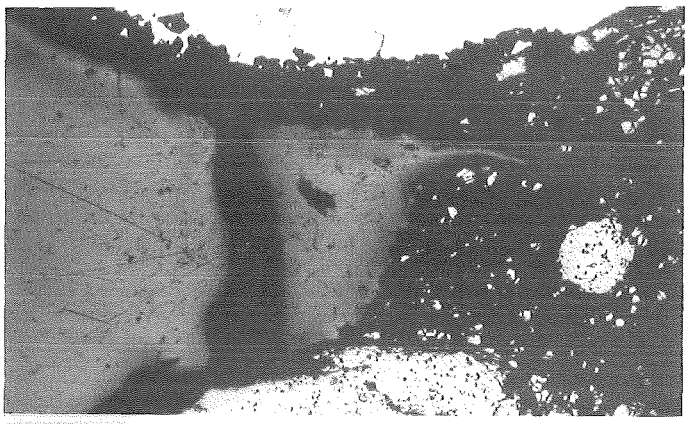

135mm

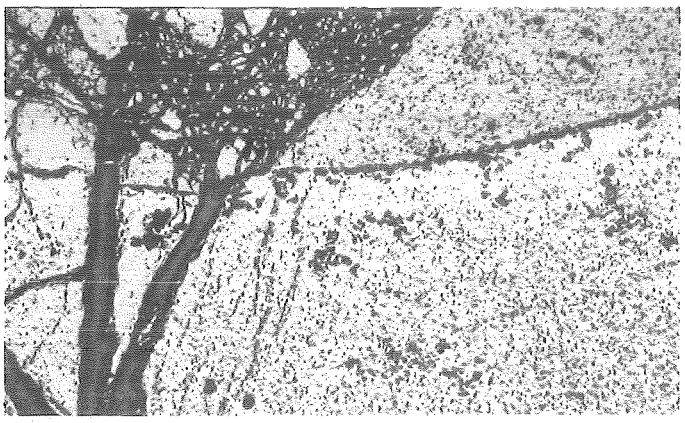

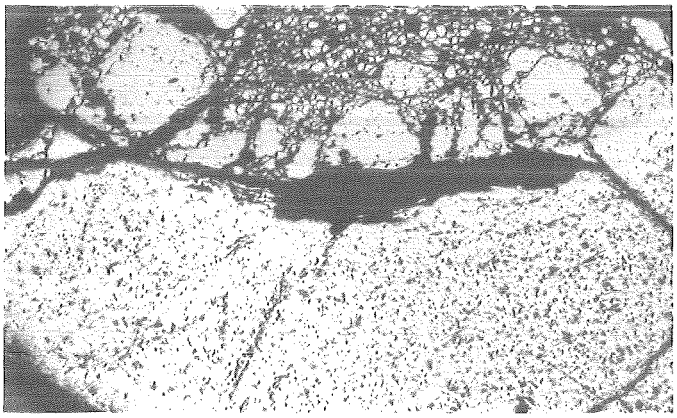

121mm

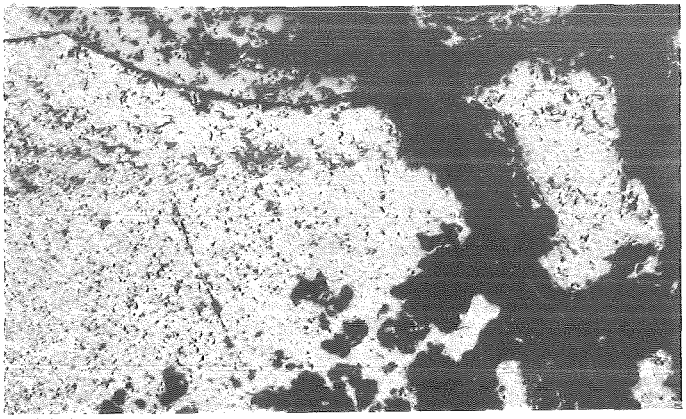

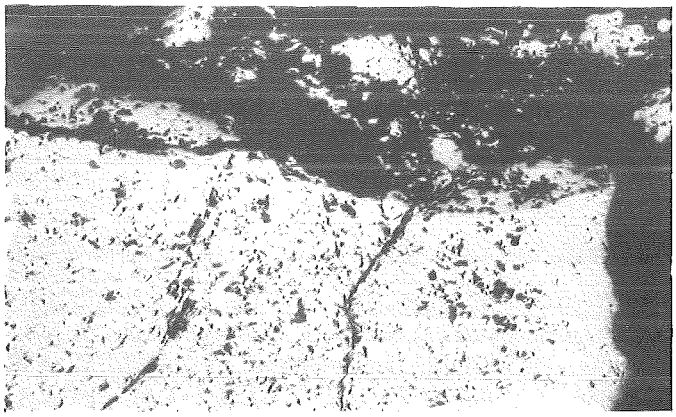

119mm

1mm

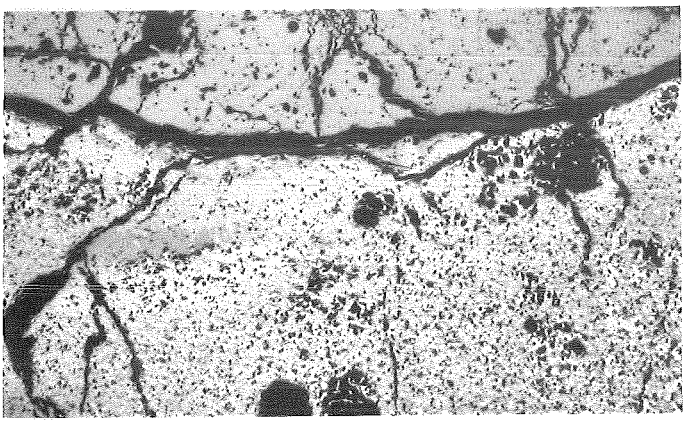

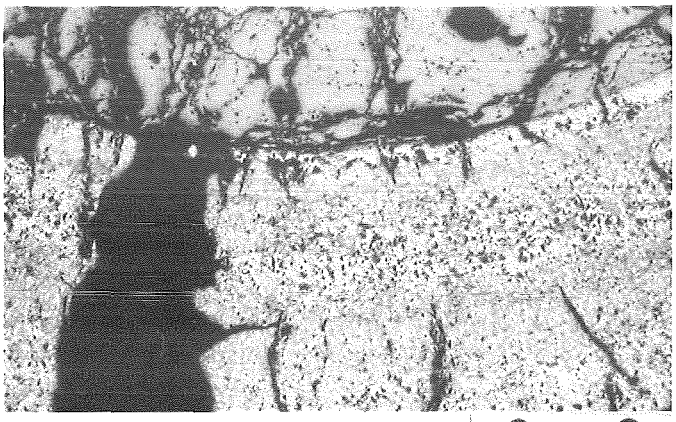

111mm

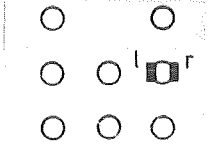

FIG.46: COMPARISON OF OPPOSITE SIDES OF SIDE ROD 6 AT VARIOUS ELEVATIONS. TEST ESBU-2A

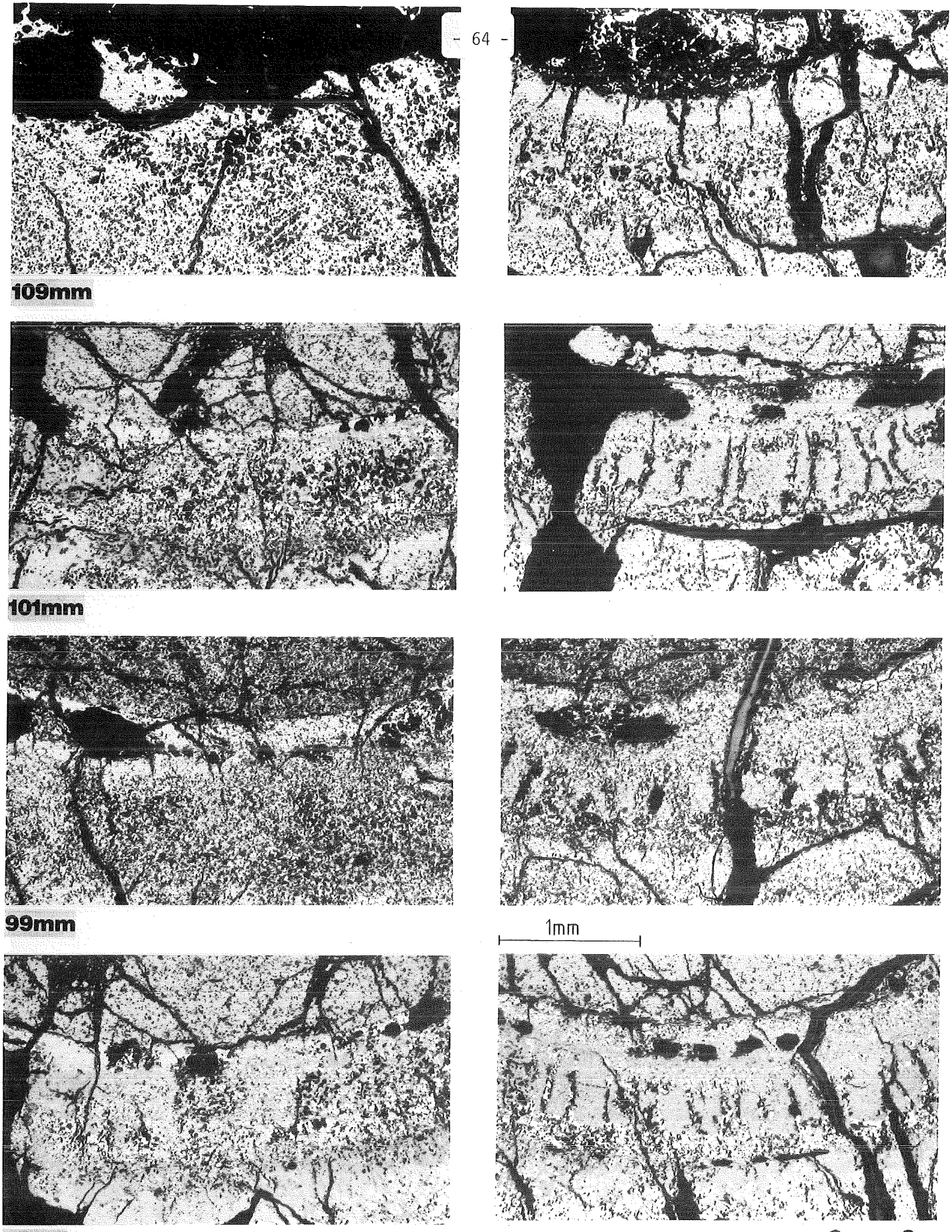

FIG.47: COMPARISON OF OPPOSITE SIDES OF SIDE ROD 6 AT VARIOUS ELEVATIONS. TEST ESBU-2A

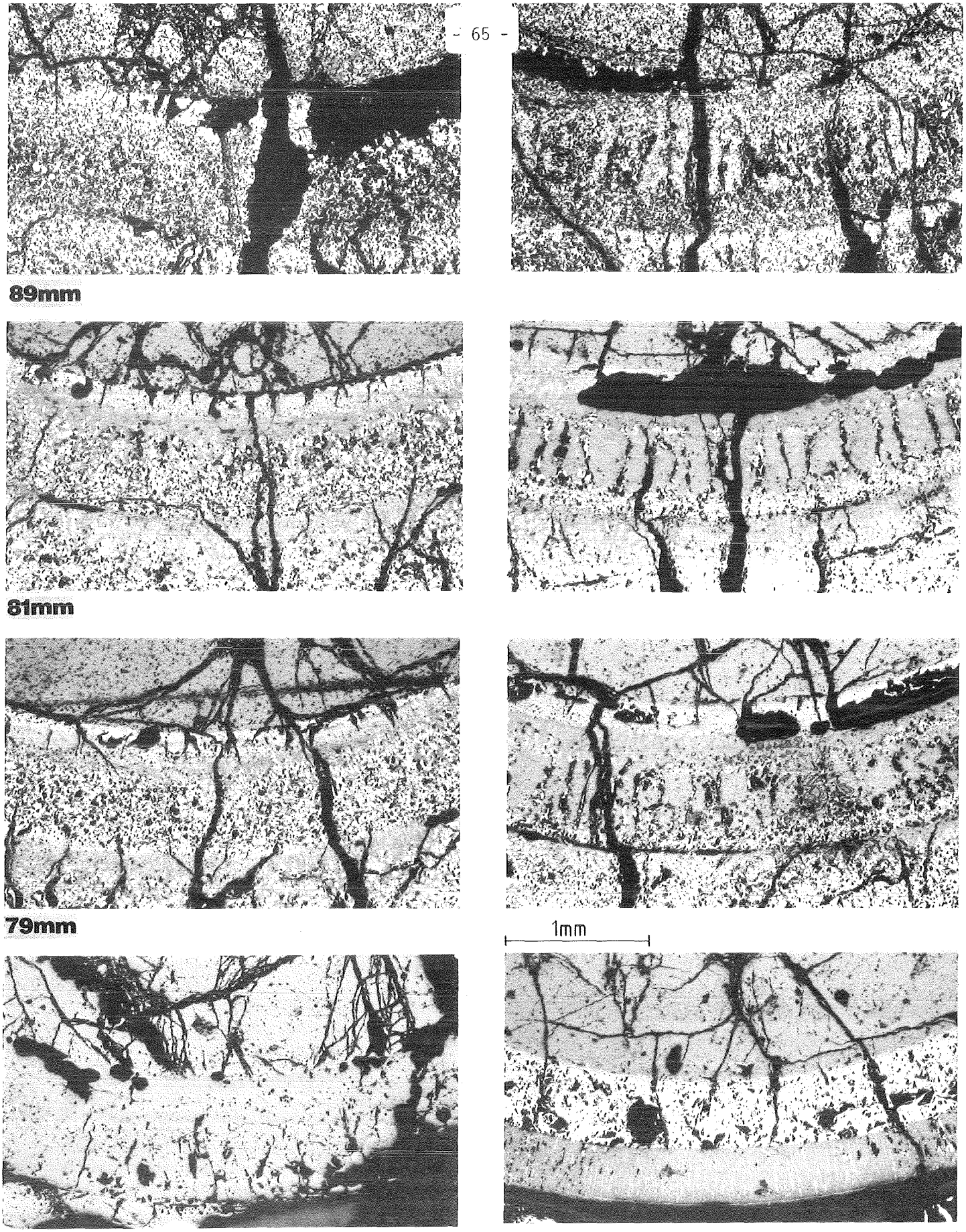

FIG.48: COMPARISON OF OPPOSITE SIDES OF SIDE ROD 6 AT VARIOUS ELEVATIONS. TEST ESBU-2A

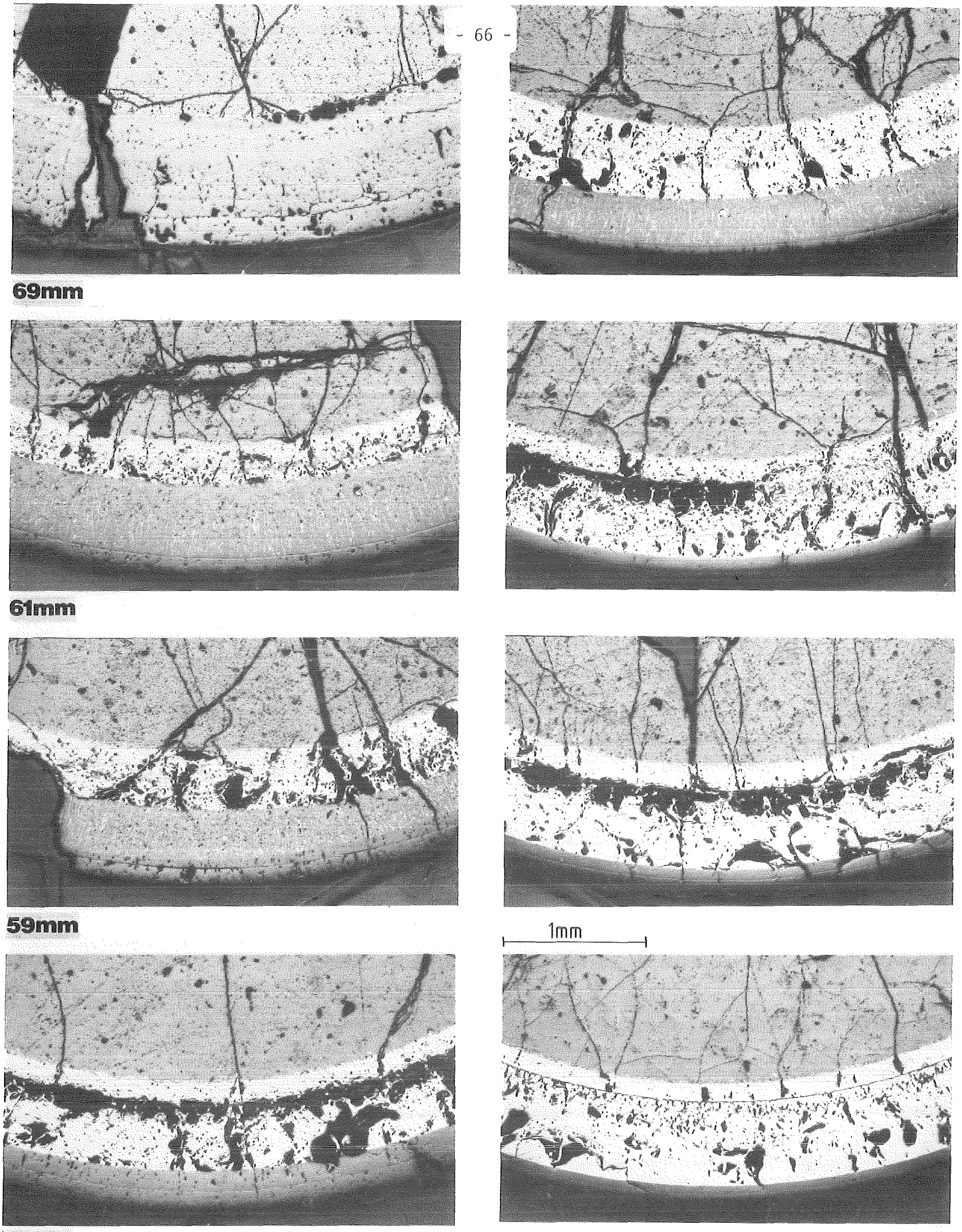

FIG.49: COMPARISON OF OPPOSITE SIDES OF SIDE ROD 6
AT VARIOUS ELEVATIONS. TEST ESBU-2A

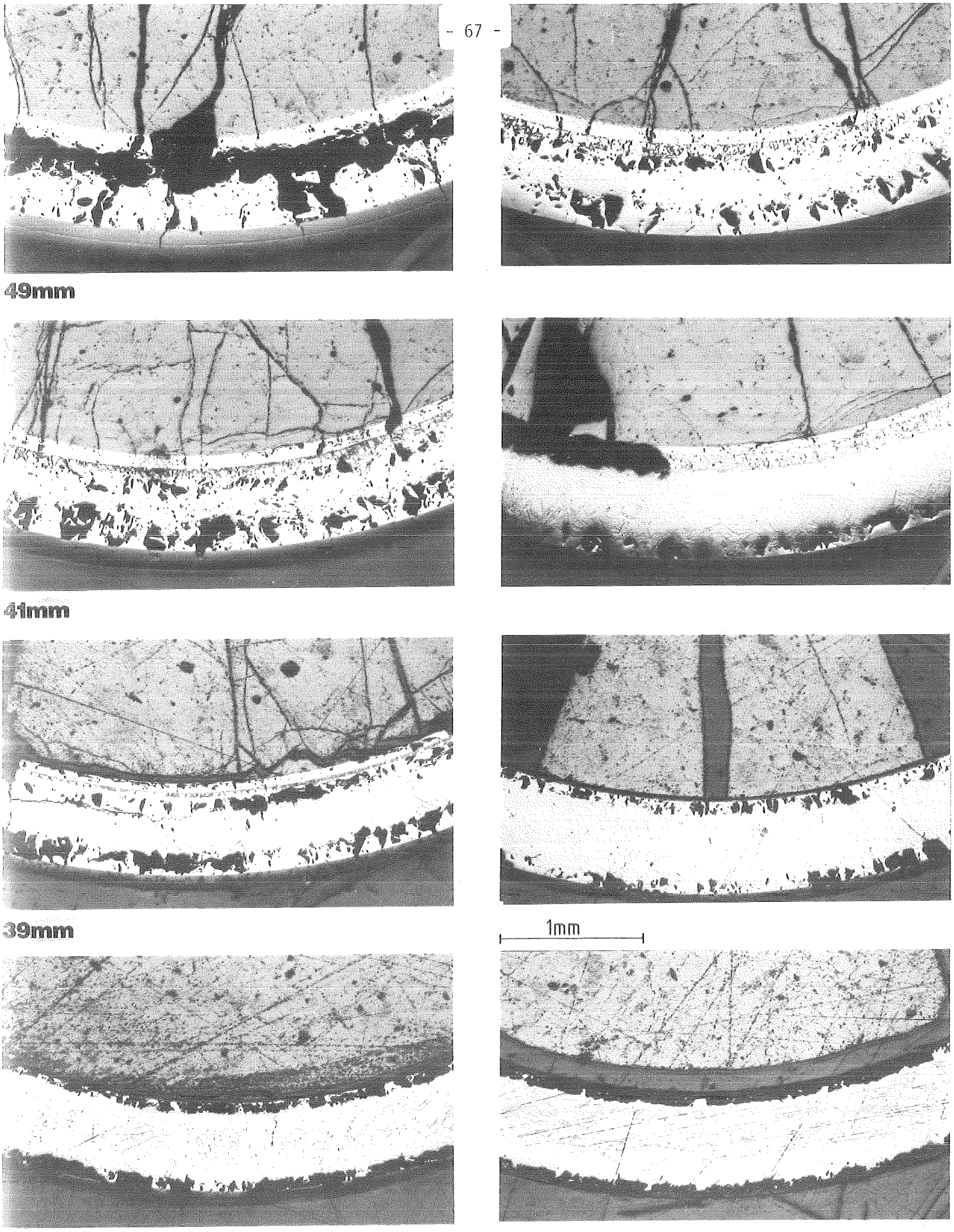

FIG.50: COMPARISON OF OPPOSITE SIDES OF SIDE ROD 6 AT VARIOUS ELEVATIONS. TEST ESBU-2A

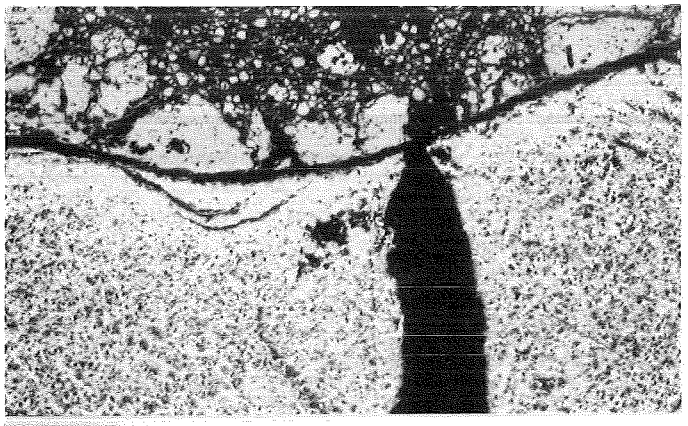

121mm

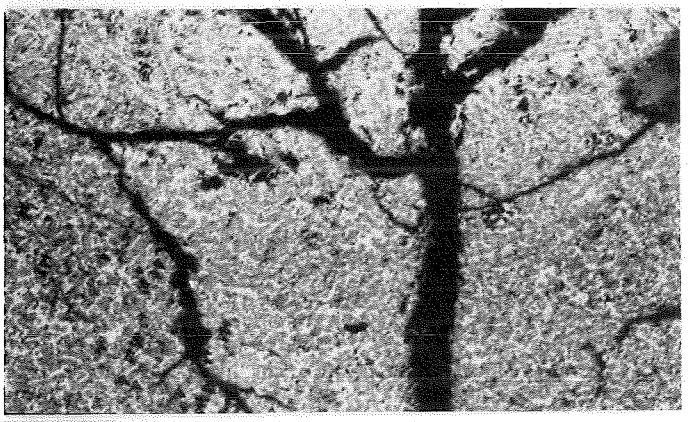

119mm

1mm

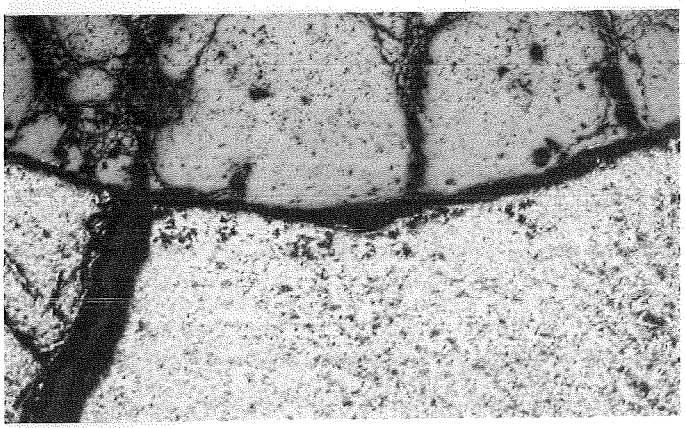

111mm

FIG.51: COMPARISON OF OPPOSITE SIDES OF CORNER ROD 9 AT VARIOUS ELEVATIONS. TEST ESBU-2A

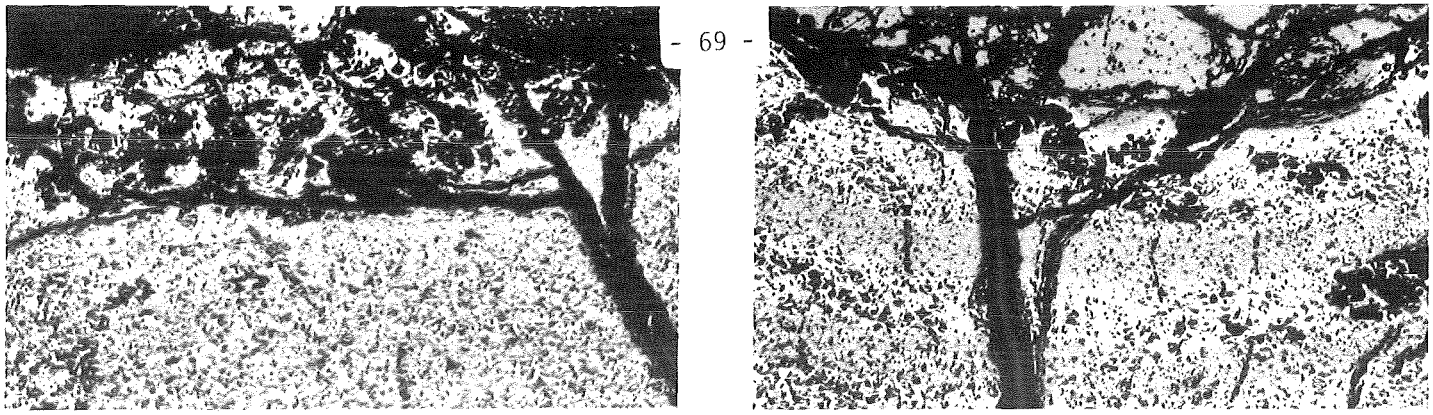

109mm

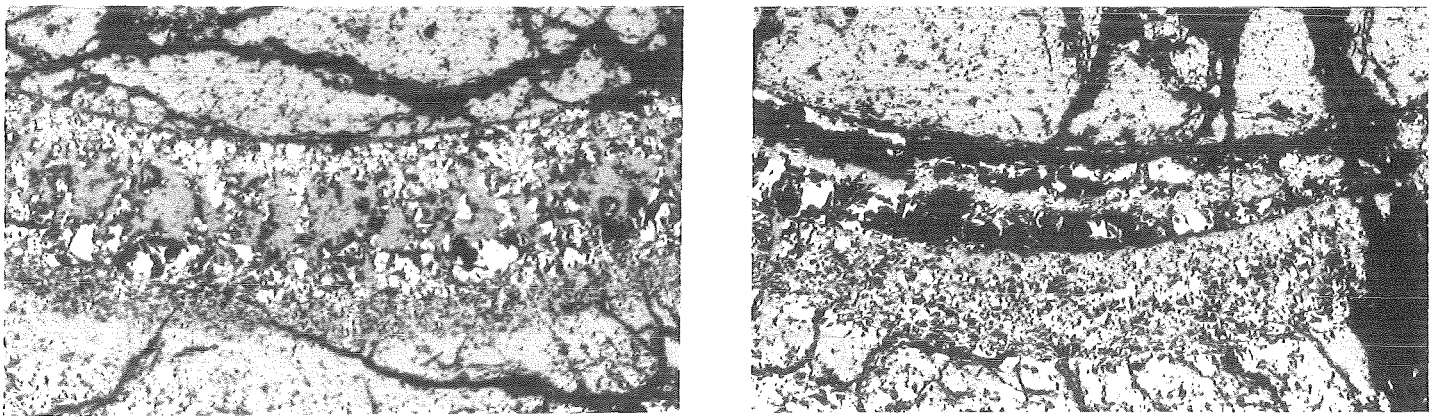

101mm

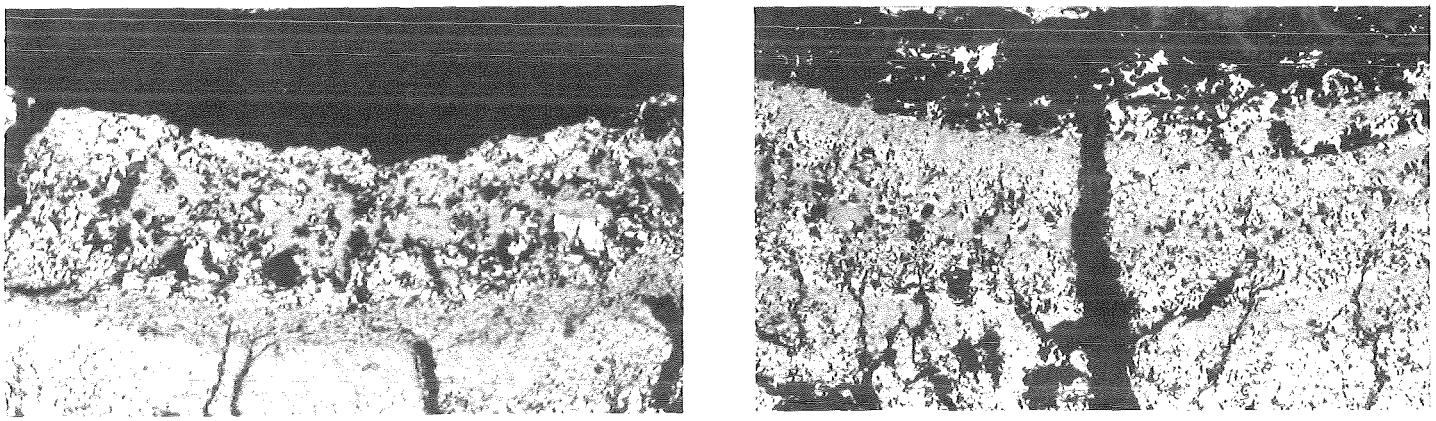

99mm

1mm

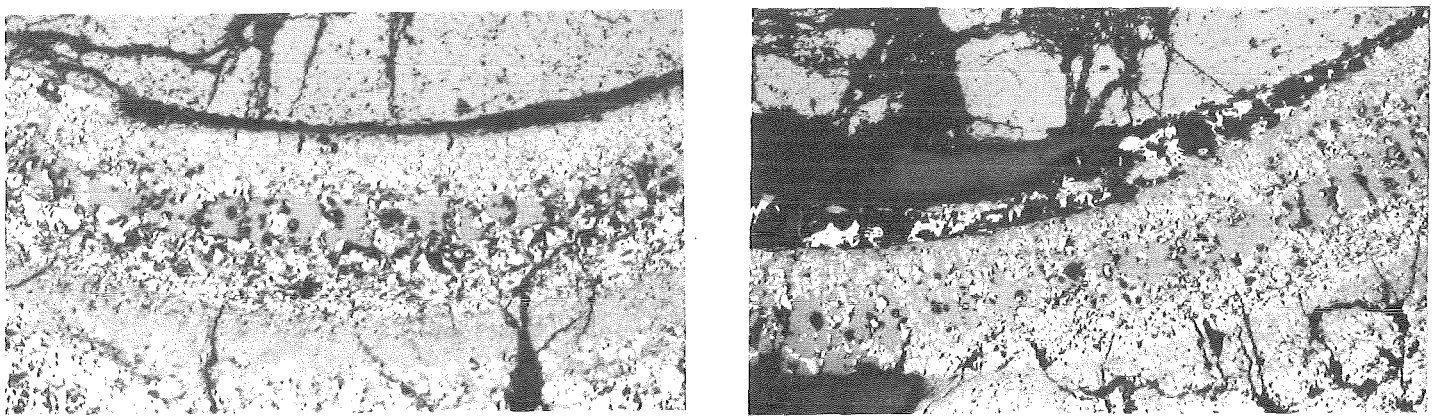

91mm

FIG.52: COMPARISON OF OPPOSITE SIDES OF CORNER ROD 9 AT VARIOUS ELEVATIONS. TEST ESBU-2A

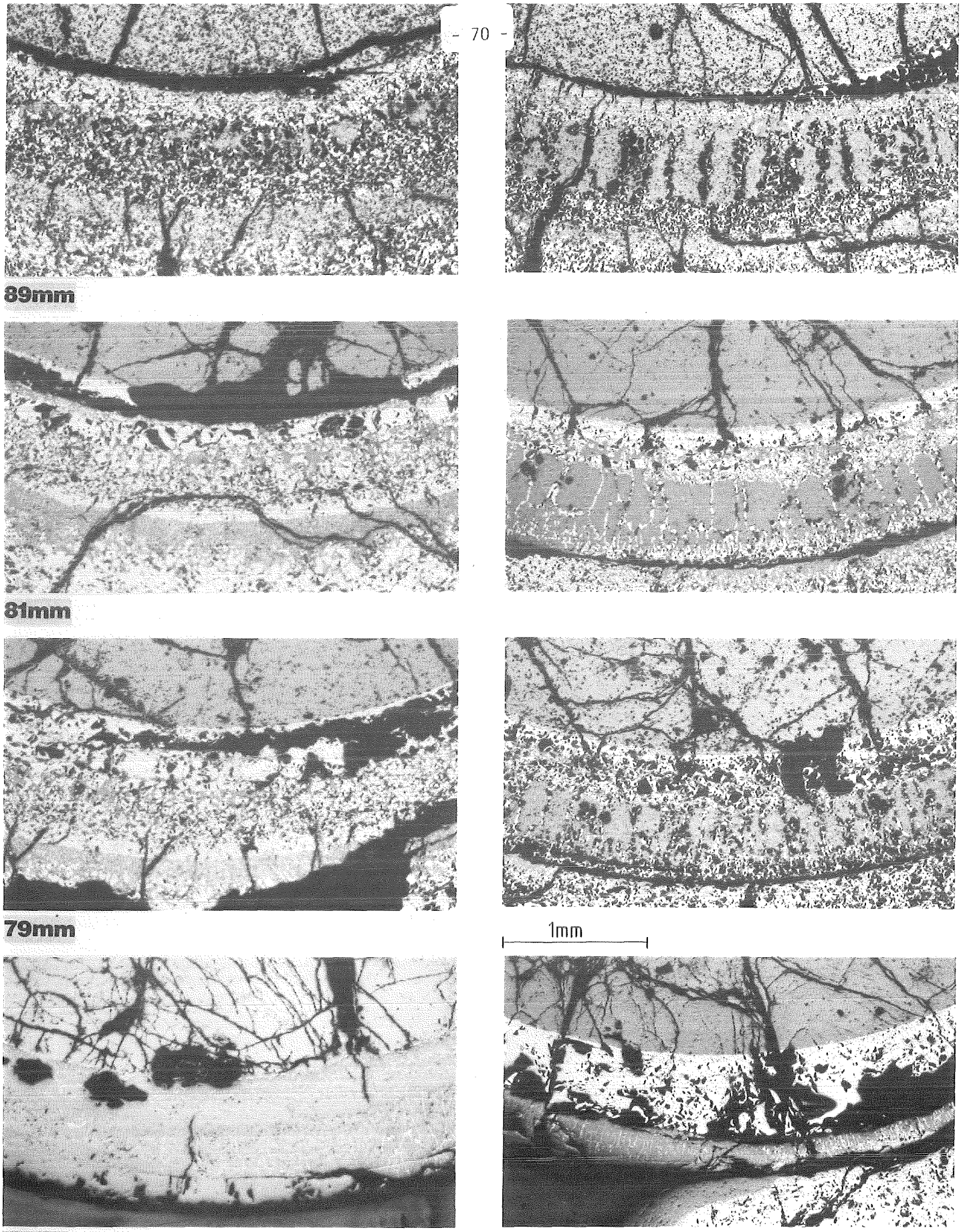

FIG.53: COMPARISON OF OPPOSITE SIDES OF CORNER ROD 9 AT VARIOUS ELEVATIONS. TEST ESBU-2A

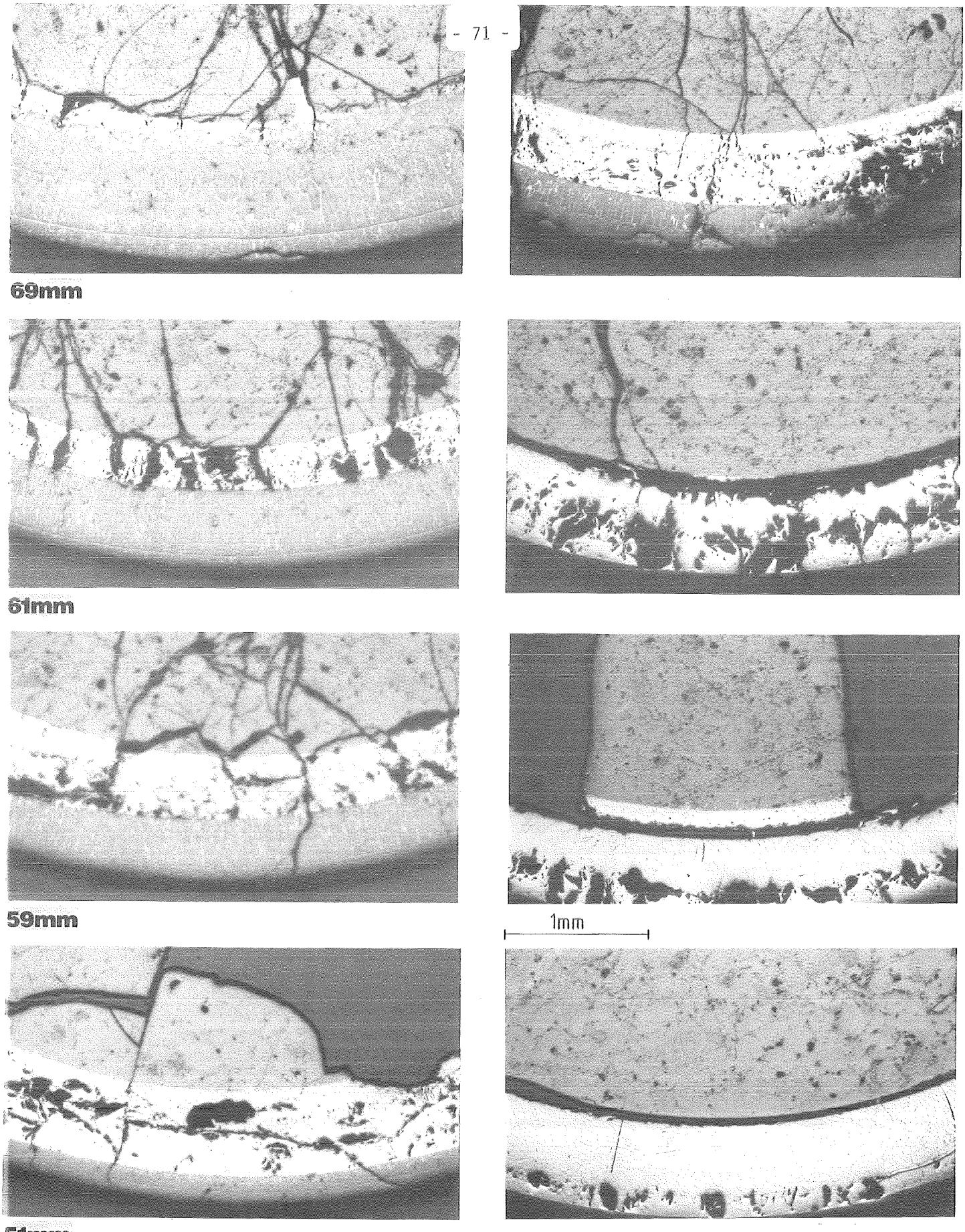

FIG.54: COMPARISON OF OPPOSITE SIDES OF CORNER ROD 9 AT VARIOUS ELEVATIONS. TEST ESBU-2A

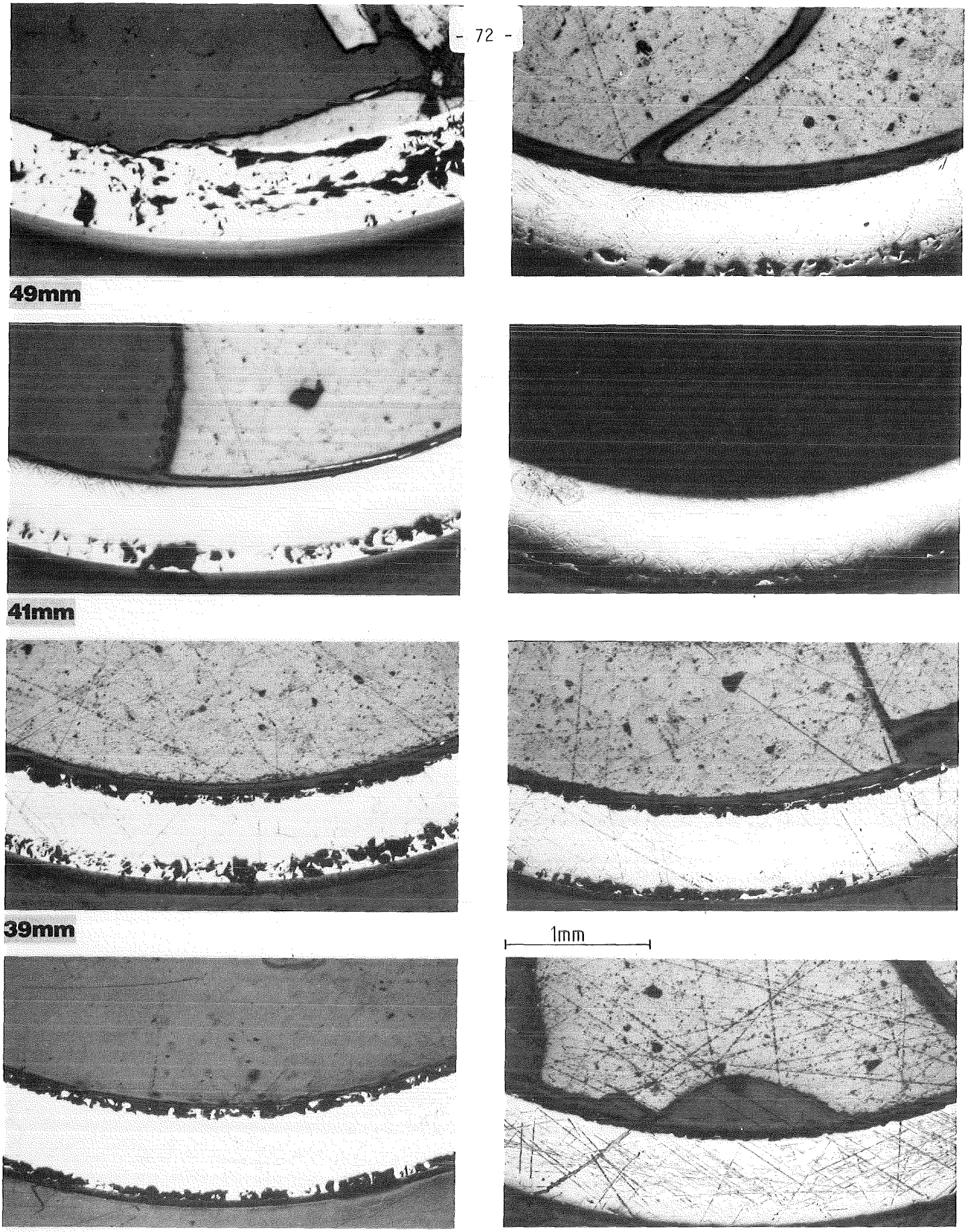

FIG.55: COMPARISON OF OPPOSITE SIDES OF CORNER ROD 9 AT VARIOUS ELEVATIONS. TEST ESBU-2A

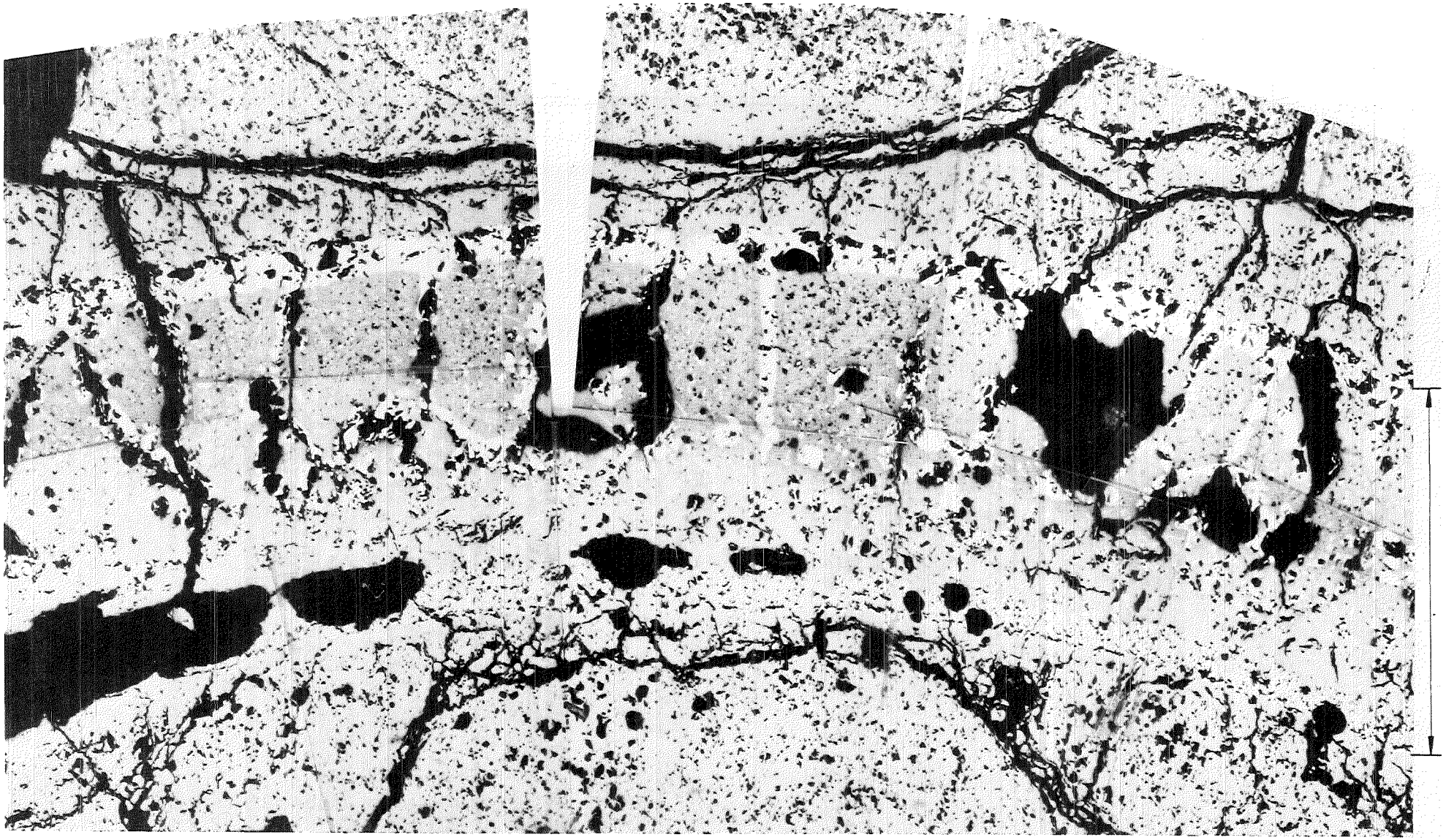

FIG. 56: INTERACTION OF MELT WITH FORMER OXIDIZED CLADDING OF CENTER ROD 5 AT 121 MM ELEVATION ESBU-2A.

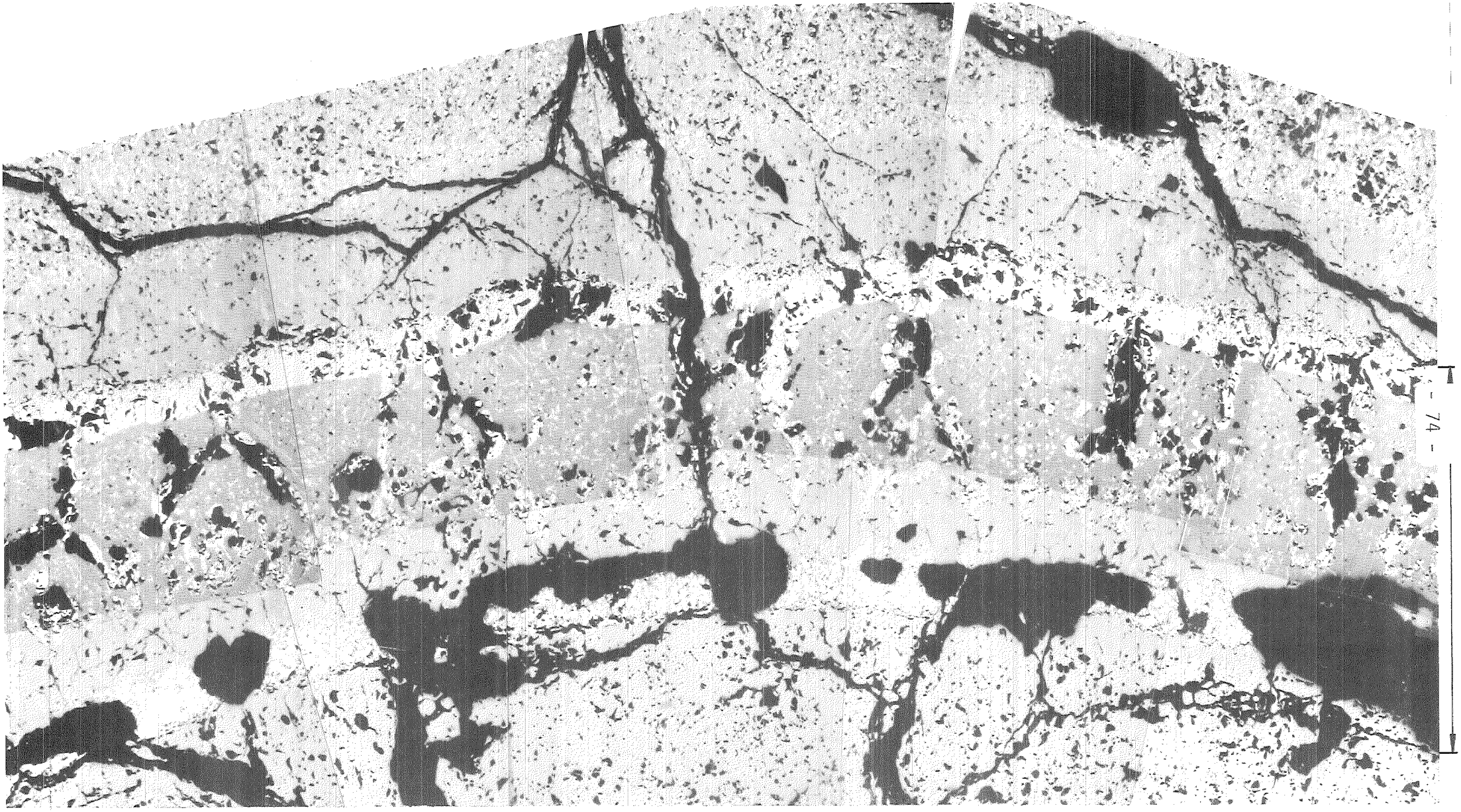

FIG.57: INTERACTION OF MELT WITH FORMER OXIDIZED CLADDING OF CENTER ROD 5 AT 119 MM ELEVATION ESBU-2A.

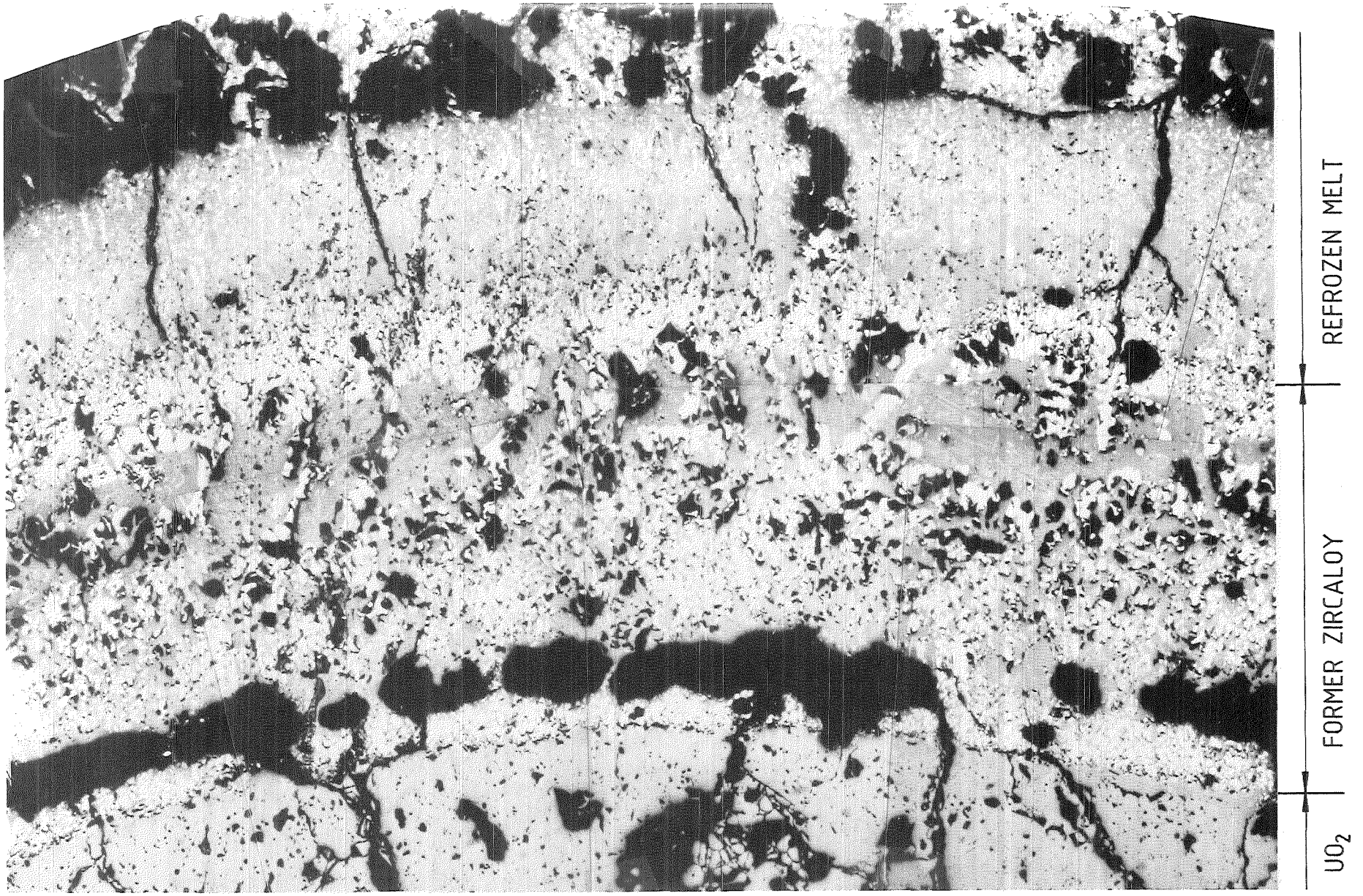

FIG.58: INTERACTION OF MELT WITH FORMER OXIDIZED CLADDING OF CENTER ROD 5 AT 111 MM ELEVATION ESBU-2A.

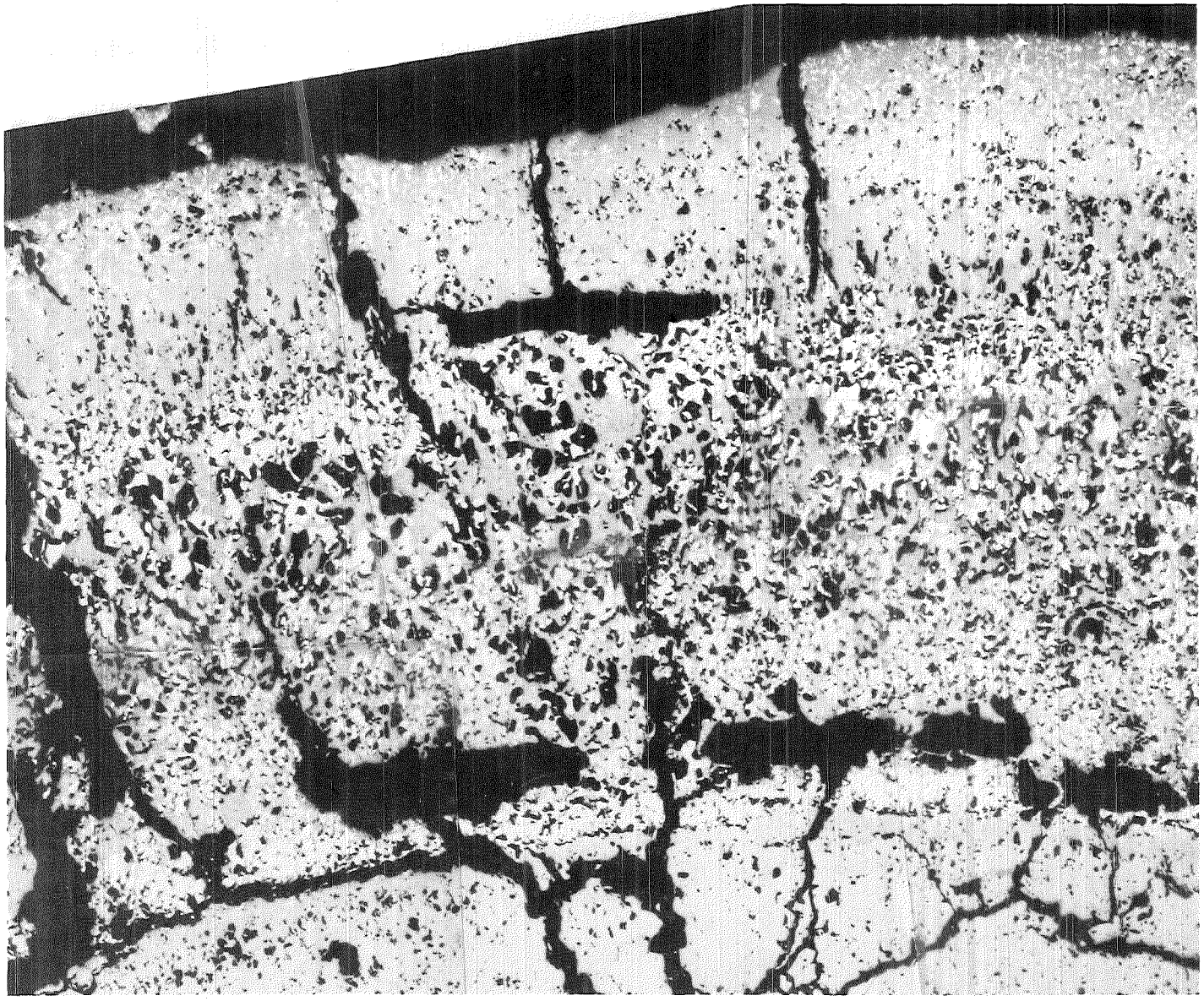

FIG.59: INTERACTION OF MELT WITH FORMER OXIDIZED CLADDING OF CENTER ROD 5 AT 109 MM ELEVATION ESBU-2A.

FIG.60: INTERACTION OF MELT WITH FORMER OXIDIZED CLADDING OF CENTER ROD 5 AT 101 MM ELEVATION ESBU-2A.

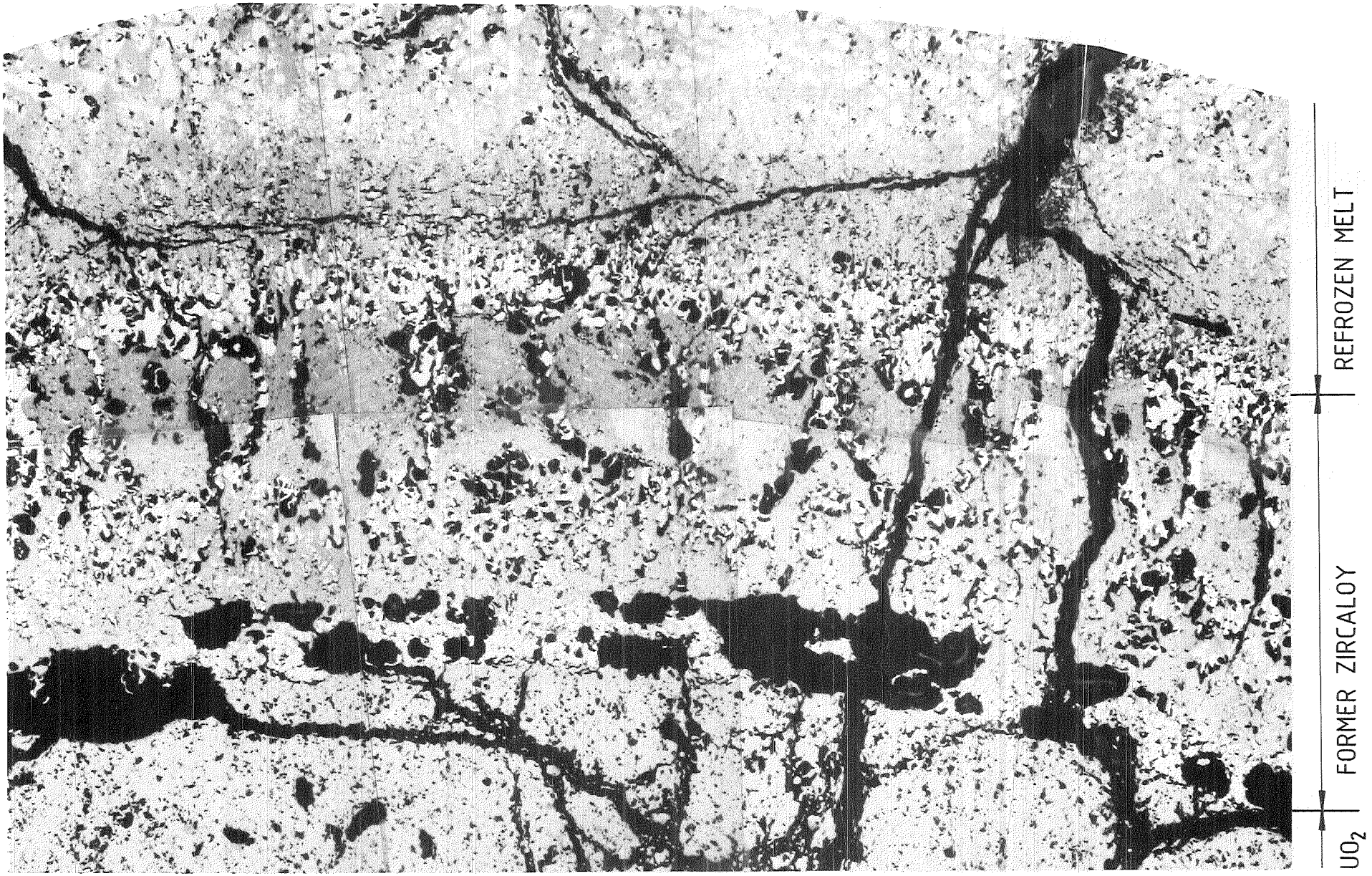

HAGEN ET AL. KFK-REPORT 3789

PNS KfK IT

FIG.61: INTERACTION OF MELT WITH FORMER OXIDIZED CLADDING OF CENTER ROD 5 AT 91 MM ELEVATION ESBU-2A.

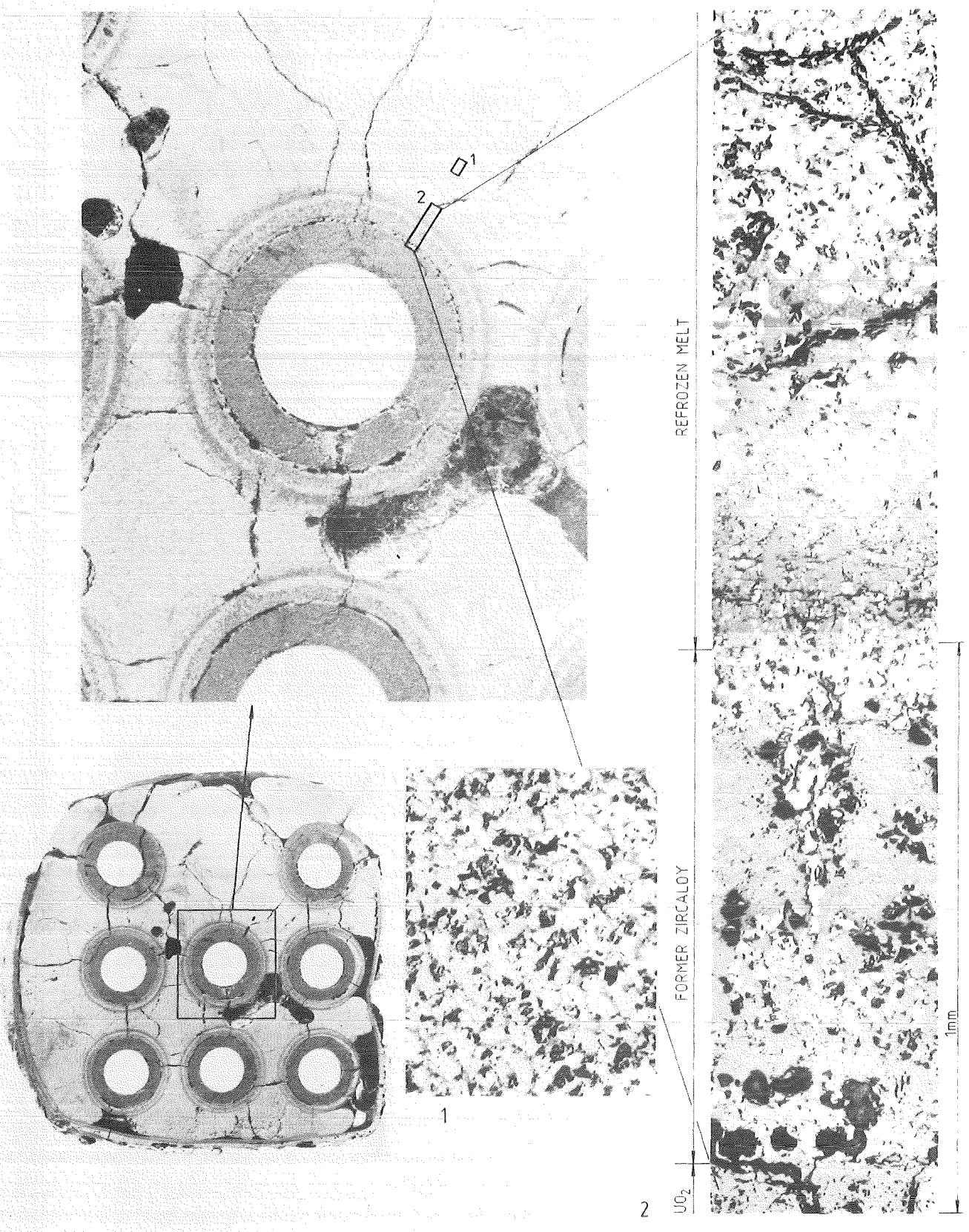

HAGEN ET AL. KfK-REPORT 3789

FIG.61a: Details of Cross Section at 91mm Elevation from Test ESBU-2A

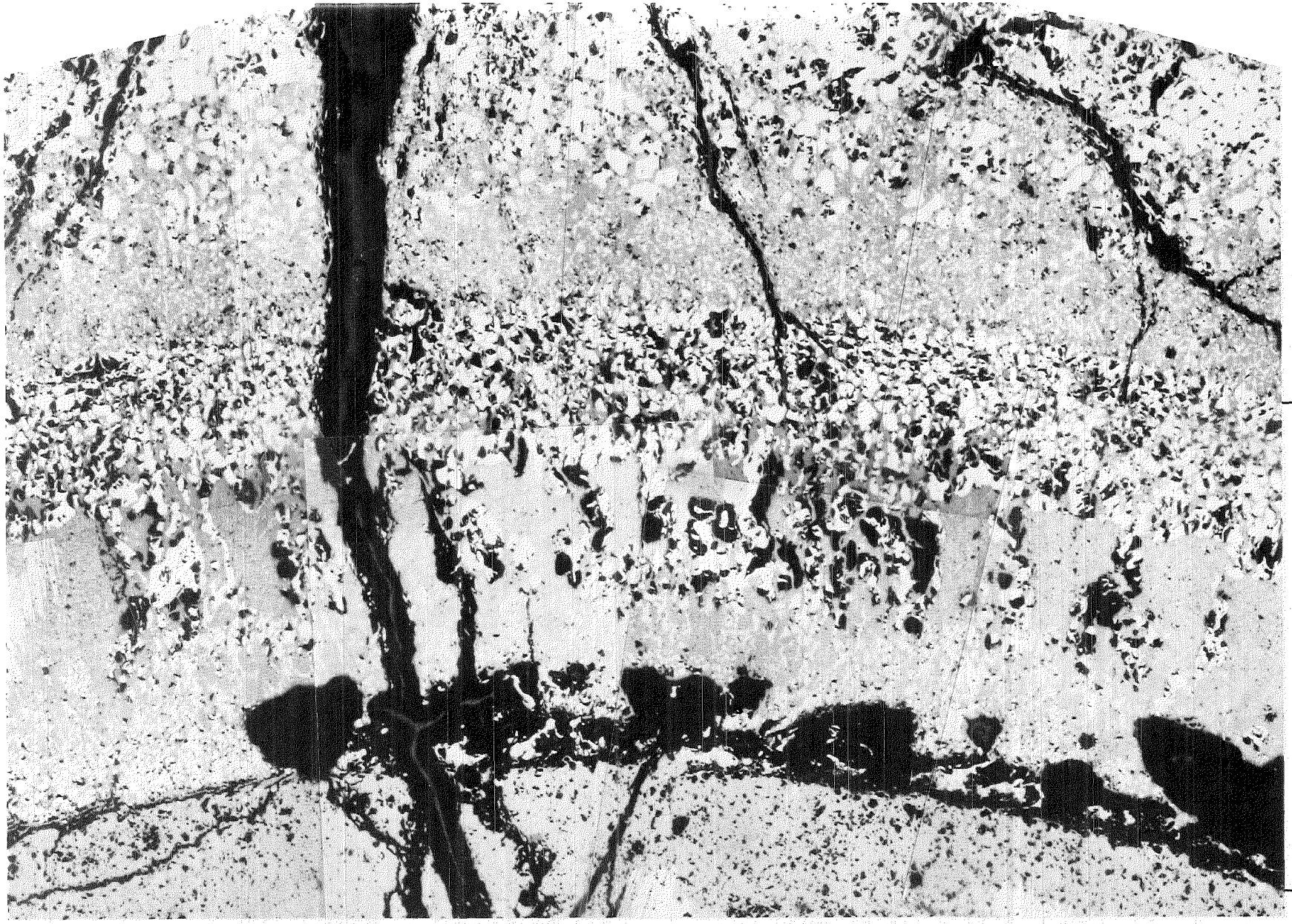

HAGEN ET AL. KFK-REPORT 3789

PNS KfK IT

FIG.62: INTERACTION OF MELT WITH FORMER OXIDIZED CLADDING OF CENTER ROD 5 AT 81 MM ELEVATION ESBU-2A.

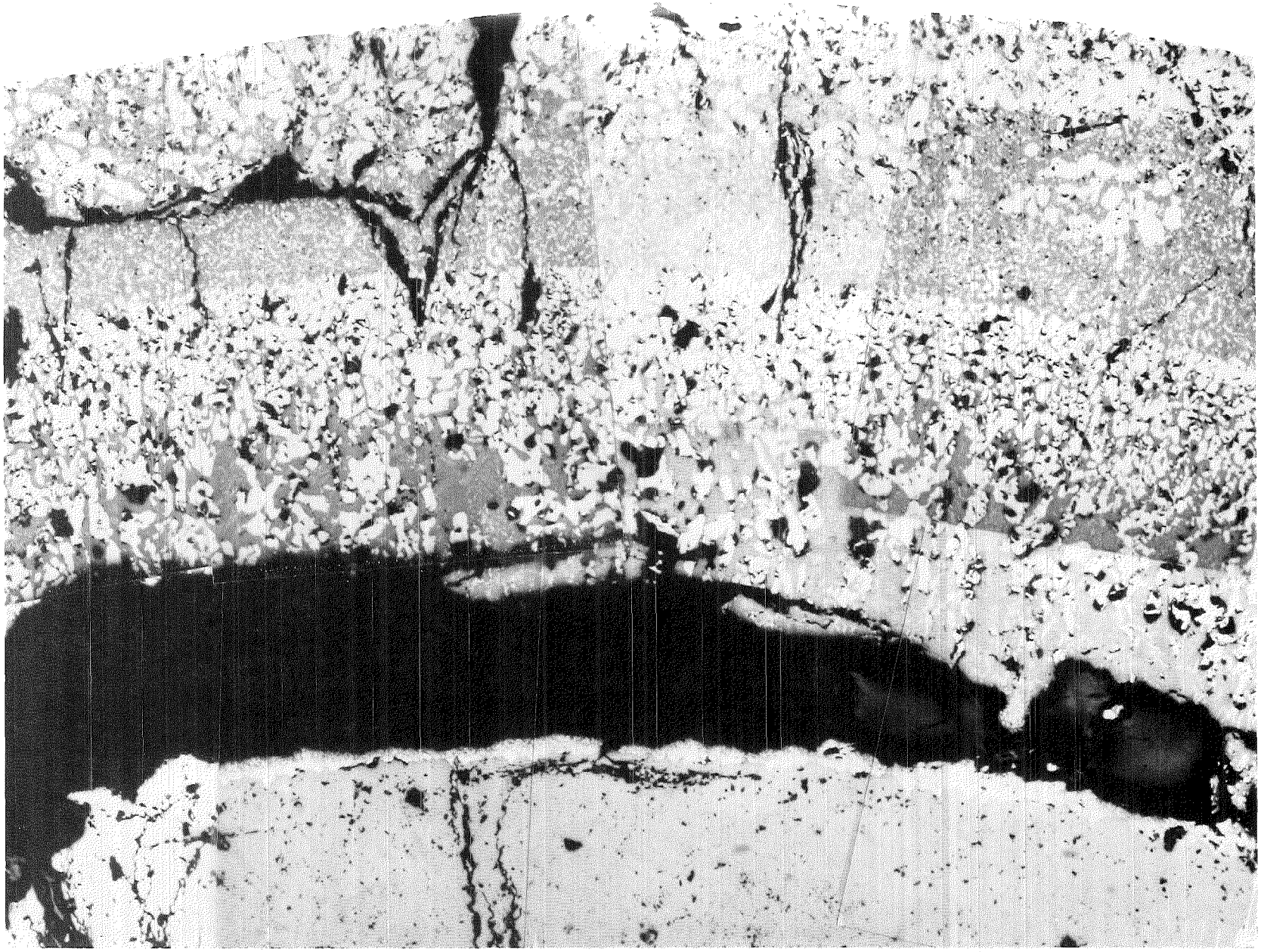

FIG.63: INTERACTION OF MELT WITH FORMER OXIDIZED CLADDING OF CENTER ROD 5 AT 79 MM ELEVATION ESBU-2A.

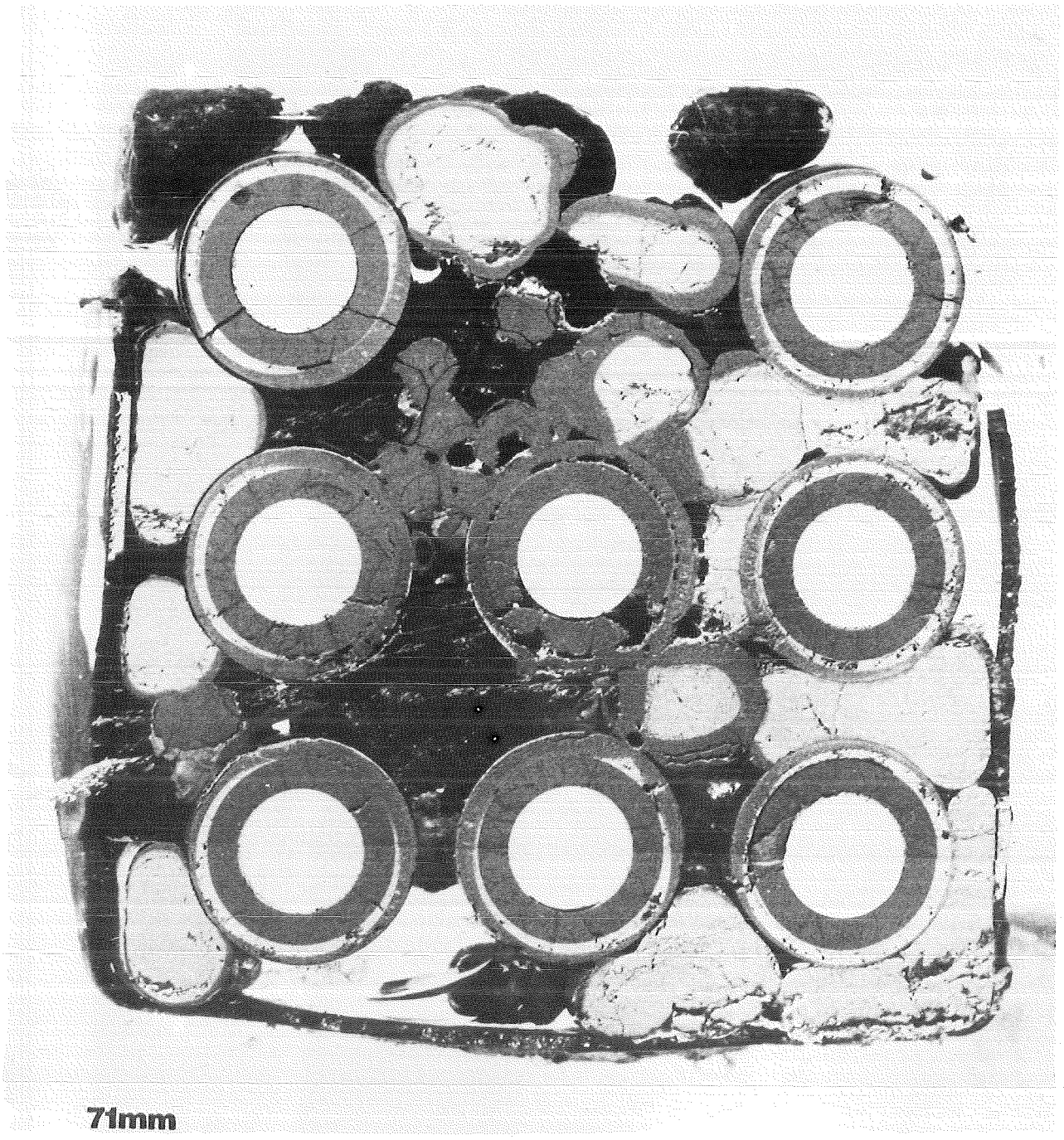

Fig. 64: Cross Section of ESBU-2A demonstrating the azimutal differences of the cladding oxidation

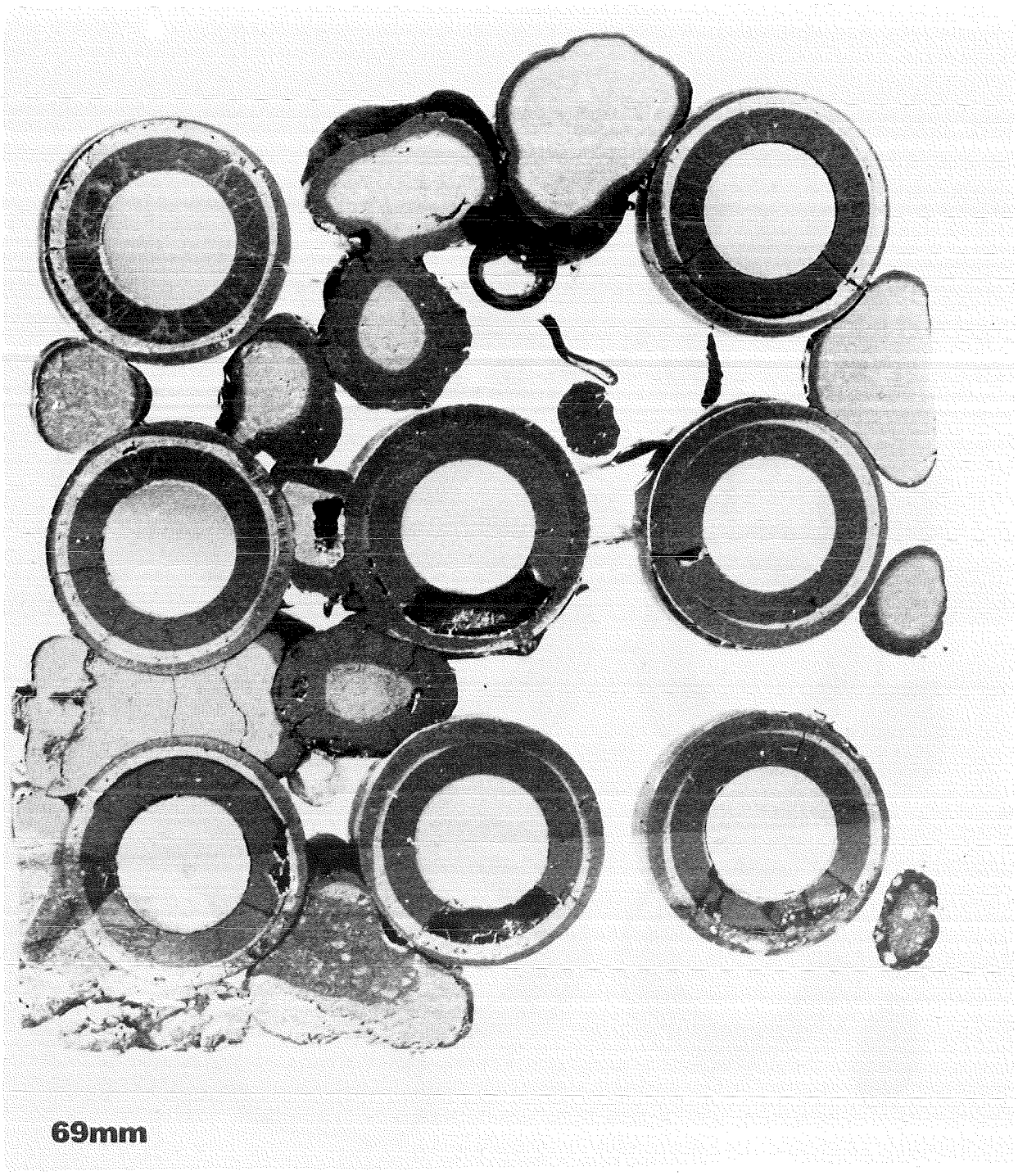

Fig. 65: Cross Section of ESBU-2A demonstrating the azimutal differences of the cladding oxidation

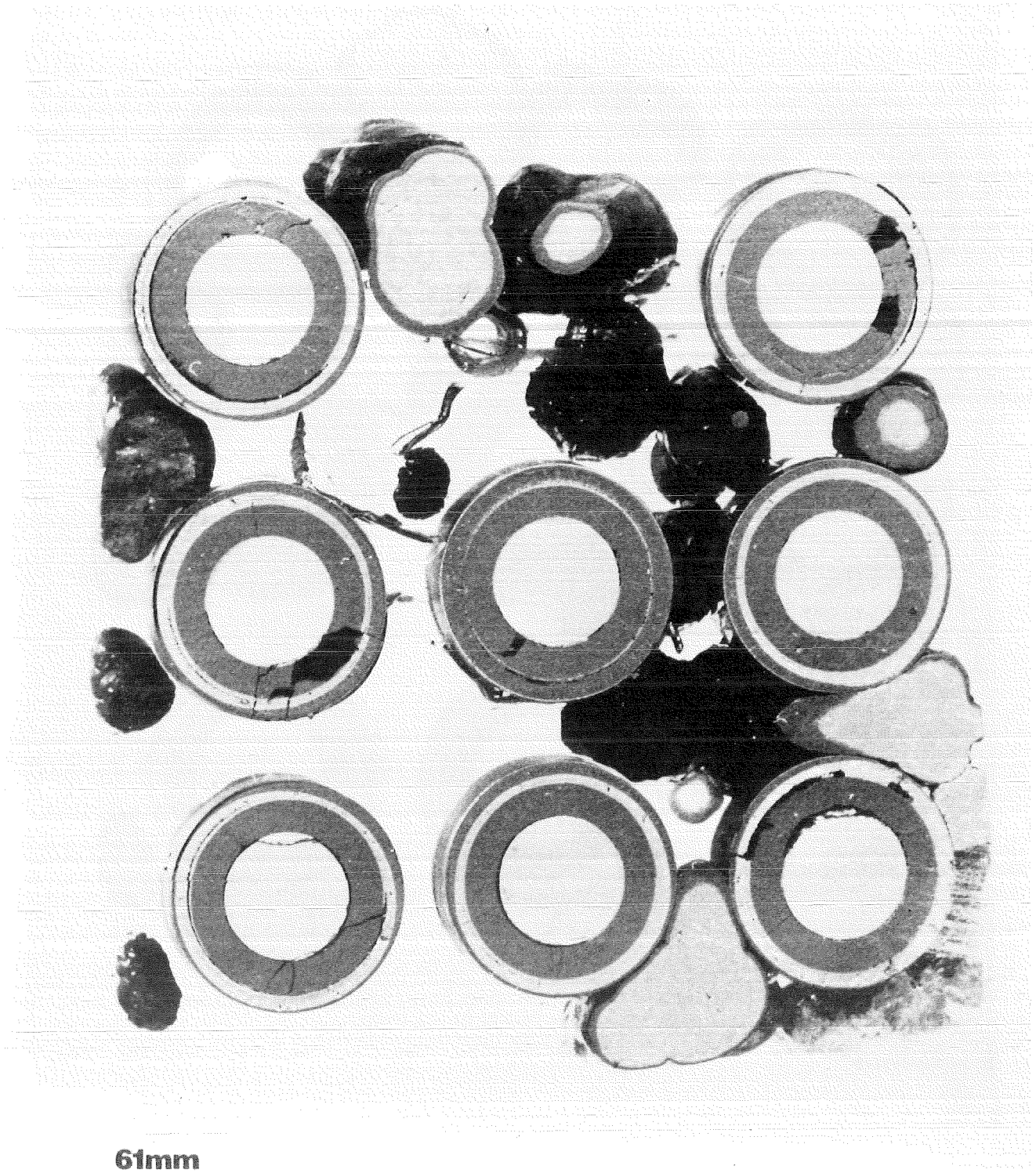

Fig. 66: Cross Section of ESBU-2A demonstrating the azimutal differences of the cladding oxidation

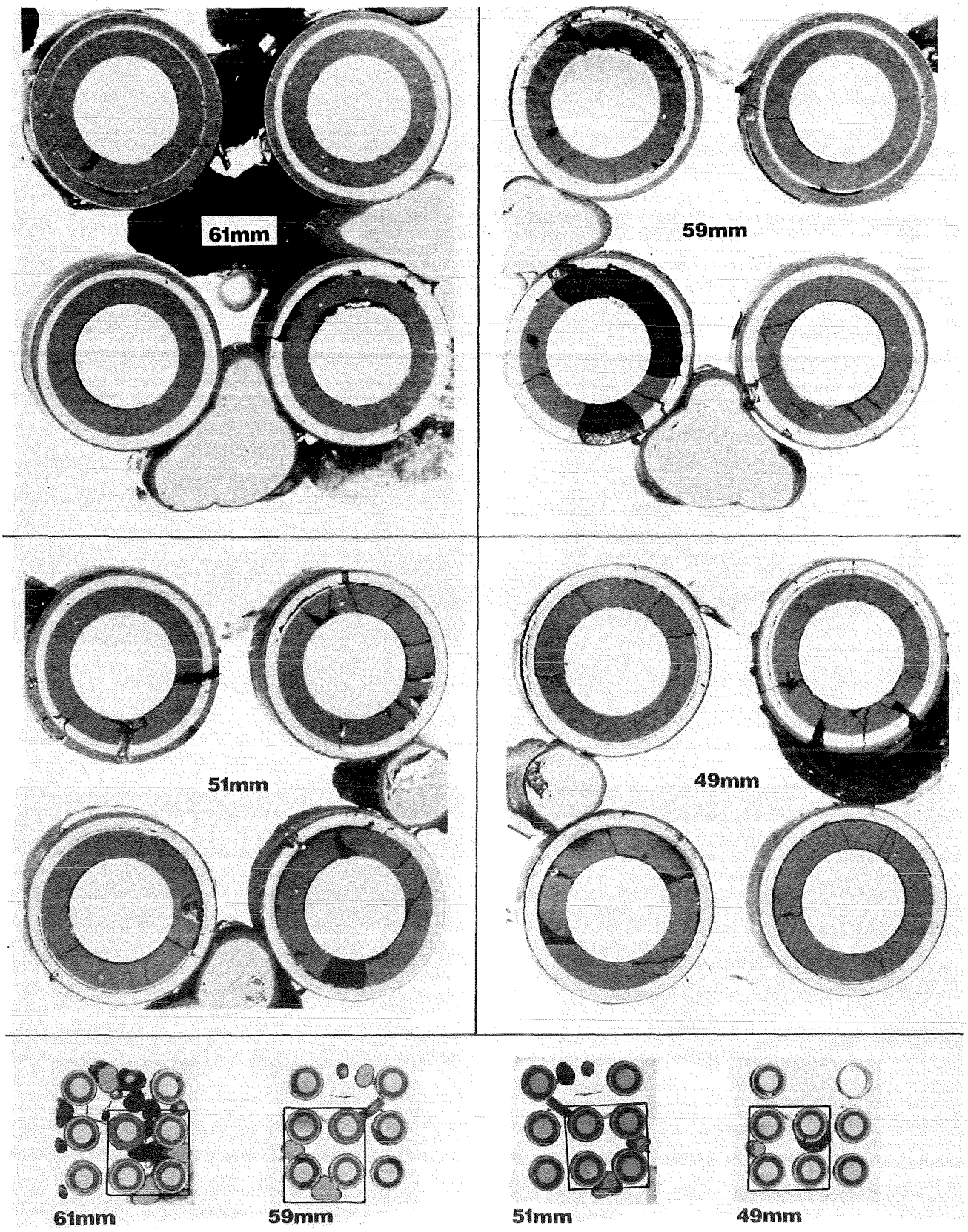

Fig. 67: Comparison of oxidation of cladding and melt for ESBU-2A

Fig. 68 : Details of Cross Section at 71 mm above bundle bottom of ESBU-2A

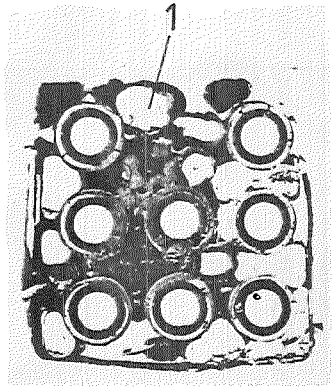

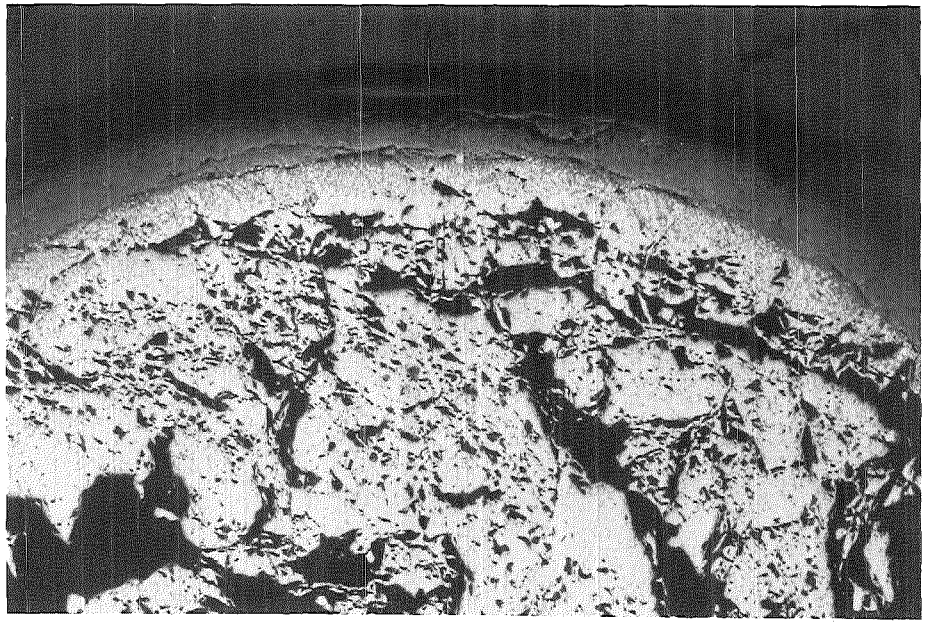

Outer region of droplet 1

25×

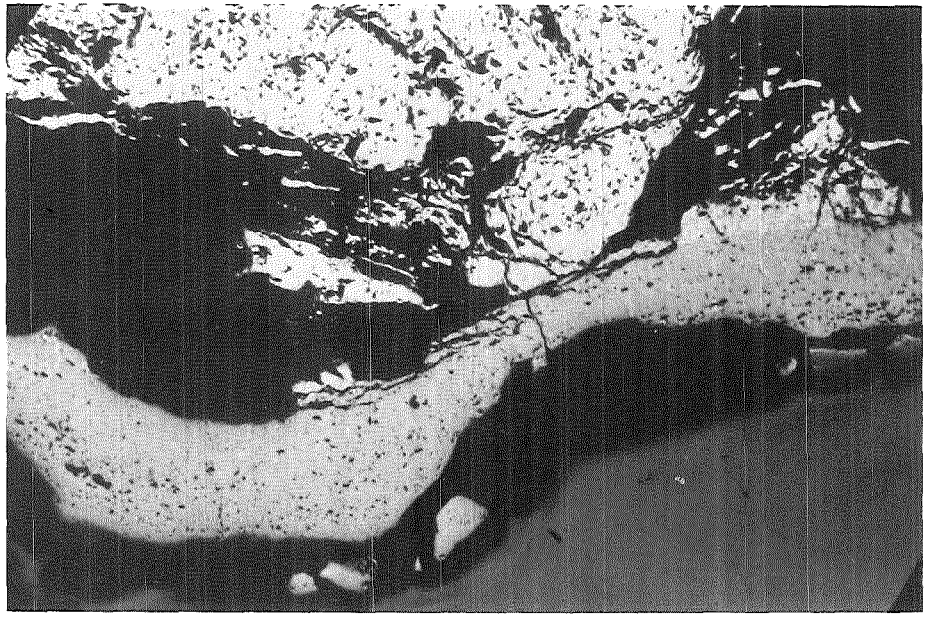

Inner region of droplet 1

200×

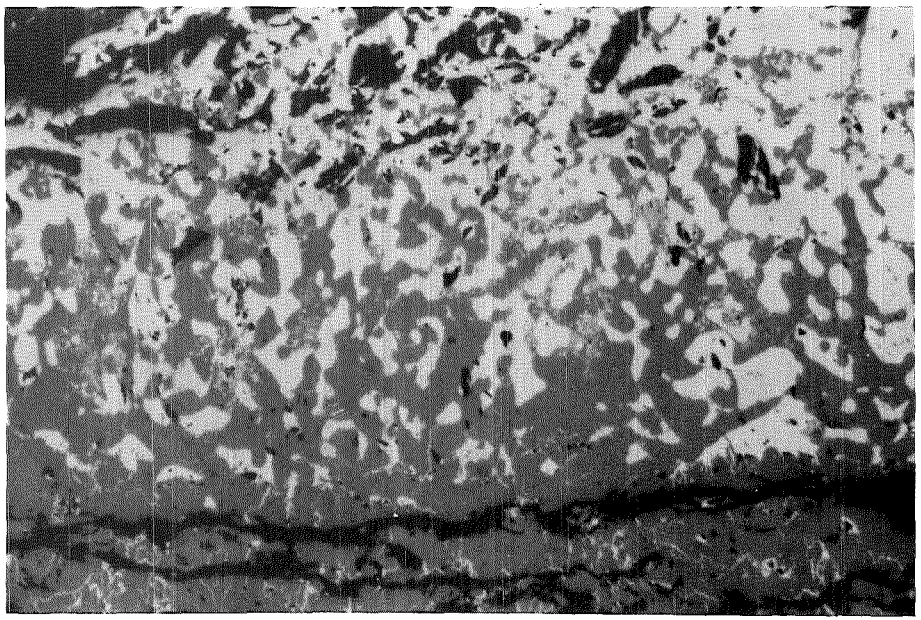

Transition of oxidized to unoxidized region

Fig. 69 : Details of Cross Section at 71mm above bundle bottom of ESBU-2A

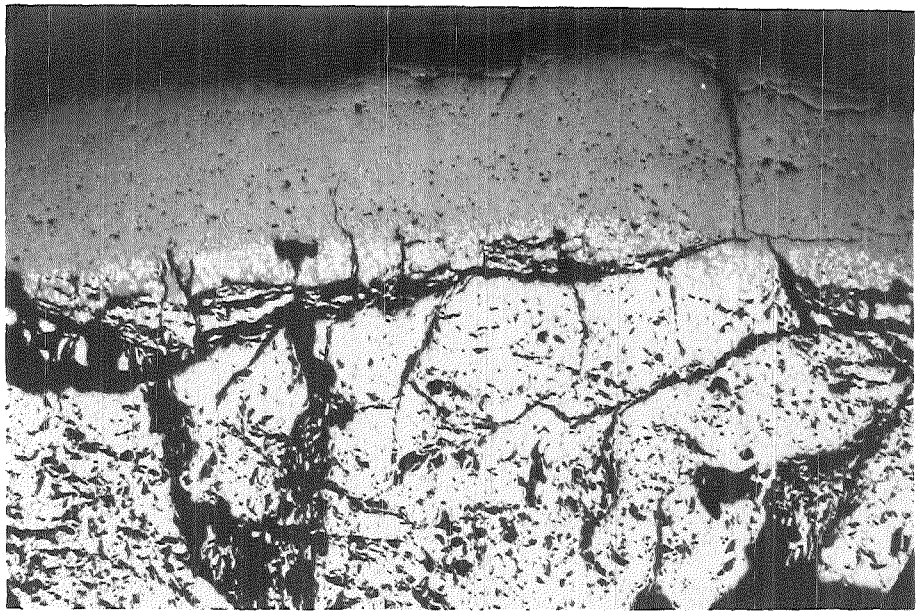

Outer region of droplet 2

25×

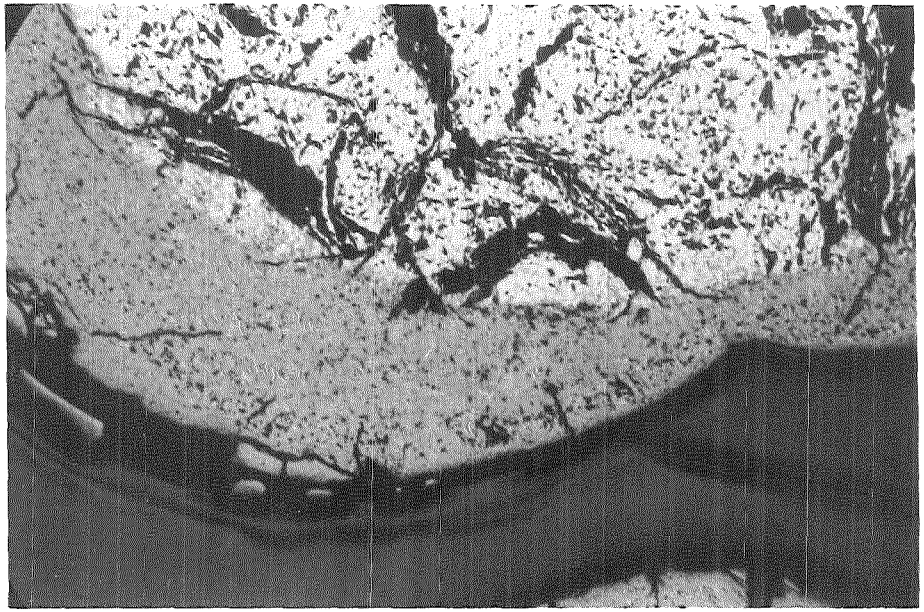

Inner region of droplet 2

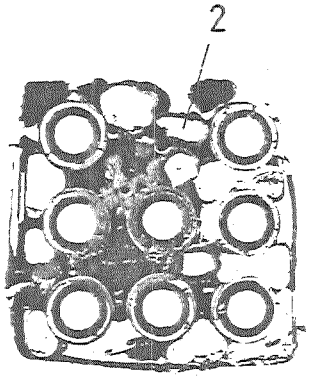

200×

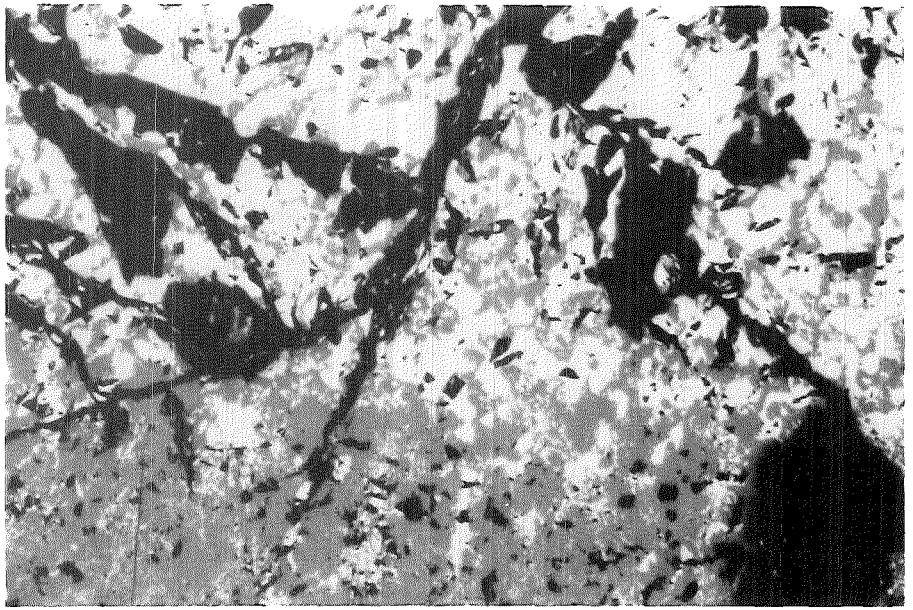

Transition of oxidized to unoxidized region

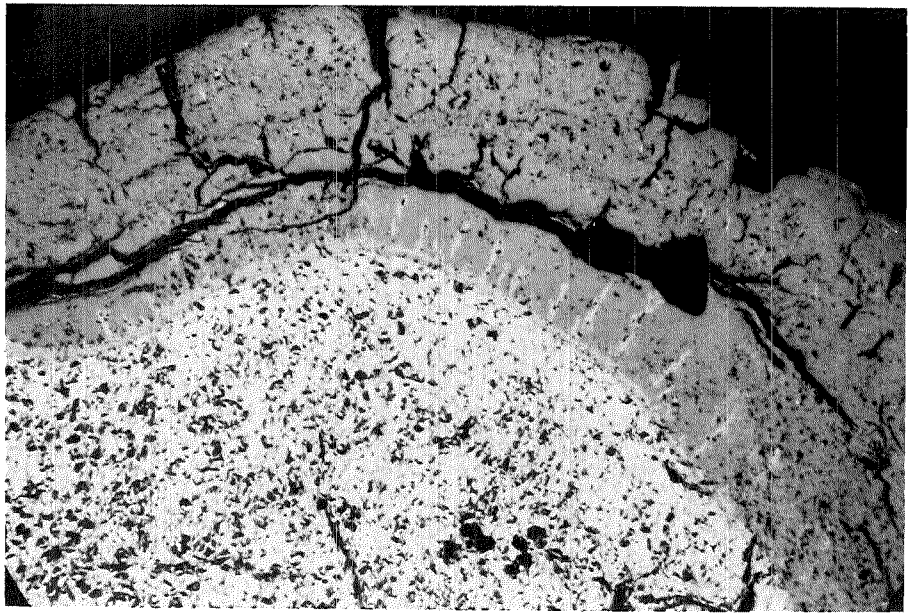

Outer region of droplet 3

25×

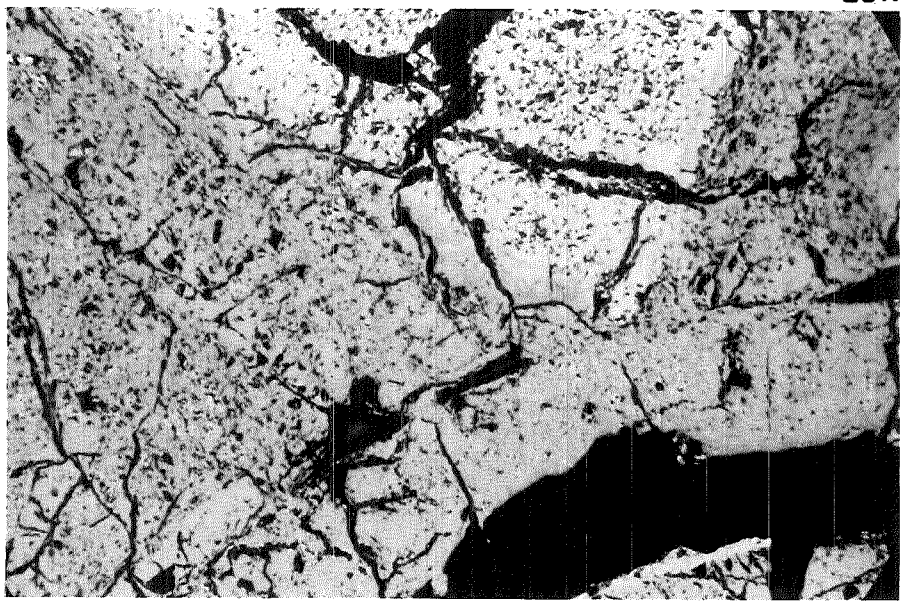

Inner region of droplet 3

Fig. 70 : Details of Cross Section at 71 mm above bundle bottom of ESBU-2A

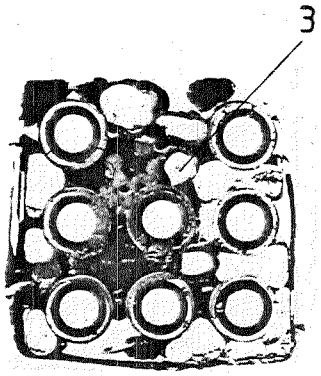

Fig. 71: Details of Cross Section at 71mm above bundle bottom of ESBU-2A

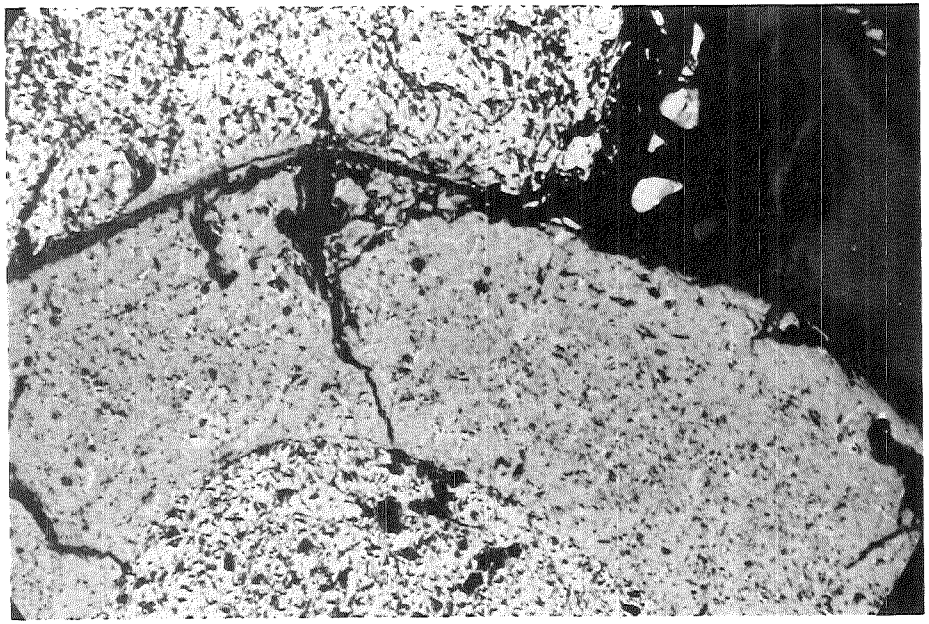

Outer region of droplet 4

25×

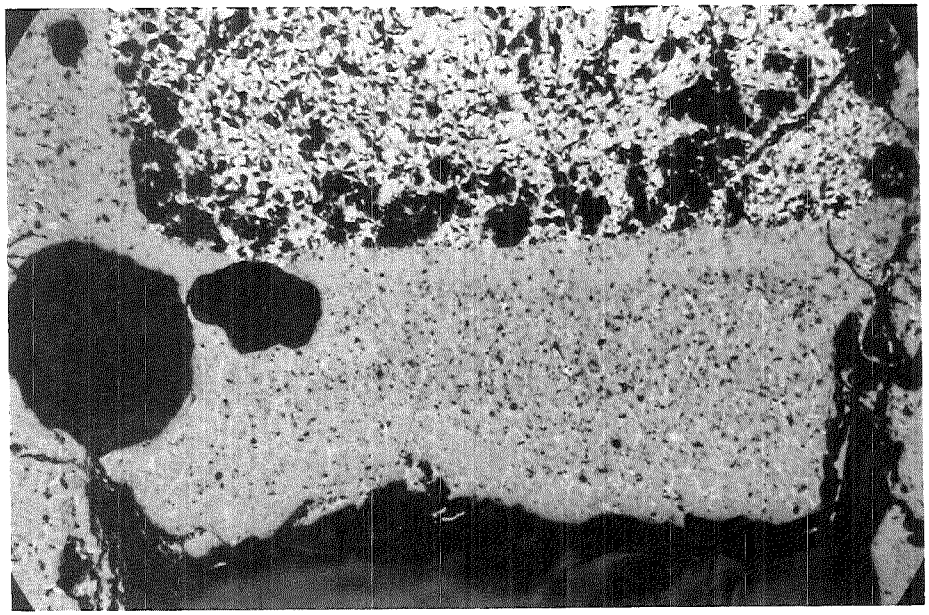

Inner region of droplet 4

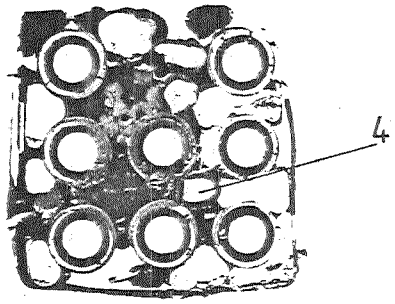

200×

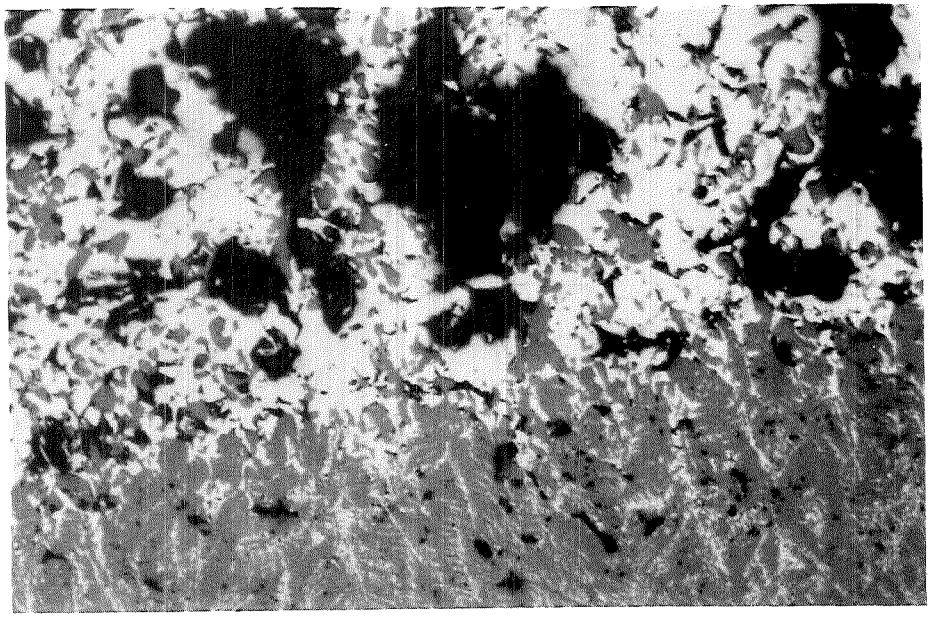

Transition of oxidized to unoxidized region

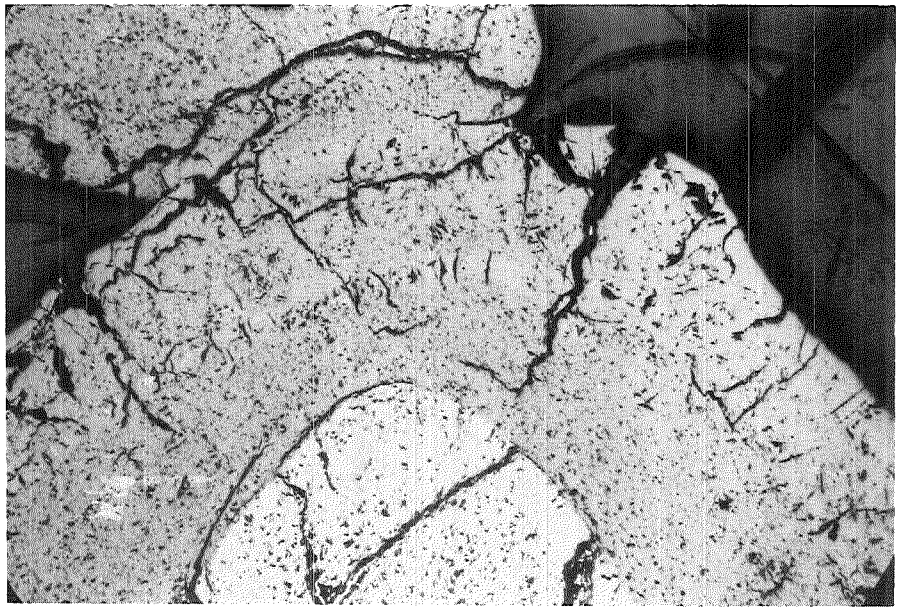

Outer region of droplet 1

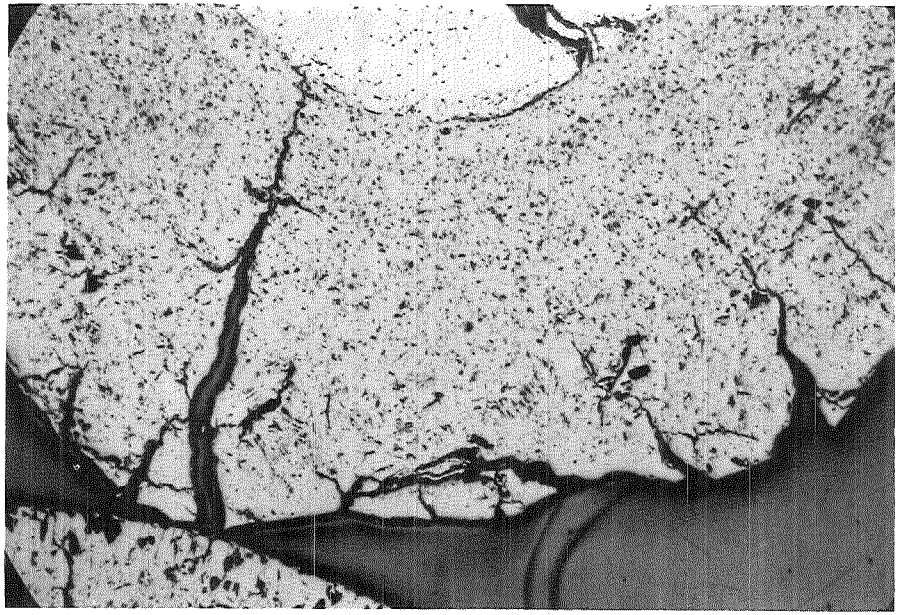

Inner region of droplet 1

Fig. 72 : Details of Cross Section at 69 mm above bundle bottom of ESBU-2A

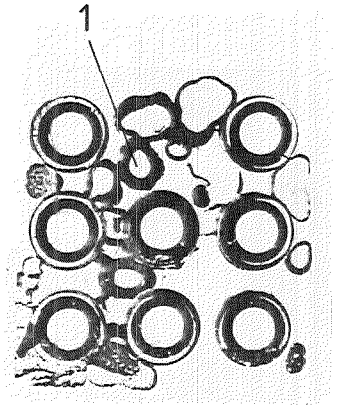

Fig. 73 : Details of Cross Section at 69 mm above bundle bottom of ESBU-2A

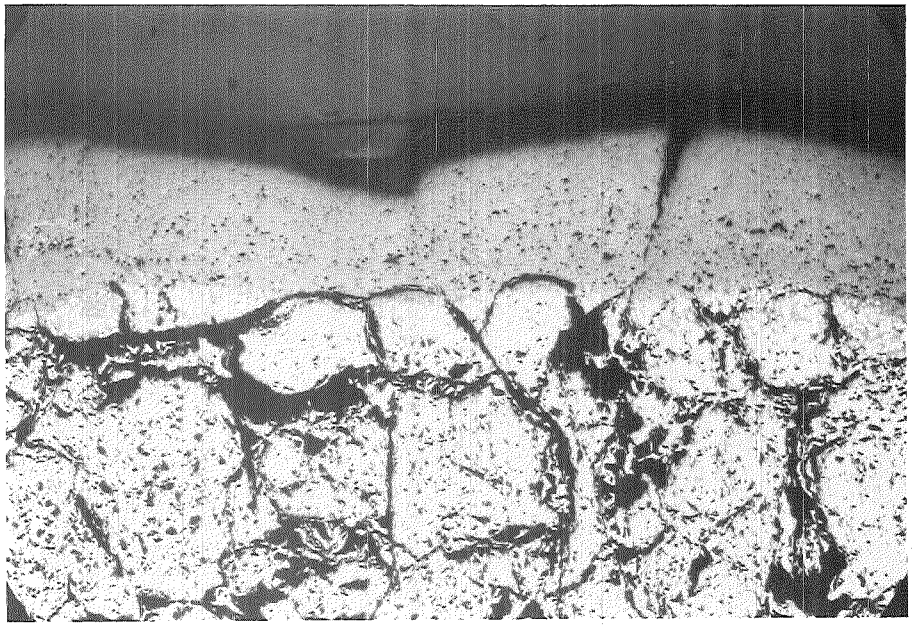

Outer region of droplet 2

25×

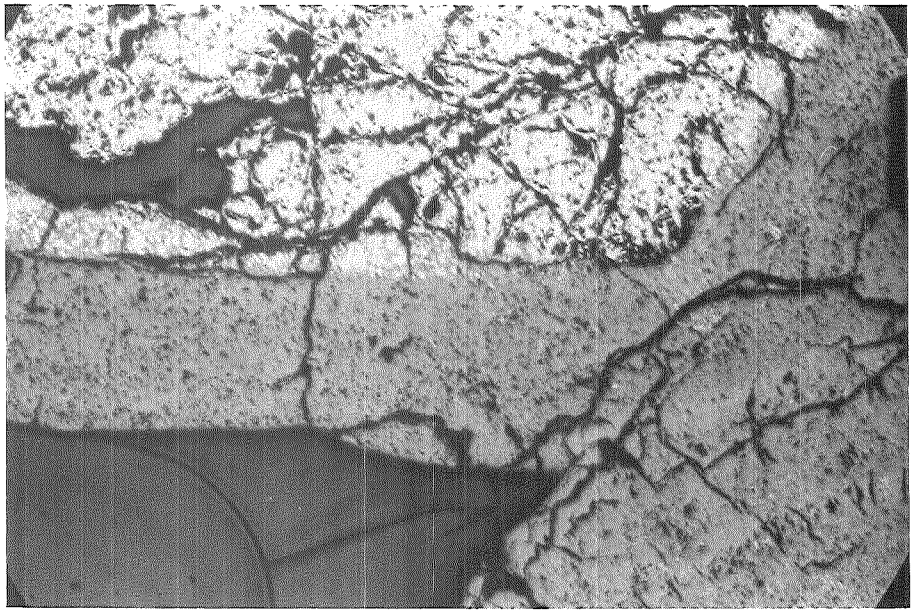

Inner region of droplet 2

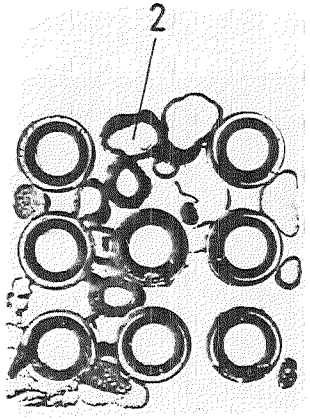

200×

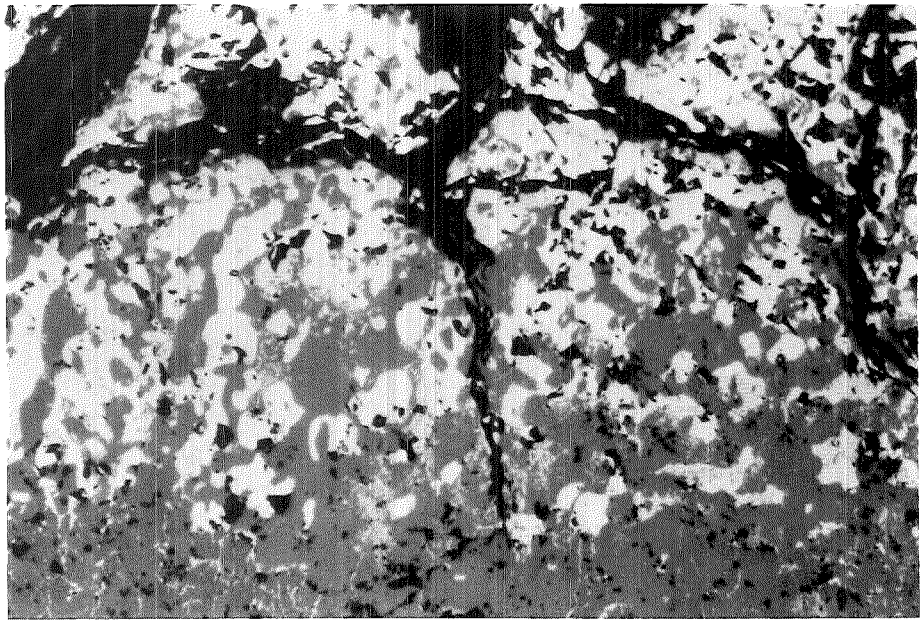

Transition of oxidized to unoxidized region

Fig. 74: Details of Cross Section at 69 mm above bundle bottom of ESBU-2A

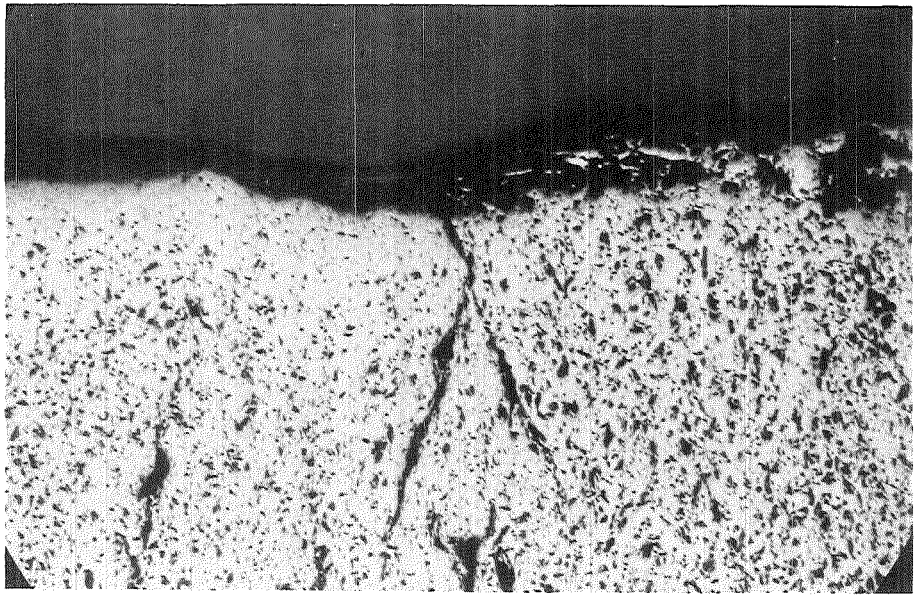

Outer region of droplet 3

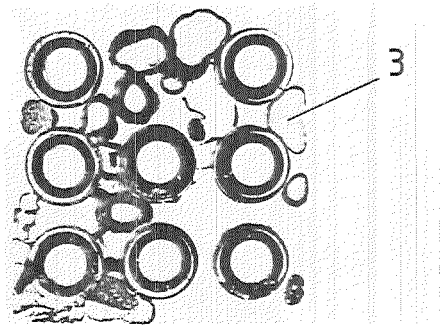

25×

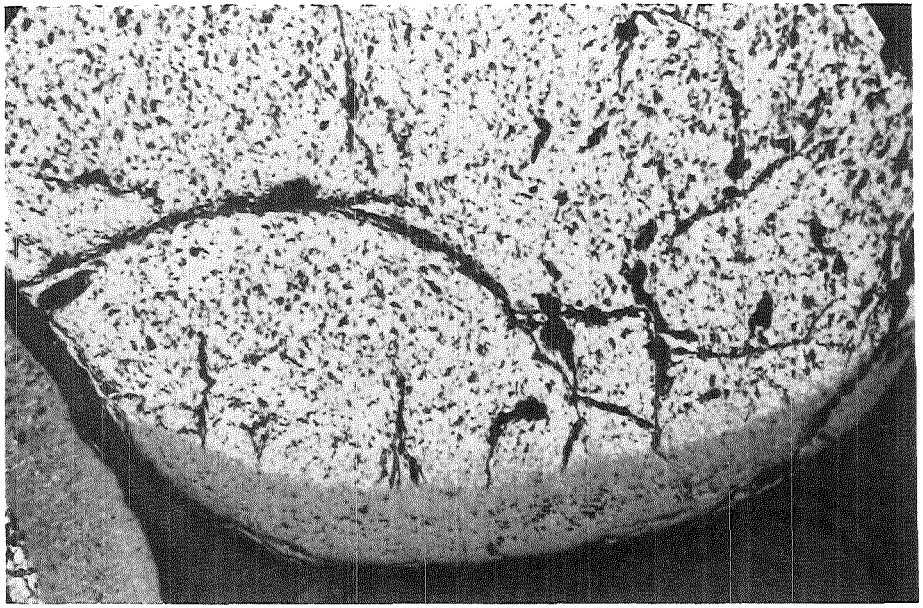

Inner region of droplet 3

200×

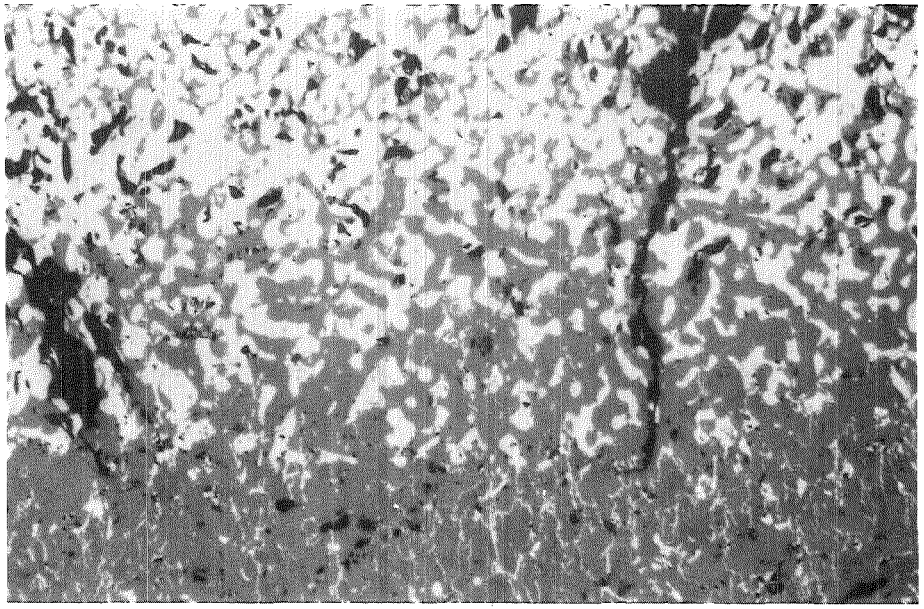

Transition of oxidized to unoxidized region

Fig. 75: Details of Cross Section at 69 mm above bundle bottom of ESBU-2A

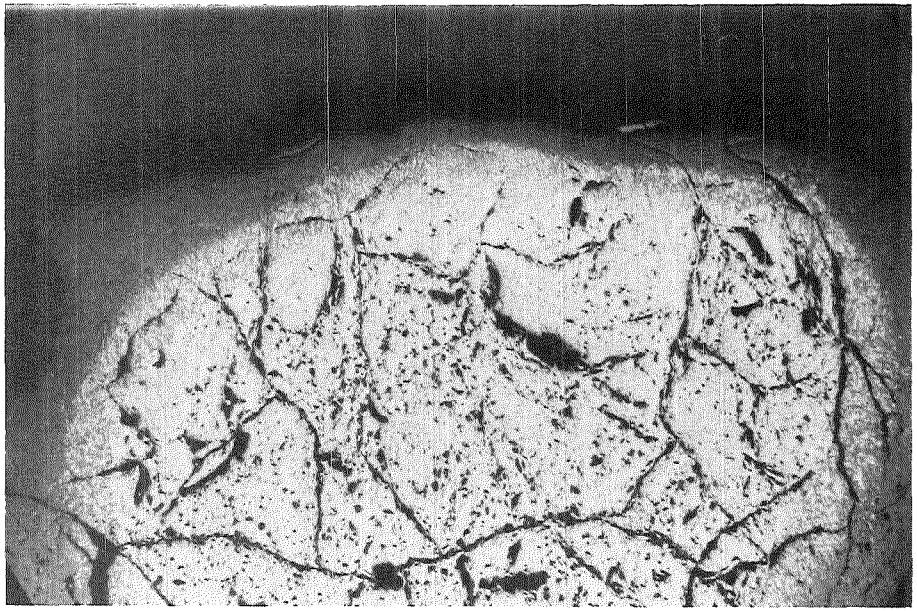

Outer region of droplet 4

25×

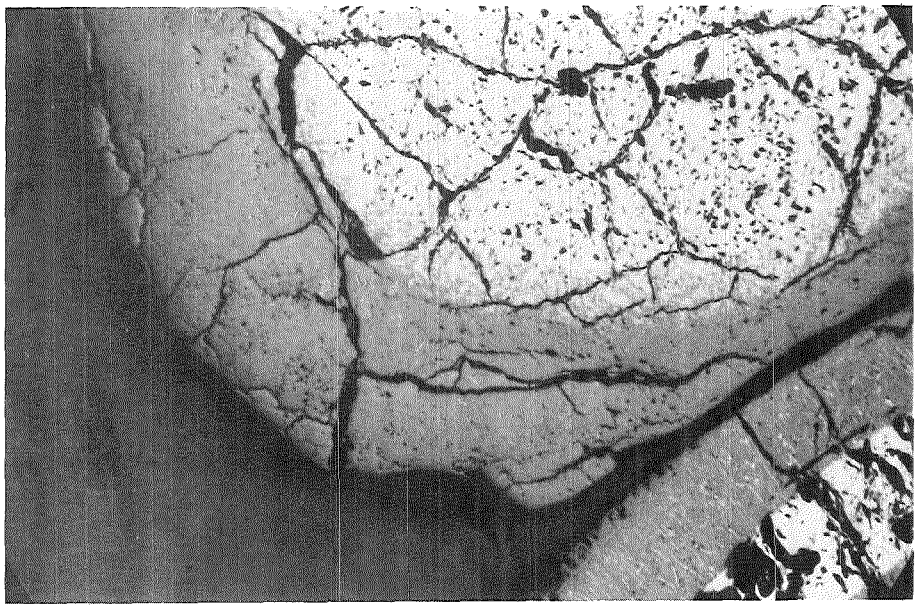

Inner region of droplet 4

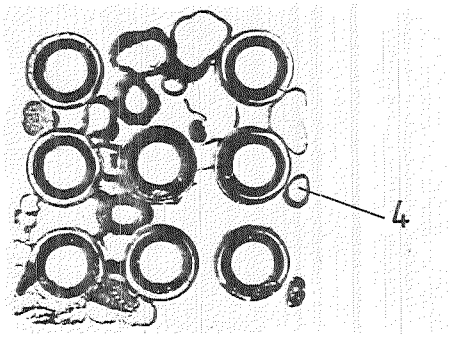

200×

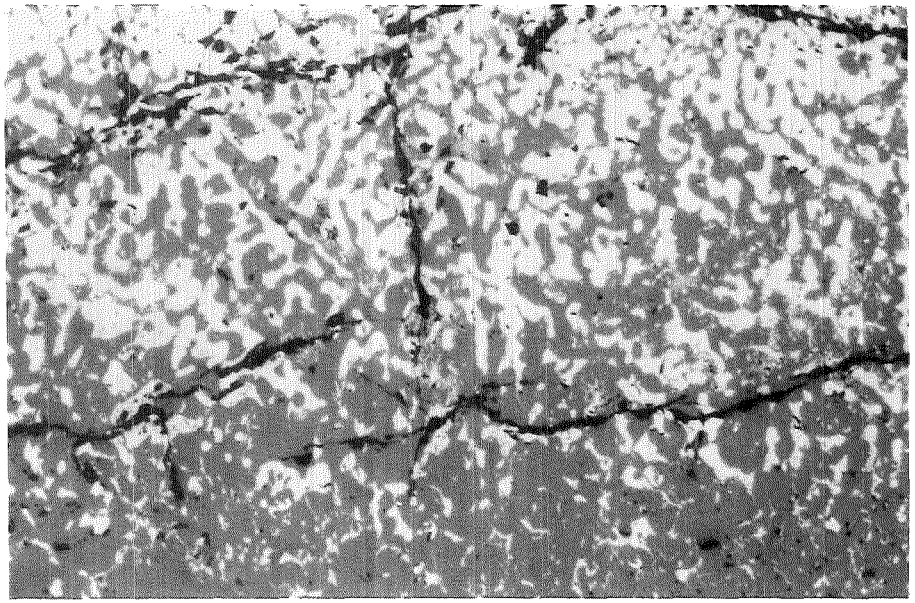

Transition of oxidized to unoxidized region

Fig. 76 : Details of Cross Section at 61mm above bundle bottom of ESBU-2A

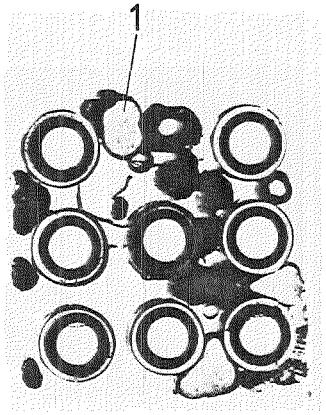

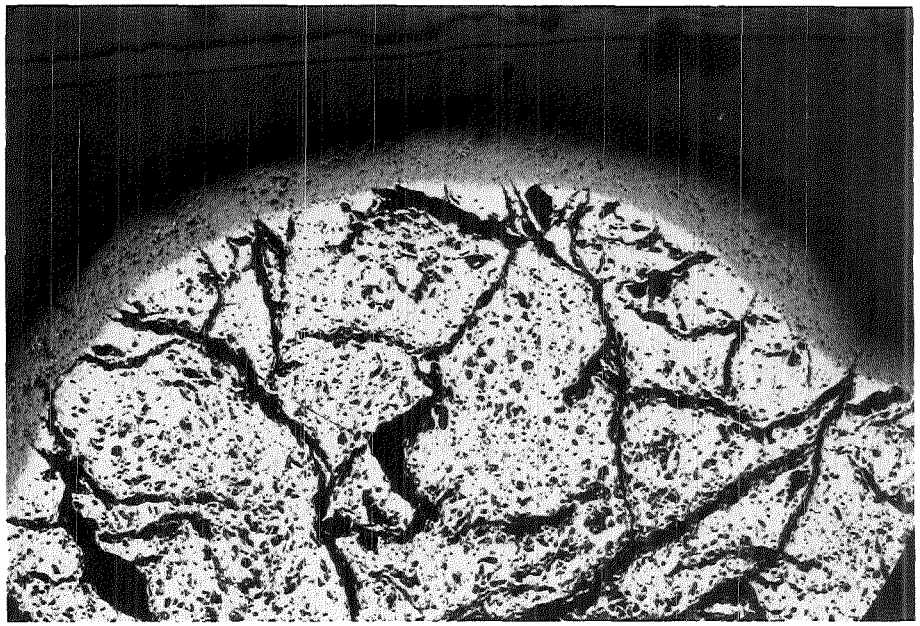

Outer region of droplet 1

25x

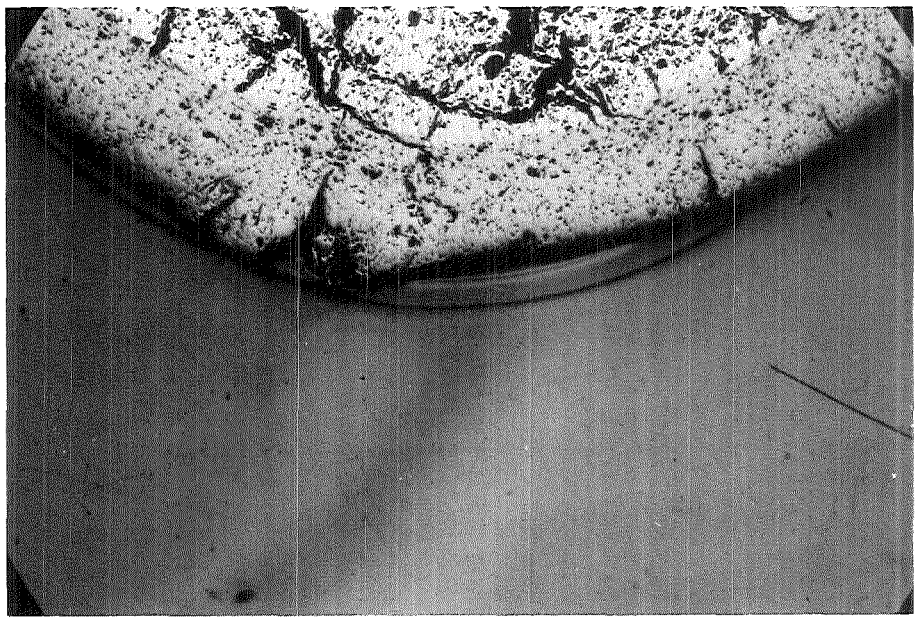

Inner region of droplet 1

200x

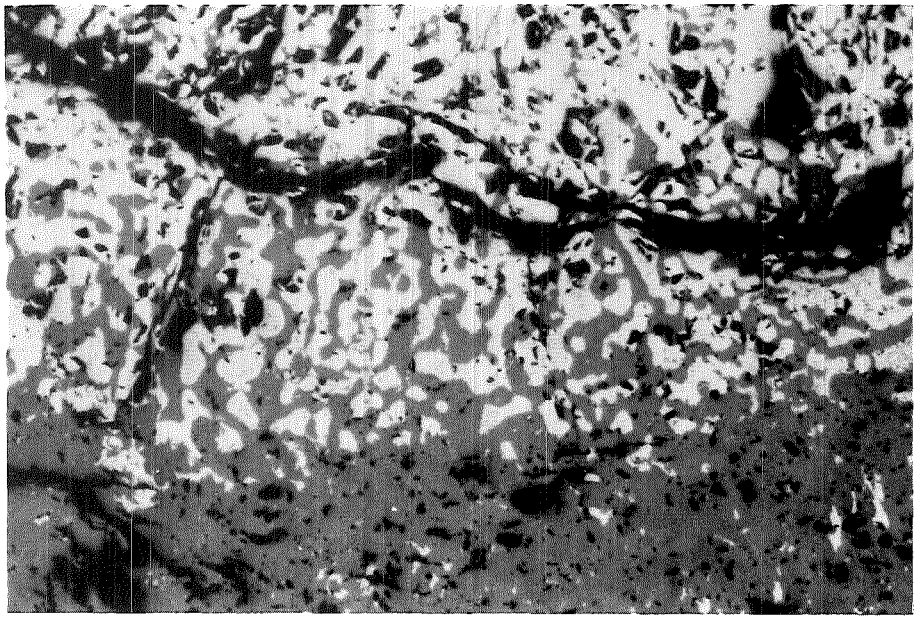

Transition of oxidized to unoxidized region

Fig. 77: Details of Cross Section at 61mm above bundle bottom of ESBU-2A

Outer region of droplet 2

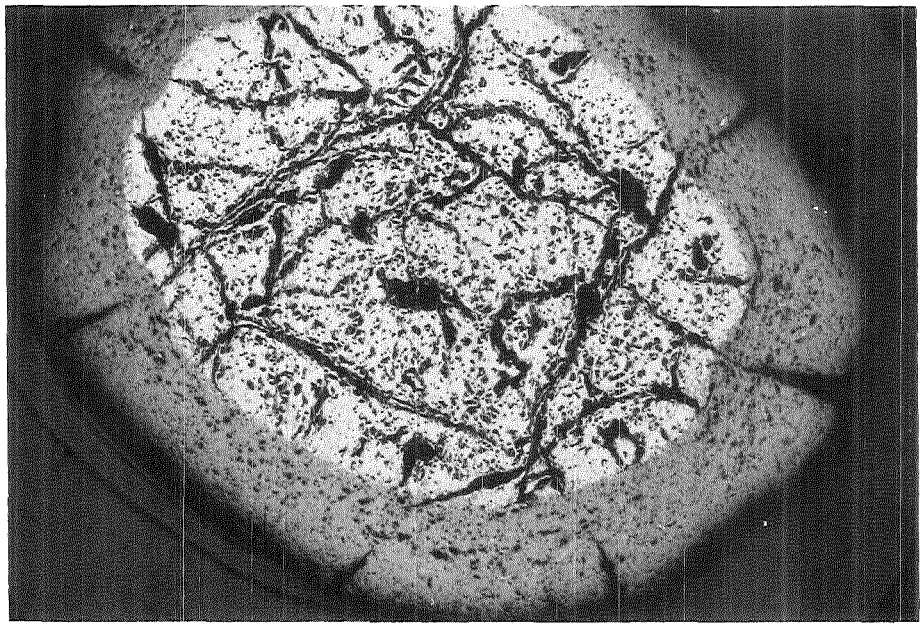

Inner region of droplet 2

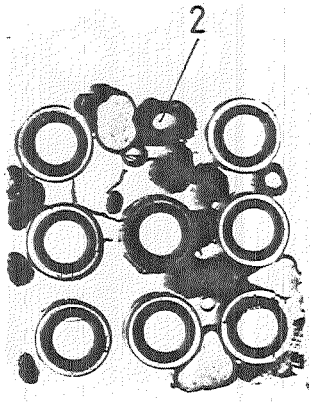

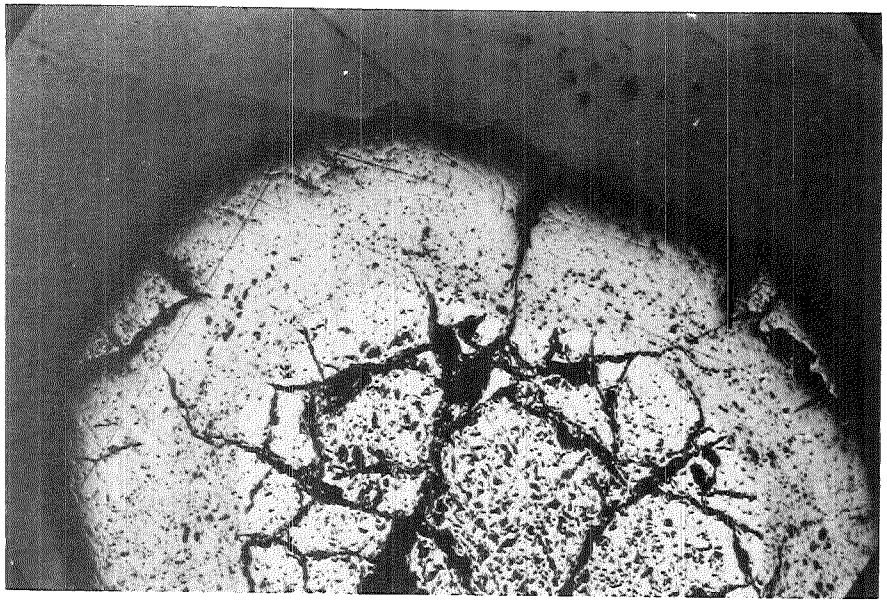

Outer region of droplet 3

Fig.78 : Details of Cross Section at 61mm above bundle bottom of ESBU-2A

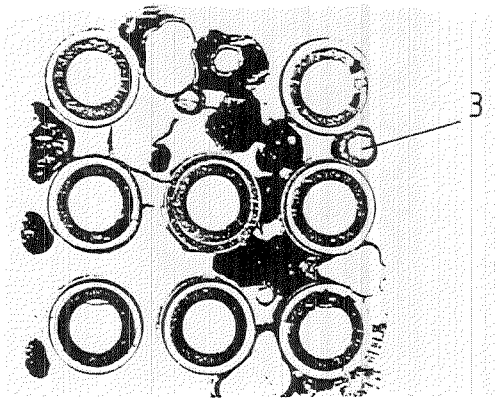

25x

Inner region of droplet 3

200x

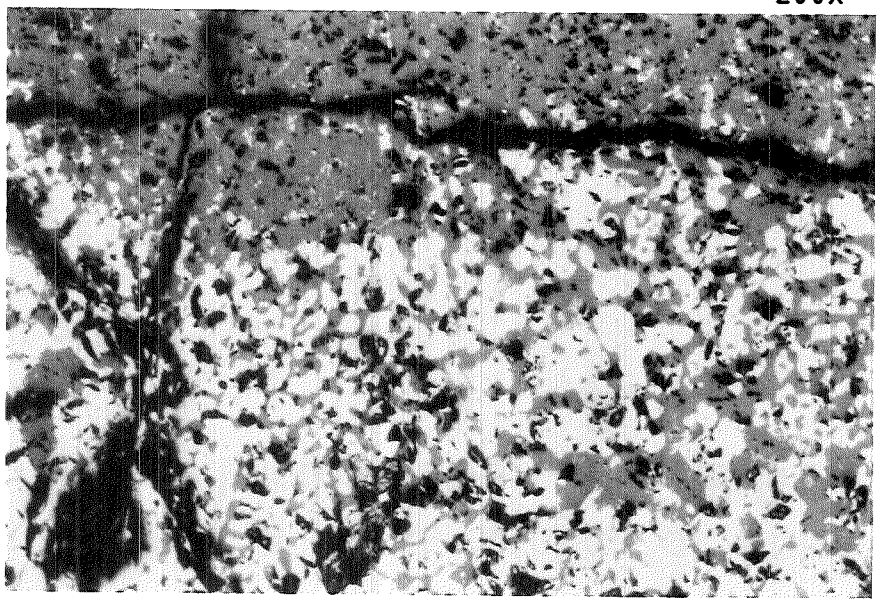

Transition of oxidized to unoxidized region

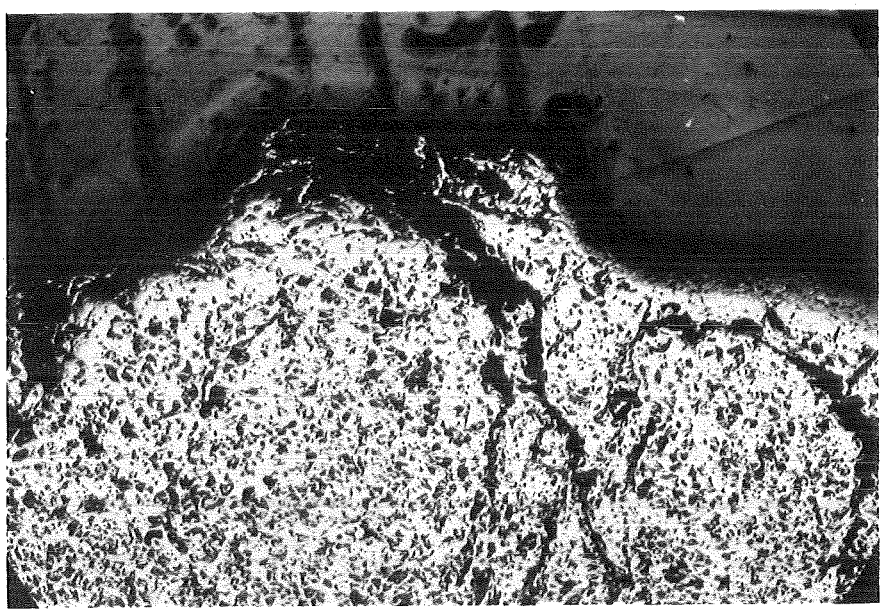

Outer region of droplet 4 25x

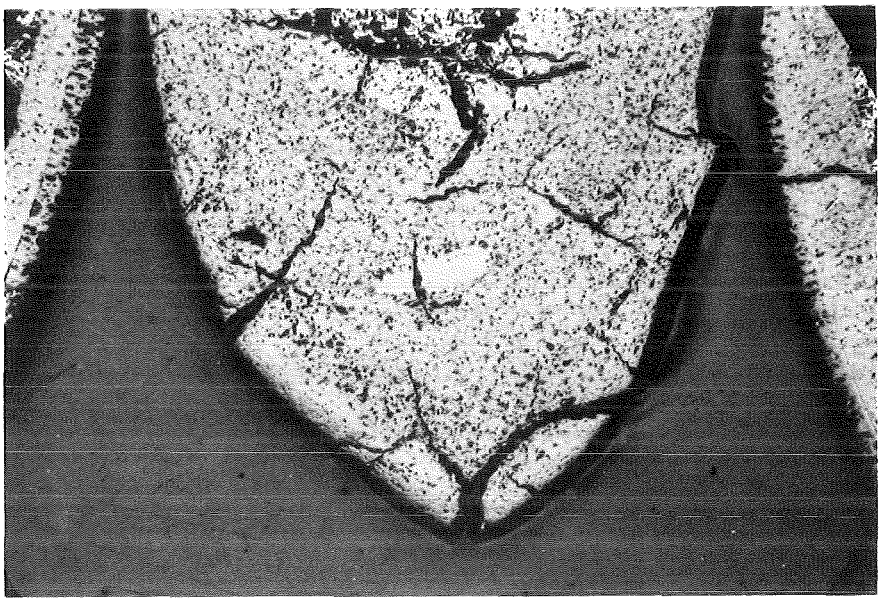

Inner region of droplet 4

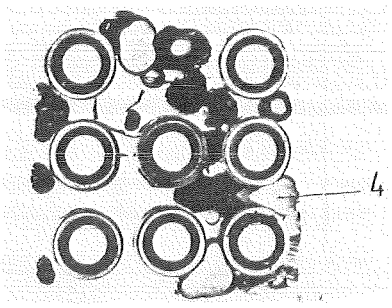

Fig. 79: Details of Cross Section at 61mm above bundle bottom of ESBU-2A

Fig. 80: Details of Cross Section at 61mm above bundle bottom of ESBU-2A

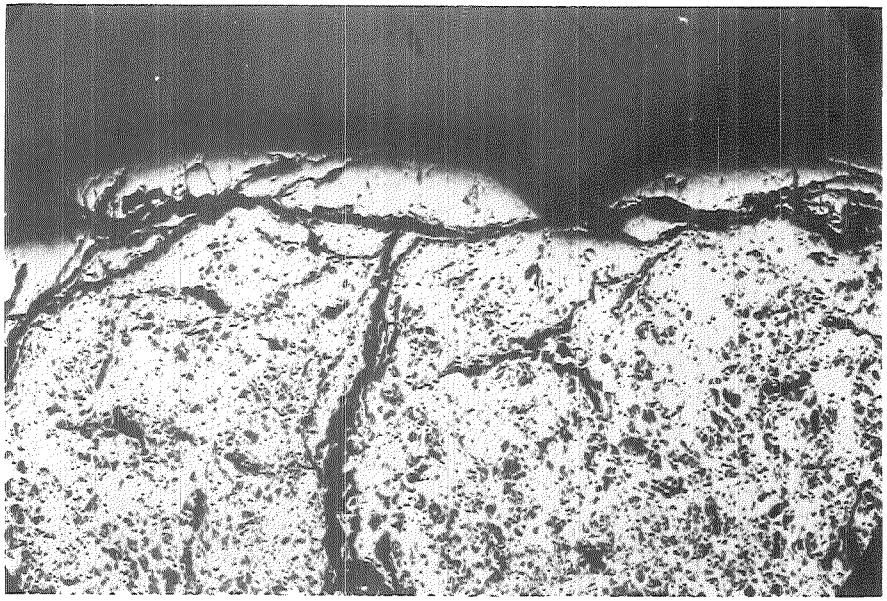

Outer region of droplet 5

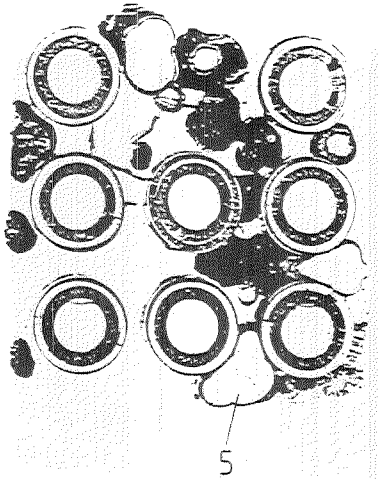

25x

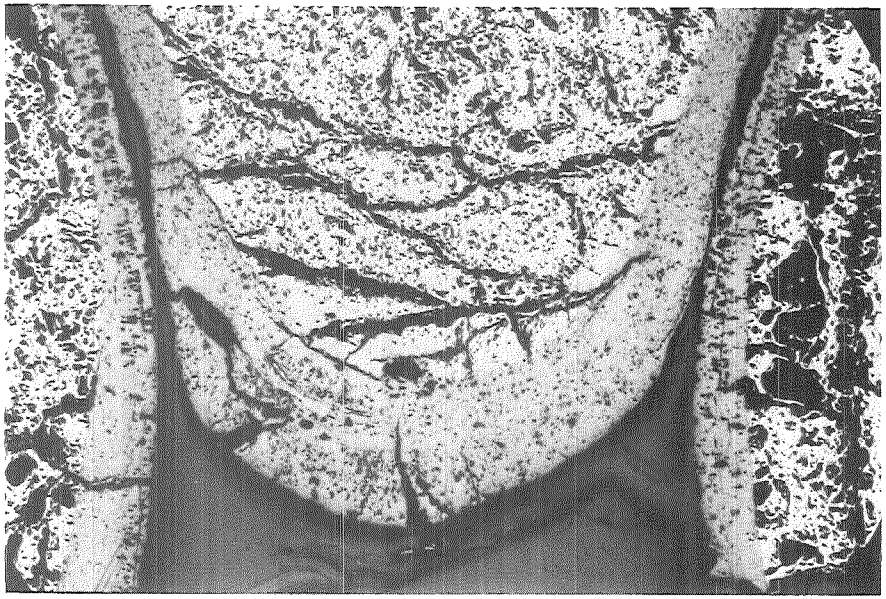

Inner region of droplet 5

200x

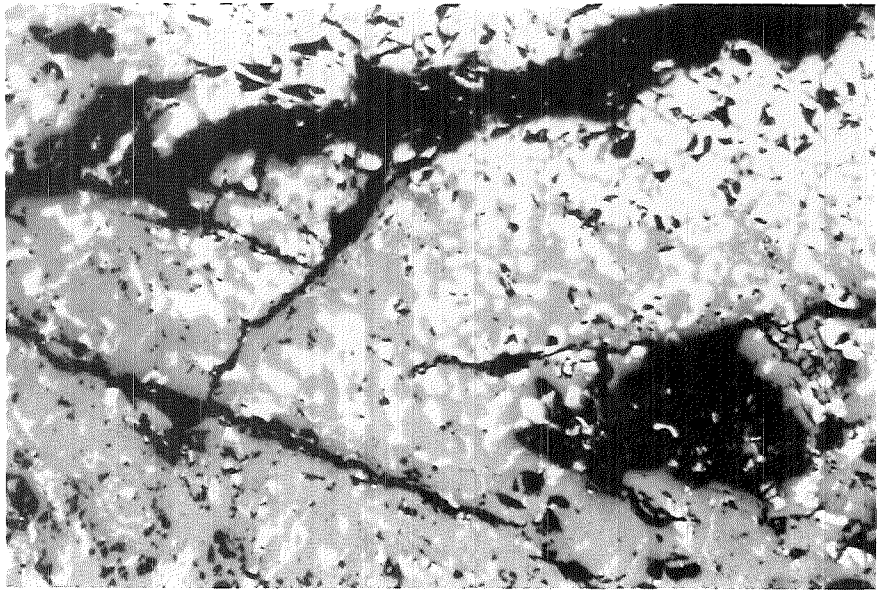

Transition of oxidized to unoxidized region

Fig. 81 : Details of Cross Section at 59 mm above bundle bottom of ESBU-2A

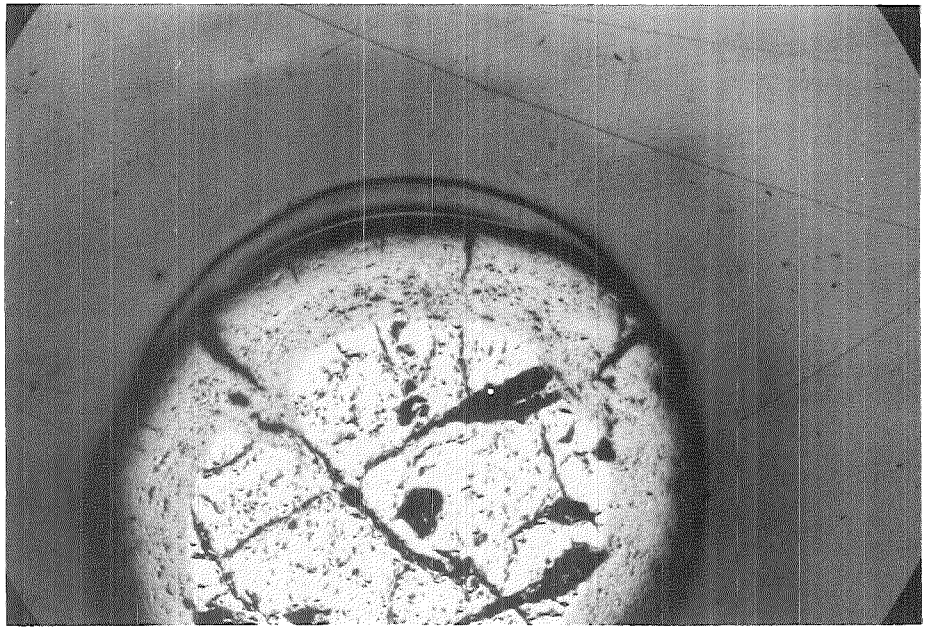

Outer region of droplet 1

25×

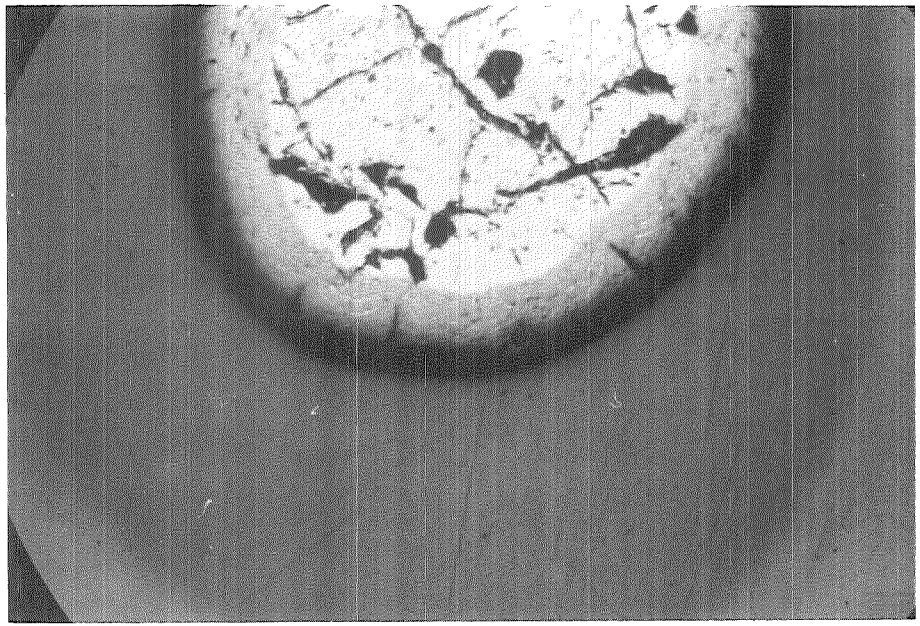

Inner region of droplet 1

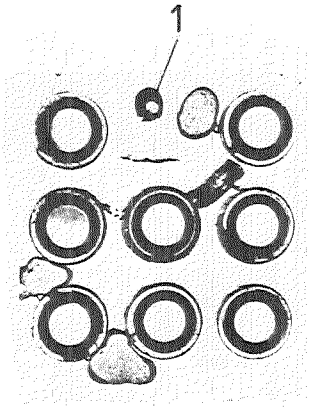

200×

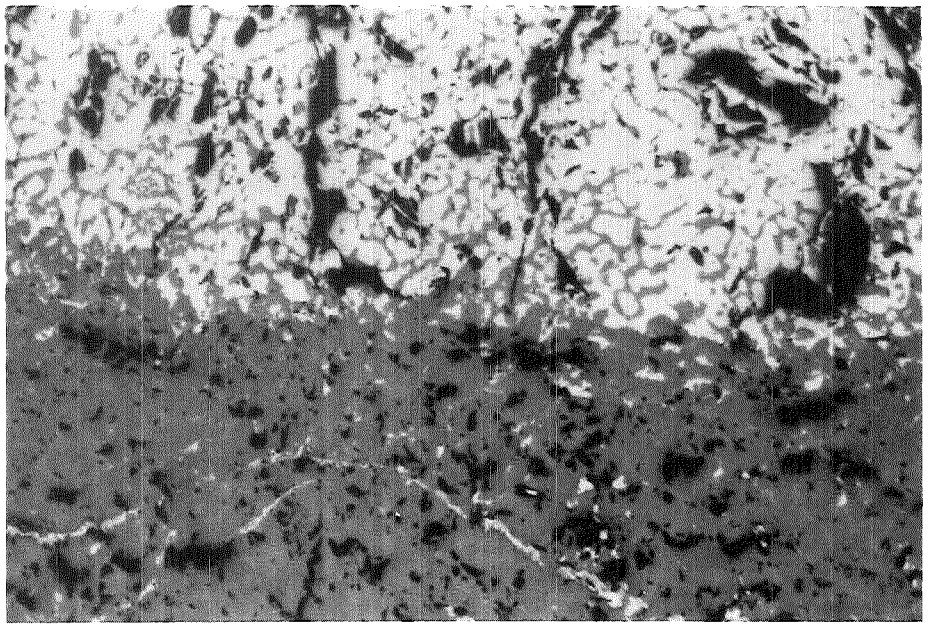

Transition of oxidized to unoxidized region

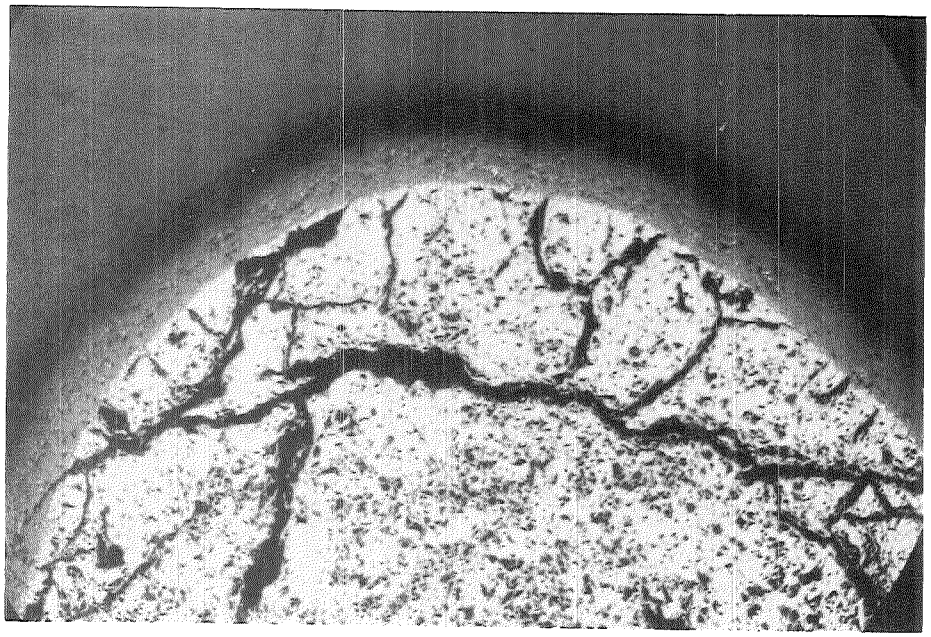

Outer region of droplet 2

25×

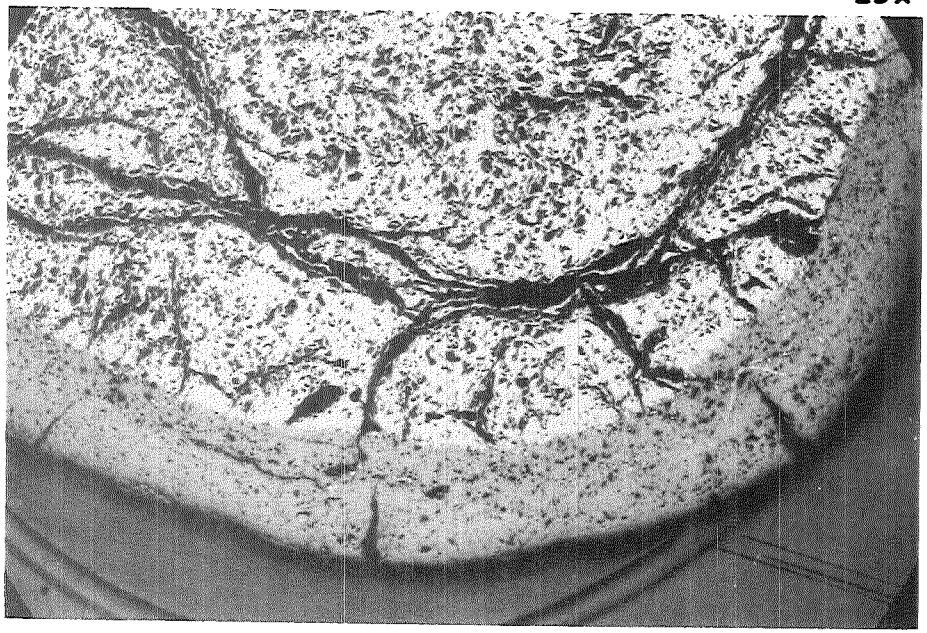

Inner region of droplet 2

Fig. 82 : Details of Cross Section at 59 mm above bundle bottom of ESBU-2A

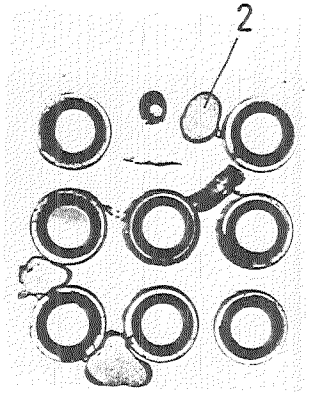

200×

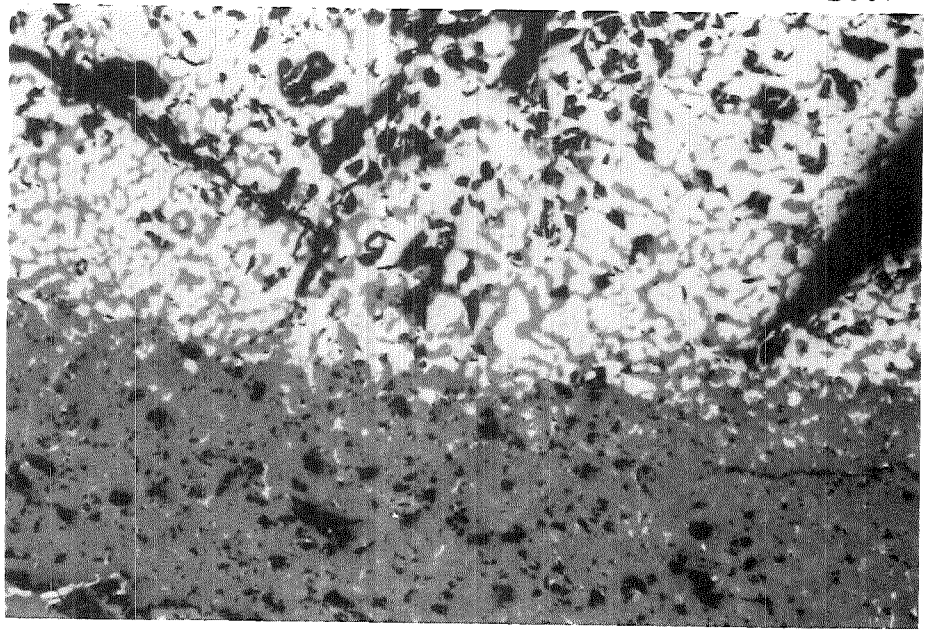

Transition of oxidized to unoxidized region

Fig. 84: Details of Cross Section at 59mm above bundle bottom of ESBU-2A

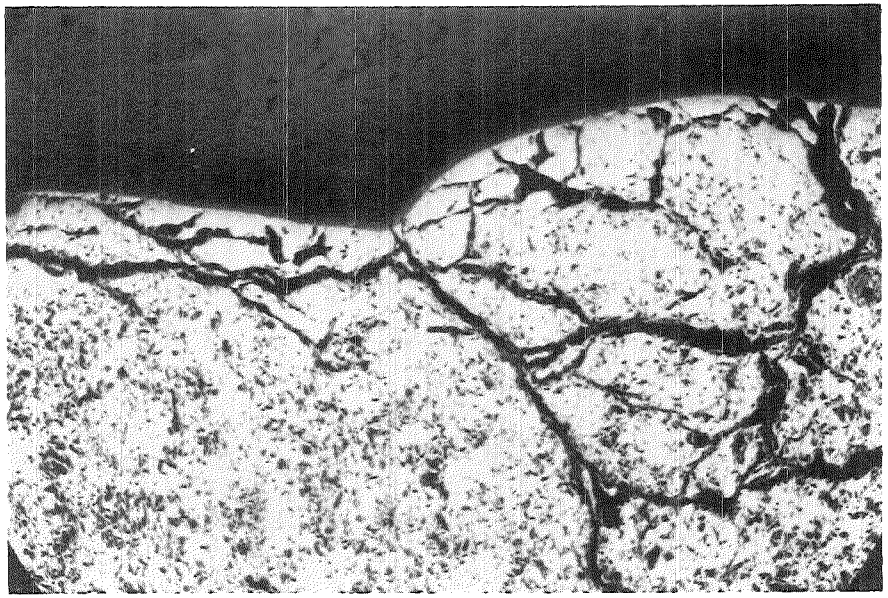

Outer region of droplet 4

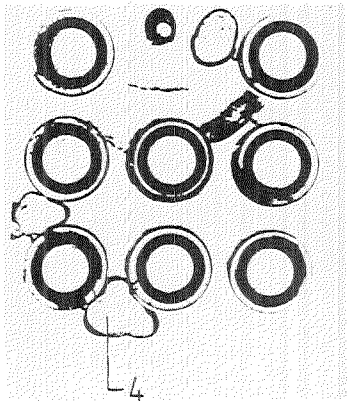

25x

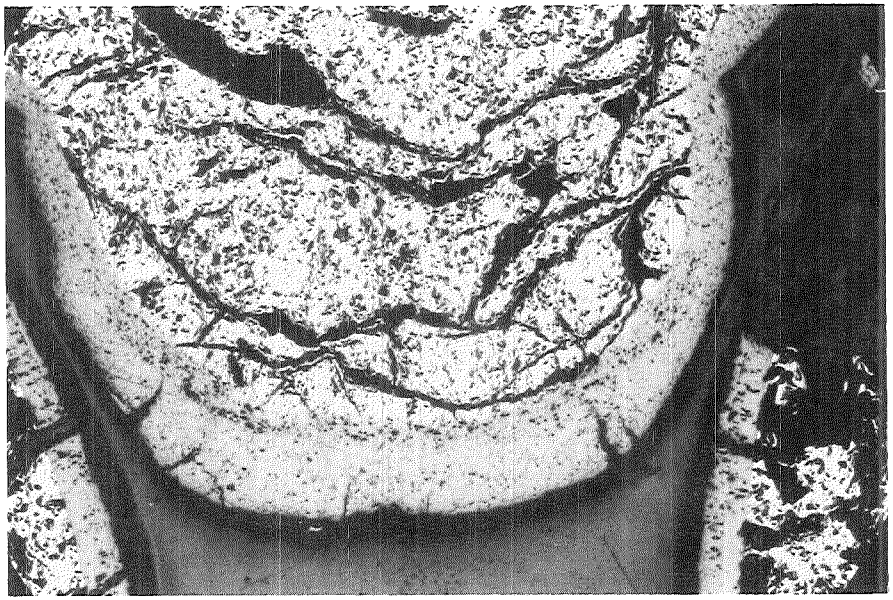

Inner region of droplet 4

200x

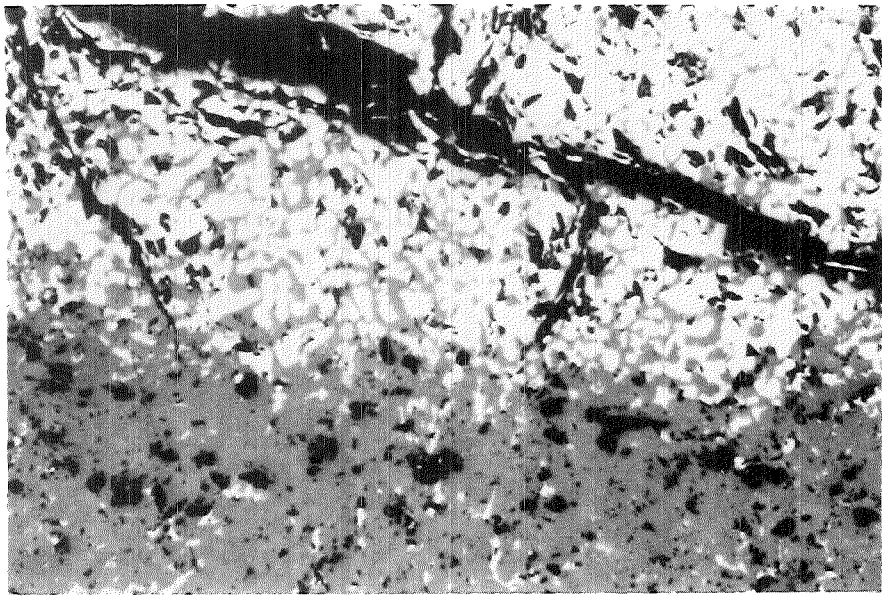

Transition of oxidized to unoxidized region

Fig. 85: Details of Cross Section at 51 mm above bundle bottom of ESBU-2A

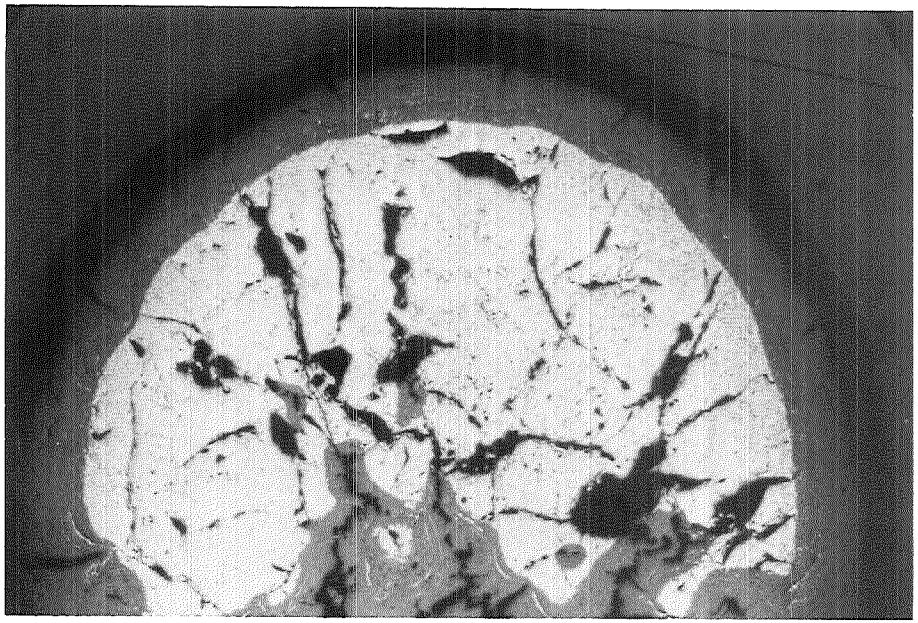

Outer region of droplet 1

25×

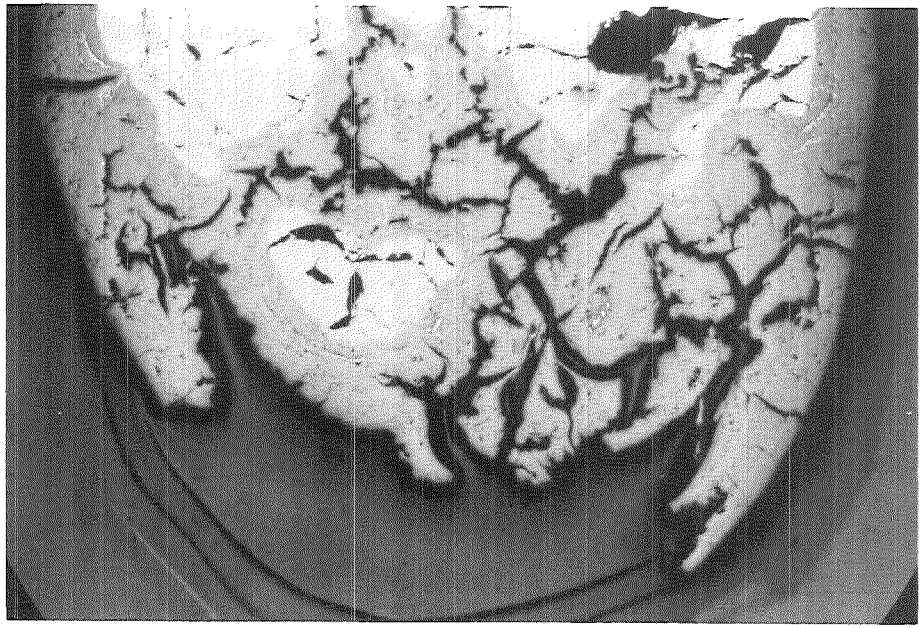

Inner region of droplet 1

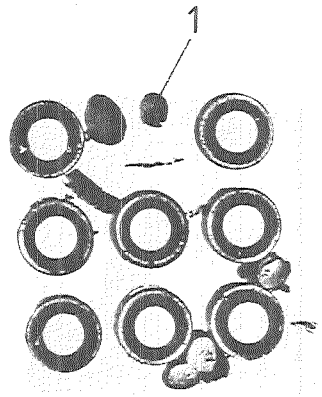

200×

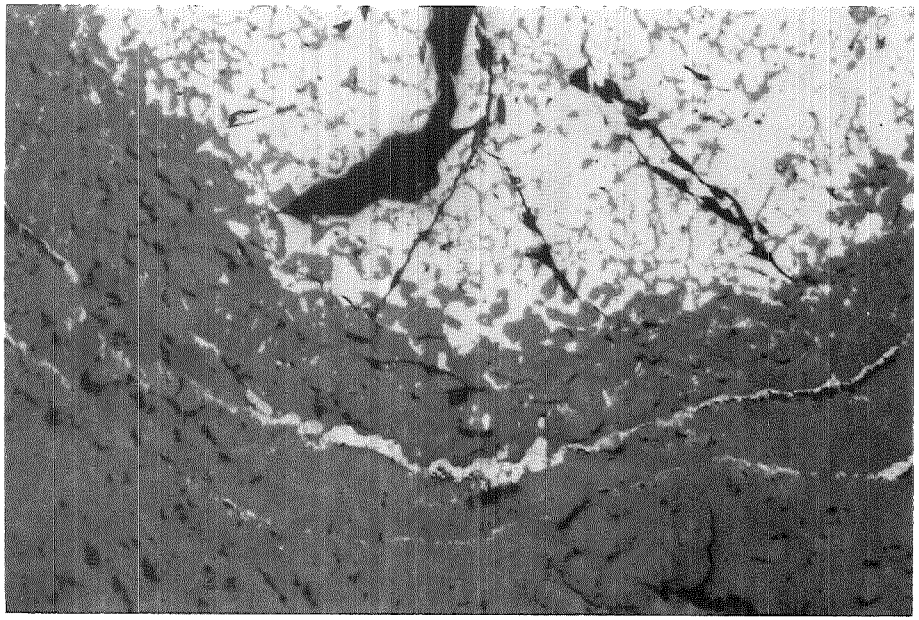

Transition of oxidized to unoxidized region

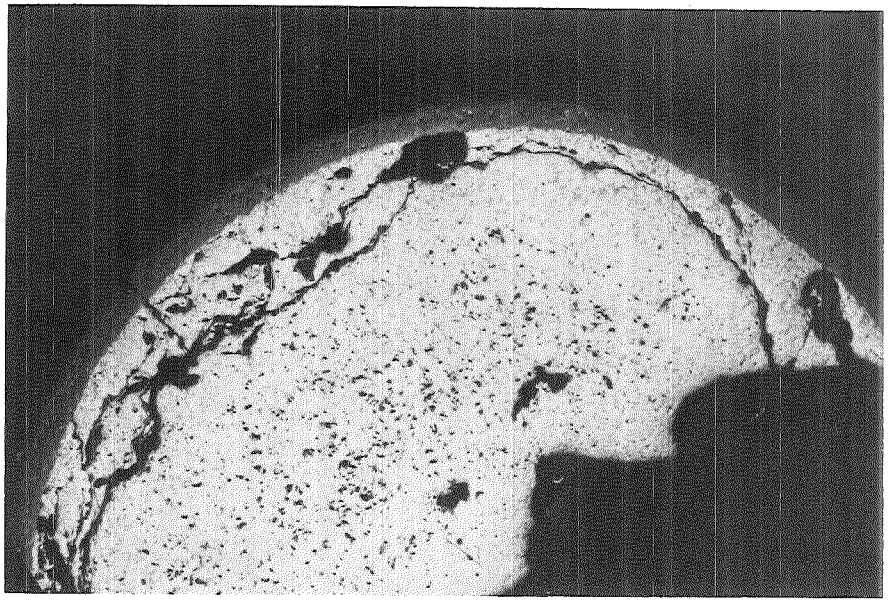

Outer region of droplet 2

Fig. 86: Details of Cross Section at 51mm above bundle bottom of ESBU-2A

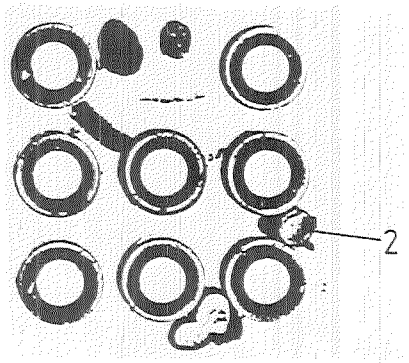

25x

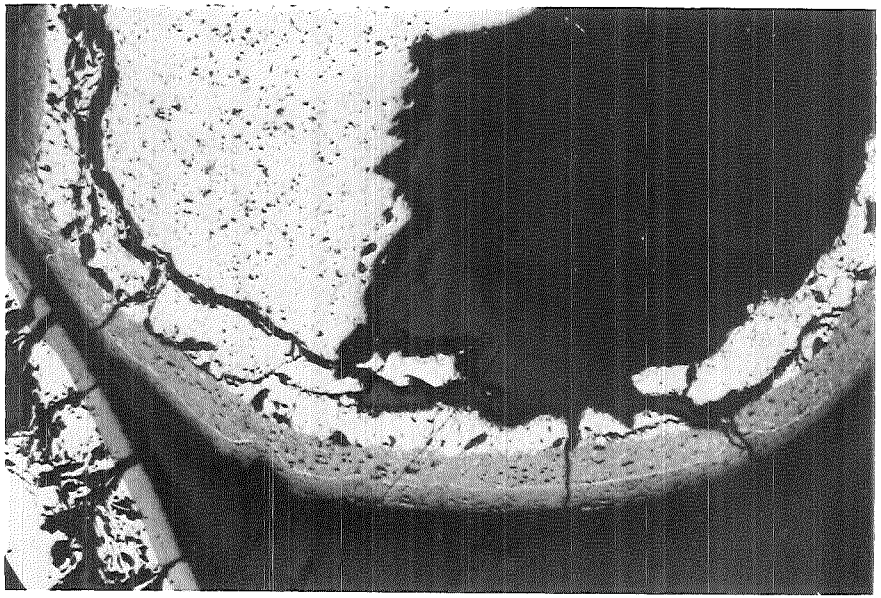

Inner region of droplet 2

200x

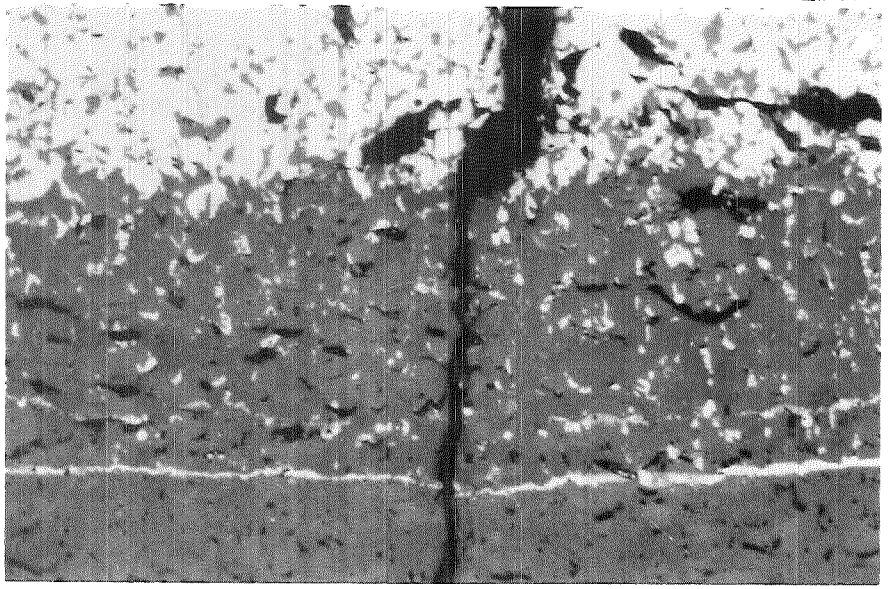

Transition of oxidized to unoxidized region

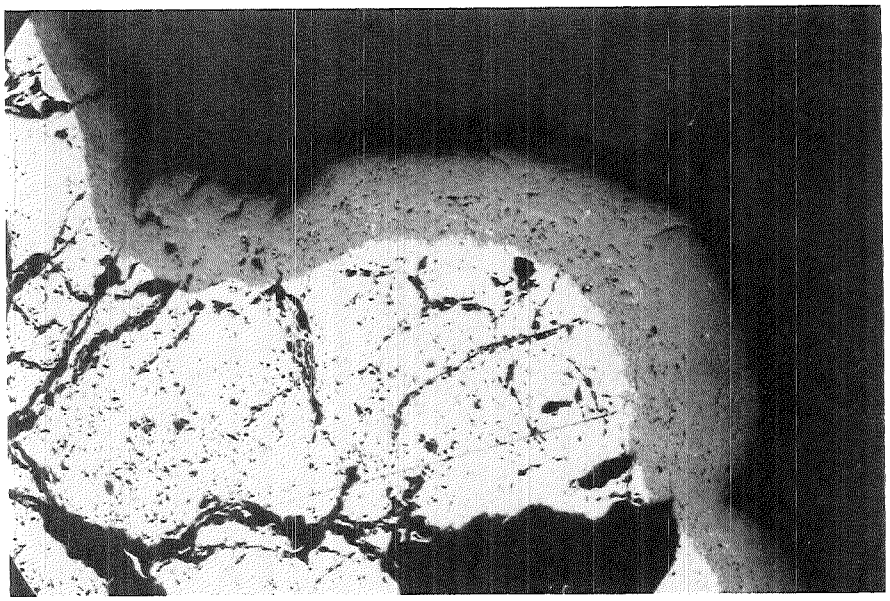

Outer region of droplet 3

Fig. 87: Details of Cross Setion at 51mm above bundle botom of ESBU-2A

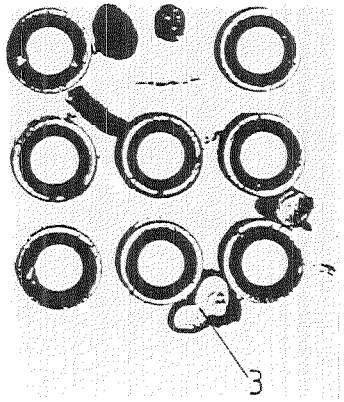

25x

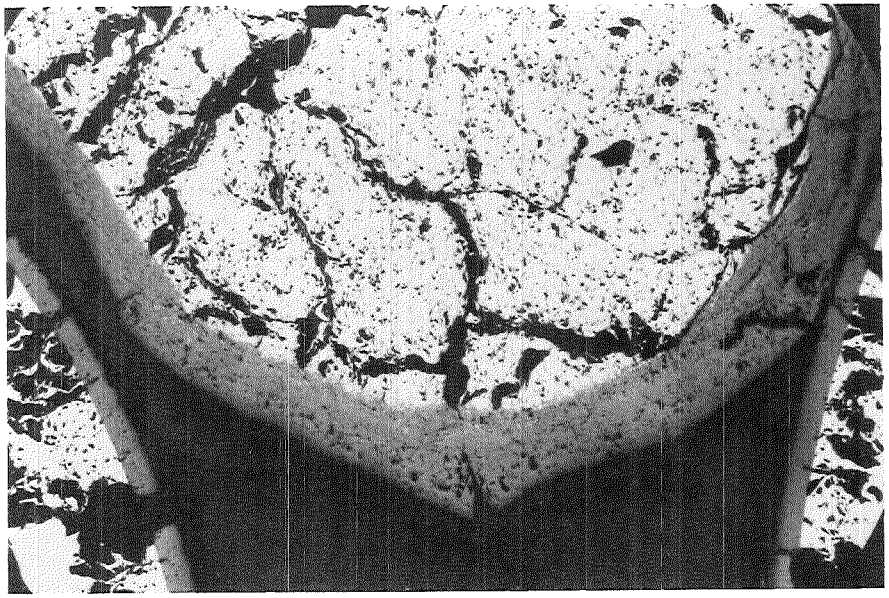

Inner region of droplet 3

200x

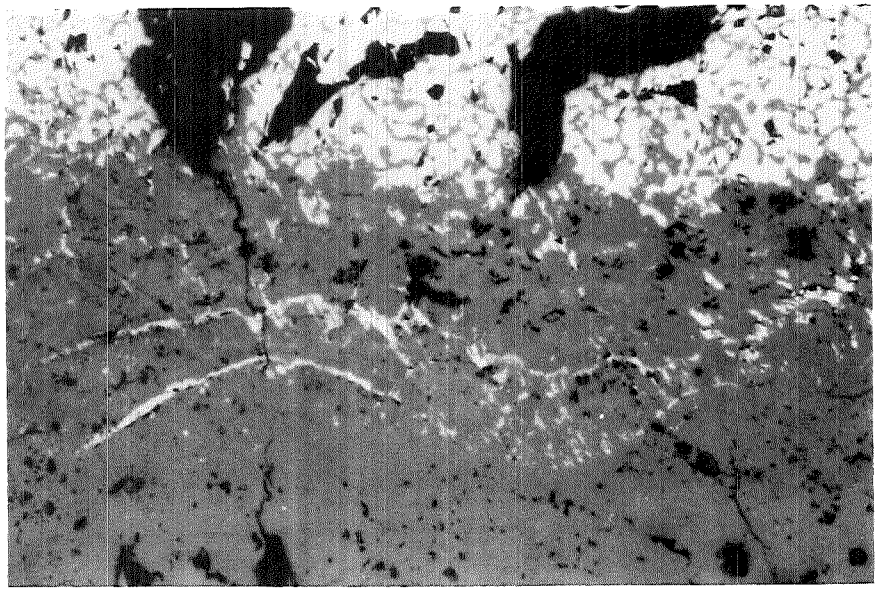

Transition of oxidized to unoxidized region

Fig.88: Detais of Cross Section at 49mm above bundle bottom of ESBU-2A

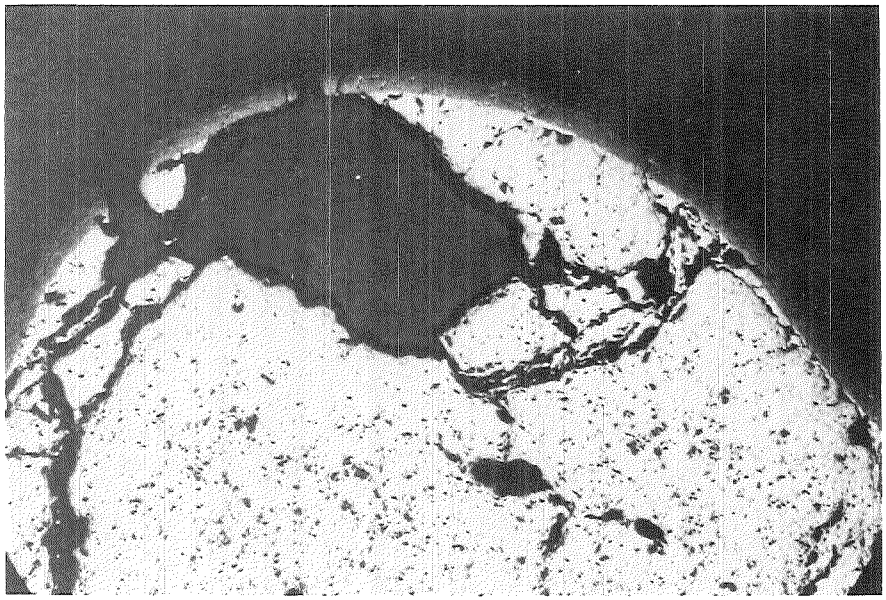

Outer region of droplet 2

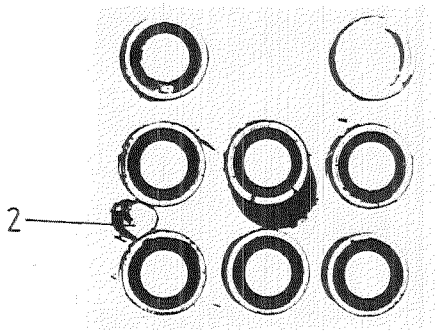

25x

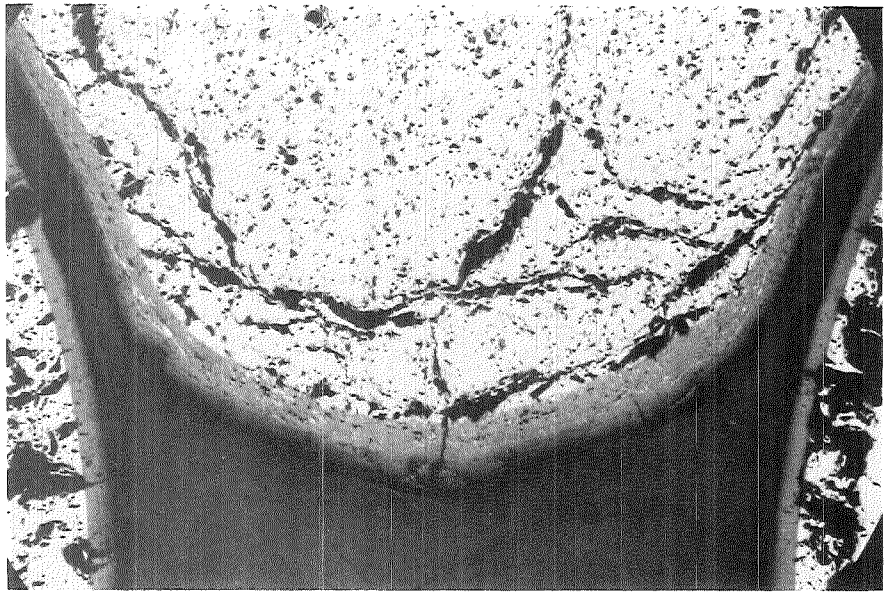

Inner region of droplet 2

200x

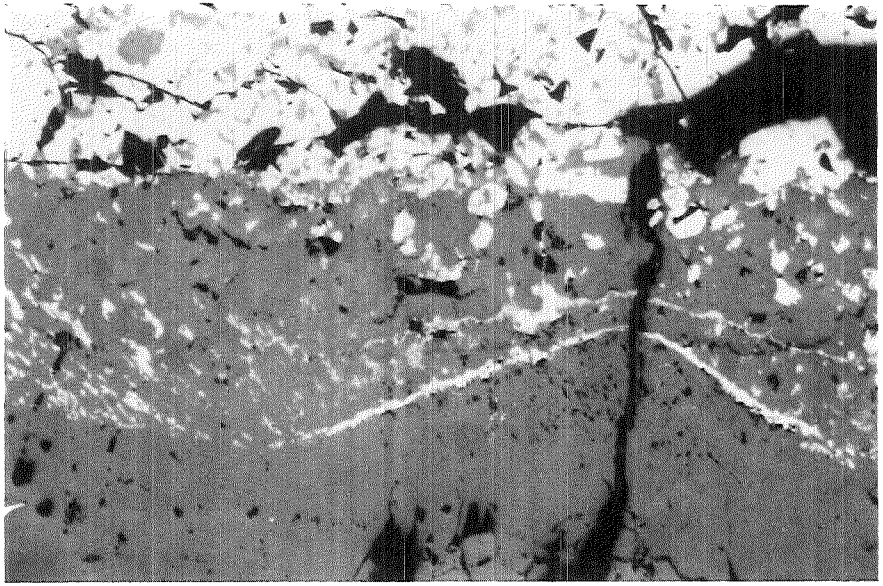

Transition of oxidized to unoxidized region

Fig. 89 : Details of Cross Section at 41 mm above bundle bottom of ESBU-2A

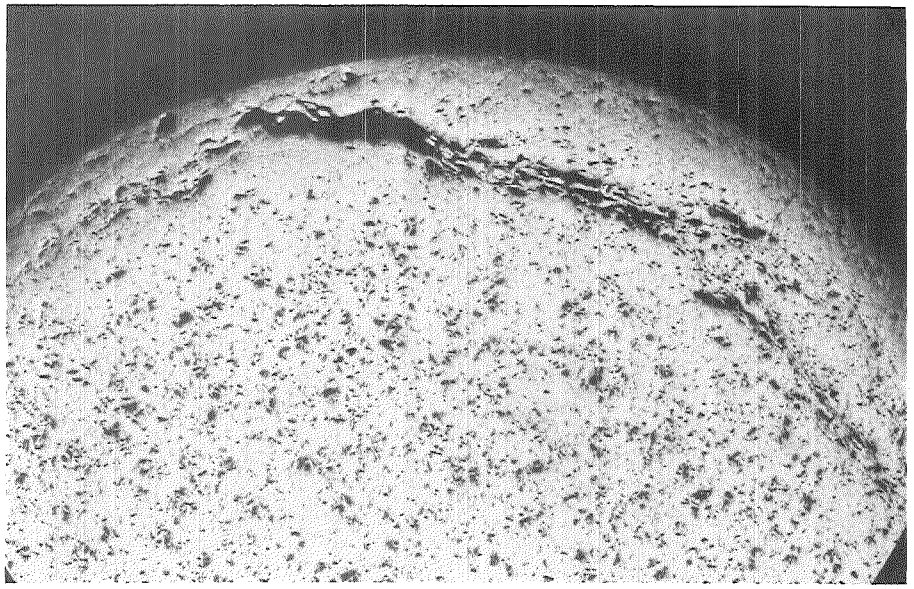

Outer region of droplet

25×

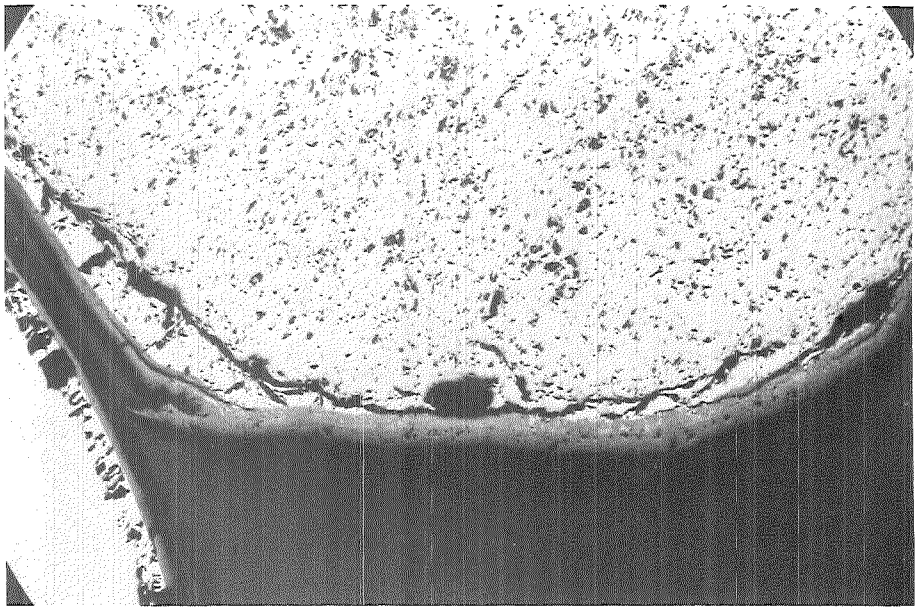

Inner region of droplet

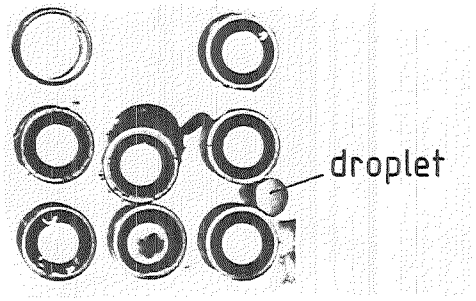

200×

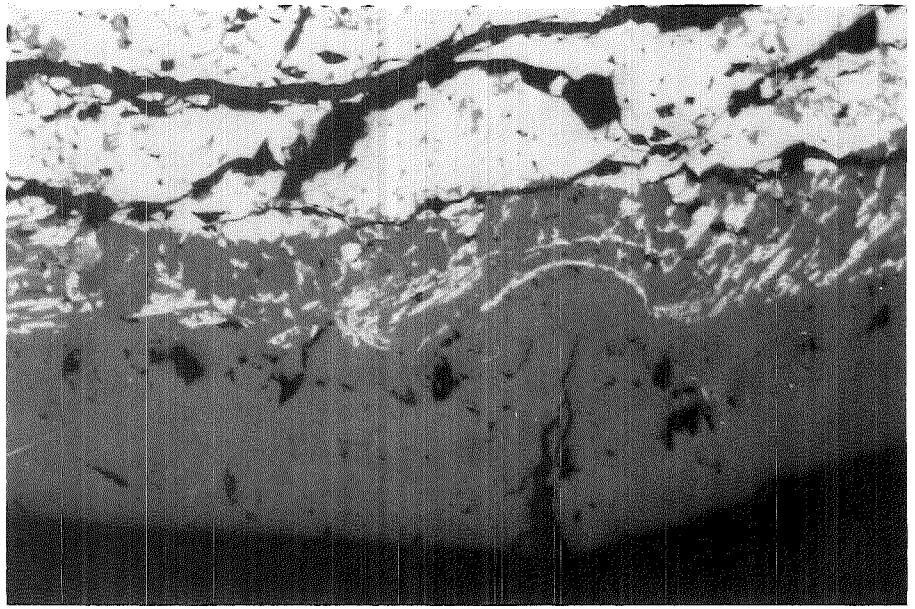

Transition of oxidized to unoxidized region

Fig. 90 : Details of Cross Section at 39 mm above bundle bottom of ESBU-2A

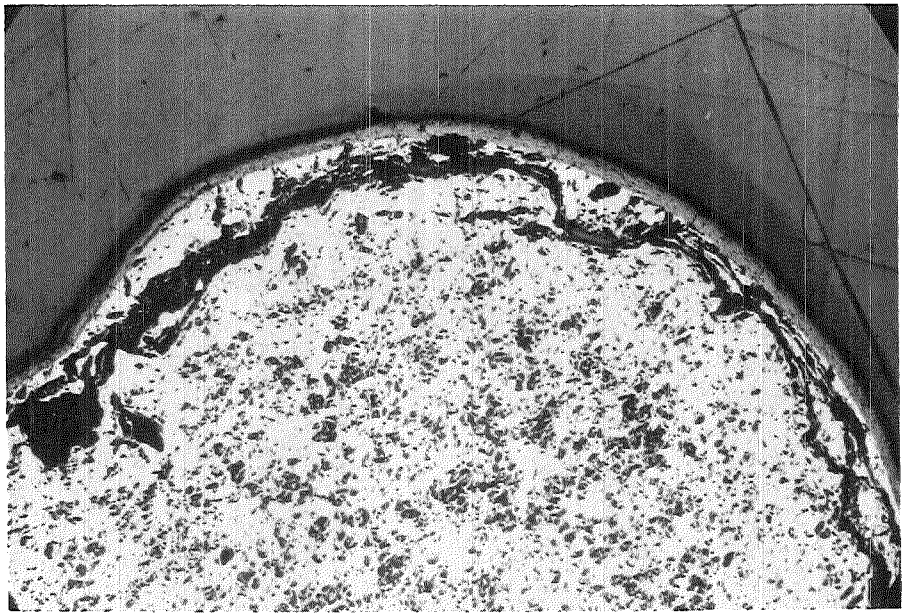

Outer region of droplet

25×

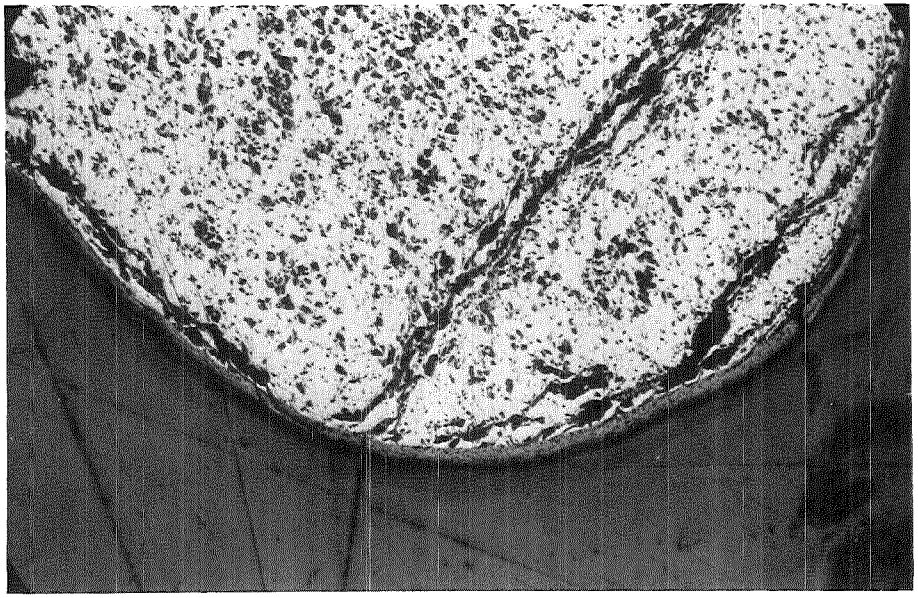

Inner region of droplet

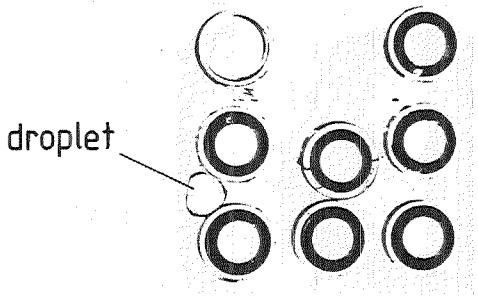

200×

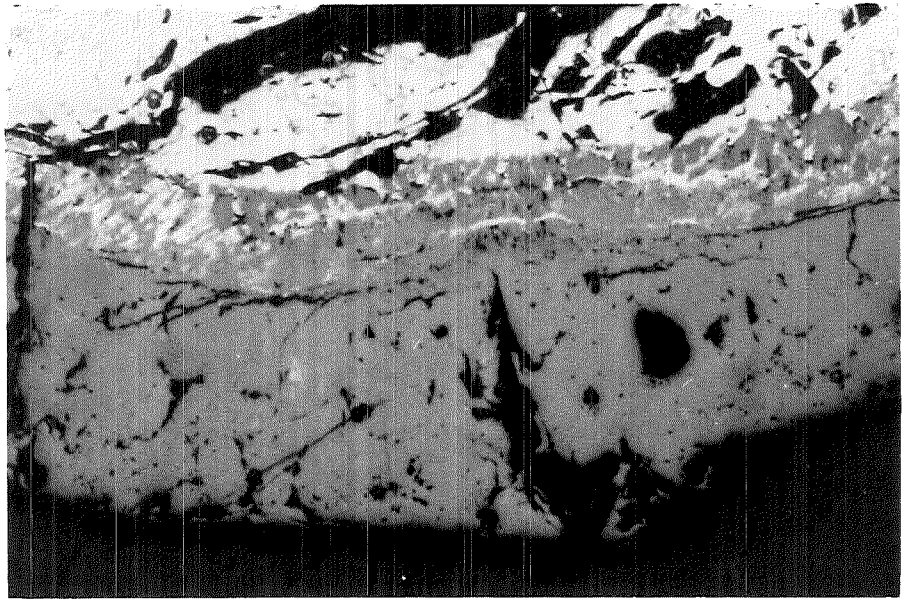

Transition of oxidized to unoxidized region

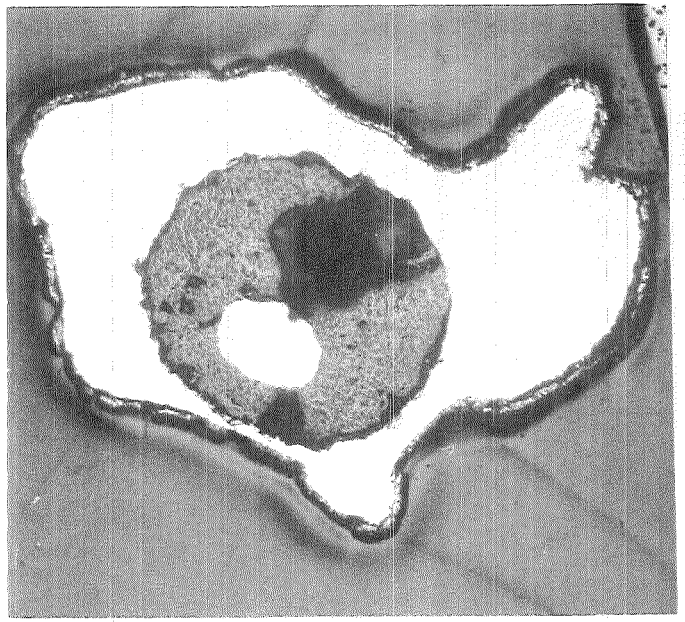

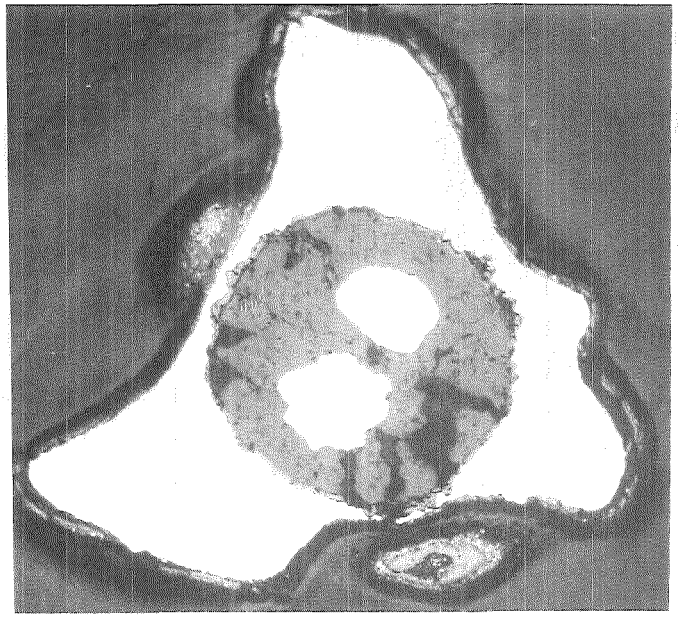

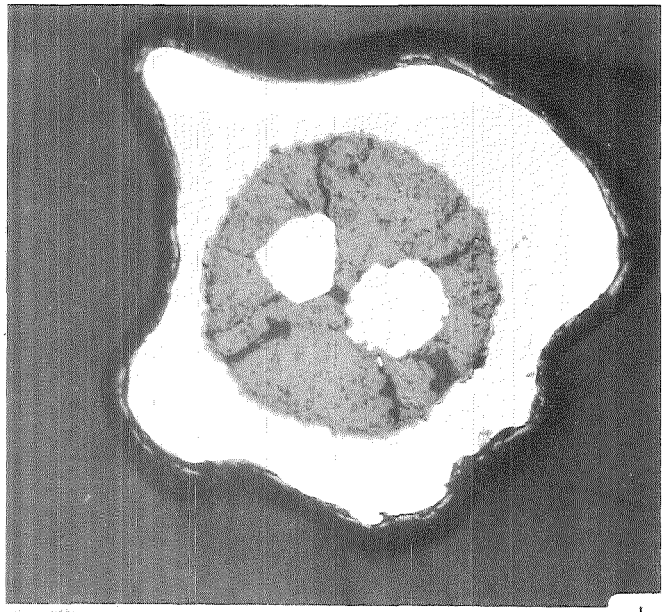

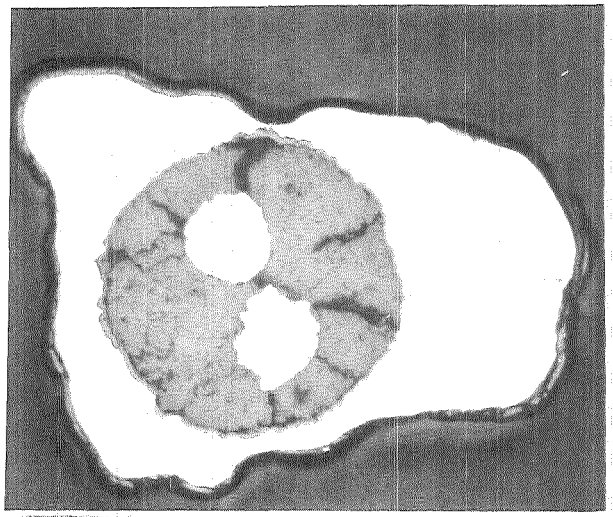

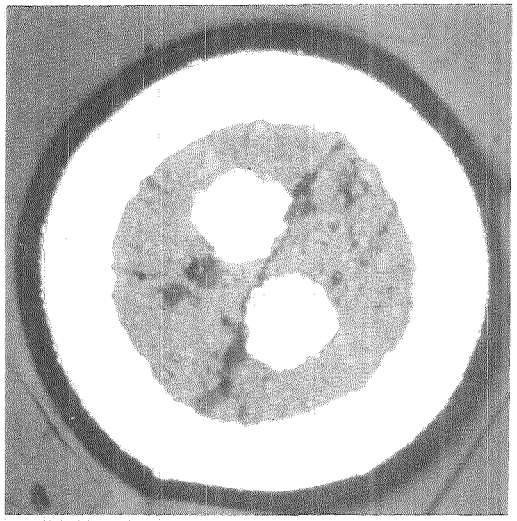

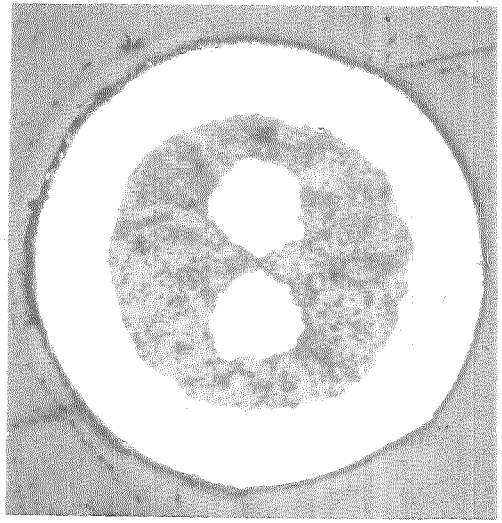

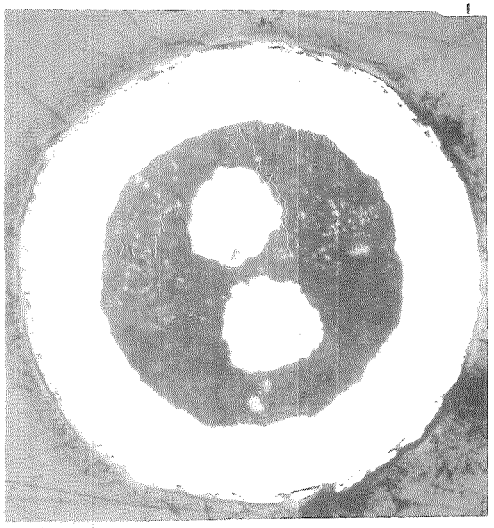

FIG.91: CROSS SECTIONS OF A NICRNI THERMOCOUPLE AT VARIOUS ELEVATIONS (ALUMINA INSULATED, INCONEL-SHEATHED) TEST ESBU-2A

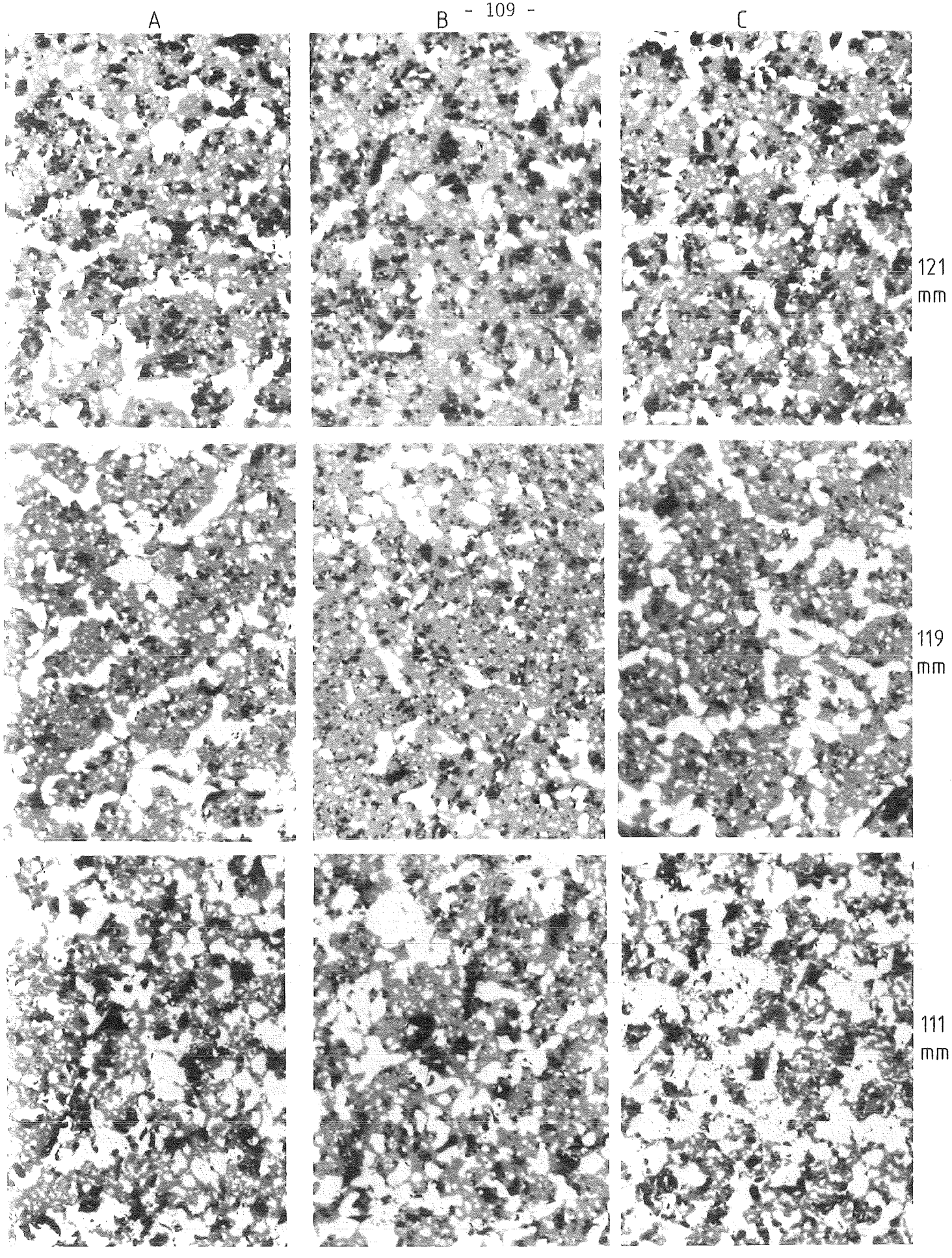

Fig. 92: Structure of the refrozen melt at the elevations given for the positions shown in fig.94 (ESBU-2A).

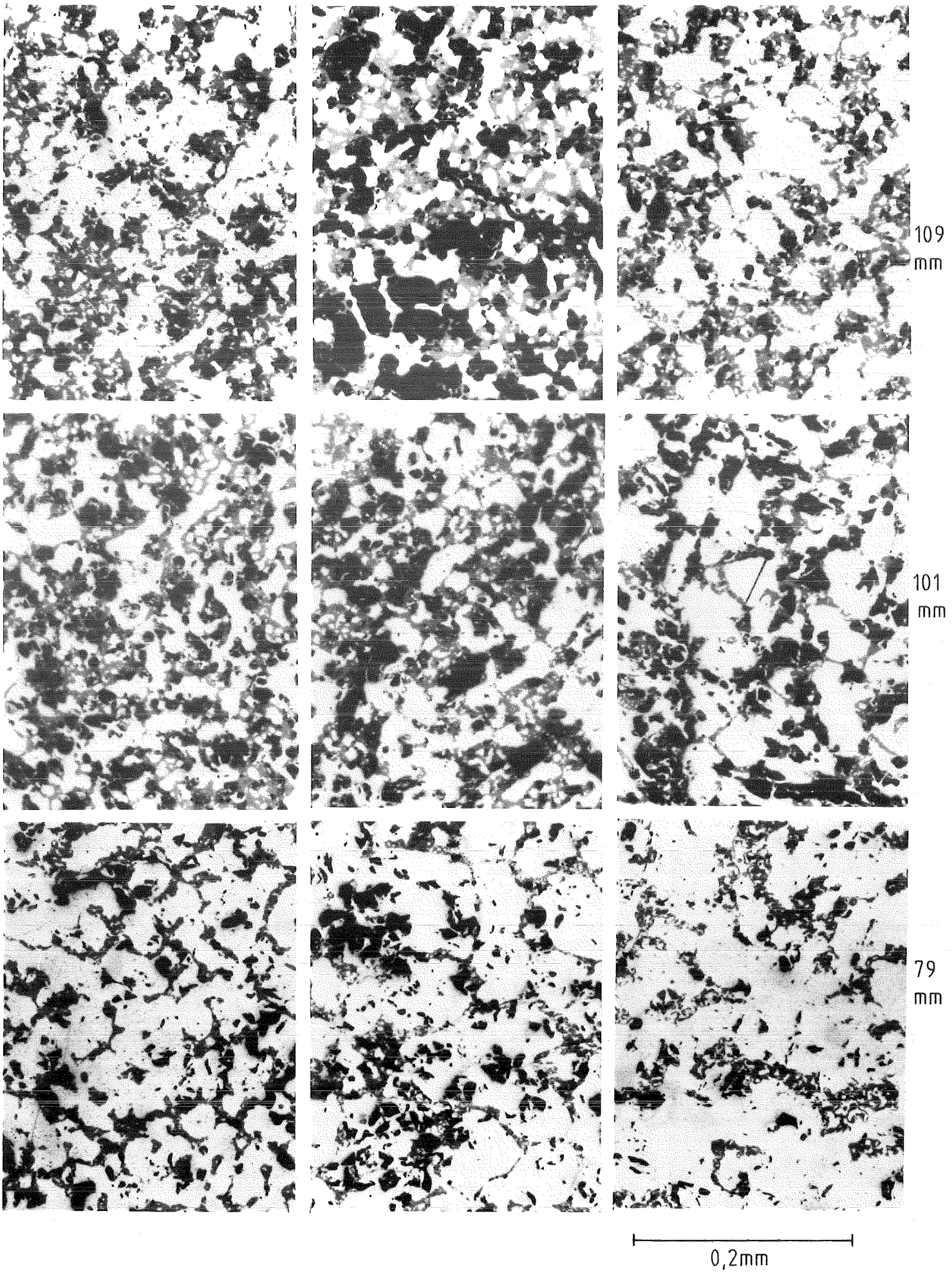

Fig. 93: Structure of the refrozen melt at the elevations given for the positions shown in fig. 94 (ESBU-2A).

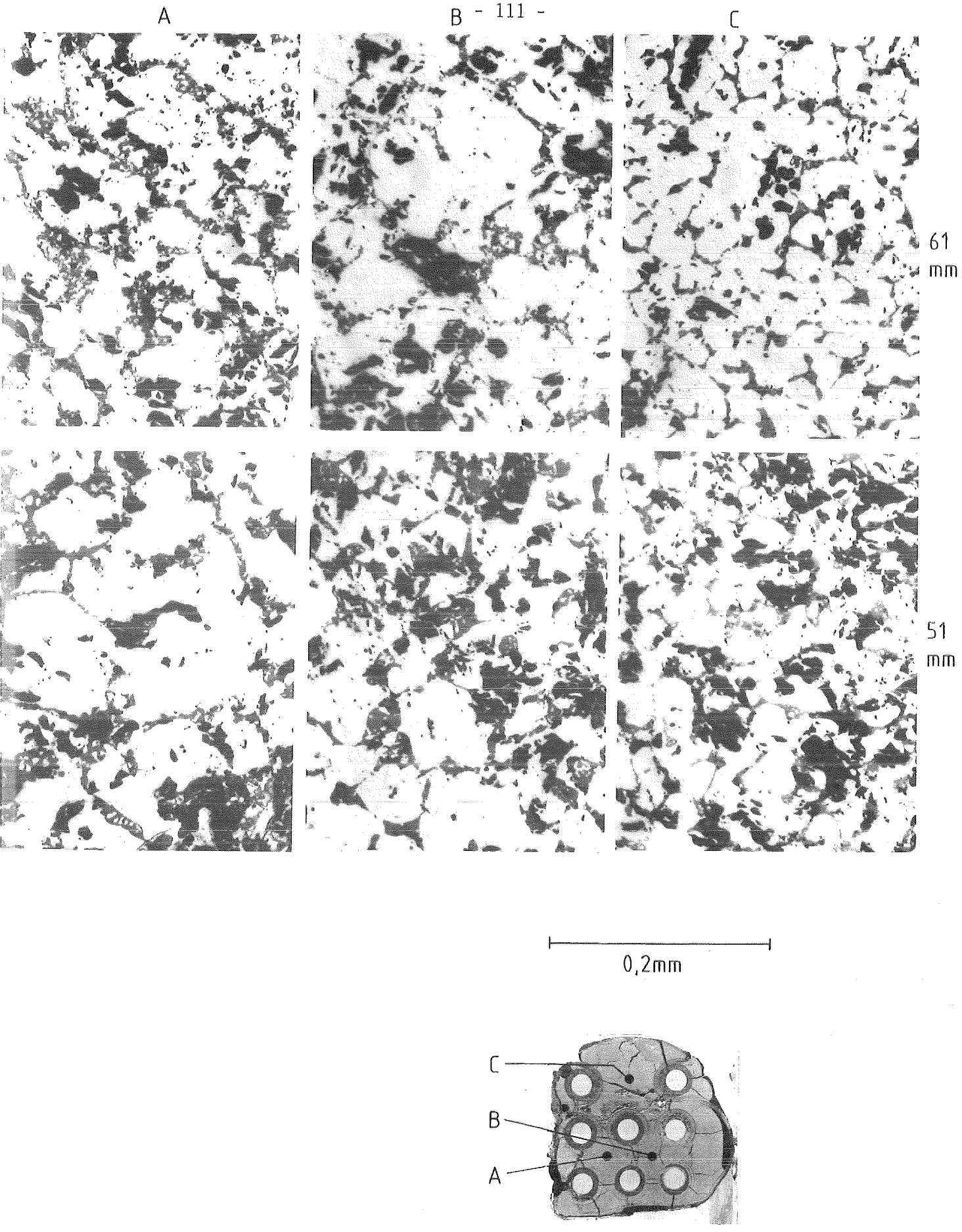

Fig. 94: Structure of the refrozen melt at the elevations given for the positions shown below (ESBU-2A).

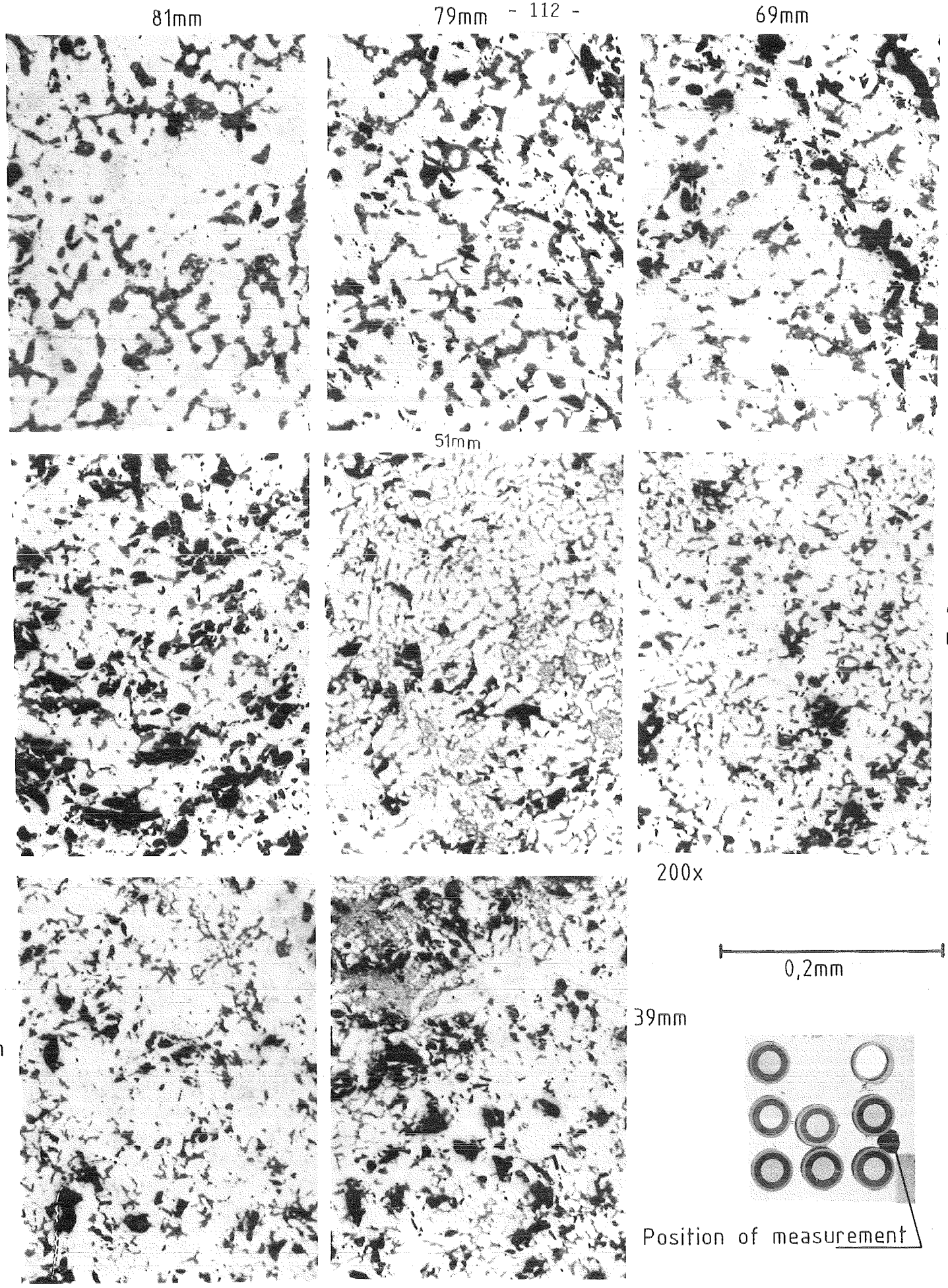

Fig. 95: Structure of the refrozen melt at the elevations given (ESBU 2A).

Fig.96 Remnants of the sieve analysis on the sieve with mesh size 1mm. (ESBU-2A)

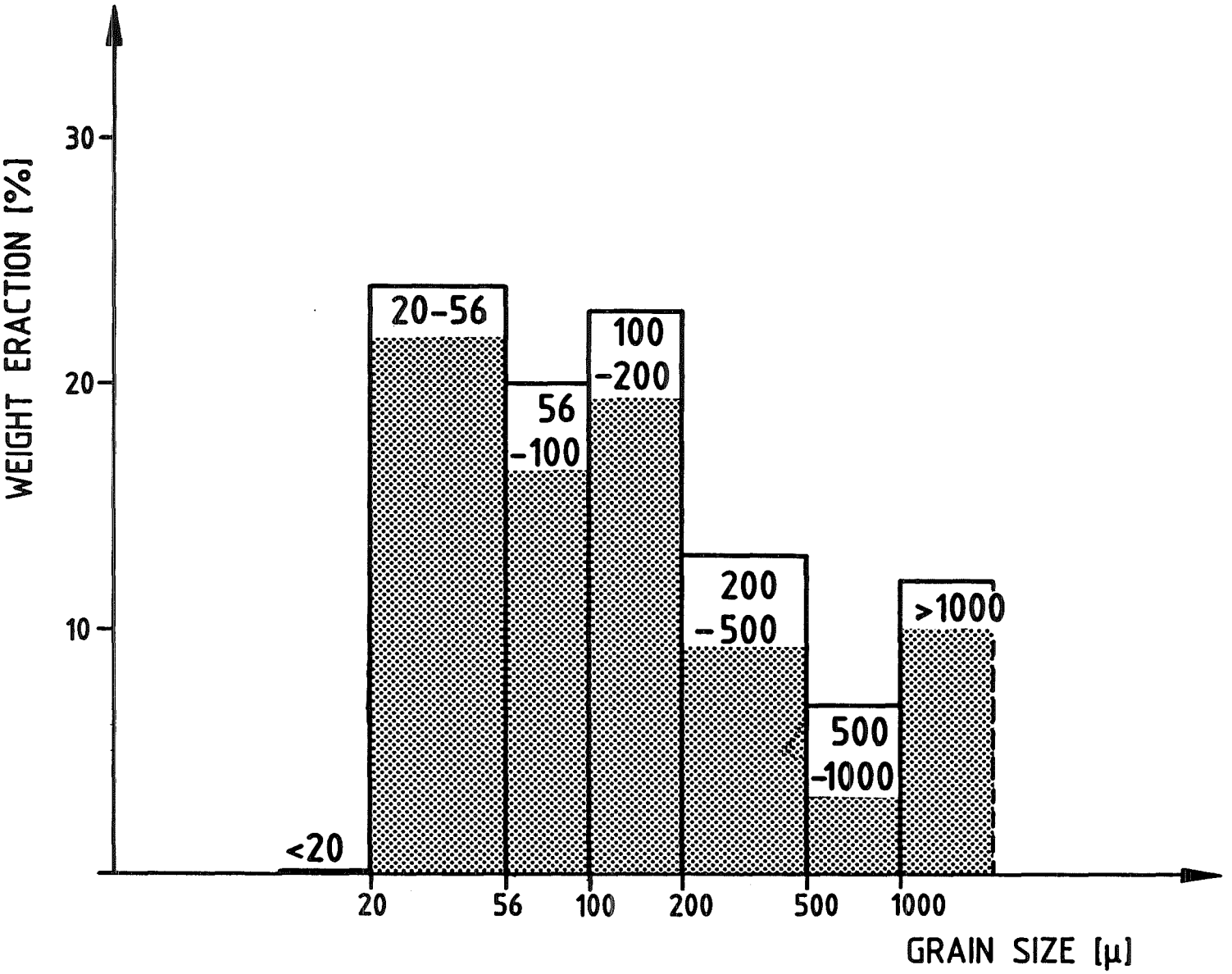

FIG.97: SIEVE ANALYSIS OF POWDER FORMED IN TEST ESBU-2A.